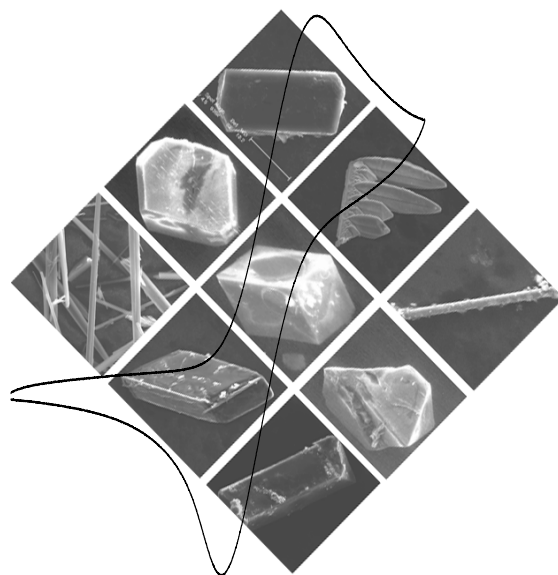


Electrochemical synthesis of new coordination
compounds with divalent silver, metallo-
phthalocyanines and organic charge transfer
crystals

Sakthivel Kandaiah



Max-Planck-Institut für Festkörperforschung Stuttgart , Germany

2010

Electrochemical synthesis of new coordination compounds with
divalent silver, metallo-phthalocyanines and organic charge
transfer crystals.

Von der Fakultät Chemie der Universität Stuttgart
zur Erlangung der Würde eines Doktors der Naturwissenschaften
(Dr. rer. nat.) genehmigte Abhandlung

Vorgelegt von

Sakthivel Kandaiah

aus Tamilnadu, Indien

Hauptberichter: Prof. Dr. Dr. h. c. Martin Jansen

Mitberichter: Prof. Dr. Robert E Dinnebier

Mitprüfer und Prüfungsvorsitzender: Prof. Dr. Thomas Schlied

Tag der Einreichung : 16.06.2010

Tag der mündlichen Prüfung: 28.07.2010

Max-Planck-Institut für Festkörperforschung, Stuttgart
2010

Table of contents

1. Introduction	10
2. General	
2.1 ElectrocrySTALLIZATION	13
2.2 Thermodynamics and electrochemistry	14
2.3 ElectrocrySTALLIZATION techniques	16
2.4 Experimental methods	16
2.4.1 Electrochemical work station	16
2.4.2 Electrochemical cell setup	17
2.4.3 Working under Inert conditions	18
2.4.3.1 Schlenk line techniques	18
2.4.3.2 Glove box	20
2.4.3.3 Solvent distillation	20
2.5 Analytical methods	20
2.5.1 X-Ray diffraction methods	20
2.5.2 Single crystal diffraction	21
2.5.3 X-ray powder diffraction	22
2.5.4 Energy Dispersive X-ray spectrometry (EDX-SEM)	22
2.5.5 Precession technique	23
2.5.6 UV-Vis-NIR spectrometry	24
2.5.7 Magnetic susceptibility measurements	24
2.5.8 Conductivity measurement	25
3. Special section	
3.1. A higher oxidation state of silver: ElectrocrySTALLIZATION of Silver (II) complexes with different coordination environments	26
3.1.1 Hexa-coordinated Ag ^{II} (4, 4' dimethyl Bipyridine) ₂ (NO ₃) ₂	29
3.1.2 Tetra-coordinated Ag ^{II} (4, 4' dimethyl Bipyridine)(NO ₃) ₂	29

Table of Contents

3.1.3	Hexa-coordinated Ag ^{II} (Bipyridine)(NO ₃) ₂	38
3.1.4	Penta-coordinated Ag ^{II} (tetramethyl tetraazacyclotetradecane) ₂ (PF ₆) ₂	43
3.1.5	<i>Cis</i> coordinated Ag ^{II} (pyridine) ₄ (NO ₃) ₂	52
3.1.6	Ag ^{II} (Bipyridine) ₂ (ClO ₄) ₂	58
3.1.7	Ag ^{II} (4,4; dimethyl Bipyridine) ₂ (ClO ₄) ₂	64
3.2	Electrochemical synthesis and structure of phthalocyanine compounds	66
3.2.1	Lithium Phthalocyanine tetrabutyl ammonium hexafluorophosphate	68
3.2.2	Disodium Phthalocyanine	80
3.2.3	Monosodium Phthalocyanine	82
3.2.4	Silver Phthalocyanine	89
3.2.5	Mercury Phthalocyanine	93
3.2.6	Fluorinated Phthalocyanine	94
3.3	Electrochemical synthesis of organic charge transfer crystals	97
3.3.1	Tetrapropylporphycene tetracyanoquinodimethane	99
3.3.2	Tetrahexyl ammonium tetracyanoquinodimethane	105
3.3.3	Tetrabutyl ammonium tetracyanoquinodimethane	110
3.3.4	Tetraphenylphosphonium tetracyanoquinodimethane	115
3.3.5	Trimethylphenylphosphonium tetracyanoquinodimethane	119
3.4	Electrocrystallization of Ag₇O₈HF₂ from aqueous medium without HF	120
4	Summary	126
5	Zusammenfassung	131
6	References	137
7	Appendix	145

Table of Contents

Acknowledgements	202
List of Figures	203
List of Tables	207
List of Abbrevations	210
List of Publications	211
Curriculum vitae	213

1. Introduction

The synthesis of new compounds, their crystal structures, as well as the electronic and magnetic properties of solids are of principal interest in the field of solid state chemistry [1,2,3]. There are several methods adapted for the preparation of new crystalline, amorphous, polymeric and glassy materials [3]. The physical properties of such solids are directly dependent on their solid state structures, i.e. the way that the atoms or molecules are packed together. Moreover, depending on the solidification conditions, the solids may comprise a single crystal or be polycrystalline. Polycrystalline solids (which represent more than 95% of solid state materials) may be thought of as an assembly of microscopic single crystals with random orientation, held together with a maze structure by the interwoven irregular shapes of the individual crystals. The electrochemical method of synthesis of solids enjoys some advantages over other methods, though it also has some limitations [4,5,6]. An important characteristic of electrocrystallization techniques is that they usually produce large, good-quality single crystals. In addition, the reaction selectivity, product formation, kinetics of reaction, crystal growth, phase purity and reproducibility are major advantages. Within the scope of this thesis the advantages of the electrochemical route for synthesis of selected crystalline solids is demonstrated. In contrast to solid state synthesis, which typically employs rather harsh conditions for the synthesis of solids, electrochemical synthesis mostly requires mild conditions for synthesis, but often affording good quality single crystals.

The thesis is organized as follows. Within chapter 2 a description of the general methodology, i.e. experimental and analytical methods, is given. Chapter 3, where the results are presented, is broken down into four subsections. In section 3.1 higher oxidation states of silver, and the synthesis of new Ag^{+2} coordination complexes with different coordination geometries via the electrochemical method, is detailed. This is followed in section 3.2 by the description of new phthalocyanine compounds prepared by electrochemical and other synthetic methods. Section 3.3 gives an

account of the electrochemical synthesis of organic crystals featuring the tetracyanoquinodimethane anion. Finally, section 3.4 discusses the electrocrystallization of the compound $\text{Ag}_7\text{O}_8\cdot\text{HF}_2$ utilizing aqueous media, and without the need for dangerous HF.

Compounds featuring higher-valent silver are potentially strong oxidants, but they remain of interest since mixed-valent silver compounds were predicted to become superconducting in an analogous manner to the copper systems. The oxidation state +2 is readily accessible and stabilized by several ligands. The general method for the preparation of this oxidation state is the oxidation of silver salts in solution in the presence of an excess of ligands, which mostly results in microcrystalline precipitates. Thus preparation of larger crystals suitable for further studies is often hampered by these hard oxidation processes. The higher oxidation state of silver as stabilized within the coordination complexes was achieved by electrochemical synthesis. This also allowed various coordination geometries of the silver complexes to be prepared. The most significant experimental parameters in electrochemical synthesis are the current and the potential, as they have a major influence on the product formation. However, the influence of solvent on the phase formation was also demonstrated in the electrochemical synthesis of some compounds. The major challenges involved in stabilizing the higher oxidation states of silver (e.g. +2 and +3) have greatly limited the number of exemplary compounds as far as pure inorganic systems are concerned. However, in contrast to the latter, the interplay of organic ligands allows for a relatively large number of such compounds to be prepared.

Metallo-phthalocyanine compounds exhibit a high potential for various applications. Thus a steep growth in the discovery of new phthalocyanine-based compounds has already been observed. In the current work, the electrochemical method is employed for the synthesis of co-crystals of lithium phthalocyanine. In addition, the electrocrystallization of monovalent sodium phthalocyanine and synthesis of other phthalocyanine compounds is also demonstrated.

Electrochemical organic synthesis has seen enormous advances in recent years. One of the most promising areas for development of electrochemical methodology is within the field of organic synthesis, where it can facilitate the simplification of synthetic routes. In fact, the synthesis of new organic compounds, organic conducting polymers and organic charge-transfer crystals has already made a significant impact on organic chemistry. In particular, electrochemical organic synthesis has substantial advantages over traditional organic synthesis, since the latter typically involves numerous intermediate steps. In the current work, we show the electrochemical synthesis of some new organic charge-transfer crystals with different organic cations and tetracyanoquinodimethane anion.

2. General

2.1. Thermodynamics and Electrochemistry

Electrochemistry is essentially based on the relationships between chemical changes and flows of electrons (i.e. the passage of electricity). It deals mainly the dynamic conditions of a given system under the perturbation of applied potential and applied current. [4,5]. In general, the heterogeneous electron transfer kinetics can be controlled mainly by those parameters. The electron transfer kinetics is also influenced by mass transfer parameters such as, diffusion, convection of the electro active species from the solution to electrode surface. Other parameters also play a significant role, like electrode, surface, supporting electrolyte, solvent, and temperature.

Using thermodynamic definitions, the spontaneity of the chemical reaction is predicted from the free energy values involved in the reaction. The free energy related with the cell potential as

$$\Delta G = -nFE_{\text{cell}} \quad [1]$$

The relation between the equilibrium constant K , and the Gibbs free energy for an electrochemical cell is expressed as follows:

$$\Delta G^{\circ} = -RT \ln K = -nFE_{\text{cell}}^{\circ} \quad [2]$$

Relating the free energy equation 1, standard free energy with equation 2, for any reversible electrochemical reaction the Nernst equation was derived as

$$E = E^{\circ} + (RT/nF) \ln [a_{\text{Ox}} / a_{\text{Red}}] \quad [3]$$

Mainly the electrode potentials determine the product formation in electrochemical synthesis. For any electrochemical reaction taking place within a cell, the potential, V of the cell is given by the formula

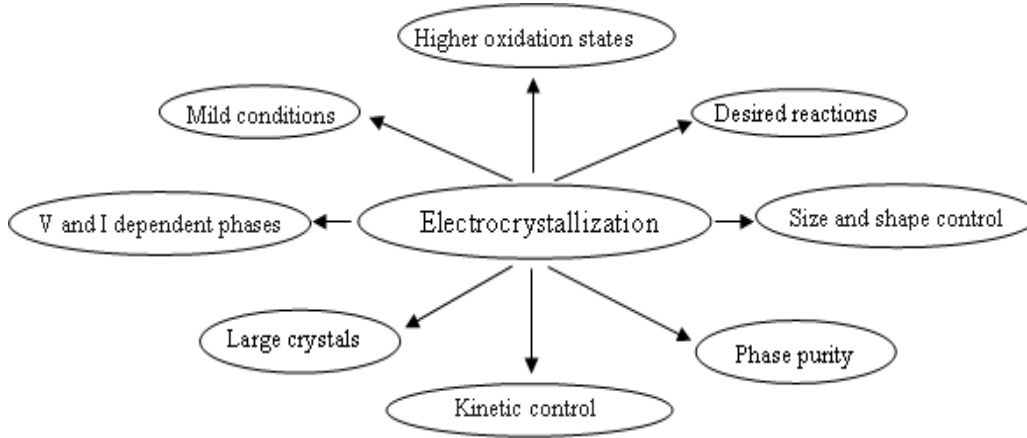
$$V = iR \quad [4]$$

where i is the current and R is the resistance of the cell, given in Ohms (Ω). The resistance of a cell is directly related to the concentration of the electrolytes in solution. As the concentration of these electrolytes decreases, the resistance increases. This accounts for the drop in current during a constant potential experiment. Likewise, for a constant current experiment, as the resistance increases, the potential also increases. The electrochemical investigations were used to measure the electrode potentials at which the eventual redox processes take place.

2.2. Electrocrystallization

Electrocrystallization is the soft synthetic route for preparation of single crystals. The electrochemical methods enjoy special advantages over other crystal growth techniques. In recent years many newer techniques have led to new understanding of electrode reactions. The term electrocrystallization was first used by Fischer [7-9]. The current and potential has ability of control of nucleation and growth rate. The crystals can be grown from the solution or melt. The current, potential, solvent, supporting electrolyte, operating temperature are the parameters that can affect the product formation. There were reports on the potential and current dependent phase formation. These two are the key parameters that affect the electrochemical crystallization. The kinetics of crystal growth can be fine tuned by varying these parameters. The current step methods were used to detect the nucleation and growth mechanism. By means of a potentiostat, the over-potential can be imposed at will, changed instantly or varied linearly with time. Alternatively, in the galvanostatic method, the nucleation process can be forced to take place at a predetermined rate and the degree of supersaturation monitored as over-potential throughout the process. The

main advantages of electrocrystallization method are schematically represented below.



Scheme 1. Advantages of electrocrystallization method

The linear rate of electrocrystallization, v , is directly related to the current density, j , and it is given as

$$v = jV_m/nF \quad [5]$$

where

V_m - molar volume

F - Faraday constant

High localized values will results in higher rate of growth.

The driving force for electrocrystallization is provided by the deviation of the electrode potential from its equilibrium value, which is known as the overpotential, η .

$$\eta = E - E_e \quad [6]$$

Electrocrystallization not only represents an interesting case of phase formation and crystal growth but is also a powerful method for various technological applications.

Especially in the field of nanotechnology and thin film processes, because the driving force of the process can be easily controlled by the current density and the electrode potential. The discovery of scanning tunneling microscopy and atomic force microscopy (STM and AFM) offered new exciting possibilities for in situ studies of the electrocrystallization phenomena down to an atomic level [10]. It would be not an overstatement to say that during the past two decades the application of these techniques has revolutionized the experimental work in this field and led to significant progress in the understanding of the atomistic aspects of electrocrystallization processes [11–16]. It helps for a better understanding of both the nucleation and growth phenomena at an atomic level and the preparation of various nanostructures by electrochemical means. It has to be mentioned, although synthetic chemists have long appreciated the value of electrochemistry as a tool for numerous organic transformations (often on an industrial-scale), the use of electrochemical methods in complex molecule synthesis remains rare.

2.3. Electrocrystallization techniques

Cyclic voltammometry, galvanostatic, potentiostatic methods were usually used to study the electrochemical nucleation and growth mechanisms [6]. The cyclic voltammometry gives information regarding the redox processes, electron transfer reactions, adsorption processes involved under potentiodynamic conditions. Hence it can be potential tool to decide at what potential or current the electrocrystallization should be carried out. From the wave form we can also arrive at conclusion how many different chemical phases could be synthesis by electrochemical oxidation or reduction.

2.4 Experimental methods

2.4.1. Electrochemical work station

The general potentiostat/galvanostat consist of a electrode connection terminals, where the potential is applied between the working and the reference electrode, while

current is measured between the working and counter electrode. In our laboratory we use multichannel VMP electrochemical workstation, provided with 16 channels. It is controlled by E-lab software. Each channel board of the instrument is an independent potentiostat/galvanostat is controlled by the EC-Lab software. The instrument and the software provide different categories of electrochemical techniques and electrochemical applications.

2.4.2. Electrochemical cell setup:

In general, an electrochemical cell consists of a working electrode, counter electrode and a reference electrode. The working and counter electrodes are usually inert, in the potential range. Platinum metal was used as working and counter electrode. The area of the counter electrode is about twice that of working electrode. The electrochemical cell was made in home (Max Planck glass workshop). It was home made, with glass with preferred outlets for three electrodes, vacuum line and Argon supply. The schematic representation of the electrochemical cell is given in figure 1, in some electrochemical synthesis there is need of separate reaction compartment, hence a two electrodes cell setup was used as shown in figure 2.

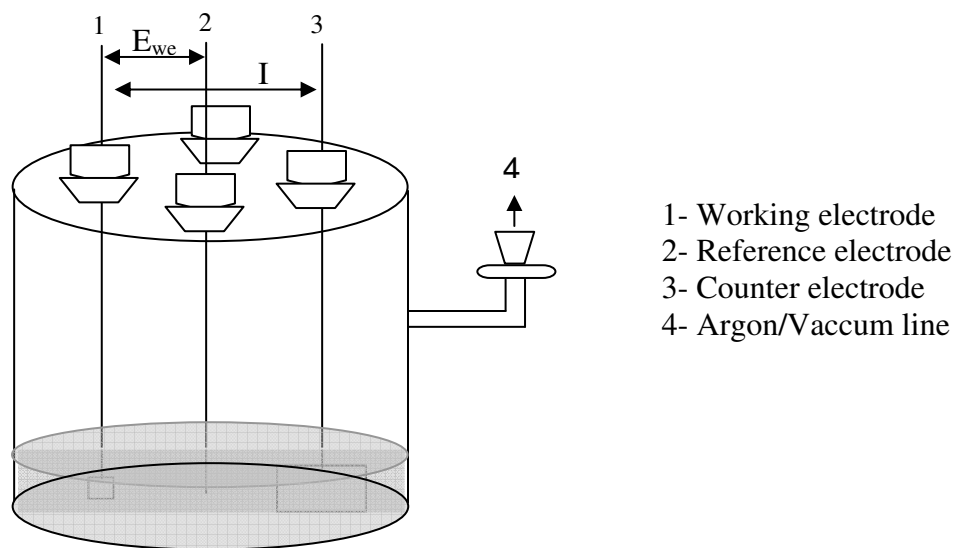


Figure 1. Pictorial representation of three electrode electrochemical cell

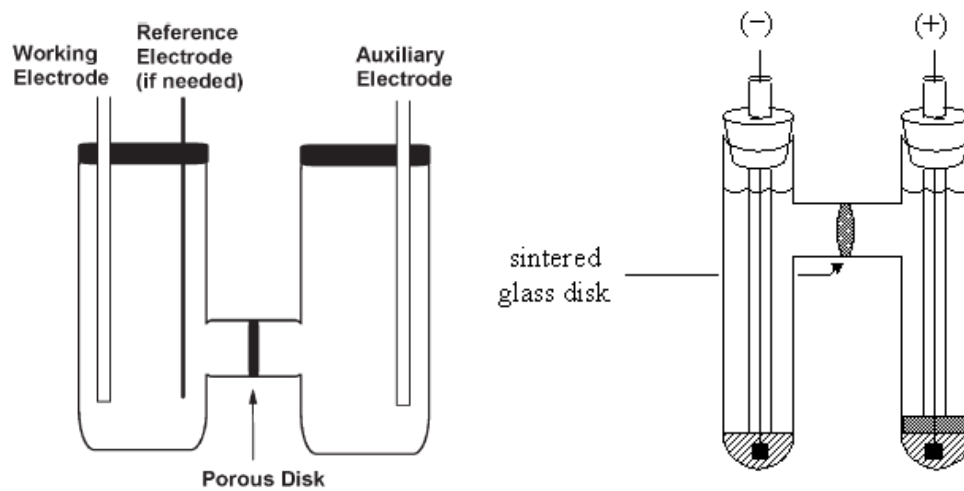


Figure 2. Three and two electrodes divided cell setup used for electrochemical synthesis

2.4.3. Working under Inert conditions

Solvents are dried in appropriate conditions and stored in the inert atmosphere. These solvents handled in the dry and inert conditions using *Schlenk* line techniques. Since the water content in the solvent will certainly affect the product formation, hence it must be taken care in the electrocrystallization experiments. The electrochemical cell setup was made in such a manner that could be assembled in the dry conditions using Schlenk line techniques.

2.4.3.1. Schlenk line techniques

This setup is used to assemble electrochemical cell, solvent handling and for other requirements of dry conditions. The schematic representation of the *Schlenk* line is shown in figure 3.

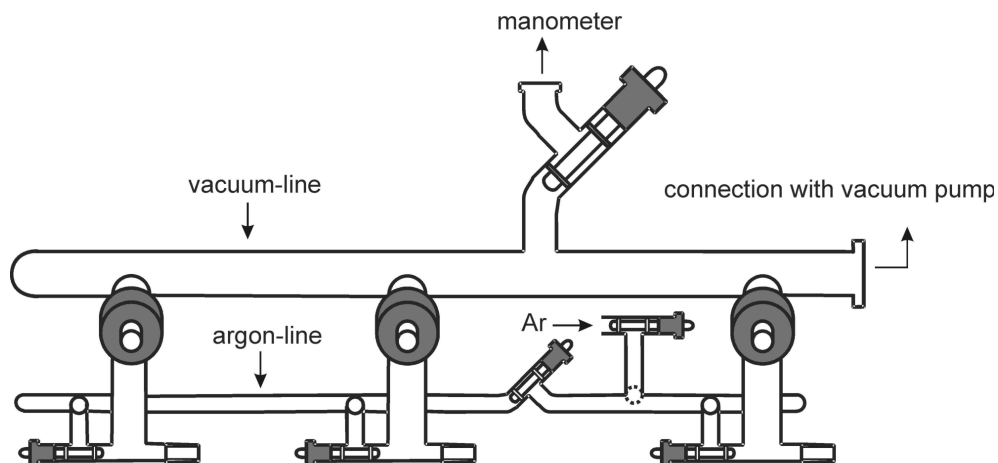


Figure 3. Schematic representation of Schlenk line

The argon was supplied by the low temperature service department of Max-Planck Institute, Stuttgart, Germany. The *Schlenk* apparatus is shown in figure 3. It is made up of Duran glass with desired connection for Argon and Vacuum lines. Evacuation was done using a rotary valve oil pump. The vacuum level is monitored using a Pirani manometer (Thermovac TM20, Company: Leybold) within a range of 10^{-3} - 10^3 mbar. This apparatus is filled with either argon. Before use, the Argon gas is passed through four successive drying towers of blue gel, potassium hydroxide, molecular sieve (mesh size 3 Å) and phosphorous pentoxide on an inert substrate (Sicapent, Company: Merck), respectively. This setup is used to remove the residual humidity from the gas. To check leakage in the glass tubes, a high frequency vacuum examiner (VP 201, Company G. Lauer) is used. L-shaped angled glasses connect the glass apparatus. The electrochemical cell is connected by glass spirals or angled glasses can be evacuated and filled with argon by opening the concerned valve. Before use, the electrochemical cell and the necessary glassware are heated under vacuum and were immediately rinsed with dried argon. The solvents were transferred into the electrochemical cell under the flow of Argon. The solvents used were pre-distilled and held in air tight container filled with Argon gas.

2.4.3.2. Glove box

The required sample preparations, handling of the air and/or moisture sensitive compounds, picking single crystals were done inside the glove box. The model of glove box compartment available is MT 200 (Company: M. Braun). The purity of the inert gas is maintained by passing it over the molecular sieves and its quality is examined by the gas analyzers. The moisture content inside the glove box compartment is maintained below 0.2 ppm while the oxygen content below 0.5 ppm. The chambers are filled with argon and evacuated a number of times (big chamber for 45 minutes and small chamber for 10 minutes) to ensure the atmosphere inside the chamber and the glove box is completely inert.

2.4.3.2. Solvent distillation

It is very important to notice on several occasions the effect of reaction medium in electrochemical product formation. The medium influence first the electrode reaction, and second, the chemical reactions which are coupled to the electron transfers. Especially special care has to taken in the residual water content in the organic solvents. Hence, the organic solvents used in electrochemical synthesis were initially dried and handled under inert condition. The appropriate distillation methods were used to dry the solvents, for every experiment. The solvents addition to the electrochemical cell setup was handled using the *schlenk* line technique.

2.5. Analytical methods

2.5.1. X-ray diffraction methods

This is a non destructive analytical method used to obtain the information about crystal structures from single crystals as well as from polycrystalline samples [17]. X-rays were scattered, or diffracted, by crystals in a way that could be interpreted to yield the absolute arrangement of the atoms in a crystal, the crystal structure. X-ray diffraction remains the

most widespread technique used for structure determination, but diffraction of electrons and neutrons is also of great importance, as these reveal features that are complementary to those observed with X-rays. The crystalline substances can be measured as single crystal or finely ground powder. In general the measurement of a single crystal gives primarily the solution of the atomic structure of a substance. The powder method is used to check the purity, for rapid substance identification, phase identification and to investigate phase transitions in substances. Also the powder diffraction data is used to solve and refine structures. The structure models of the powder or single crystal samples are visualized with the help of the program DIAMOND [18].

2.5.2. Single crystal diffraction

The single crystal was mounted on the glass capillaries with special wax or glue. Then it was subjected to quality test through precession measurement. Diffraction experiments on single crystals collect the reflexes in the three-dimensional area individually and thus make a simpler task to solve crystal structures in contrast to powder diffraction. By means of film methods all reflexes of one layer can be collected at the same time and thus elementary cell, Laue group and extinction conditions are easily accessible. For the determination of integral reflection intensities additionally a single crystal diffractometer is used. The single crystal diffraction measurements are carried out with a dual circuit plane detector diffractometer IPDS II (Company: Stoe & Cie, Darmstadt) and a three circle diffractometer AXS Smart with CCD 1000-Detector (Company: Bruker, Karlsruhe), both with a fine focus tube with Mo-anode (Mo-K α - radiation: $\lambda = 71.073$ pm) as source of X-rays and a graphite single crystal monochromator. From the experimentally measured reflections and intensities the data are processed using the programs X-area [19] or SMART32 [20], further the data reductions are performed using the programs X-red [21] or SAINT32 [22]. The absorption corrections are carried out with the programs X-shape [23] or SADABS [24]. The structure solution was done with the help of direct methods using SHELXS- 97 [25] and SHELXTL [26]. The refinements of structures determined are carried out by the least squares refinement procedure with the help of the SHELXTL [26] program package, or with the minimisation of the

difference of the squares on the basis of the structure refinement program, JANA2000 [27].

2.5.3. Powder X-ray diffraction

Powder X-ray diffraction was used for ascertaining the phase purity and also determining the crystal structure of polycrystalline powder samples. Stadi P and D8 powder diffractometer (Company: Stoe & Cie, Darmstadt, Bruker D8 flat plate and capillary mode) were used for this purpose. The crystalline sample was applied either to a surface carrier between two X-ray-amorphous polyethylene foils, low-background flat Si-(911) sample holder or filled into a glass capillary and rotated in the path of X-rays. The air and moisture sensitive samples were filled in the capillaries and sealed inside the glove box. The X-rays are generated in a fine focus tube with Cu anode using Ge (111)-single crystal as a monochromator (Cu-K α 1-radiation $\lambda = 1.54.06 \text{ \AA}$). A position sensitive detector (PSD) was used as a proportional counter with an opening angle 2θ of 6° (linear PSD, resolution $D2\theta = 0.06^\circ$) and a image plate detector with an opening angle 2θ of 140° (IP-PSD, Company: Stoe & Cie, Darmstadt, resolution $D2\theta = 0.12^\circ$). The correction of measured values was achieved by using elemental Si as an external standard. Identification of the substances was accomplished by comparing with the database (e.g. ICDD-JCPDS) [28, 29] of powder diffractograms for already known compounds. The evaluation of the diffractograms was carried out using WinXPow, Topas and DASH programs. The first step is the indexing of the pattern to find a unit cell. The Le Bail method is a peak extraction method used to refine the background, lattice parameters and the peak profiles. Next, the Rietveld method was used to refine the model-dependent parameters, such as atomic coordinates, thermal parameters, and atomic occupancy. The structure model for a large organic molecule is given as z-matrix file. The refinement is based on the variation of profile parameters, background coefficients and structure parameters with the least squares method until the calculated profile matches with the observed powder pattern as precise as possible. The structure refinement from powder data was carried out by using GSAS [30], DASH [31] or Topaz [32].

2.5.4. Precession technique

This method is used to test the quality of the single crystals. The single crystals in a thin glass capillary is mounted on the goniometer head and adjusted in the precession camera. The crystal position is adjusted to be inline with the X-ray beam position. The precession photographs were taken using image plates. The measurements were done using MoK α - radiation (0.7107 Å).

2.5.5. Energy Dispersive X-ray spectrometry (EDX-SEM)

Energy Dispersive X-ray Spectroscopy (EDX) is used to probe the presence of heavier elements in the sample. Mostly this is not a quantitative technique, but it is used to probe the crystals when obtained products where of lower amounts. The principle involved in EDX is the interaction of incident electrons (electron beam) with inner-shell electrons of the sample. When the sample is bombarded with fast moving electrons the characteristic X-rays are produced. During the ionization process, a high-energy electron ejects an electron from the inner-shell of the atom, leaving a vacancy in the shell. The excited atom returns to its initial state filling the vacant place with an electron from an outer-shell (recombination). Because of the difference in bonding-energy, the recombination process results in the emission of characteristic X-rays. The intensity and the wave length of this X-rays yield quantitative and qualitative information on the elements present in the sample. Scanning electron microscopy and Energy dispersive microanalysis was carried out on XL 30 TMP (Company: Philips, Eindhoven, NL), equipped with a energy dispersive unit for microanalysis (Model: Phoenix, Company: EDAX, Mahwah, NJ, USA). The images of the single crystals were taken using SEM. Observations of the shapes of crystals, the crystal morphology, can suggest the regular external form of a crystal and shape can be an expression of internal order.

2.5.6. UV-Vis-NIR spectrometry

The solid state spectra of the crystals were taken using The UV-Vis-NIR spectrum can be measured with Lambda 19 spectrometer in range of 200-2400 nm range. The solubility of solid in the desired solvents and phase transition limits one to examine the solid state spectra compounds. Here the spectra were taken by using a solid pellet made by mixing finely grounded sample with dry KBr. Here we used transmission mode for measurements.

2.5.7. Magnetic susceptibility measurements

The temperature dependent measurement of the magnetic susceptibility of any substance gives an idea about the presence of the unpaired electrons in that substance. The magnetic moment values gives the information about the compound whether it is diamagnetic or paramagnetic, or ferromagnetic or antiferromagnetic or ferrimagnetic substances. The plot of χ^{-1} vs T also gives the vivid details about the magnetic characteristic of the compound. The determination of the magnetic susceptibility was achieved in a spin quantum interference device (SQUID magnetometer), MPMS 5.5 (Company: Quantity Design, San Diego, CA, USA). For the air stable compounds the sample was prepared in a gelatine capsule (in powder form) or into a quartz capillary sealed under helium in the case of air sensitive samples. The diamagnetic correction was done for the sample data from the standard values obtained from the literature [33]. The magnetic moments for the compounds were calculated from the plot of χ^{-1} vs T. The paramagnetic substance obeys the curie law given below.

Curie Law

$$\chi = \frac{C}{T} = \frac{M}{H}$$

$$\frac{C}{T} = \frac{N\mu_0 g^2 j(j+1) \mu_B^2}{3KT}$$

$$\mu_{\text{eff}} = g \sqrt{j(j+1)} \mu_B$$

2.5.8. Conductivity measurements

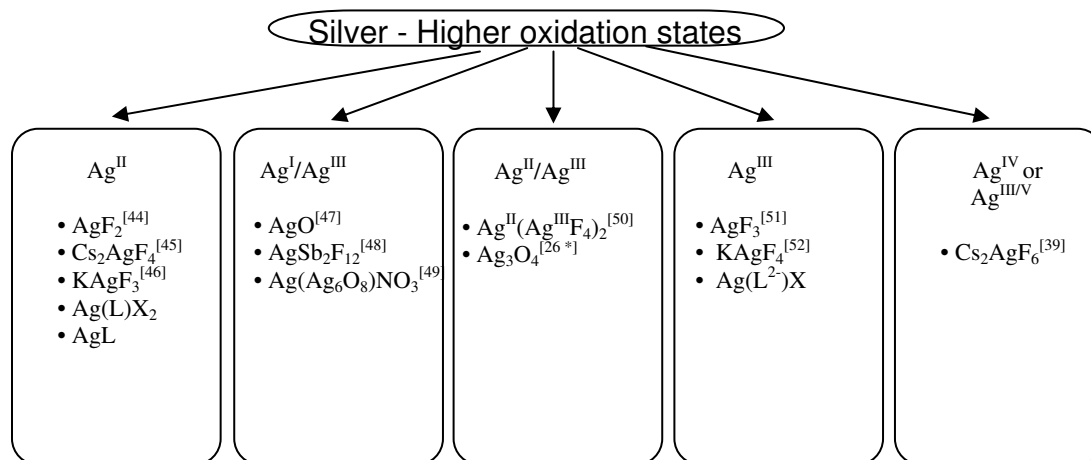
The electrical impedance measured with application of AC potential of very small amplitudes. This is mainly used to separate the ionic conductivity of the given system. This was done using two electrode setup with symmetrical electrodes such as Pt, Au, and Ag. The compound is made as pellet and assembled inside the glove box setup. The temperature dependent conductivity was done using a high resolution dielectric analyzer (Novocontrol GmbH Germany). The resultant impedance data were subjected to fitting using equivalent circuit program. The controlling and analysis of the data is carried out with the programs Sigma measurement [34], Sigma evaluation [35], and Equivalent Circuit [36]. The ionic conductivity can be calculated from the high frequency region of the Nyquist plot.

3. Special section

3.1. A higher oxidation state of silver: Electrocrystallization of Silver(II) complexes with different coordination environments

Introduction

High temperature superconductivity in mixed-valent compounds has been of great interest for some time now [37, 38]. The discovery of high T_c superconductors based on cuprates resulted in the search for other materials with similar structures. Ag compounds similar to Cu-based superconductors can also show mixed valences in some instances [39]. The commonest and most stable oxidation state of silver is +1. Yet higher oxidation state compounds of silver that also exhibit high stability, are of great interest in research and applications. Despite sharing the same formal oxidation states, copper and silver show marked differences in the respective stabilities. While the common oxidation states for silver and gold (M) are +1 and +3, paramagnetic mononuclear d^9 M(II) complexes are especially rare in pure inorganic systems. In particular, genuine mononuclear Au(II) compounds are very rare, although mononuclear, paramagnetic Ag(II) centers are more common, and mostly found in organometallic compounds. Ag(II) species have been identified in the processing of radioactive waste at room temperature [40] and are known as effective oxidants for organic substrates. The chemistry of higher oxidation states of silver and its various potential applications was reviewed by several authors [39, 41, 42]. Silver in the +1 and +3 oxidation states is frequently encountered in solid state compounds, whereas silver in the +2 oxidation state is rather uncommon [39, 43]. However, properly hole-doped silver in +2 oxidation state compounds can possibly be superconducting. Silver in the +2 state appears to be very rare and is still regarded as an unusual oxidation state in pure inorganic solids. It is observed that the stabilization of this oxidation state is mainly achieved via some organic-based macrocycles. A schematic diagram of various oxidation states of silver are represented Scheme 2.



Scheme 2. Silver in different oxidation states

The silver fluorides AgF₂ and AgF₃ are known to be among the strongest oxidizing agents [53, 54]. In particular hole- or electron-doped silver(II) fluorides have been predicted to be potential superconductors [39]. The fluorides of silver with M₂AgF₄ are of particular interest because they are layered and have a strong two dimensional character. The fluoroargentates are difficult to prepare due to their high reactivity. In contrast, it is well established that amine and imine ligands can be utilized to stabilize silver cations in their high oxidation states of +2 and +3 [41, 42]. These valence states of silver are rather rare in inorganic systems; the oxidising capability of silver (II) is strikingly high [39, 53]. In fact, the divalent fluoride is known to be the strongest oxidising agent among all M²⁺ based compounds [55]. It is shown that it readily oxidizes many different materials, even glass, due to its strong fluorinating character. Experiments show that Ag²⁺ in HF can even oxidize Xe to Xe²⁺ [55]. By contrast, the stability of silver(II) in coordination complexes is impressively high and most of the complexes are stable towards air and moisture. Usually Ag(II) is stabilized with organic based ligands in varieties of nitrogen containing heterocyclic compounds. The most noticeable point in the current work is that the electrocrystallized crystals exhibit different coordination environments for the Ag²⁺ cation. The complexes of formal Ag(II) centers are dominated by porphyrin [56-58] and aza macrocyclic [59, 60] species in which the Ag(II) center is coordinated to all four N-

donors of the ligand in a square planar geometry with potential weak axial interaction(s) to counter-anions or co-ligands. In these studies the preparation of Ag(II) compounds with different coordination environments as organometallic complexes is described. The potential-dependent phase formation of Ag(II) compounds with different coordination environments is shown. Usually d^9 silver is six-fold coordinate and subject to Jahn Teller distortion. The distortion and lengthening of the long bonds can be of differing extents. Highly oxidizing Ag(II) compounds stabilized with N-heterocyclic ligands can be prepared via oxidation of precursor Ag(I) salts along with the ligands. Also, the electrocrystallization of Ag(II) complexes with weakly coordinating anions using selective experimental conditions, are discussed.

3.1.1. Electrocrystallization of Tetra- and Hexa-coordinated Ag (II) Compounds based on 4, 4' - Dimethyl - 2, 2' - Bipyridine Ligand:

Introduction

In this section we describe the potential dependent electrocrystallization of $\text{Ag}(4,4'$ dimethyl 2,2' Bipyridine) $_2(\text{NO}_3)_2$ (**1**) and $\text{Ag}(4,4'$ - dimethyl - 2,2' -bipyridine) $(\text{NO}_3)_2$ (**2**) from the same electrolytic bath. Thus it has been shown for the first time that the coordination number of silver ion to ligands can be tuned by the electrocrystallization potential. Usually silver(II) is stabilized with organic based ligands in varieties of nitrogen containing heterocyclic compounds. Chemical synthesis of respective complexes has been mostly achieved by the oxidation of silver(I) in the presence of the respective ligands. A detailed preparation and single crystal structure investigations of a series of Ag^{+1} bipyridine adduct with oxyanions was recently reported [61]. Electrocrystallization is a potential tool for the preparation of chemical phases which could be difficult to access by chemical synthetic routes [43, 62]. In this study we show the electrocrystallization of a higher coordinated $\text{Ag}(4,4'$ - dimethyl - 2,2' - bipyridine) $_2(\text{NO}_3)_2$ **1** and a lower coordinated $\text{Ag}(4,4'$ - dimethyl - 2,2' -bipyridine) $(\text{NO}_3)_2$ **2** Ag^{2+} compound. Both were prepared from the same electrolysis bath, just by varying the potential of the electrocrystallization process. In the literature a single crystal structure of $\text{Ag}(\text{bipyridine})_2(\text{NO}_3)_2 \cdot \text{H}_2\text{O}$ which is similar to **1**, was prepared by a chemical route, is reported [63].

Experimental

Electrocrystallization experiments

Silver nitrate (Alfa Aesar, 99.9%) 4, 4' - Dimethyl - 2, 2' - bipyridine (DMBPY) (Alfa Aesar, 98%), Tetrabutyl ammonium hexafluorophosphate (TBAPF₆)(Fluka 99%),

chemicals were used as supplied by the manufacturers. Acetonitrile (Merck, 99.5%) was dried under CaH_2 (Alfa Aesar 95 %) before use in the electrocrystallization experiments.

Electrocrystallization experiments were carried out in the three electrode electrochemical cell setup. Pt foil was used as working and counter electrode, silver wire was used as the reference electrode. Dry acetonitrile solution containing AgNO_3 : DMBPY in 0.1 M: 0.05 M (2:1) molar ratio and 0.1M TBAPF_6 as the supporting electrolyte was prepared for the electrocrystallization experiments. The electrochemical cell setup was assembled by maintaining argon atmosphere using a Schlenk line technique. The potential for electrocrystallization was decided from the cyclic voltammetric investigation of the reaction solution. Potentiostatic oxidation of the above solution at two different potentials 0.55 V and 1.1 V resulted in growth of black and deep red coloured crystals respectively. These crystals grew on the electrode surface in higher yields. The crystals were separated, washed with dry acetonitrile and dried under vacuum at room temperature. The crystals were mounted on the glass capillary tip and subjected to single crystal x-ray structural characterization with a Bruker-AXS- APEX Smart-CCD diffractometer. Details of the structure determination are given in tables 1-2 (Crystal data, selected geometric parameters. The atomic coordinates and displacement parameters are tabulated in appendix section table 17, 18. The magnetic measurements of the crystals were carried out in the temperature range of 1.8 – 300 K using a MPMS SQUID magnetometer, upto 7 tesla. Diamagnetic corrections were performed for both the samples.

Electrochemical characterization – Cyclic voltammetry

Electrochemical cyclic voltammetric measurements basically show two irreversible processes. A steep increase in the current beyond 0.7 V vs Ag wire is observed. Figure 4 shows the cyclic voltammograms of two consecutive cycles, this allows us to choose the desired potentials for electrocrystallization. The basic mechanism of electrooxidation at higher positive potential is exactly like maintaining acidic conditions. This is due to the higher rate of reduction of Ag^{1+} to Ag at the counter electrode and electrochemical generation of higher concentration of nitrate anion in the electrolytic bath.

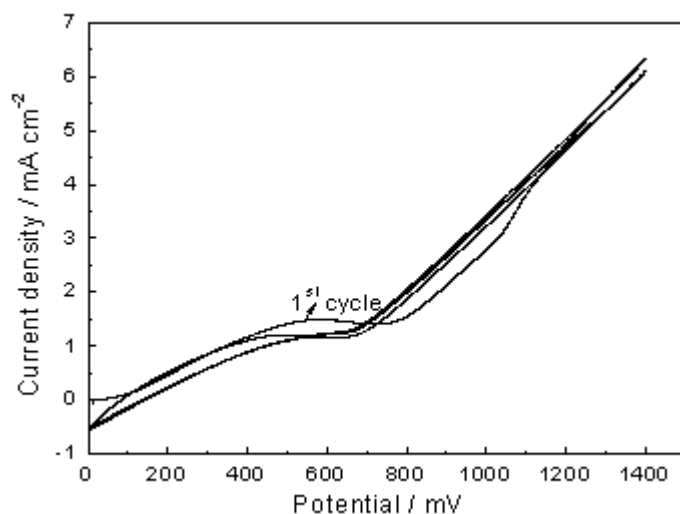


Figure 4. Cyclic Voltammograms of $\text{AgNO}_3 + \text{DMBPY} + \text{TBAPF}_6$ in dry acetonitrile at 20 mV sec^{-1} .

These conditions favour the crystallization of $\text{Ag}(4,4' - \text{dimethyl} - 2,2' - \text{bipyridine})(\text{NO}_3)_2$ and results in a potential dependent phase formation. The crystals obtained at 0.55 V and 1.1 V are different in colour and visually discernable when viewed under optical microscope. This is also clearly evident from the scanning electron micrographs, shown in figure 5. Both the crystals are basically stable in air and free of water.

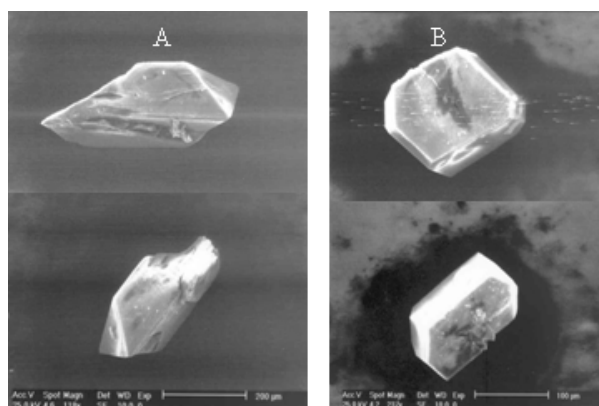


Figure 5. Scanning electron micrograph of $\text{Ag}(4,4' \text{ dimethyl } 2,2' \text{ Bipyridine})_2 (\text{NO}_3)_2$ (A) and $\text{Ag}(4,4' - \text{dimethyl} - 2,2' - \text{Bipyridine})(\text{NO}_3)_2$ (B)

Structure description

The crystal structure solution show the crystals to be $\text{Ag}(4,4' \text{ dimethyl } 2,2' \text{ bipyridine})_2(\text{NO}_3)_2$ (**1**) and $\text{Ag}(4,4' \text{ dimethyl } 2,2' \text{ bipyridine})(\text{NO}_3)_2$ (**2**) . In compound **1** silver is coordinated to four nitrogen donors from two 4, 4'- dimethyl – 2, 2' bipyridine ligands. The bond lengths observed in this compound are as expected. The complex cation significantly deviates from the expected planar geometry. The torsion angle between the two planar ligands is $24.335(80)^\circ$. Ag(II) is coordinated additionally by two nitrate anions in monodentate manner. In contrast, silver is coordinated by only one 4, 4'- dimethyl – 2,2' bipyridyl ligand in **2**, in a slightly distorted square planar arrangement. The two nitrate anions are *cis* coordinated with the silver (II) ion. The anions are slightly shifted from the exact square planar configuration by 16.45° and 5.65° respectively. The oxygen coordinated to silver in the nitrate anion shows a longer N-O bond length in comparison with other uncoordinated N-O bonds. It is interesting and worthwhile to compare the bonding parameters of both these crystals. In compound **2**, the nitrate anion is strongly coordinated to the Ag(II) metal ion, because of the lower coordination environment. This is clear from bond length of Ag-O in **2**, which is about 0.75 \AA shorter in comparison with compound **1**, shown in table 2 and also in figure 6, 7. Furthermore, silver to donor nitrogen bond length is also slightly shorter in comparison to compound **1**.

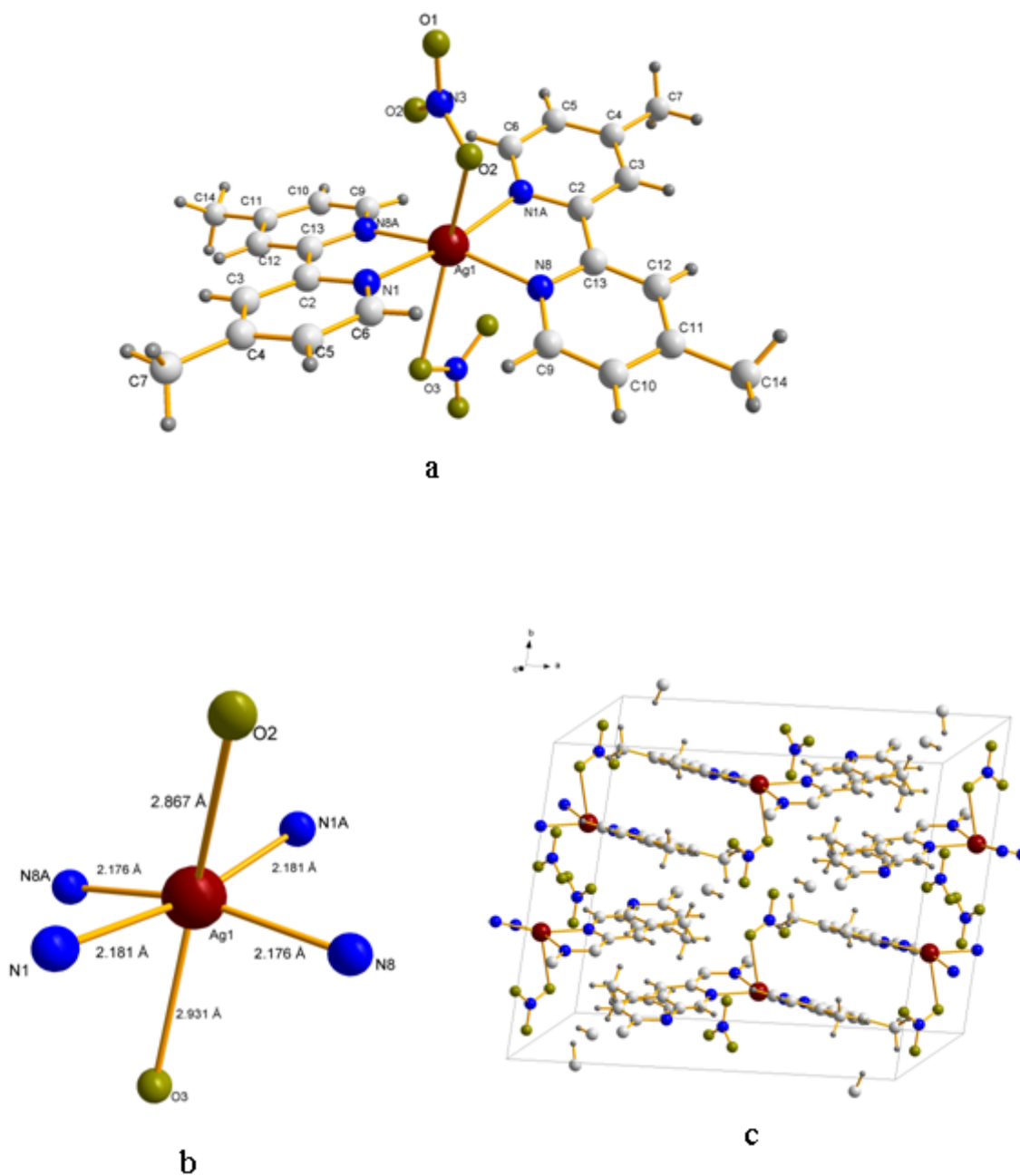


Figure 6. a) View of molecular structure of $\text{Ag}(4,4' - \text{dimethyl} - 2,2' - \text{bipyridine})_2(\text{NO}_3)_2$; b) the view of hexa-coordinated silver(II), with bond lengths given; c) the unit cell view of the compound.

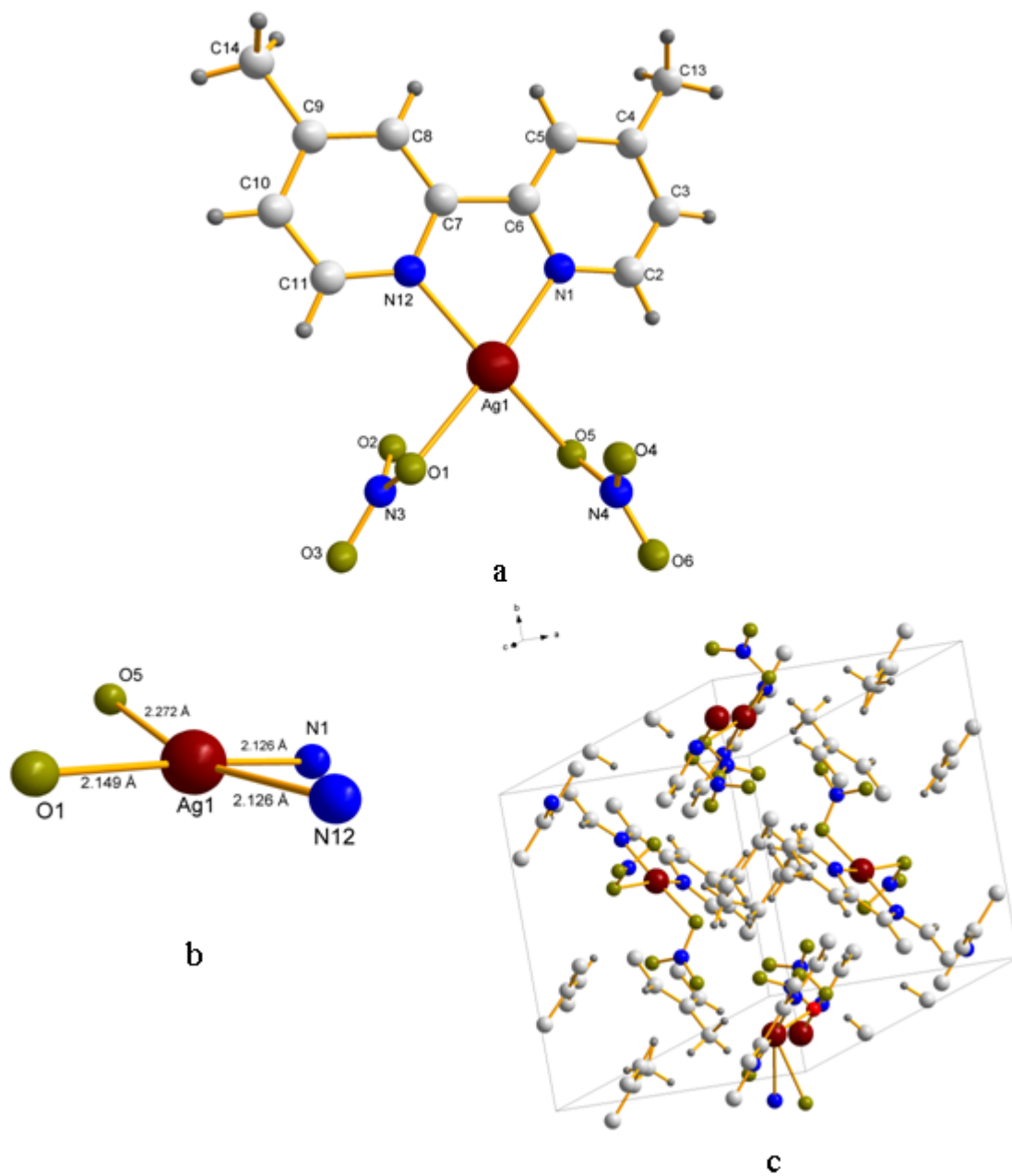


Figure 7. a) View of molecular structure of $\text{Ag}(4,4'\text{-dimethyl-2,2'\text{-bipyridine})(\text{NO}_3)_2$; b) view of tetra coordinated silver(II), with bond lengths given.

Magnetic measurements

The magnetic susceptibility measurements of the crystals are illustrative of d^9 electronic configuration of silver in these compounds. It is clearly evident from the plots of magnetic susceptibility and reciprocal magnetic susceptibility that silver is in +2 oxidation state in both the compounds. Plots of reciprocal susceptibility vs temperature

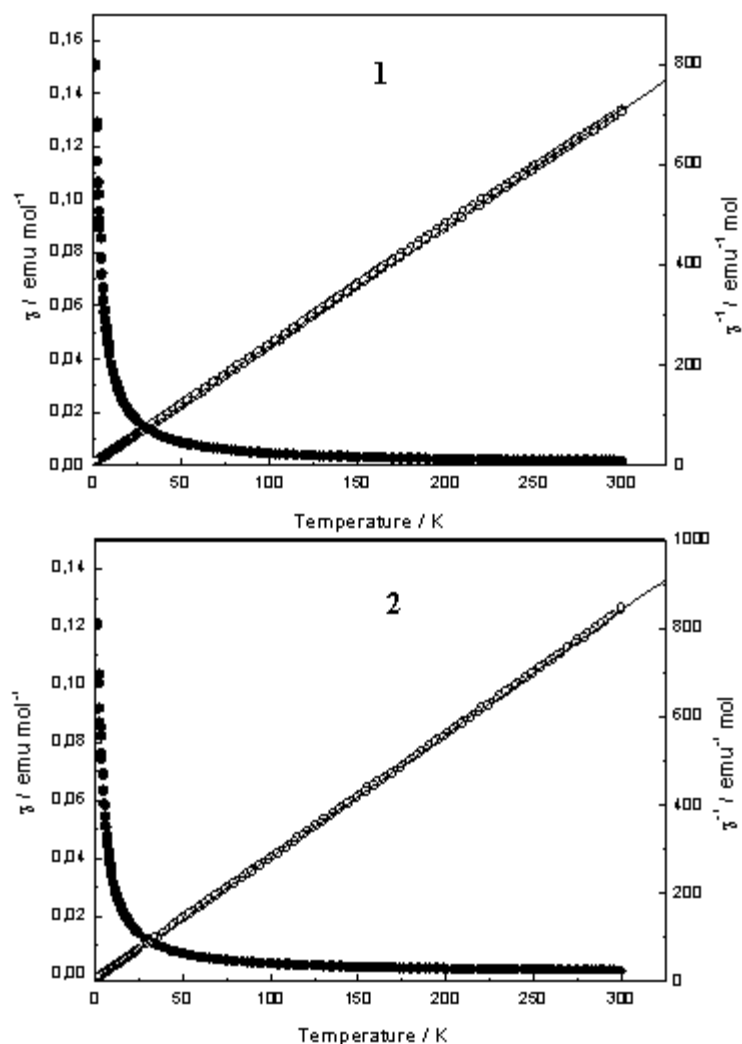


Figure 8. Magnetic susceptibility and reciprocal magnetic susceptibility of compounds $\text{Ag}(4,4' - \text{dimethyl} - 2,2' - \text{bipyridine})_2(\text{NO}_3)_2$ **1** and $\text{Ag}(4,4' - \text{dimethyl} - 2,2' - \text{bipyridine})(\text{NO}_3)_2$ **2**

(figure8) clearly pass through the origin and show both the compounds obey the *Curie* law. The effective magnetic moment is calculated from the slope of the reciprocal susceptibility plots. The values are $1.84 \mu_B$ and $1.72 \mu_B$ for 1 and 2 respectively at 3 telsa. This is a clear indication of highly dilute magnetic systems. The values are typically found for silver (II), showing spin only behaviour with only slight orbital momentum contribution for **1** and pure spin only behaviour for compound **2**.

Table 1. Crystal data and structure refinement for compounds 1 and 2

	1	2
Empirical formula	C ₂₄ H ₂₄ Ag N ₆ O ₆	C ₁₂ H ₁₂ Ag N ₄ O ₆
Crystal system	Monoclinic	Monoclinic
Formula weight	600.36	416.13
Pearson symbol	<i>mC</i> 244	<i>mC</i> 280
Wavelength / Å	71.073	71.073
Space group	<i>C</i> 2/ <i>c</i> (15)	<i>P</i> 21/ <i>c</i> (14)
Unit cell dimensions		
a / Å	18.6308(15)	8.5865(11)
b / Å	14.5708(12)	11.0157(14)
c / Å	11.5867(10)	16.4554(10)
β / °	126.5910(10)	111.102(10)
Volume / nm ³	2.5255(4)	1.4521(3)
Formula per unit cell / Z	4	4
Density (calculated) / Mg/m ³	1.579	1.903
Absorption coefficient / mm ⁻¹	0.850	1.427
F (000)	1220	828
Crystal size / mm ³	0.360x0.180x0.100	0.150x0.060x0.045
Crystal colour	Black	Deep red
Theta range for data collection	1.95 to 35.02	2.28 to 25.75°
Refinement method	F ²	F ²

3. Special section: Higher oxidation state of silver

Index ranges	-29<=h<=29	-10<=h<=10
	-22<=k<=22	-13<=k<=13
	-18<=l<=18	-20<=l<=20
Reflections collected	19693	11014
Independent reflections	5300[R _{int} = 0.0254]	2775 [R _{int} = 0.0284]
Completeness to theta = 35.02°	95.1 %	99.9 %
Data / restraints / parameters	5300 / 0 / 173	2775 / 0 / 210
Goodness-of-fit on F2	1.029	0.991
Final R indices [I>2sigma(I)] R1	0.0398	0.0350
wR2	0.1024	0.0802
R indices (all data) R1	0.0509	0.0493
wR2	0.1117	0.0883
Largest diff. peak and hole(e.Å ⁻³)	0.858 and -0.447	1.212 and -1.145

Table 2. Selected interatomic distances (Å) and bond angles (°) of compounds 1 and 2

1		2	
Bond lengths (Å)			
Ag(1)-N(8A)	2.175(2)	Ag(1)-N(12)	2.126(3)
Ag(1)-N(8)	2.176(2)	Ag(1)-N(1)	2.126(3)
Ag(1)-N(1)	2.181(2)	Ag(1)-O(1)	2.149(3)
Ag(1)-N(1A)	2.181(2)	Ag(1)-O(5)	2.272(4)
Ag(1)-O(3)	2.930(4)		
Ag(1)-O(2)	2.867(3)		
Bond angles(°)			
N(8A)-Ag(1)-N(8)	163.65(9)	N(12)-Ag(1)-N(1)	77.35(1)
N(8A)-Ag(1)-N(1)	75.58(6)	N(12)-Ag(1)-O(1)	97.42(1)
N(8)-Ag(1)-N(1)	106.44(6)	N(1).Ag(1)-O(1)	174.35(1)
N(8A)-Ag(1)-N(1A)	106.44(6)	N(12)-Ag(1)-O(5)	163.49(1)
N(8)-Ag(1)-N(1A)	75.58(9)	N(1)-Ag(1)-O(5)	96.79(1)
N(1)-Ag(1)-N(1A)	166.27(9)	O(1)-Ag(1)-O(5)	88.82(1)
N(1)-Ag(1)-O(3)	154.68(9)		

3.1.3. Electrocrystallization of Ag(II)(Bipyridine)(NO₃)₂

Introduction

Ag(Bipyridine)₂(NO₃)₂.H₂O is prepared by chemical oxidation of silver nitrate in presence of Bipyridine with strong oxidising agents(27). Here in this section we show the electrocrystallization of the title compound under definite electrochemical conditions. The composition of the electrochemical bath and the electrode potential plays a significant role in electrocrystallization of this compound. Unlike in Ag(II)(4,4' Dimethyl Bipyridine)(NO₃)₂, the structure of this compound shows significant change in the axial coordination environment. This is described in the structure description section.

Experimental

Electrocrystallization experiment was done with the acetonitrile containing AgNO₃, Bipyridine (BPy) and tetrabutylammonium hexafluorophosphate at 0.9 V vs Ag wire. Cyclic voltammetric experiments were performed with the three electrode electrochemical cell setup, with the solution. From the cyclic voltammograms the desired potential or current conditions were decided for the potentiostatic or galvanostatic electrocrystallization experiments. Here electrocrystallization was done at 0.9 V to obtain the single crystals grown on the platinum electrode surface.

Result and discussion

Electrochemical oxidation at higher oxidation potential results in Ag(II) coordinated by only one 2,2' bipyridyl ligand. The cyclic voltammograms is similar as with DMPY. The concentration of the reactants also plays key role in the product formation. Electrocrystallization at higher oxidation potential can preferentially form high quality single crystals of the title compound, which could be rather difficult by direct chemical oxidation method.

Crystal structure description

The crystal structure determination shows that molecular composition of crystal is $\text{Ag}(\text{Bipyridine})(\text{NO}_3)_2$ (figure 9). The silver ion is in a slightly distorted square planar arrangement with two *cis* coordinated nitrate anions. The anions are slightly shifted from the exact square planar configuration by 4.84° and 4.18° respectively. The bond lengths of the two *cis* coordinated oxygen of nitrate anions show considerable variations. The oxygen coordinated to silver in the nitrate anion shows a longer N-O bond length in comparison with other uncoordinated N-O bonds. In this compound, the nitrate anion is strongly coordinated to the Ag(II) metal ion, because of one coordinating Bipyridine ligand. The two *cis* coordinated nitrate anions are about 0.6 \AA shorter in comparison with axially weakly coordinated oxygen of the neighboring nitrate. This is shown in table 4 and also in figure 9. The axial contact with the oxygen of neighboring anion is in the order of $2.7 - 2.8 \text{ \AA}$. This coordination is absent in case of $\text{Ag}(\text{DMBPY})(\text{NO}_3)_2$. Thus here a chain like contact through the nitrate is observed in between the molecules, shown in figure 10. Thus here the compound exhibits a 4+2 coordination environment around Ag^{+2} cation which is rather different in $\text{Ag}(\text{DMBPY})(\text{NO}_3)_2$.

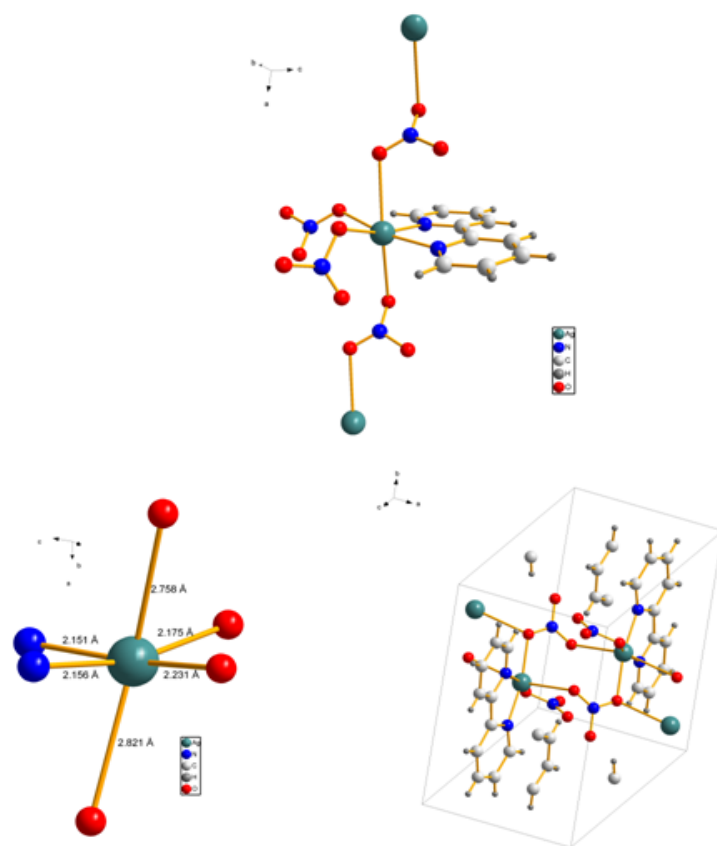


Figure 9. a) A view of $\text{Ag(II)(BPY)(NO}_3)_2$ axially coordinated with the oxygen of neighboring nitrate anion b) the view of hexa-coordinated silver(II), with bond lengths given.

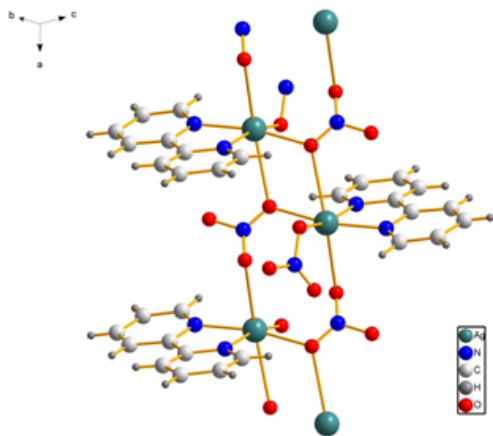


Figure 10. A chain structural view of $\text{Ag(II)(BPY)(NO}_3)_2$ axially coordinated with neighboring molecule.

Table 3. Crystal data for Ag(II)(Bipyridine)(NO₃)₂

Chemical formula	C ₁₀ H ₈ AgN ₄ O ₆
Formula weight (g/mol)	388.07
Crystal system	<i>Triclinic</i>
Space group	<i>P-1</i>
<i>a</i> (Å)	7.0000(14)
<i>b</i> (Å)	10.1450(2)
<i>c</i> (Å)	10.3830(2)
α (°)	113.440(3)
β (°)	100.220(3)
γ (°)	95.620(3)
<i>Z</i>	2
<i>V</i> (Å ³)	654.1(2)
<i>T</i> (K)	293(2)
ρ_{calc} (g/cm ³)	1.970
λ (Å)	0.71073
μ (mm ⁻¹)	1.58
F(000)	382
θ range for data collection	2.2 , 30.8
Refinement method	F ²
Index range	-9<= <i>h</i> <=9 -14<= <i>k</i> <=14 -14<= <i>l</i> <=14
$R[I > 4(\sigma(I))]$ (%)	11.7
$wR(F^2)$ (%)	30.8
<i>S</i>	0.91
No. of reflections	7195
No. of independent reflections	3981

No. of observed reflections [$I > 4(\sigma(I))$]	3981
Completeness to theta = 30.8°	97.5
$R_{\text{int}}, R_{\text{sigma}}$ (%)	14.9, 27.7
No. of parameters	191
No. of restraints	0
$\Delta\rho_{\text{min}}, \Delta\rho_{\text{max}}$ ($\text{e } \text{\AA}^{-3}$)	-1.30, 3.13
$(\Delta/\sigma)_{\text{mean}}, (\Delta/\sigma)_{\text{max}}$	<0.001, 0.04
Largest diff. peak and hole ($\text{e } \text{\AA}^{-3}$)	3.13 and -1.30

Table 4. Selective interatomic distance and bond lengths $\text{Ag(II)(BPY)(NO}_3)_2$

Bond lengths (\AA)		Bond angles ($^\circ$)	
Ag(1)-N(1)	2.156(2)	N(1)-Ag(1)-N(1A)	77.37(4)
Ag(1)-N(1A)	2.151(2)	N(1)-Ag(1)-O(1)	99.31(4)
Ag(1)-O(1)	2.175(4)	N(1A)-Ag(1)-O(2)	90.48(4)
Ag(1)-O(2)	2.231(3)	N(1)-Ag(1)-O(1)	99.31(5)
Ag(1)-O(3)	2.757(2)	O(1)-Ag(1)-O(2)	90.95(6)
Ag(1)-O(4)	2.821(1)		

3.1.4. Electrochemical synthesis and crystal structure of a penta-coordinated silver(II) macrocyclic complex

Introduction

A recent theoretical analysis of complex compounds derived from AgF_2 and various aza ligands has illustrated the spin density shift from the silver(II) centers towards the ligands [64], a phenomenon that might explain the stability of the respective complexes. To date, there aren't any experimental reports on the preparation and characterization of $\text{Ag(L)}_4\text{F}_2$ representatives and some promoting suggestions have been made on this aspect [64]. In our study we use a tetraaza macrocycle to prepare silver(II) complexes with the larger PF_6^- anion instead of F^- as the counterion. It is known from earlier studies that some porphyrin or N-confused porphyrin macrocyclic ligands can be used to stabilize higher oxidation states of silver [65, 66]. This is also reflected by the fact that the redox potential of Ag(I)/Ag(II) can be distinctly reduced to lower values in the presence of an aza based organic base. The electrochemical synthetic approach and the structural aspects of such silver(II) complexes with aza macrocycles is also the focus of our work. In this present study we use a macrocyclic chelating ligand and a sterically larger anion to stabilize silver in the +2 oxidation state. The chelating tetramethyltetraazacyclotetradecane (TMTACTD) was chosen here as a ligand because its size is suitable to accommodate the higher valent silver cations in the central cavity [67]. In contrast to the earlier structural report [67] on $\text{Ag(II)(TMTACTD)(ClO}_4)_2$, the stereo chemical aspects of the ligand and coordination geometry in our compound are different. In this paper, we describe the electrochemical synthesis and the single crystal structure analysis of compound containing silver(II) stabilized by the tetramethyltetraazacyclotetradecane macrocyclic chelating ligand and PF_6^- as counterions.

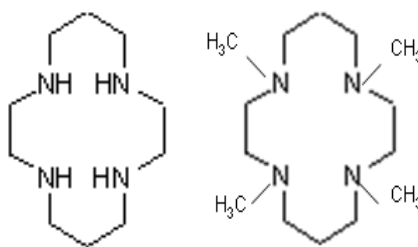


Figure 11. Molecular view of Tetraazacyclotetradecane and Tetramethyl Tetraazacyclotetradecane

Electrochemical Synthesis

Silverhexafluorophosphate (Aldrich, 99.9%), Tetramethyltetraazacyclotetradecane, (TMTACTD) (Alfa Aesar, 99.9%) and Tetrabutyl ammonium hexafluorophosphate (TBAPF₆) (Fluka 99%) were used as supplied by the manufacturers. Acetonitrile (Merck, 99.5%) was dried over CaH₂ (Alfa Aesar 95 %) and distilled before use in the electrocrystallization experiments. A three electrode electrochemical cell setup with Pt foil as working and counterelectrode and silver wire as the reference electrode were used in the electrochemical experiments. The electrochemical cell was assembled and loaded in inert and dry conditions using Schlenk line techniques. A preliminary electrochemical test was done by cyclic voltammetry. The electrolytic bath contains a solution of 0.1 M AgPF₆, 0.025 M TMTACTD and 0.1 M TBAPF₆ in dry acetonitrile. A galvanostatic electrooxidation experiment was done at 0.025 mA cm⁻². There was no product deposited on the electrode surface even after a long reaction time, hence the galvanostatic electrooxidation was continued for 10 hours. The solution turned completely brown after this prolonged electrochemical oxidation, however, no crystals had grown on the anode. Then the electrolyzed solution was slowly evaporated and large needle-shaped dark brown crystals were obtained. The crystals were separated and washed with *n*-hexane and have been found to be stable in air.

Crystal structure determination

X-ray diffraction data collection was performed at room temperature using a Bruker-AXS APEX Smart-CCD diffractometer equipped with MoK α source with the crystal mounted on the tip of a glass capillary. The cell parameters were determined using reflections within the range $1.76 < \theta < 27.11^\circ$. The crystal structure was solved by the direct method (SHELXS-97) in the orthorhombic $Pna2_1$ space group and refined by full matrix least squares (SHELXL-97) [11]. All non hydrogen atoms were refined using an anisotropic model for their displacement parameters. Hydrogen atoms were placed on their calculated positions and refined using the riding model with a U_{iso} value equal to 1.2 U_{eq} of the parent carbon atom in case of methylene groups and equal to 1.5 U_{eq} in case of methyl groups. Some bond length restraints on carbon-carbon and carbon-nitrogen bonds of the ligand were introduced as well as restraints on anisotropic displacement parameters. From the general appearance of atoms' ellipsoids, it seems that libration of the cation about the Ag–N(CH₃CN) bond is significant but full TLS analysis was not pursued because restraints were imposed on ADP parameters. Both of the PF₆[−] anions were found to be disordered over two positions. The two orientations of one PF₆[−] anion are rotated by almost exactly 45° around the F-P-F bonds approximately perpendicular to the (*b*, *c*) plane. The other PF₆[−] anion was modeled with two positions of the whole molecule. In each anion, the two positions contribute equally. Each orientation was refined with P-F bond lengths restrained to be equal but without giving a restraint value. F-P-F angles were restrained to 90° by restraining all of the F-F distances of adjacent fluorine atoms to be equal. General information and details of the structure refinement are given in Table 5. Table 6 Lists some bond distances and bond angles.

Electrochemical characterization - Cyclic voltammogram

Electrocrystallization of the title compound on the electrode surface has failed due to its high solubility of the products in acetonitrile. The proposed mechanism is the Ag⁺ ion

being oxidized at the anode surface and the resulting Ag^{2+} being stabilized in solution by the macrocyclic chelating ligand. This is clearly in accordance with the cyclic voltammograms recorded (Figure 12). Simultaneously, Ag^+ is reduced to elemental silver at the cathode. Hence, as mentioned in the experimental section, the crystals were prepared from the resulting electrolyzed solution by allowing the solvent to slowly evaporate. The crystals obtained were large, stable in air and suitable for single crystal X-ray diffraction analysis. A scanning electron micrograph of a single crystal is shown in figure 13.

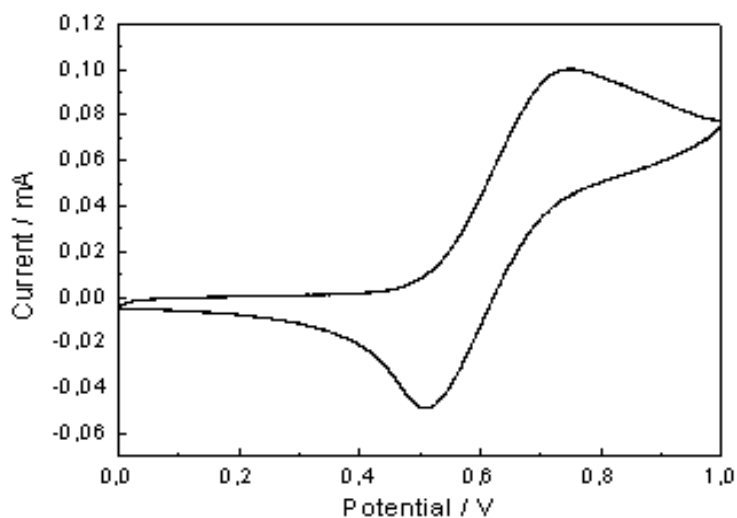


Figure 12. Cyclic voltammogram of $\text{AgPF}_6 + \text{TMTACTD} + \text{TBAPF}_6$ in acetonitrile at 20 mV/sec.

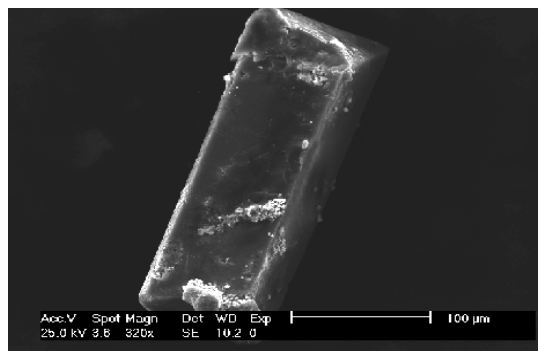


Figure 13. Scanning electron micrograph of $\text{Ag(II)(TMTACTD)(PF}_6)_2(\text{CH}_3\text{CN)}$

Structure description

The results of the structure solution revealed that the formula of the obtained compound is $\text{Ag(II)(TMTACTD)(PF}_6)_2(\text{CH}_3\text{CN)}$. A view of the complex cation is shown in Figure 14. The crystal structure obtained here exhibits the coordination of a solvent acetonitrile molecule to the silver(II) center. By contrast, the crystals grown by electrocrystallization on the electrode usually don't have the solvent coordinated. It is worth highlighting the coordination environment of silver(II) in the prepared complex. The Ag-N bond lengths are very similar and are found in the range from 2.187 Å to 2.227 Å (Table 6) and the silver(II) ion is not in a perfect rectangular planar configuration as is in the case in $\text{Ag(II)(TMTACTD)(ClO}_4)_2$ [67] but is displaced by 0.2780(3) Å from the mean plane formed by nitrogen atoms of the macrocyclic ligand. As another marked difference, there is a weak axial coordination of the acetonitrile molecule with the Ag-N bond length of 2.528 Å. The Figure 16a depicts the penta-coordinated environment of the silver(II) center. The shortest distance between silver(II) and the fluorine of the PF_6^- is as long as 3.32 Å and cannot be regarded as a donor bond. In the crystal structure both the PF_6^- ions exhibit a twofold disorder (Figure 16). The disorder of one of the PF_6^- ions can be visualized as the anion rotation around one F-P-F axis by $\sim 45^\circ$, shown in the inset of Figure 3b. The second PF_6^- anion is disordered over two positions and oriented towards the silver(II) center but tilted by 24.4° from the axis of the Ag-N5 bond. It is also interesting to note that the position of all four N-methyl groups are arranged in *cis* configuration; this is different in case of $\text{Ag(II)(TMTACTD)(ClO}_4)_2$ where each two methyl groups on one side of the AgN_4 plane give a *trans* configuration. A view of silver(II) in penta-coordinated geometry along with four N methyl groups in *cis* configuration is shown in Figure 16a,. Finally, the conformation of the macrocyclic ligand is different in comparison with the situation encountered in $\text{Ag(II)(TMTACTD)(ClO}_4)_2$. In our compound the macrocycle shows a boat conformation while in the perchlorate complex it is of chair conformation. This is a direct consequence of the presence of an acetonitrile molecule as the fifth ligand, and the larger PF_6^- anion approaching the coordination sphere additionally. Also the cavity enlargement of the ligand results in a planar coordination geometry of Ag (II) in the

Ag(II)(TMTACTD)(ClO₄)₂ [67]. In contrast, a non planar rectangular pyramidal coordination is found for the title compound with the N-Ag-N angles in the range from 82.61(2)^o to 101.6(2) °. This type of coordination geometry for Ag²⁺ is somewhat unusual. The C-H...F hydrogen bonds are formed between the macrocyclic ligand and PF₆⁻, which is oriented towards Ag cation, are the H...F distances are in the range of 2.441 – 2.592 Å except the shortest one which is 2.290 Å (Table 7). The atomic coordinates and anisotropic displacement parameters are given in table 23, 24 in appendix section

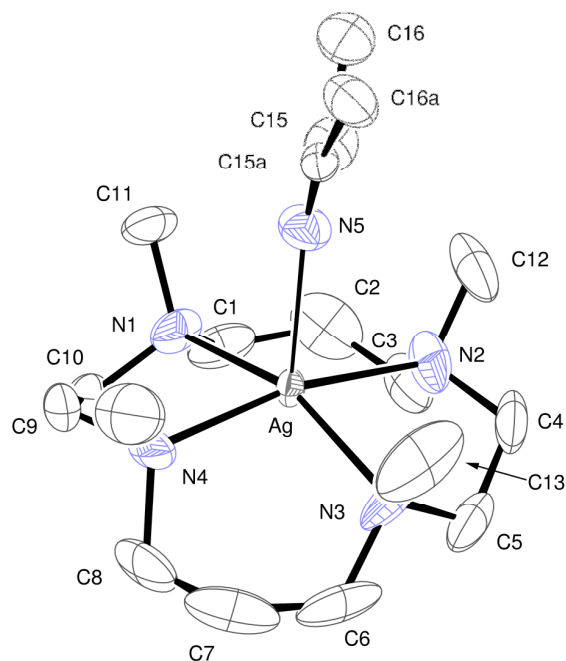


Figure 14. ORTEP representation of the cation in Ag(II)(TMTACTD)(PF₆)₂(CH₃CN). Ellipsoids are drawn at 50 % probability level and hydrogen atoms are omitted for clarity.

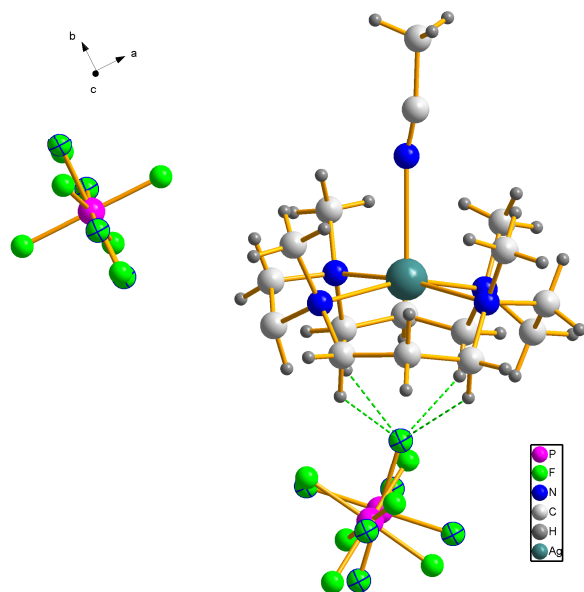


Figure 15. (a) A molecular view of $\text{Ag(II)(TMTACTD)(PF}_6)_2(\text{CH}_3\text{CN)}$ in a pentacoordinated environment, with twofold disorder of PF_6^- anion with two orientations rotated by approximately 45° relatively to each other

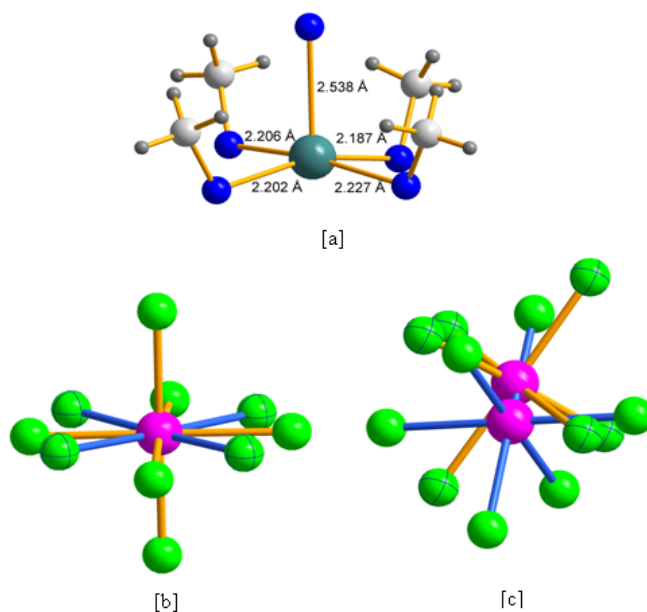


Figure 16. (a) A view of Ag^{2+} in a pentacoordinated environment. (b) Twofold disorder of PF_6^- anion with two orientations rotated by approximately 45° relatively to each other and (c) two position disorder of the whole anion. Two orientations of disordered anions are in each case designated with different bond colours.

Table 5. General and crystallographic parameters for Ag(II)(TMTACTD)(PF₆)₂(CH₃CN).

Chemical formula	[Ag(C ₁₆ H ₃₅ N ₅)](PF ₆) ₂
Formula weight (g/mol)	692.3
Crystal system	<i>Orthorhombic</i>
Space group	<i>Pna</i> 2 ₁ (33)
<i>Z</i>	4
<i>a</i> (Å)	17.5542(7)
<i>b</i> (Å)	14.7216(6)
<i>c</i> (Å)	10.1157(4)
<i>V</i> (Å ³)	2614.2(2)
<i>T</i> (K)	100
ρ_{calc} (g/cm ³)	1.76
λ (Å)	0.71073
μ (mm ⁻¹)	0.995
$R[I > 4(\sigma(I))]$ (%)	5.5
$wR(F^2)$ (%)	13.7
<i>S</i>	1.06
No. of reflections	48775
No. of independent reflections	12658
No. of observed reflections [$I > 4(\sigma(I))$]	9520
$R_{\text{int}}, R_{\text{sigma}}$ (%)	4.41, 1.55
No. of parameters	449
No. of restraints	477
<i>x</i> (Flack parameter)	0.50(5)
$\Delta\rho_{\text{min}}, \Delta\rho_{\text{max}}$ (e Å ⁻³)	-2.79, 6.59
$(\Delta/\sigma)_{\text{mean}}, (\Delta/\sigma)_{\text{max}}$	<0.001, 0.03

Table 6. Selected geometrical parameters for Ag(II)(TMTACTD)(PF₆)₂(CH₃CN).

Bond lengths (Å)	
Ag-N1	2.202(7)
Ag-N2	2.228(8)
Ag-N3	2.187(7)
Ag-N4	2.206(6)
Ag-N5	2.538(4)
Angles (°)	
N1-Ag-N3	160.0(3)
N3-Ag-N4	89.3(2)
N1-Ag-N4	83.3(2)
N2-Ag-N3	82.61(2)
N1-Ag-N2	101.6(2)
N2-Ag-N4	168.5(3)
N1-Ag-N5	99.0(3)
N2-Ag-N5	97.9(3)
N3-Ag-N5	99.7(3)
N4-Ag-N5	91.6(3)

Table 7. Hydrogen bonds of the C-H...F type between the macrocyclic ligand and one of the PF₆⁻ anions.

	$d(D\cdots A)$ (Å)	$d(H\cdots F)$ (Å)	$\angle(D-H\cdots A)$ (°)
C6-H6A...F11A ⁱ	3.343(12)	2.440	154.7
C1-H1B...F11 ⁱ	3.331(12)	2.591	133.2
C8-H8B...F11 ⁱ	3.381(13)	2.505	150.2
C8-H8B...F11A ⁱ	3.451(12)	2.554	153.8
C3-H3A...F11 ⁱ	3.371(13)	2.566	140.5
C6-H6A...F11 ⁱ	3.388(12)	2.573	141.7
C10-H10...F9 ⁱ	3.558(10)	2.594	172.9
C10-H10...F9A ⁱ	3.218(9)	2.290	159.7

ⁱ = -x+1/2, y+1/2, z-1/2

3.1.5. Electrocrystallization and Single Crystal structural Investigation of *cis*- Coordinated Tetrapyridine Silver(II) dinitrate.

Introduction

The stability of $4d^9$ silver with pyridine heterocycles in air and moisture is one of challenging factors in its earlier single crystal synthesis and structure elucidation [42, 68]. Silver in the +2 oxidation state, as stabilized with pyridine ligands are less stable to air and moisture. Hence it readily decomposes upon exposure to the atmosphere over longer periods of time. A detailed literature survey shows that the crystal structure of bivalent silver with the pyridine ligand as a *cis* coordinated anion is not yet reported. Preparation of high-quality single crystals via normal chemical synthetic routes is difficult. Experiments have to be performed under stringent, inert conditions, and the separation of products should be executed in the absence of moisture. It can, in fact, be readily observed how the crystals readily decompose by reacting with atmospheric moisture. The structural aspects of the title compound are interesting in comparison with the Cu(II) analog. The Cu(II) complexes with four pyridine show that all the ligands were coordinated in square planar configuration [69]. But here, with Ag(II), two of the pyridine ligands were axially coordinated and two nitrate anions were *cis* coordinated. Also, the specific electrocrystallization conditions necessary to prepare high quality single crystals are shown.

Experimental section

Chemicals. Silver nitrate (Alfa Aesar, 99.9%), pyridine (PY) (Alfa Aesar, 98%) and tetrabutyl ammonium hexafluorophosphate (TBAPF₆) (Fluka 99%) were used as supplied by the manufacturers. Acetonitrile (Merck, 99.5%) was dried under CaH₂ (Alfa Aesar 95%) before use in the electrocrystallization experiments. A three electrode cell setup was kept under inert conditions via Schlenk line techniques. The product formed is highly sensitive on exposure to air and moisture so great care was taken in every step of the product synthesis. Platinum foil was used as working and counter electrode while silver

wire was used as quasireference electrode. Dry acetonitrile containing pyridine (0.001 mmol), Silver nitrate (0.005 M), and TBAPF₆ (0.05 M) was subjected to electrochemical cyclic voltammetric investigation for the preliminary information. The potential for the potentiostatic electrocrystallization was decided from the cyclic voltammograms. Unlike most Ag(II) coordination compounds these crystals are highly unstable on prolonged exposure to air and moisture. The crystals obtained are of good quality and suitable for single crystal X-ray measurements. Hence the separation of crystals and all other processes were performed under dry conditions using Schlenk line techniques and in a glove box. The single crystals were separated and mounted on a glass capillary. The crystal was carefully mounted on the tip of a 0.1 mm diameter glass capillary and sealed inside another capillary of 0.3 mm diameter. Then the crystal was subjected to single crystal X-ray structural characterization with a Bruker-AXS- APEX Smart-CCD diffractometer. The data collection was performed at room temperature and the cell parameters were determined from the reflections collected in the range $2.45 < \theta < 28.2^\circ$.

Details of the structure determination are given in Tables 8 & 9 (crystal data, selected geometric parameters, while the atomic coordinates, anisotropic displacement parameters are given in appendix section Table 25,26).

Results and Discussion

The electrochemical oxidation of the silver salt in the presence of pyridine affords deep red crystals, which grow on the electrode surface. It is observed that these crystals are unstable when exposed to air for prolonged periods, transforming to a white powder. This confirms the reactivity of the Ag(II) center within this complex. The cyclic voltammetric investigations prove that the electrooxidation readily converts Ag⁺¹ to Ag⁺² in the presence of pyridine. In the case of bipyridine no second phase formation at higher potentials was observed. The cyclic voltammograms only show a steady increase in current as the potential is increased. On the other hand, when dimethyl bipyridine was used, there were two distinct electrochemical processes observed in the cyclic voltammograms. The electrooxidation experiments performed at higher positive potential gave a thick deposit, where the reaction rate is higher. The powder X-ray analysis shows

that the product is the same phase as the title compound. Hence the electrocrystallization was done in a galvanostatic mode to obtain larger and better quality single crystals. The requirement for good quality single crystals and the high sensitivity of the crystals to air and moisture may have impeded structural determination in earlier studies. The single crystal structure elucidation proves the molecular composition as $\text{Ag(II)(Pyridine)}_4(\text{NO}_3)_2$, as shown in figure 17. The crystal structure with the pyridine heterocycle is significantly different to the Cu(II) analog. The positions of the ligands and anions ought to be taken note of. The two nitrate anions in the hexacoordinated silver with the pyridine ligand are in *cis* configuration. This observation of *cis* coordinated nitrate anions is unusual in a hexa-coordinated silver(II) compound. The Ag(II) is almost in a planar arrangement while the angles and bond distances between the coordinating atoms imply that it is not in a perfect square planar configuration. In this compound the angles between the coordinating atoms are highly different (see Table 9). It is interesting to note that the two axially-coordinated, *trans* pyridine ligands are in a mutually staggered conformation with a bond angle of 179.6° , whereas the two *cis* pyridine ligands are coplanar. Hence the highly distorted octahedral coordination of Ag(II) in this compound, which is shown by the polyhedron in figure 17c. The axially-coordinated pyridine shows a slightly shorter Ag-N bond length compared to the planar ones. By contrast, for copper complexes featuring pyridine ligands and SCN^- anions or aminopyridine ligands and nitrate anions, the *trans* pyridine ligands are observed to be coplanar. Finally, the magnetic susceptibility measurements show the silver to be a paramagnetic center, with d^9 configuration.

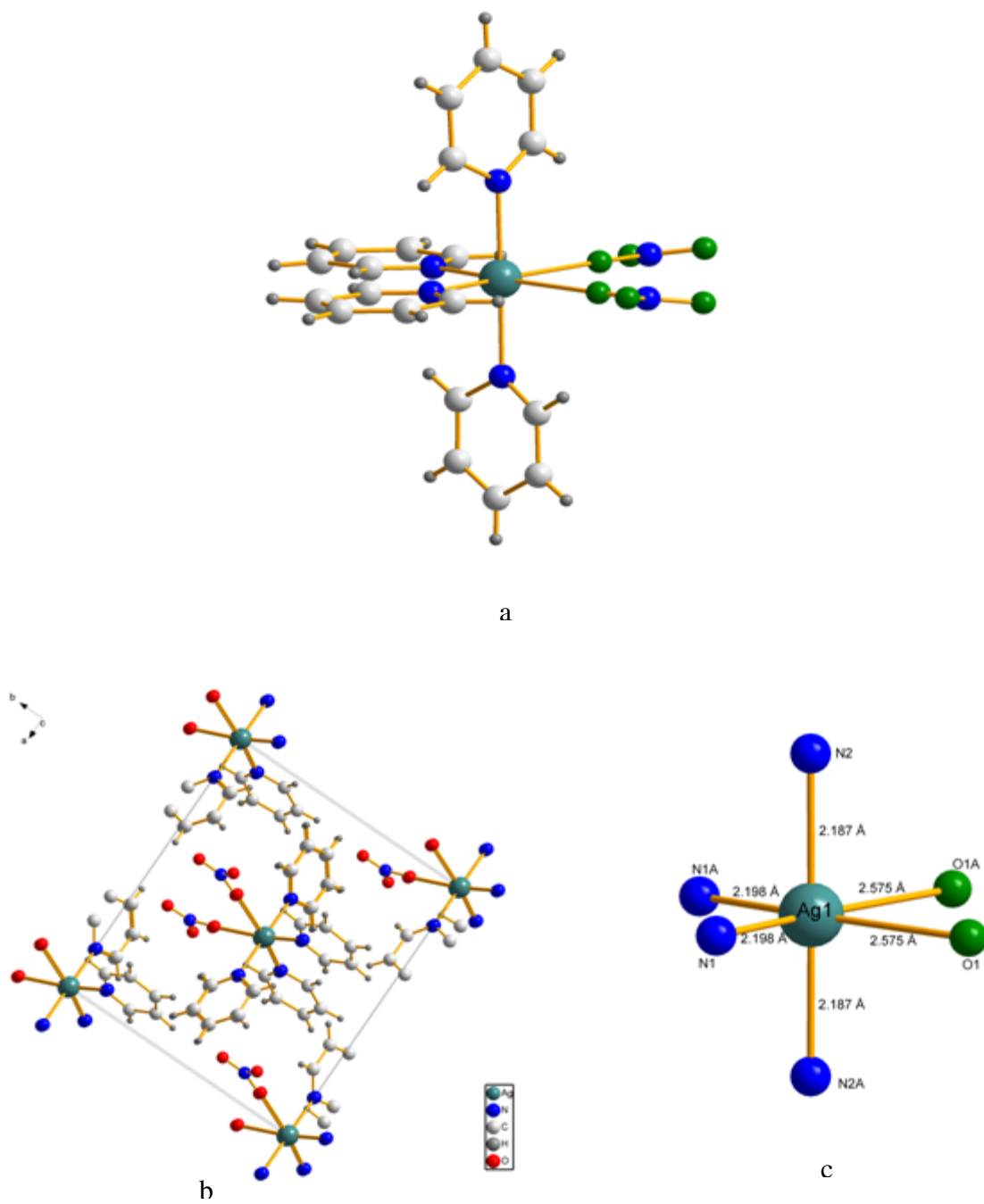


Figure 17. (a) A molecular view of Ag(II)(Pyridine)₄(NO₃)₂, b. unit cell view and c. *cis* coordinated Ag(II)

Table 8. Crystal data and structure refinement of $\text{Ag}^{\text{II}}(\text{pyridine})_4(\text{NO}_3)_2$

Empirical formula	C ₂₀ H ₂₀ Ag N ₆ O ₆
Crystal system	Monoclinic
Formula weight	548.29
Temperature	273(2) K
Wavelength	71.073 pm
Space group	C2
Unit cell dimensions	a = 14.587(17) Å b = 11.017(13) Å c = 7.972(9) Å $\beta = 119.45^\circ$
Volume	1115.6(2) Å ³
Z	2
Density (calculated)	1.632 Mg/m ³
Absorption coefficient	0.953 mm ⁻¹
F(000)	554
Theta range for data collection	2.45 to 28.22°
Index ranges	-18 ≤ h ≤ 19, -14 ≤ k ≤ 14, -10 ≤ l ≤ 10
Reflections collected	4776
Independent reflections	2447 [R(int) = 0.0241]
Completeness to theta = 28.22°	93.7 %
Refinement method	Full-matrix least-squares on F ²
Data / restraints / parameters	2447 / 1 / 151
Goodness-of-fit on F ²	1.033
Final R indices [I > 2σ(I)]	R1 = 0.0476, wR2 = 0.1203
R indices (all data)	R1 = 0.0477, wR2 = 0.1212
Flack parameter	0.50(4)
Largest diff. peak and holes	1.186 and -0.420 e.Å ⁻³

Table 9. Selected interatomic distances (Å) and bond angles (°) for the Ag(II)(Pyridine)₄(NO₃)₂

Bond lengths (Å)		Bond angles(°)	
Ag(1)-N(1)	2.186(4)	N(8A)-Ag(1)-N(8)	163.65(9)
Ag(1)-N(1A)	2.186(4)	N(8A)-Ag(1)-N(1)	75.58(6)
Ag(1)-N(2)	2.197(1)	N(8)-Ag(1)-N(1)	106.44(6)
Ag(1)-N(2A)	2.197(1)	N(8A)-Ag(1)-N(1A)	106.44(6)
Ag(1)-O(3)	2.576(1)	N(8)-Ag(1)-N(1A)	75.58(9)
Ag(1)-O(2)	2.576(1)	O(1)-Ag(1)-O(1A)	80.29(4)

3.1.6. Single crystal structures and magnetic studies of electrocrystallized silver(II) compounds containing weakly coordinated perchlorate anions.

Introduction

The electrocrystallization method gives access to the single crystals of chemical phases which are difficult to prepare by usual synthetic routes. Higher oxidation state silver compounds are of great interest due to their potential applications. In Section 3.1.1 the potential-dependent phase formation of bivalent silver complexes was shown. The electrochemical synthetic conditions, esp applied potential and current densities, clearly affect the crystal growth. The kinetically-controlled electrocrystallization reactions usually produce good-quality crystals with high purity and yield. However, the use of weakly coordinating and bulky anions results in disorder in the structure, and it is hard to prepare single crystals of these compounds, especially in case of Ag(II) compounds. Hence, to the best of knowledge there are no single crystal structure reports of bivalent silver stabilized with bipyridine and weakly-coordinating anions such as perchlorate. The difficulties in preparing single crystals by the chemical method would have limited attempts at structural elucidation. However, here an electrocrystallization method for preparing a high yield of good-quality single crystals of $\text{Ag}^{\text{II}}(\text{BPy})_2(\text{ClO}_4)_2$ followed by structural elucidation and magnetic characterization, is presented. The selective electrocrystallization conditions for obtaining single crystals of the title compound are described.

Experimental section

Silver perchlorate (Aldrich, 99.9%), Bipyridine (BPY) (Alfa Aesar, 99.9%) and tetrabutyl ammonium hexafluorophosphate (TBAPF₆) (Fluka 99%) were used as supplied by the manufacturers. Acetonitrile (Merck, 99.5%) was dried over CaH₂ (Alfa Aesar 95 %) and distilled before use in the electrocrystallization experiments. A three electrode

electrochemical cell setup with Pt foil as working and counter electrode, and silver wire as the reference electrode, were used in the electrochemical experiments. The electrochemical cell was assembled and loaded under inert conditions via Schlenk line techniques. A preliminary electrochemical test was performed by cyclic voltammetry. The electrolytic bath contains a solution of 0.1 M AgClO_4 , 0.025 M BPY and 0.1 M TBAPF₆ in dry acetonitrile. A galvanostatic electrooxidation experiment was carried out at 0.025 mA cm⁻². The dark red crystals grew on the anode surface. The crystals were separated and washed with dry acetonitrile and were found to be air-stable. Magnetic measurements were performed at 5kOe using a Quantum Design MPMS XL SQUID magnetometer. Gelatin capsules were used as sample containers for the measurements taken in the temperature range 1.9 – 300 K. The substance shows paramagnetic behaviour.

Results and Discussion

Cyclic voltammograms

Electrocrystallization techniques give access to chemical phases of high purity in a selective manner. The electrochemical reaction conditions influence the product formation, especially here the starting materials used for electrolysis. The electrocrystallization was conducted from acetonitrile containing silver perchlorate, bipyridine and tetrabutyl ammonium perchlorate as supporting electrolytes. Only the use of silver perchlorate and the perchlorate-containing support-electrolyte afforded the title compound. The cyclic voltammogram of the above solution shows two redox processes. Unlike with the nitrate anion, the potentiostatic conditions do not yield two different phases. The potentiostatic crystallization gave poor quality crystals which were not suitable for single crystal structural studies. In the galvanostatic method good quality crystals of high yield were prepared by 25 $\mu\text{A cm}^{-2}$ applied current density. Thus only electrocrystallization under galvanostatic conditions gave single crystals of the above compound. This was difficult to do by chemical synthesis routes, even under potentiostatic conditions. Also, no potential-dependent phase formation was observed.

Furthermore, it ought to be mentioned that Galvanostatic electrocrystallization experiments executed with silver salts containing PF_6^- , SbF_6^- , BF_4^- or AsF_6^- show no product formation on the electrode surface.

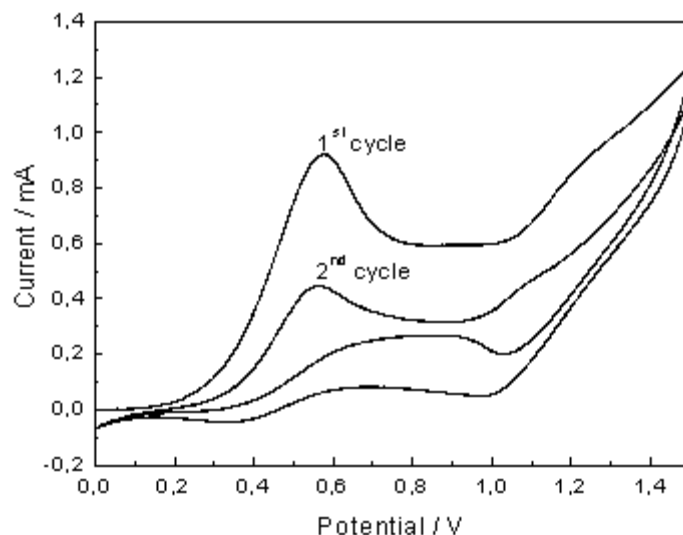


Figure 18. Cyclic voltammograms of $\text{AgClO}_4 + \text{Bipyridine} + \text{TBAClO}_4$ in acetonitrile at 20 mV/sec.

Crystal structure determination.

Single crystal X-ray structural characterization was conducted with a Bruker-AXS-APEX Smart-CCD diffractometer. Cell parameters were determined from the reflections collected in the range $2.06 < \theta < 28.4^\circ$. The crystal structure was solved by direct methods using the program SHELXS-97. The structure refinement calculations were done with SHELXL-97. Crystal data and further experimental details are summarized in Table 10 together with the parameters of the structure refinement. The single crystal structure solution shows that the obtained compound is $\text{Ag(II)(BPy)}_2(\text{ClO}_4)_2$. The structure of this compound is described here for the first time. The silver metal center in this complex is weakly coordinated with perchlorate anion. This is inferred from the observed bond lengths of Ag-O (about 3.22 Å). The metal center is coordinated by two

bipyridine ligands in a manner that deviates from the ideal square planar coordination as a result of a torsion angle of 20.45°.

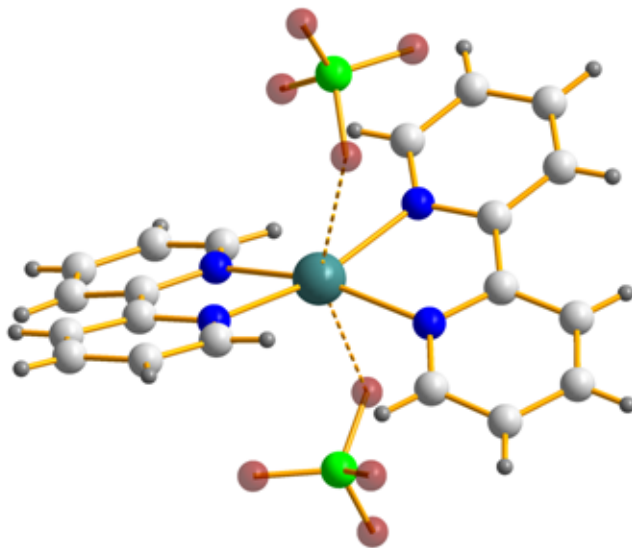


Figure 19. Molecular view of Ag(II)(Bipyridine)₂(ClO₄)₂

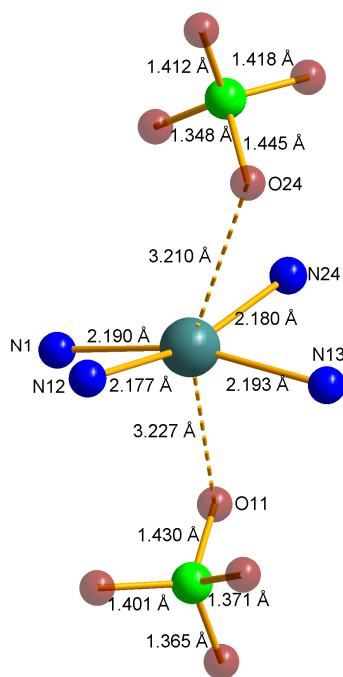


Figure 20. Ag(II) ion in 4+2 coordination. The weak coordination denoted by broken line.

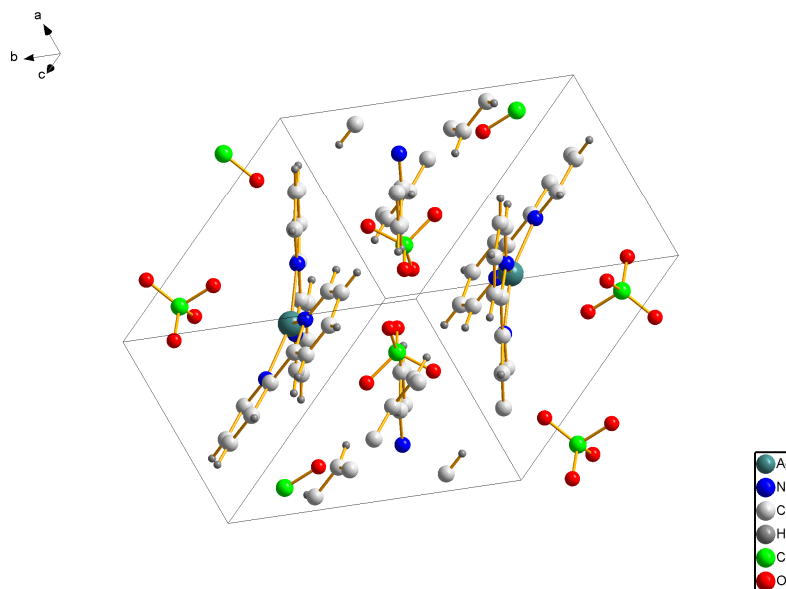


Figure 21. A view of unit cell of $\text{Ag(II)(Bipyridine)}_2(\text{ClO}_4)_2$

Table 10. Crystal data and structure refinement for $\text{Ag}^{\text{II}}(\text{BPy})_2(\text{ClO}_4)_2$

Empirical formula	C ₂₀ H ₁₆ Ag Cl ₂ N ₄ O ₈
Formula weight	619.14
Temperature	293(2) K
Wavelength	71.073 pm
Crystal system	Triclinic
Space group	P-1
Unit cell dimensions	a = 794.91(16) pm b = 1023.6(2) pm c = 1463.9(3) pm
Volume	1.1409(4) nm ³
Z	2
Density (calculated)	1.802 Mg/m ³
Absorption coefficient	1.174 mm ⁻¹

3. Special section: Higher oxidation state of silver

F(000)	618
Theta range for data collection	2.06 to 28.24°.
Index ranges	-10<=h<=10, -13<=k<=13, 0<=l<=19
Reflections collected	5553
Independent reflections	5553 [R(int) = 0.0000]
Completeness to theta = 28.24°	98.5 %
Refinement method	Full-matrix least-squares on F ²
Data / restraints / parameters	5553 / 48 / 317
Goodness-of-fit on F ²	0.621
Final R indices [I>2sigma(I)]	R1 = 0.0505, wR2 = 0.1248
R indices (all data)	R1 = 0.0984, wR2 = 0.1376
Extinction coefficient	0.0131(12)
Largest diff. peak and hole	1.299 and -1.097 e.Å ⁻³

3.1.7. Electrocrystallization of $\text{Ag}(\text{DMBPY})_2(\text{ClO}_4)_2$

Experimental

Silver perchlorate (Aldrich, 99.9%), 4,4'-dimethyl 2,2'-Bipyridine, (DMBPY) (Alfa Aesar, 99.9%) and tetrabutyl ammonium hexafluorophosphate (TBAPF₆) (Fluka 99%) were used as supplied by the manufacturers. Acetonitrile (Merck, 99.5%) was dried over CaH₂ (Alfa Aesar 95 %) and distilled before use in the electrocrystallization experiments. A three electrode electrochemical cell setup with Pt foil as working and counter electrode, and silver wire as the reference electrode, were used in the electrochemical experiments. The electrochemical cell was assembled and loaded under inert conditions using Schlenk line techniques. A preliminary electrochemical test was conducted by cyclic voltammetry. The electrolytic bath contained a solution of 0.1 M AgClO₄, 0.025 M DMBPY and 0.1 M TBAPF₆ in dry acetonitrile. A galvanostatic electrooxidation experiment was carried out at 0.025 mA cm⁻². The dark red product was grown on the anode surface. The crystals were separated and washed with dry acetonitrile and were found to be air-stable.

Result and discussion

The cyclic voltammograms show two distinct redox processes (see Figure 22). Hence it was decided to carry out the potential-dependent electrocrystallization experiments in a similar manner to the nitrate system described in Section 3.1.1. In contrast, no potential-dependent phase formation was observed with the perchlorate anion. Galvanostatic electrocrystallization with silver perchlorate and 4,4' dimethyl bipyridine produced small, poor-quality single crystals. Hence the power X-ray diffraction pattern was measured for the sample (Figure 23) and was indexed with the program Topas. The results indicate a monoclinic unit cell with $a = 23.5063 \text{ \AA}$, $b = 5.8629 \text{ \AA}$, $c = 21.3368 \text{ \AA}$, $\beta = 93.092^\circ$, within space group P21/m (Rwp = 4.9%). Electrocrystallization experiments attempted

with the anions PF_6^- , SbF_6^- and BF_4^- did not result in the growth of crystals on the electrode surface.

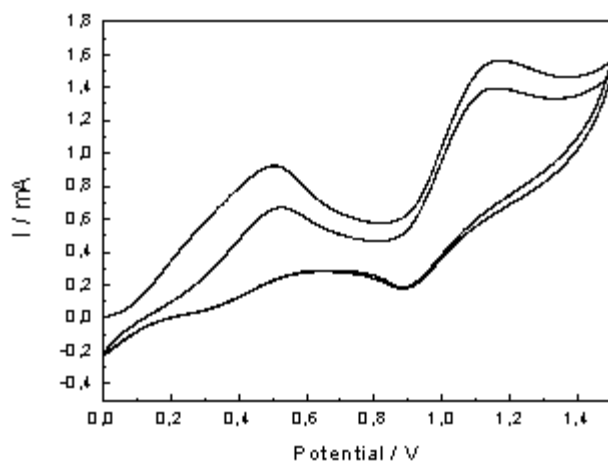


Figure 22. Cyclic voltammograms of acetonitrile containing AgClO_4 + 4,4' dimethyl 2,2' Bipyridine + TBAPF_6

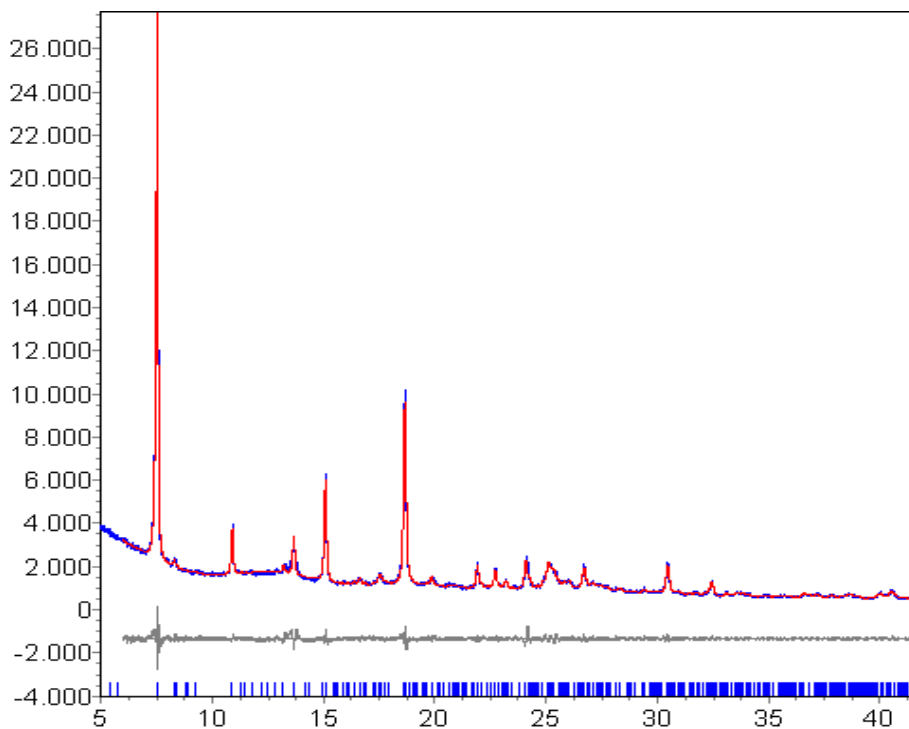


Figure 23. X-Ray powder pattern $\text{Ag}^{\text{II}}(4,4'$ dimethyl 2,2' Bipyridine) $_2(\text{ClO}_4)_2$ showing Le Bail fit for

3.2. Electrochemical Synthesis, Crystal Structure and Optical Properties of Phthalocyanine compounds

Introduction

Metal(II) phthalocyanines are planar complexes based on the structure shown in Figure 25. They are of great technological as well as fundamental interest, due to their properties and as a result of their similarity to other classes of compounds [70]. In Figure 24, the histogram shows the development of research and new findings with phthalocyanine-based compounds since the discovery of the compound itself. The steady increase in the number of hits shows an upsurge in the interest in phthalocyanine compounds. The phthalocyanines are extensively used as pigments and dyes, and they are models for biologically-important species such as porphyrins, hemoglobin, and chlorophyll. They can serve as the active elements in chemical sensors, especially for the detection of NO₂ [71, 72]. They are of great interest for use in optoelectronic devices [73] and solar cells [74]. Their catalytic properties have also been studied for some time, most recently as redox catalysts in fuel cell applications [75-77]. They are semiconducting, and can be used to form well-behaved field effect transistors. [78, 79]

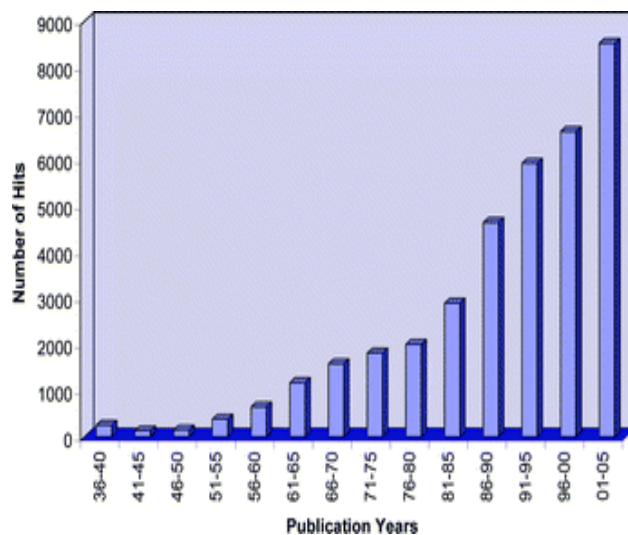


Figure 24. Histogram of research articles on phthalocyanine compounds for every 5 years

The chemical properties of the ligand and its remarkable physico-chemical stability have extended its application in many vital areas [70]. This inner-complexing ligand can stabilize metal atoms in the +2 oxidation state. The higher oxidation state can also be stabilized with the axial coordination of counter anions. Mostly, the optical properties of metal-phthalocyanines have attracted much attention due to their intense absorptions in the UV-Visible-NIR range, and their non-linear optical behaviour [80]. The electron- or hole-doped metal-phthalocyanines show specific optoelectronic properties, electrical properties (as ‘molecular metals’) [81] and magnetic properties (as “magnetic switches”) properties [82]. These properties are influenced by the packing of the molecules in the solid state and in particular by effective intermolecular stacking [82, 83]. One factor that crucially limits the processing of most metal phthalocyanines is their poor solubility in common solvents. Hence, in order to improve on this aspect, significant efforts have been made in modifying the periphery of the ring. Axial substitution of phthalocyanines generally increases their solubility and, therefore, reduces molecular aggregation [84, 85]. The axial substitution can improve the efficiency of non-linear optical materials [86, 87]. However, the low solubility of unsubstituted metal phthalocyanines has continued to be, and still is, the major limiting factor. For the solution phase, electrochemical characterization [88] and further processing this is a problem.

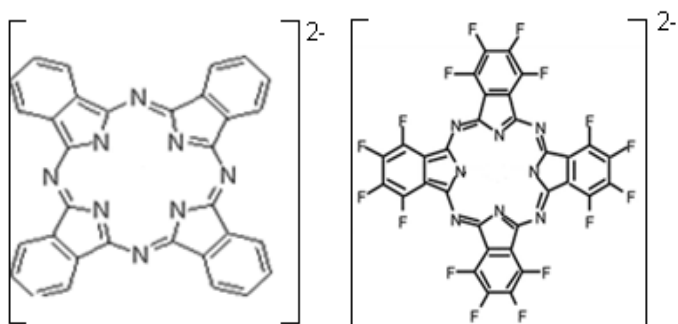


Figure 25. View of phthalocyanine and hexadecafluorinated phthalocyanine ligand.

3.2.1. Electrochemical synthesis of Lithium Phthalocyanine-Tetrabutylammonium Hexafluorophosphate and Lithium Phthalocyanine radical.

Introduction

Among the metal phthalocyanines, dilithium phthalocyanine is exceptional as it shows a remarkable solubility in most organic solvents. Hence it is often used as a starting material for the synthesis of many other metal-phthalocyanines. The solution phase electrochemistry of some metal phthalocyanines and peripherally modified forms has been investigated [88]. Electrocrystallization experiments carried out by electrooxidation of dilithium phthalocyanine (Li_2Pc) gave the monolithium phthalocyanine radical (LiPc^\cdot) [89]. This represents the only known air stable monovalent phthalocyanine radical [89]. There are still debates ongoing on the synthesis of monopotassium phthalocyanine and on its structure [90] and the higher alkali metal phthalocyanines are even less investigated because of their low solubility in organic solvents. Lithium phthalocyanine radical synthesized by electrocrystallization method has shown a potential [91] and solvent [92, 93] dependent phase formation. Electron paramagnetic measurements (EPR), oxygen sensitivity studies, magnetic and electric properties of these phases were investigated in detail [94 – 101]. The α , β , χ modifications of LiPc^\cdot differ in the mode of stacking [92], and there is some correlation between the crystal structure and the physical properties. Theoretical calculations and electrochemical characteristics of the LiPc^\cdot radical reveal that it is less stable than $[\text{LiPc}]^-$ by 66.17 kcal/mol [101]. Electrocrystallization experiments carried out by oxidation of Li_2Pc in acetonitrile and acetone gave long needle like crystals of LiPc^\cdot , while an adherent deposit of lithium phthalocyanine on the electrode as a thick film from dimethyl sulphoxide solvent and its characterization was reported earlier [102]. Synthesis and characterizations of different structural phases of LiPc^\cdot and its halogen adducts were reported [103, 104]. All modifications of LiPc^\cdot radical reported so far

contain the phthalocyanine stacked to form columns, implying strong intermolecular interactions. We were interested in studying isolated LiPc units embedded in a crystalline matrix. In order to realize such a situation we have been aiming at co-deposition of LiPc with a second salt by electrosynthesis. For this purpose we have tested various combinations of solvents and salts consisting of varied (complex) anions and cations. With tetrabutyl ammonium hexafluorophosphate and with Li_2Pc in dimethoxyethane a co-crystal of LiPc and tetrabutyl ammonium hexafluorophosphate was obtained. In this study we have shown the influence of solvent and the applied potential on product formation. These parameters are important, especially in the field of electro-organic synthesis [105]. In some cases conventional chemical methods of synthesis of metal phthalocyanine are difficult to perform, while the electrochemical route can be a simple way to obtain the desired product with high purity. Here in this paper we describe the electrochemical synthesis, structure and optical properties of mono-lithium phthalocyanine-tetrabutyl ammonium hexafluorophosphate.

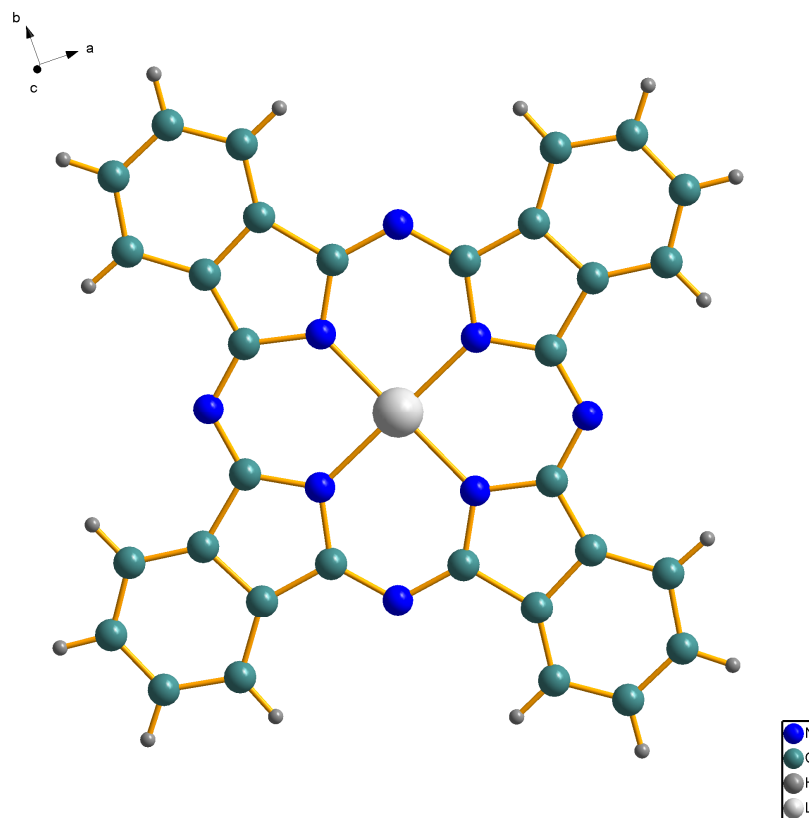


Figure 26. (a) Molecular view of Lithium phthalocyanine radical

Experimental Section

Dilithium phthalocyanine (Li_2Pc) (Aldrich), Tetrabutyl ammonium hexafluorophosphate (TBAPF_6) (Fluka 99%), Dimethoxyethane (DME) (Fluka 98%) chemicals were used in the electrochemical synthesis. All the electrochemical synthesis was performed in a one-compartment, three-electrode cell with a Pt foil working; counter electrode and silver wire as the reference electrode. The electrochemical cell was assembled under inert and dry conditions using *schlenk* line techniques. The electrolytic bath contains a mixture of 0.001 M Li_2Pc , 0.01M TBAPF_6 in 20 ml DME. The preliminary electrochemical test was done by cyclic voltammetric experiments. From the cyclic voltammograms the electrooxidation potential for the potentiostatic oxidation experiments was chosen. Large crystals had grown at the bottom of the electrochemical cell after a prolonged potentiostatic oxidation, about 12 hours. These crystals are insoluble in DME and hence they are separated and washed with dry n-hexane. LiPc^- is soluble in dimethoxyethane in contrast to acetonitrile. Hence no large needle like crystal growth was observed in DME as in acetonitrile. The electrooxidation potential also plays an important role in the product formation; the details are discussed in the results section. The crystals are stable in air. They were separated, washed, dried and individual ones selected under an optical microscope for single crystal measurement. The best crystal was subjected to single crystal x-ray structural characterization with a Bruker-AXS- APEX Smart-CCD diffractometer. The data collection was performed at room temperature and the cell parameters were determined from the reflections collected in the range $1.4 < \theta < 27.0^\circ$. The structure was solved by the direct method (SHELXS-97) and refinement done by the full matrix least square method (SHELXL-97). Details of the structure determination are given in tables 1-2 (Crystal data, selected geometric parameters). Metal phthalocyanines are well known to form aggregates in the organic solvents due to their limited solubility. Hence the solid state spectrum of the compound and LiPc^- was collected in the range of 400-1100 nm using Perkin Elmer instruments.

Result and Discussion

Cyclic voltammograms

According to cyclic voltammograms of dilithium phthalocyanine in acetonitrile and dimethoxyethane the electrochemical redox processes are reversible (figure 1). While in dimethoxyethane the current associated with the oxidation process is low and there is a positive shift in the oxidation potential. The voltammograms also infer the reaction rate is low in dimethoxyethane. Electrocrystallization carried out in acetonitrile results in long needle-like crystals grown at the anode, which correspond to the tetragonal phase (χ form) of lithium phthalocyanine radical. While in dimethoxymethane the electrooxidation performed at 0.1 V vs Ag wire gave no deposit on the electrode surface. The applied potential and the solubility of the electrooxidised product in the given solvent determine the deposition on electrode surface, growth of crystal and also the phase formation [43, 105]. The mechanism involved in the product formation electrochemical oxidation followed by chemical co-crystallization in the solution. The relative solubility of LiPc[•] in DME plays an important role in formation of the resultant co-crystal with TBAPF₆. These crystals were grown at the bottom of the electrochemical cell in the DME. These crystals are insoluble in DME, hence it can be separated. Also the rate of oxidation is lower in DME solvent; hence they support the chemical interaction with TBAPF₆ in the solution, following the electrochemical reaction. The electrooxidation potential is also an important parameter in preparation of this compound. The electrochemical oxidation of dilithium phthalocyanine results in lithium phthalocyanine radical, but due to its solubility in dimethoxymethane solvent it results in lithium phthalocyanine tetrabutylammonium hexafluorophosphate crystal. LiPc[•] is almost insoluble in acetonitrile, hence the title compound was not formed in this solvent.

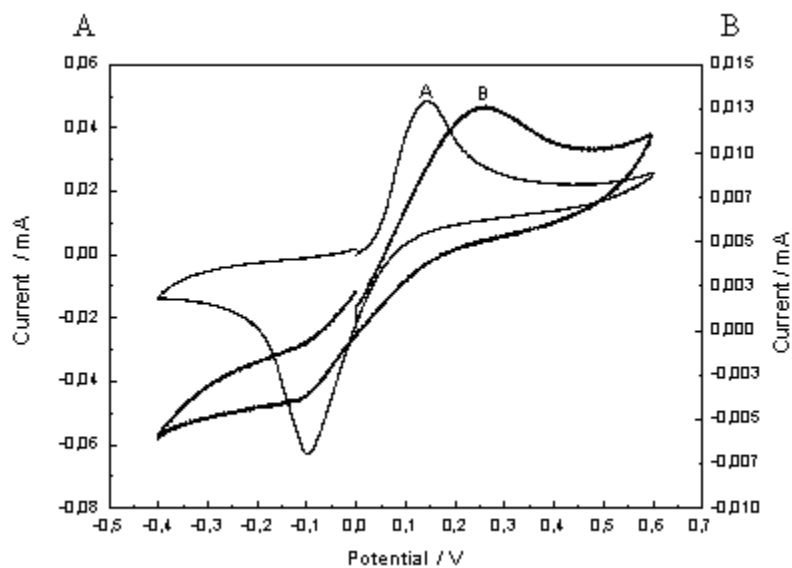


Figure 27. Cyclic Voltammograms of $\text{Li}_2\text{Pc} + \text{TBAPF}_6$ in dry acetonitrile (A) and in dimethoxyethane (B) at 20 mV sec^{-1} .

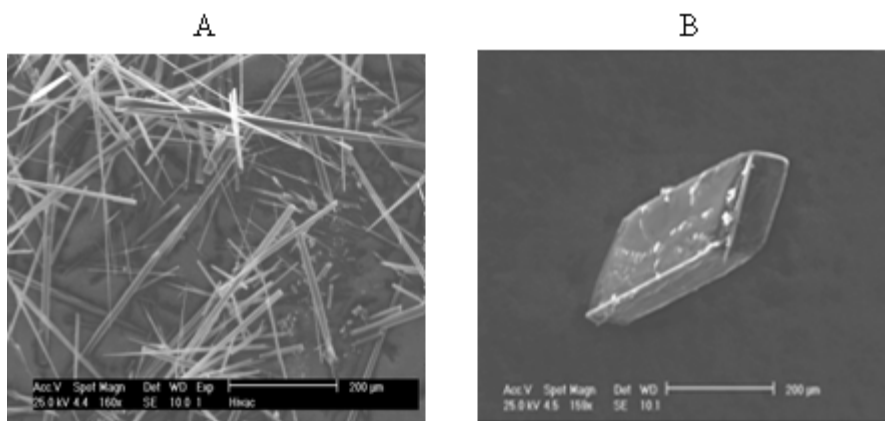


Figure 28. Scanning electron micrographs of (A) Lithium phthalocyanine radical, (B) Lithium phthalocyanine Tetrabutyl ammonium hexafluorophosphate

Structure description

The crystal structures of metal-phthalocyanines highly determine their physical properties. The crystal structure analysis has shown that the title compound crystallizes in the triclinic system and confirmed the molecular composition of monolithium phthalocyanine tetrabutylammonium hexafluorophosphate (LiPc-TBAPF₆) (figure 2). The intermolecular π - π interactions between the phthalocyanine rings as found in other crystal structures of metal-Phthalocyanine is here modified by the presence of the tetrabutylammonium cation. The nearest lying phthalocyanine units are separated by the interlaying tetrabutylammonium cation. The distance between them is therefore much higher in comparison to the tetragonal phase of LiPc. In particular in comparison to the χ form of the LiPc radical where the intermolecular distances are even less than the sum of corresponding van der Waals distances. In LiPc radical the close packing results in the semiconducting behaviour, higher oxygen sensitivity and EPR sensitivity of tetragonal phase. In our compound the phthalocyanine ligand deviates from the planar (D_{4h}) structure due to the steric effect induced by tetrabutylammonium hexafluorophosphate. A comparative view of LiPc⁻ units in this compound and the radical compound are given in figure 3. Here we can see that the phthalocyanine ring composed of four isoindole units, deviates from the planar geometry. The two opposite lying isoindole units of the phthalocyanine macrocycle are tilted and appear in a chair conformation, while the other two are in plane. The non-planar conformation of the phthalocyanine ring could be altered depending on the size of the alkyl group. The Li-N bond length in this compound is similar as in the tetragonal phase of LiPc. The hexafluorophosphate anions located at the corner of the triclinic unit cell are shown in figure 2b. Usually the hexafluorophosphate has high propensity to disorder as in TBAPF₆ at room temperature. However, in this compound the PF₆⁻ anion is ordered. Also, the tetrabutyl ammonium cation is ordered and shows the four butyl groups are in an eclipsed conformation. The bond lengths of P-F are in the range of 1.56 Å to 1.58 Å, which are highly precise and in agreement with the ordered PF₆⁻ anion. The PF₆⁻ anions form a hydrogen-bonded network structure with the peripheral hydrogen atoms of the phthalocyanine rings. The charge associated with reduction of lithium phthalocyanine is much higher in the

electrochemical experiments. Lithium phthalocyanine-Tetrabutylammonium hexafluorophosphate is immediately soluble in acetonitrile and over the period time the LiPc powder collected at the bottom to give a colourless solution.

Table 11. Crystal data for LiPc.TBAPF₆

Chemical formula	Li ₁ C ₄₈ N ₉ H ₅₂ P ₁ F ₆
Formula weight (g/mol)	906.90
Crystal system	<i>Triclinic</i>
Space group	<i>P-1</i>
<i>a</i> (Å)	8.6423(4)
<i>b</i> (Å)	12.8196(6)
<i>c</i> (Å)	15.0189(7)
α (°)	83.0080(10)
β (°)	87.8730(10)
γ (°)	74.4480(10)
<i>Z</i>	2
<i>V</i> (Å ³)	1591.10 (13)
<i>T</i> (K)	293
ρ_{calc} (g/cm ³)	1.62
λ (Å)	0.71073
μ (mm ⁻¹)	0.058
$R[I > 4(\sigma(I))]$ (%)	5.5
$wR(F^2)$ (%)	13.7
<i>S</i>	1.06
No. of reflections	48775
No. of independent reflections	12658
No. of observed reflections [$I > 4(\sigma(I))$]	9520

$R_{\text{int}}, R_{\text{sigma}}$ (%)	4.41, 1.55
No. of parameters	449
No. of restraints	477
$\Delta\rho_{\text{min}}, \Delta\rho_{\text{max}}$ ($e \text{ \AA}^{-3}$)	-2..87, 7.38
$(\Delta/\sigma)_{\text{mean}}, (\Delta/\sigma)_{\text{max}}$	<0.001, 0.04

Table 12. Selected bond angles and bond distances for LiPc.TBAPF₆

	Bond distance (\AA)
Li-N	1.965
Li-N	1.959
Li-N	1.965
Li-N	1.959
Li-H	2.836
	Angles ($^{\circ}$)
N2-Li-N3	89.859
N2-Li-N3	90.141
N2-Li-N3	89.859
N2-Li-N3	90.141

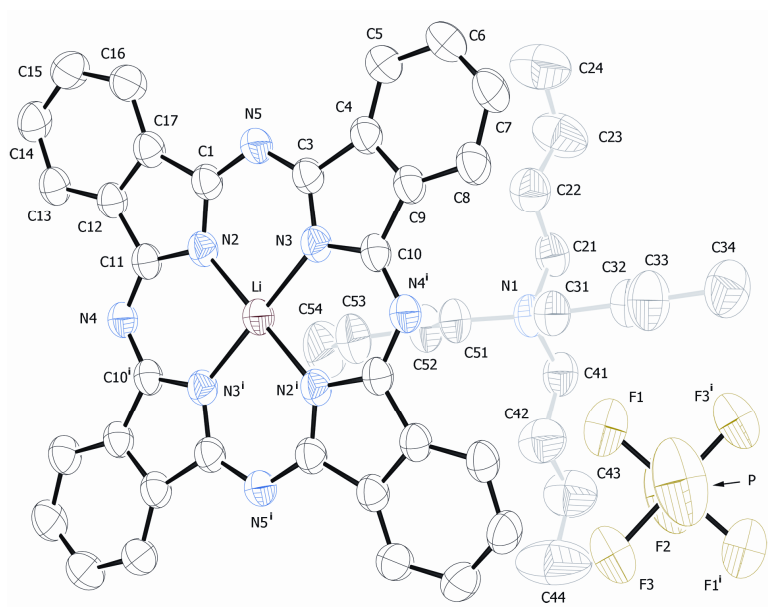


Figure 29. ORTEP representation of the cation in LiPc.TBAPF_6 . Ellipsoids are drawn at 50 % probability level and hydrogen atoms are omitted for clarity.

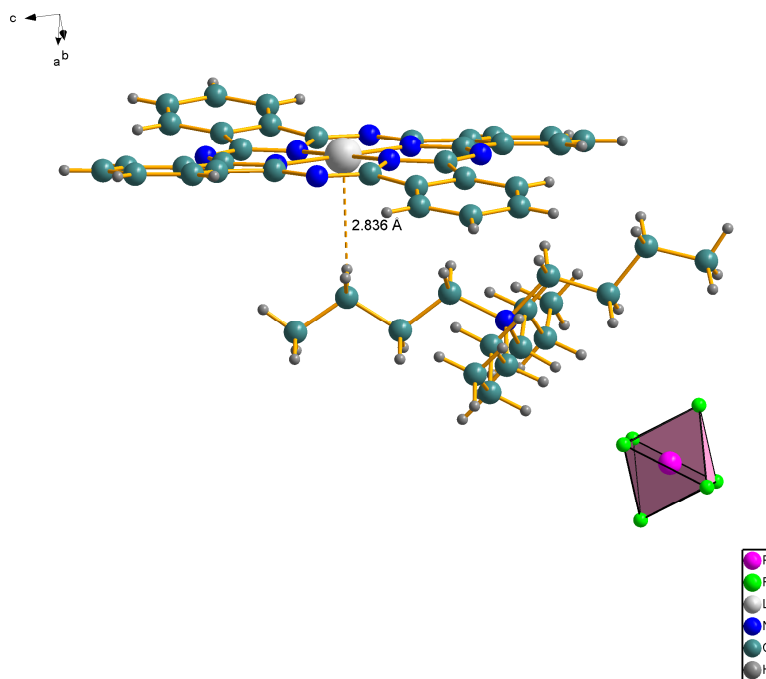


Figure 30. A view of molecular structure of lithium phthalocyanine. Tetrabutylammonium hexafluorophosphate co-crystal.

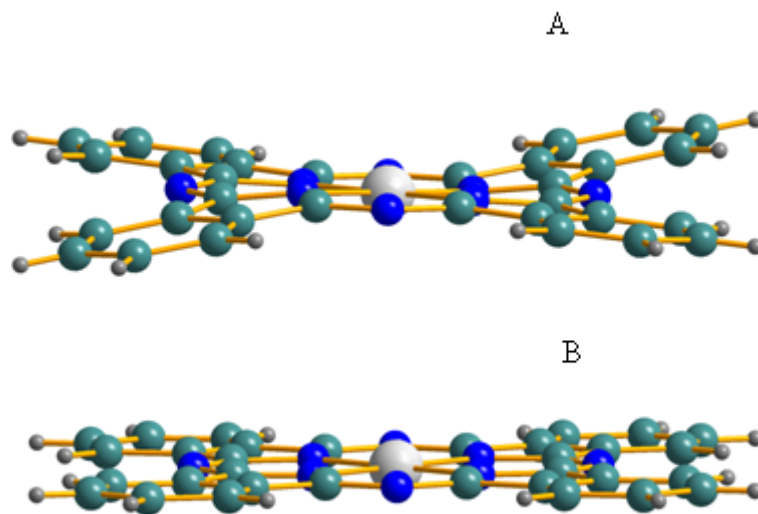


Figure 31. A comparative view of LiPc unit in this compound (A) and in the tetragonal phase of LiPc radical (B).

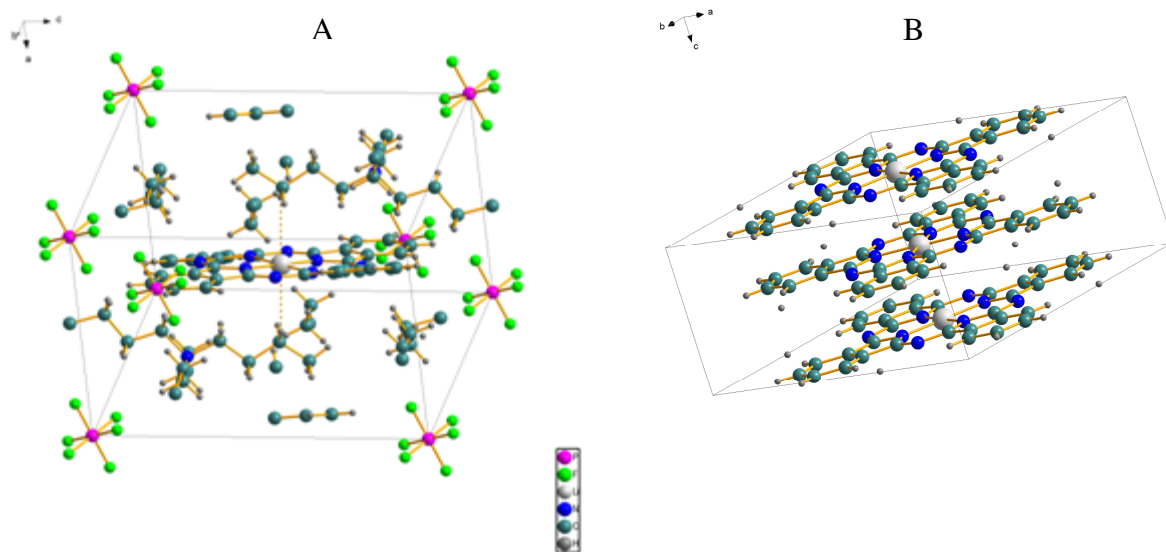


Figure 32. Unit cell structure of (A) Lithium phthalocyanine Tetrabutyl ammonium hexafluorophosphate, (B) Lithium phthalocyanine radical,

Spectroscopic characterization

The studies of the optical characteristics of phthalocyanine compounds are very informative. Their highly conjugated aromatic π - electron system can give rise to large nonlinear optical response, and can be readily modified by physical or chemical methods. The molecular packing and stacking nature of the phthalocyanine ring affects the π - π interactions. The absorption spectra of the α and β polymorphs of LiPc radical are different from the χ form. Due to limitations in the solubility of LiPc and desired solvent for the title compound the solid state spectra was taken using KBr pellets. Unlike planar LiPc, the nonplanar features of the phthalocyanine ring in this compound can also influence the optical properties. A comparative solid state spectrum of LiPc \cdot and LiPc.TBAPF₆ is shown in figure 5. There is a shift in the absorption maxima towards shorter wavelength. Usually bathochromic shifts are known to occur into the near infrared region with electron-donating groups and hypsochromic shift with electron-withdrawing groups. In the case of the LiPc radical, there a shift in absorption bands toward lower energies. While both Q and solet (B) bands are shifted towards the shorter wavelength in LiPc.TBAPF₆, in case of LiPc they are shifted towards the longer wavelength. The split and the broad absorption bands can also infer the deviation of the molecular symmetry from D_{4h} symmetry, while for the LiPc radical only a single well-defined Q band is observed. The effect on the spectral properties is also attributed to a larger extent of separation of phthalocyanine units in the crystal structure. The intensities at 900-1000 nm, near IR regions are not very much pronounced but are identifiable in the case of LiPc and LiPc.TBAPF₆. But the solution spectrum of LiPc in chloronaphthalene clearly show an absorption band centered at 975 nm. The near IR absorption property of metal phthalocyanine has been shown to be useful for optical disks and laser printers. Hence, electrochemical synthesis proved to be a facile method to prepare the title compound. The influence of the presence of tetrabutylammonium hexafluorophosphate on the stereochemistry of the phthalocyanine skeleton has been examined. The optical spectrum shows an absorption shift towards the shorter wavelength. The crystals exhibits pleochroism, ie., when the crystals were viewed under the optical microscope, shows

different colours. This depends on the optical absorption of the crystal in that particular direction.

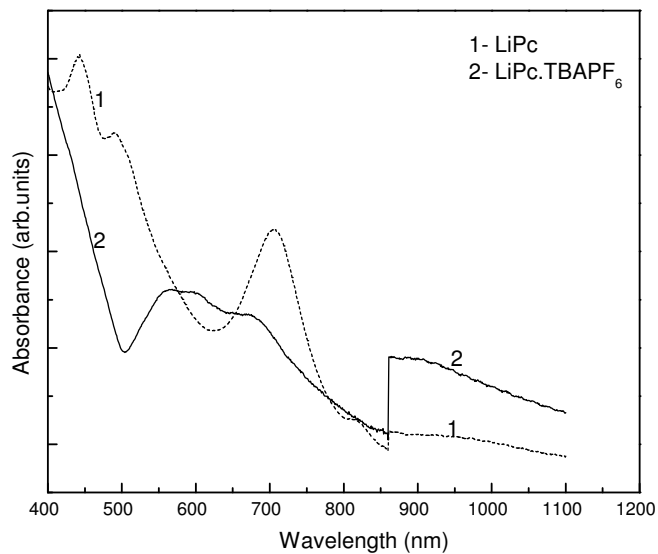


Figure 33. Solid state spectra of LiPc radical (2) and the compound (2) in the KBr pellets

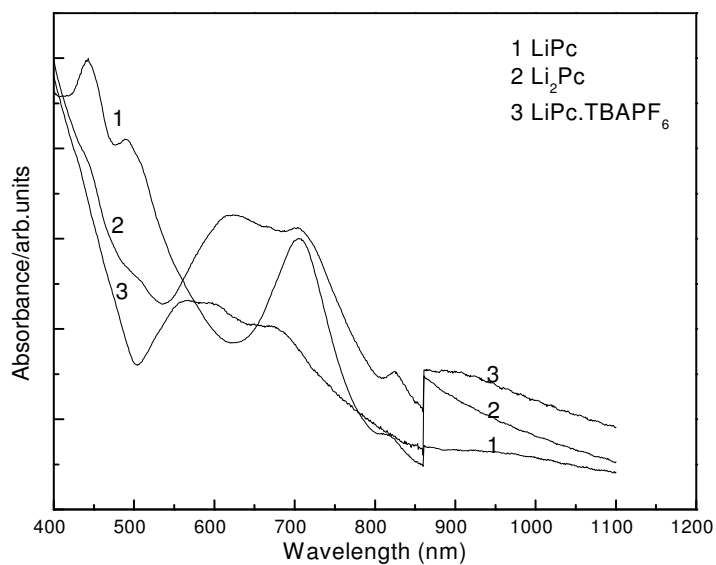


Figure 34. UV-Vis-NIR Spectra of LiPc (1), Li₂Pc (2), LiPc.TBAPF₆ (3)

3.2.2. Disodium phthalocyanine

Introduction

Dilithium phthalocyanine is very well known and well characterized among the alkali metal phthalocyanine. It is very well established as a precursor material for synthesis of other metal phthalocyanine. This is due to its high solubility it is used very much in electrochemical synthesis. When we move down in the periodic system the solubility of alkali metal phthalocyanine is very limited. Hence there are not detailed investigations on other alkali metal phthalocyanine was found in the literature.

Experimental

Disodium phthalocyanine was synthesized using fresh sodium metal, phthalonitrile in octanol solvent. Similar to dilithium phthalocyanine synthesis of disodium phthalocyanine done as reported earlier. Reaction of metallic sodium with octanol produces sodium octanolate. Phthalonitrile has to be added simultaneously with addition of sodium metal. This creates a strong reducing condition for cyclization phthalonitrile to form phthalocyanine ring. The product formed is extracted with tetrahydrofuran and acetone. The product is recrystallized with dimethoxyethane. The product purity was checked by X-ray powder with Na₂Pc received from TCI Europe.

Result and discussion.

The product obtained was subjected to X-ray powder diffraction measurement. After several trials the powder shows best solubility in dimethoxyethane. Since the recrystallization in dimethoxyethane does not yield any larger crystal single crystals. The powder pattern was indexed (Monoclinic P 2₁/m, a = 15.3104, b = 6.0752, c = 9.74626, β = 122.901) and le Bail fit was done using DASH program.

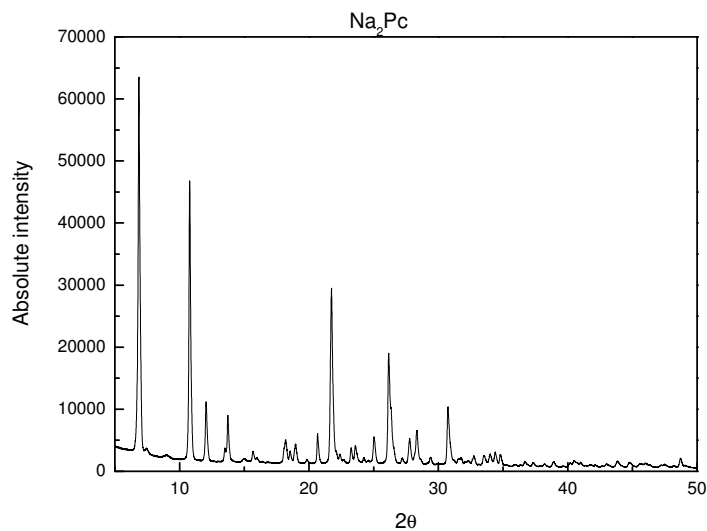


Figure 35. 1 X-Ray powder pattern disodium phthalocyanine

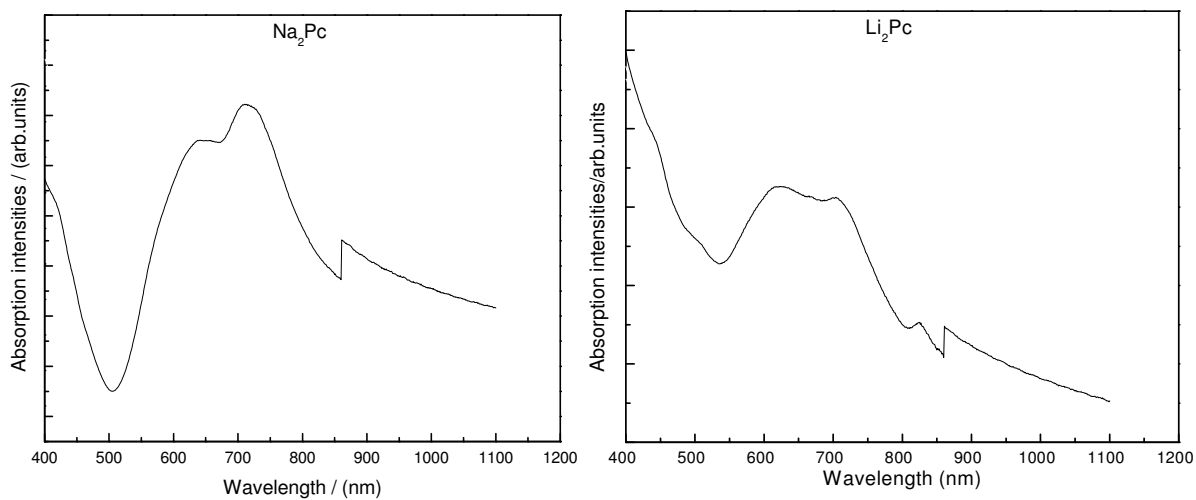


Figure 36. UV-Vis-NIR spectra of disodium phthalocyanine and dilithium phthalocyanine.

The powder was mixed with KBr and made into a pellet, and the UV-Vis-NIR spectrum measured. A comparative spectrum of Na_2Pc and Li_2Pc is shown in Figure 36. Both compounds show a split in the Q band. There is a shift towards longer wavelength in the case of Na_2Pc .

3.2.3. Electrocrystallization of monosodium phthalocyanine

Introduction

Among the metal phthalocyanines, dilithium phthalocyanine shows excellent solubility. Hence it is the precursor material for the synthesis of many other metal phthalocyanines. Upon descending the group, it is seen that the phthalocyanines of the heavier alkali metals exhibit a very low solubility. The limited solubility of many metal phthalocyanines is the main hindrance to their wide-spread processing. Hence various attempts have been made to functionalize the periphery of the phthalocyanine ring. The lithium phthalocyanine radical is the only monovalent phthalocyanine compound reported in the literature, and electrocrystallization was used to prepare single crystals of it. There is a dispute regarding the monopotassium phthalocyanine, which was recently reported [106, 107]. As reported, monopotassium phthalocyanine was prepared from copper phthalocyanine, however the product was a mixture of phases. Hence LiPc is the only well-characterized monovalent phthalocyanine. Electrochemical synthesis of the monolithium phthalocyanine radical compound shows solvent-dependent phase formation. Also, the tetragonal phase can be transformed to a monoclinic phase on exposure to acetone vapour. The ESR behaviour of this compound depends on the crystal structure. The structural features of these phthalocyanine compounds are attractive due to the one dimensional $\pi - \pi$ interaction. Due to the ionic size of sodium in this compound, the structure and properties may well be different to those of monolithium phthalocyanine. The lithium phthalocyanine radical shows D_{4h} symmetry in the tetragonal modification. The effective intermolecular packing and reduction of the distance plays an important role in its electrical and magnetic properties. In the following, the preparation of monosodium phthalocyanine by an electrochemical route is shown for the first time.

Experimental

Disodium phthalocyanine (Na_2Pc) (TCI Europe), dilithium phthalocyanine (Li_2Pc) (Sigma Aldrich), potassium hexafluorophosphate (Fluka) and dry acetone were employed. A three-electrode electrochemical cell setup with platinum foil as working and counter electrodes, along with silver wire as the quasi-reference, was used in all experiments. The electrochemical cell was assembled and operated under inert conditions using Schlenk line techniques. The cyclic voltammograms were measured with the VMP potentiostat. The potential for the electrooxidation was determined from the cyclic voltammograms. The potentiostatic electrochemical oxidation at 0.2 V vs. silver wire gave a thick deposit on the working electrode. With Li_2Pc thin needle-like crystals were grown, while with Na_2Pc flake-like deposits were formed. The product was washed with acetone and used for powder XRD, magnetic and electrical measurements.

Results and Discussion

Na_2Pc shows higher solubility in dimethoxyethane and acetone. Unlike Li_2Pc it shows very low solubility in nitrile solvents. The electrochemical characterization was performed in dry acetone and also in dimethoxyethane. The cyclic voltammograms show a similar behaviour as for dilithium phthalocyanine. The first electrooxidation peak corresponds to oxidation of disodium phthalocyanine to monosodium phthalocyanine. This behaviour is very similar to dilithium phthalocyanine; also the product was deposited on the electrode surface. The reversible behaviour of the first peak for Li_2Pc is clearly observed in the cyclic voltammograms, whilst it is almost irreversible in the case of Na_2Pc . This shows that the LiPc^\cdot radical can easily undergo reduction. This is also supported by theoretical calculations, which indicate that LiPc^\cdot is more stable than the LiPc^\cdot radical by 65 kcal/mol. However, at higher potential cycling both compounds show a different behaviour. In the case of Na_2Pc there is a peak at 0.8 V vs. Pt wire that is highly reversible, and the charge under the peak increases with cycle number. This is not observed with Li_2Pc electrooxidation. This is shown in the figure indicating the different

number of cyclic voltammograms. The electrochemical oxidation at 0.2 V gave a thick black deposit of NaPc on the electrode surface.

Thus electrooxidation of Na₂Pc at 0.4 V gave monosodium phthalocyanine. After several trials Na₂Pc showed higher solubility in dimethoxyethane / acetone. This allowed the electrocrystallization of monosodium phthalocyanine on the electrode surface to be carried out. Unfortunately, even after several trials, larger crystals could not be grown on the electrode surface. However, it represents the second monovalent phthalocyanine produced so far (after the lithium phthalocyanine radical). In the literature, there is a controversy regarding the synthesis, purity and structure of monopotassium phthalocyanine [106, 107]. The powder of the obtained crystals was subjected structure solution. The structure solution was performed using the GSAS- EXPGUI program. The crystal structure solution indicates tetragonal P4/mcc, with $a = 13.8201(12)$ Å, $c = 6.5348(5)$ Å and $V = 1248.26(14)$ Å³. A molecular representation of NaPc is shown in Figure 40a. It can be seen that the sodium cation lies above the plane of phthalocyanine ring. Furthermore, it forms a weak contact with the nitrogen atoms of the neighbouring phthalocyanine ring with respective bond lengths of 2.838 Å. The Na – N bond lengths are 0.293 Å longer than the Li–N bonds in the LiPc radical (Li-N = 1.931 Å, Na-N = 2.234 Å). Moreover, whereas the LiPc radical exhibits D_{4h} symmetry, it can be seen that NaPc deviates from D_{4h} symmetry. A comparative powder X-ray diffraction pattern of LiPc and NaPc is shown in Figure 39b. Although both patterns appear to be rather similar, there are shifts in the reflection positions as well as some new reflections for NaPc. The presence of the Na⁺ cation above the plane of phthalocyanine ring increases the *c*-axis length in comparison with the lithium phthalocyanine radical. Ion exchange could be very feasible in comparison with LiPc. Also, another solution found indicates the crystal structure to be orthorhombic, with $a = 13.8334(1)$ Å, $b = 13.8215(3)$ Å, $c = 6.48879(5)$ Å and $V = 1231.45(1)$ Å³. There is only a slight deviation in the *b*-axis, while the *c*-axis deviates largely.

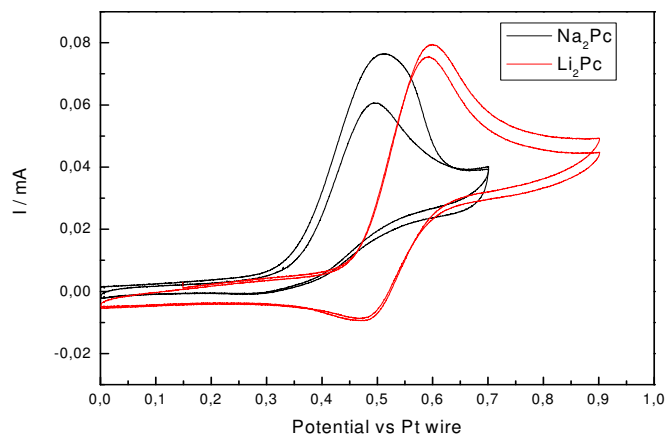


Figure 37. Cyclic voltammograms of Na_2Pc and Li_2Pc in dimethoxyethane containing 0.01 M tetrabutyl ammonium hexafluorophosphate.

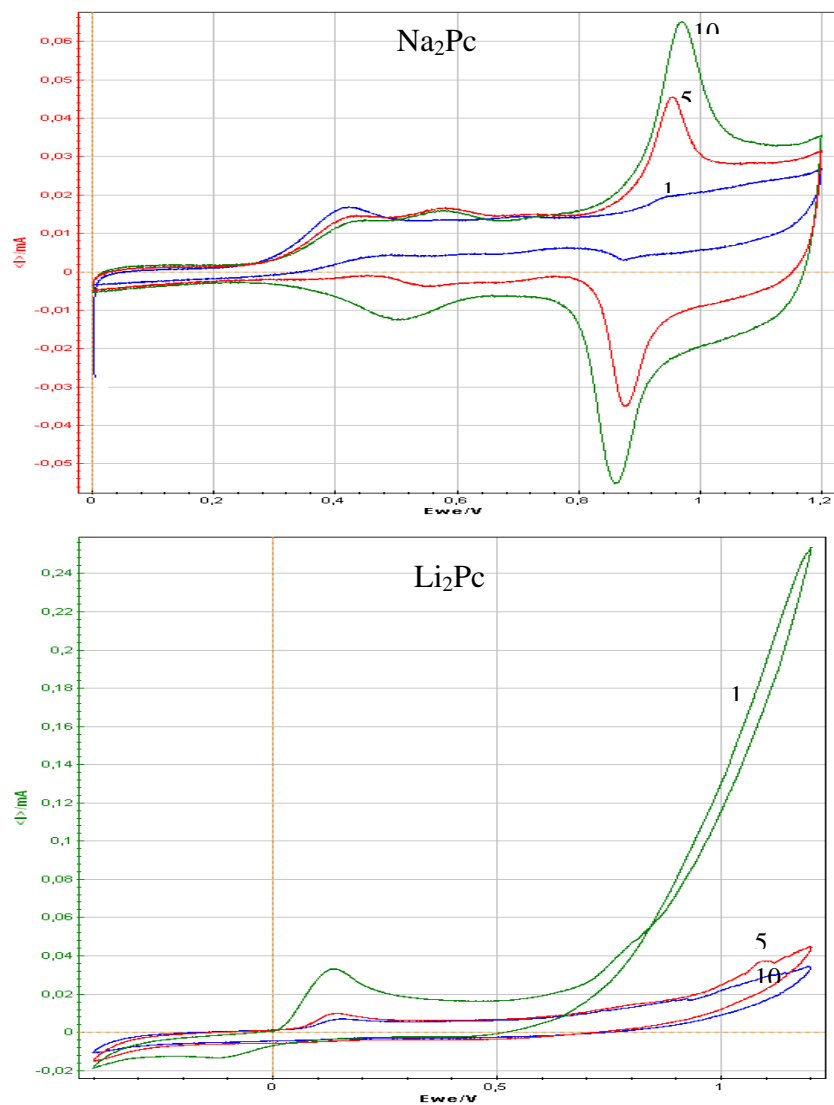


Figure 38. Cyclic voltammograms of Na_2Pc and Li_2Pc in dimethoxyethane containing TBAPF_6

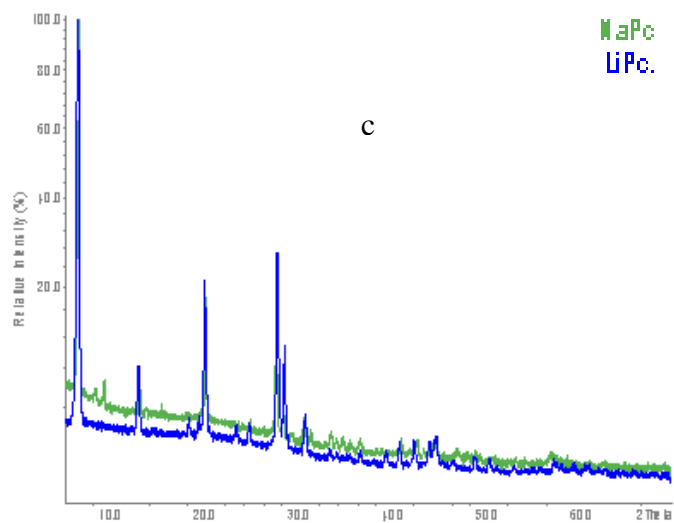
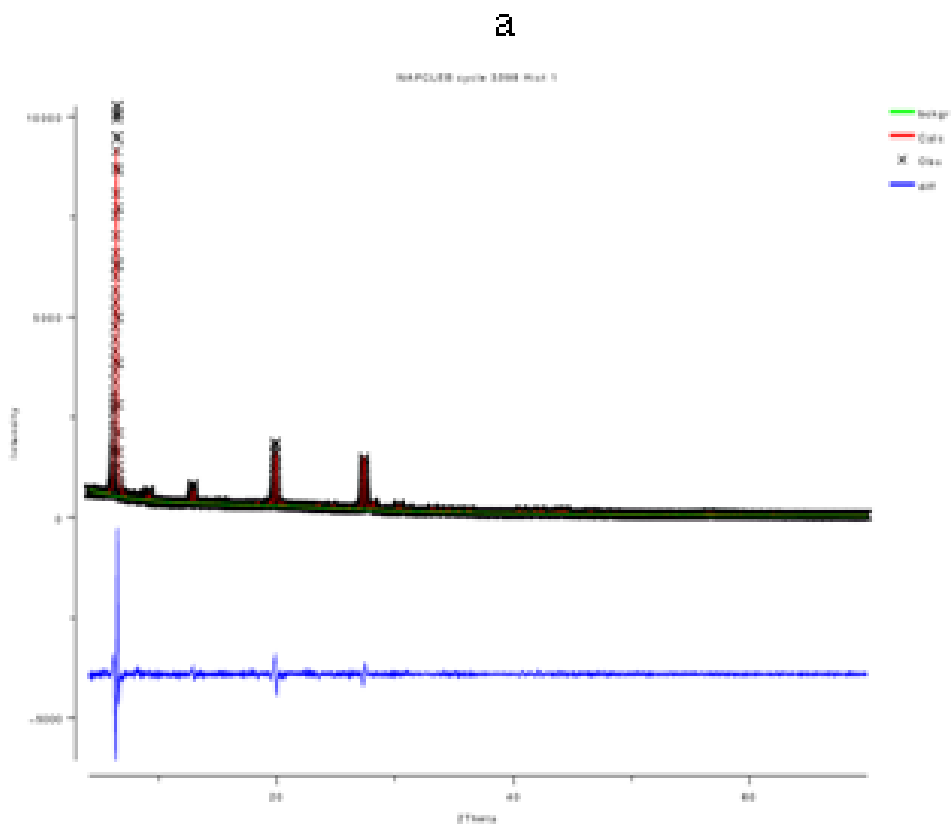


Figure 39a, powder X-ray diffraction pattern of NaPc showing Rietveld refinement profile. b. powder X-ray diffraction patterns of monolithium and monosodium phthalocyanines

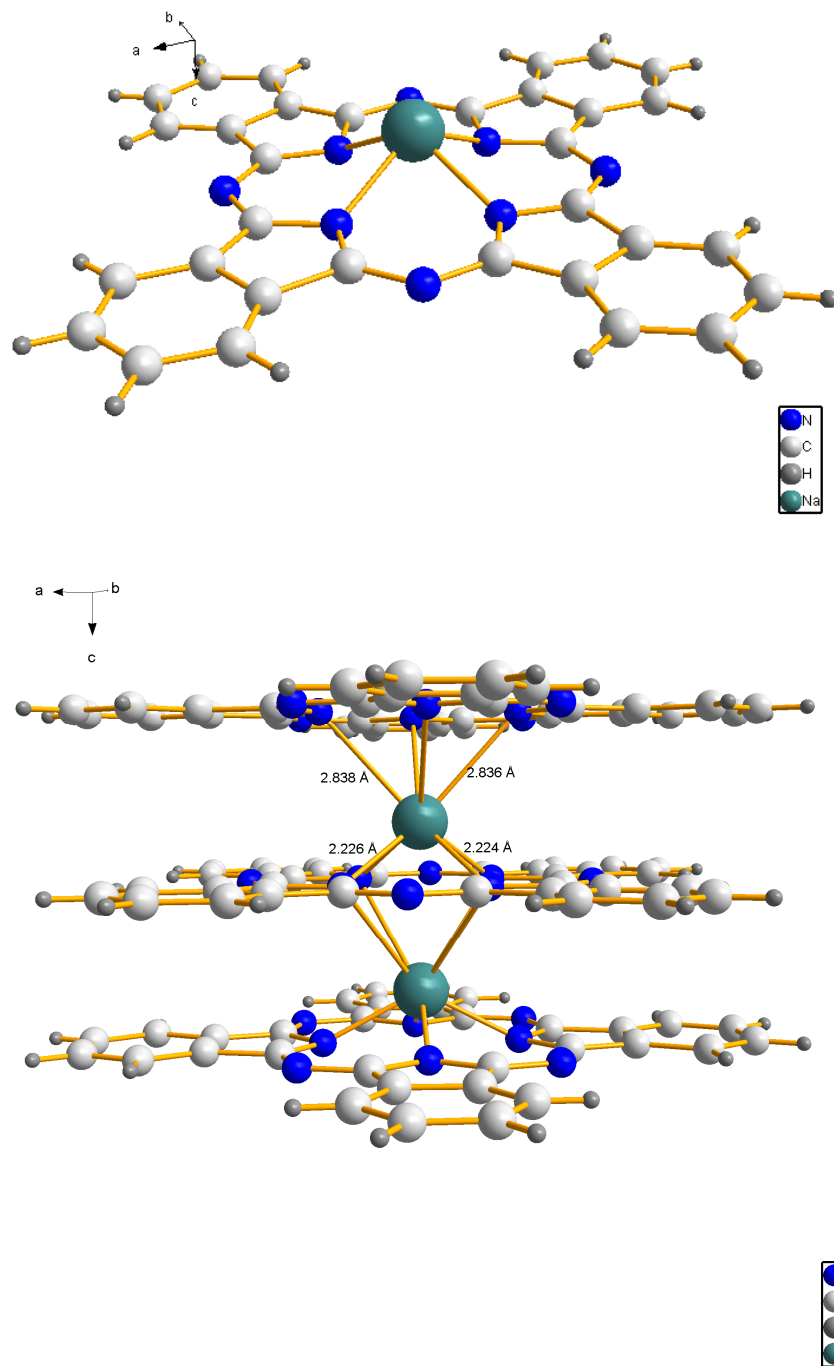


Figure 40. a - Molecular view of monosodium phthalocyanine and b- packing of neighbouring phthalocyanine molecules with intermolecular weak bonding of N-Na-N.

Spectroscopic characterization

The solid spectra of the NaPc show a shift in the band towards shorter wavelength in comparison with Na₂Pc. Unlike the LiPc radical, the absorption band shows a split and it is broad. This may be implicit of the deviation of the molecular symmetry away from D_{4h} symmetry. Comparative spectra of LiPc and NaPc are shown in figure 40.

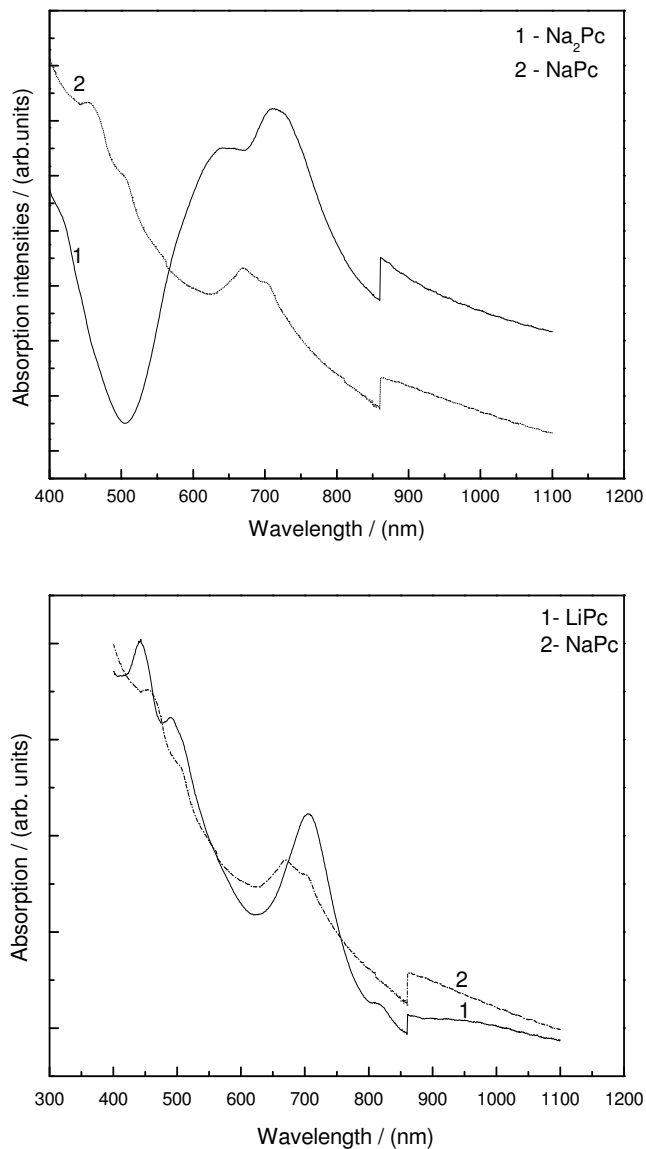
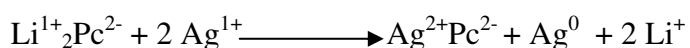


Figure 41. Solid state absorption spectra of Li₂Pc, Na₂Pc, LiPc and NaPc taken in a KBr medium.

3.2.4. Silver Phthalocyanine

Silver in phthalocyanine ligand can exist in +2 oxidation state. Attempts have been made to synthesis silver phthalocyanine from phthalonitrile and monovalent silver salt always failed. It is due to poor stability of silver in +2 oxidation in phthalocyanine ligand. Also there is dispute regarding the existence of silver in monovalent state silver hydrogen phthalocyanine, still not verified. In contrast, in our experiments, the preparation of silver phthalocyanine done using dilithium phthalocyanine and monovalent silver salt in dry acetonitrile solution, shows the product has always metallic silver impurities. It is due to the double decomposition reaction of monovalent silver with phthalocyanine. This is shown in the below reaction.



This is confirmed by the X-ray powder diffraction. Due to the solubility limitation of silver phthalocyanine there is always difficulty in separation of pure divalent silver phthalocyanine. The below X-ray powder pattern (figure 41) shows the product prepared from Li_2Pc and AgNO_3 . The presence of metallic silver is indicated.

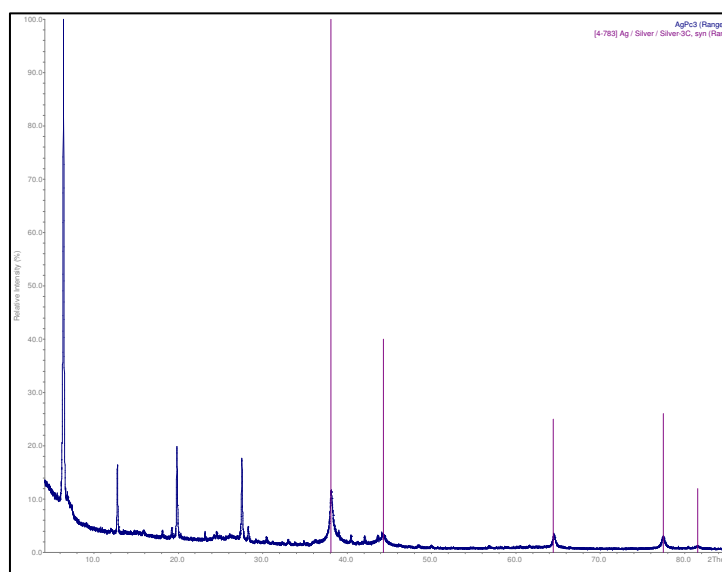


Figure 42. Powder Diffraction pattern of silver phthalocyanine prepared from Li_2Pc + AgNO_3 mixture.

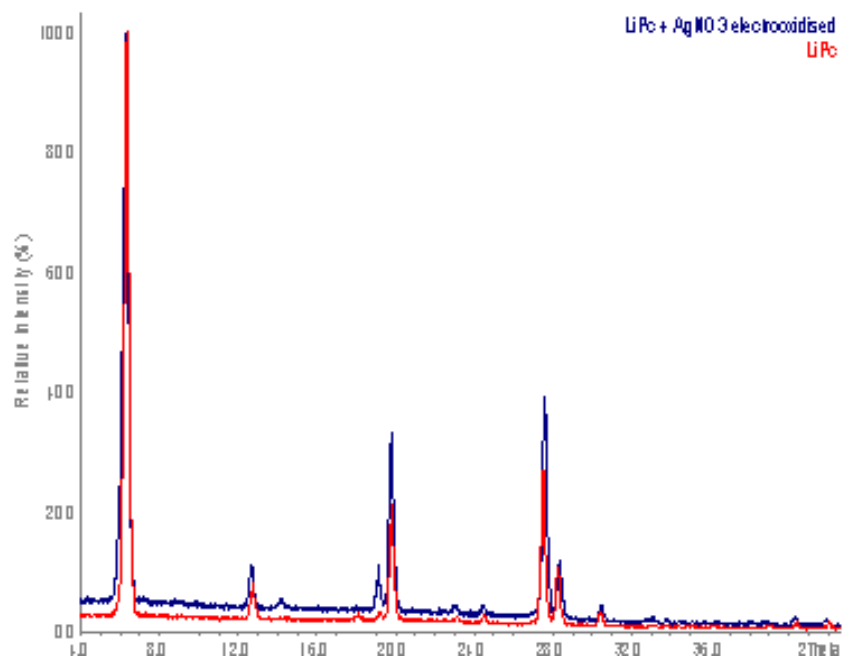


Figure 43. X-Ray powder patterns of LiPc and AgNO₃ treated LiPc.

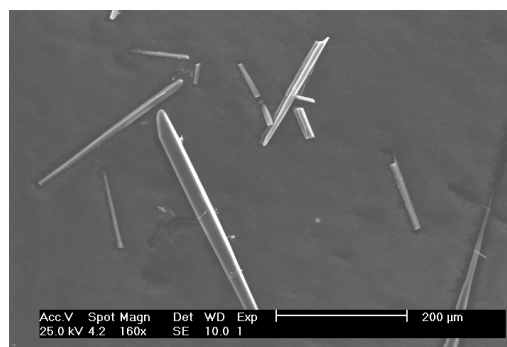


Figure 44. Solidstate silver exchange reaction of lithium phthalocyanine radical with AgNO₃ in CH₃CN - EDAX [Ag:N -0.23:8]

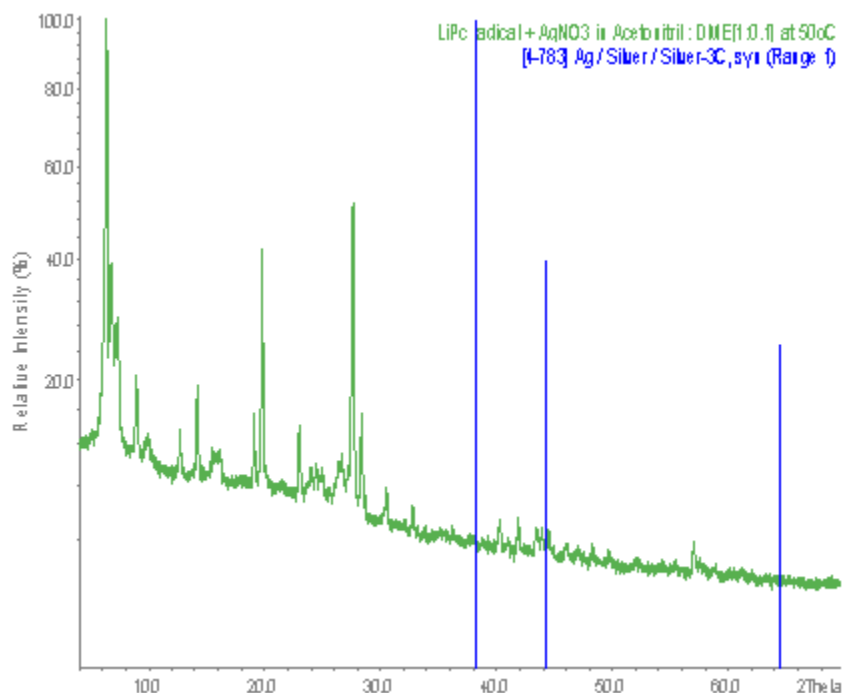
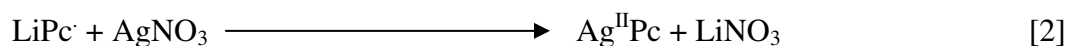


Figure 45. X-Ray powder diffraction of products obtained by treating LiPc with monovalent silver salt in dimethoxyethane.

The stability of LiPc^- is greater than LiPc^\cdot radical by 66.17 Kcal/mol. Here we make use of the reducing property of monolithium phthalocyanine radical to prepare elemental silver free silver phthalocyanine.



The above reaction is facile since the stability of Lithium Phthalocyanine in reduced state is higher than that in radical state. Tetragonal phase of lithium phthalocyanine radical synthesized electrochemically from dilithium phthalocyanine. This reacts with AgNO_3 as reaction follows. LiPc radical is soluble in THF hence mixture of dry acetonitrile and tetrahydrofuran was used for preparing AgPc from LiPc radical. The powder pattern shows clear difference from the route adapted earlier for AgPc preparation from Li_2Pc . EDAX measurement also shows the approximation in silver to nitrogen ratio (1.08:11). The sample obtained by solution phase reaction is a powder, sample still it shows good crystalline nature. Here we observe for the first time the preparation stable silver in +2 oxidation state without Ag in elemental state but may be the reaction was incomplete. Powder pattern indexing and structure determination was

not done with the powder pattern. This reaction could be carried out with monosodium phthalocyanine.

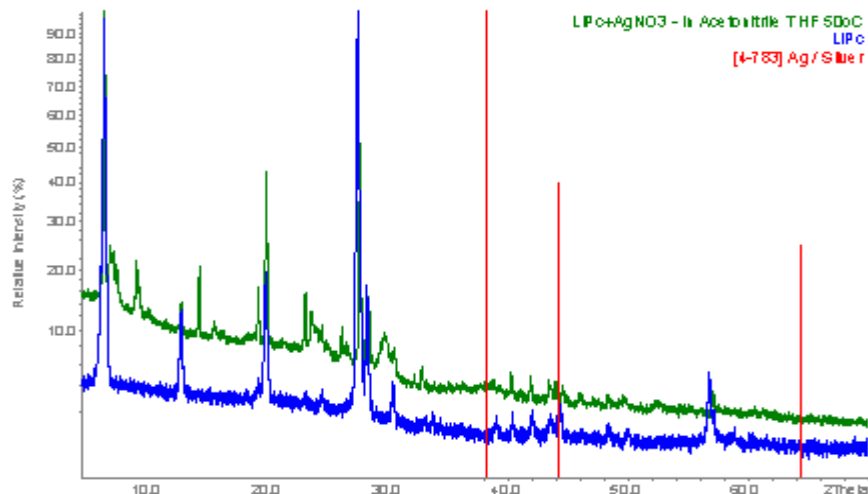


Figure 46. Powder XRD pattern of LiPc, AgNO₃ treated LiPc and ICDD peak file of elemental Ag

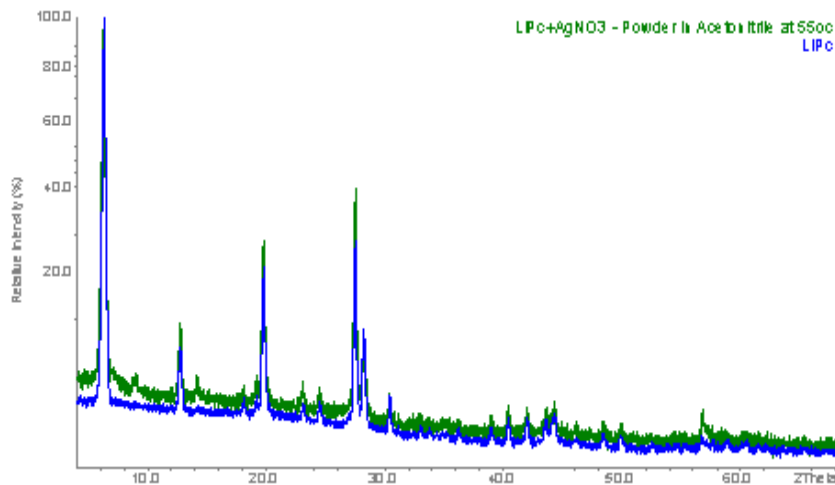
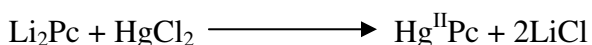


Figure 47. A comparative pattern of LiPc and solid LiPc powder treated with AgNO₃ solution

Reaction of lithium phthalocyanine radical crystal with AgNO₃ in acetonitrile gave products with lower silver content. LiPc radical shows no solubility in acetonitrile. The Powder XRD pattern of the powder of LiPc reacted with AgNO₃ is shown in figure 46.

3.2.5. Mercury phthalocyanine ($\text{Hg}^{\text{II}}\text{Pc}$)

Mercury phthalocyanine ligand can exist in +2 oxidation state. The preparation of HgPc was done by reaction of dilithium phthalocyanine and a divalent mercury salt in dry acetonitrile solution. The resulting product is always is microcrystalline powder. Due to the limited solubility of mercury phthalocyanine to prepare a large single crystal is a challenge. HgPc can be prepared by reaction of Li_2Pc with HgCl_2 , the reaction is given below.



In the above reaction was performed in dry acetonitrile medium. The rate of reaction is so rapid infer the ready exchange of mercury with two lithium ion.

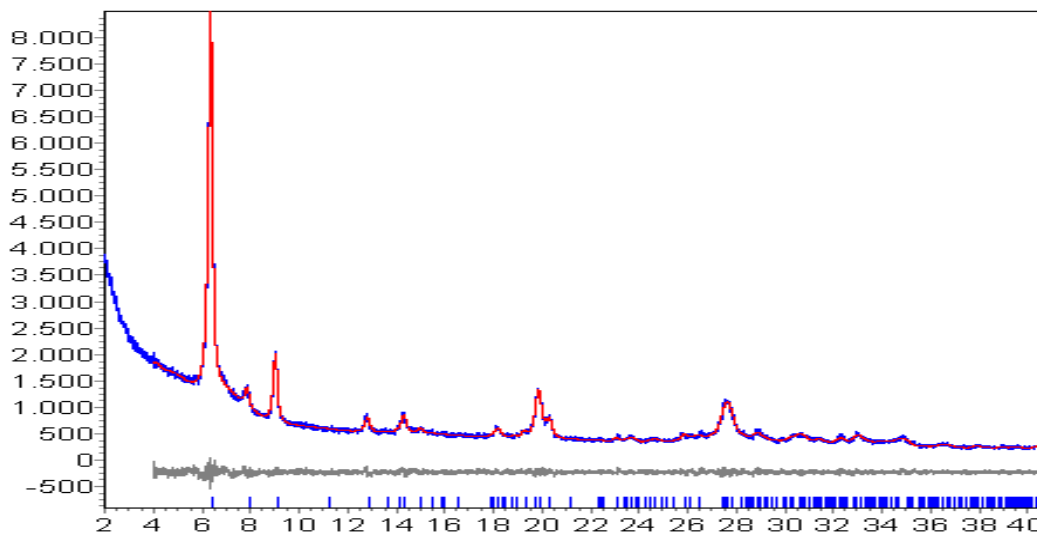


Figure 48. Powder pattern of mercury phthalocyanine synthesized from $\text{Li}_2\text{Pc} + \text{HgCl}_2$

The microcrystalline produced from the above reaction readily precipitate. The powder was separated and washed several times with dry acetonitrile and dried. The x-ray powder diffraction was measured with the sample. The sample shows high crystallinity. The data was treated with Topas structure solution programme. It was indexed in a Triclinic P-1 [$a = 14.0744$, $b = 11.9801$, $c = 6.4760$, $\alpha = 107.875$, $\beta = 88.476$, $\gamma = 102.107$ $R_{\text{wp}} = 5.74\%$]. Structure solution was unsuccessful due to quality of pattern, especially at higher angles.

3.2.6. Substituted Phthalocyanine- Hexa-deca fluorinated phthalocyanine

Peripheral substitution in phthalocyanine was done to improve the solubility characteristics [108,109]. Mainly substitution of larger alkyl group dramatically improves the solubility of metal phthalocyanine [110]. This helps in further electrochemical characterization and electrocrystallization of oxidized and reduced products. In general, the strong electron withdrawing characteristics of fluorine can enhance the stability of the higher oxidation state metal in hexadecafluorinated phthalocyanine. Here we attempt to synthesize dilithium hexadecafluorinated phthalocyanine and silver hexadecafluorinated phthalocyanine.

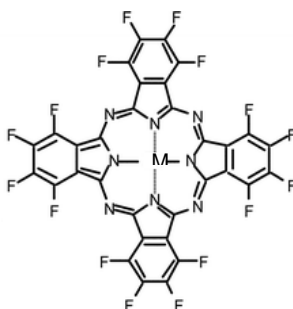
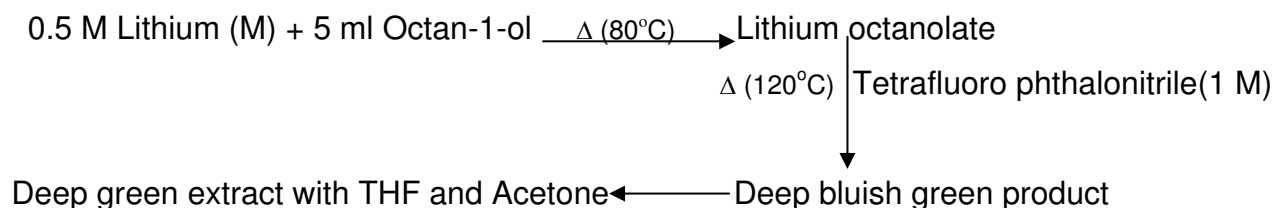


Figure 49. view of hexadecafluorinated metal phthalocyanine

Hexadecafluorinated dilithium phthalocyanine synthesis was attempted by using the synthetic route as described in scheme below.



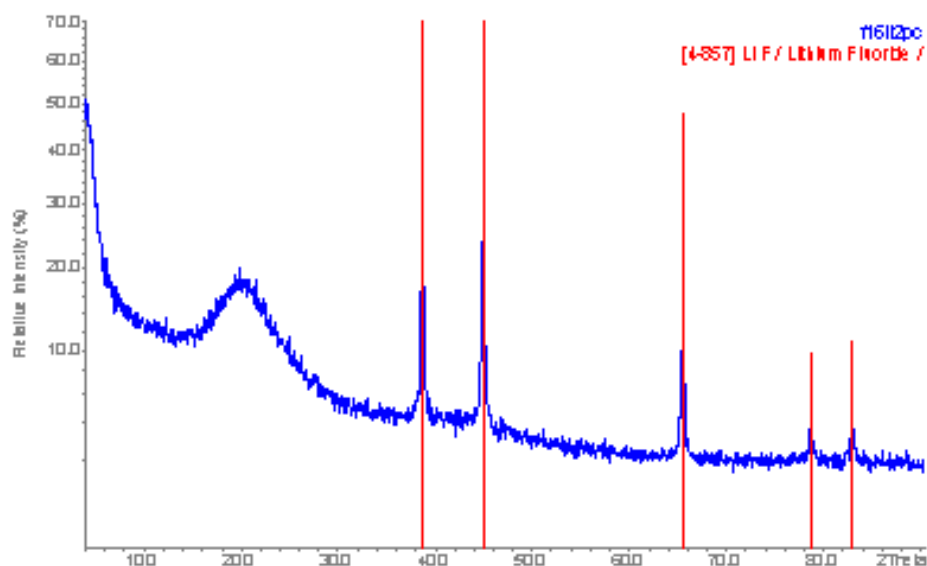


Figure 50. X-Ray powder diffraction of the resultant product of the above reaction.

The X-ray powder pattern shows presence of LiF and more amorphous. The product is completely insoluble in acetonitrile but highly soluble in THF. The fluorine in phthalonitrile ring possibly could be substituted by octanoxy group. This product obtained was subjected to crystallization for but there was no crystal formation was observed even with several trials. In the above synthesis when tetrachlorophthalonitrile was used instead of tetrafluorophthalonitrile, it shows the formation of LiCl in the product.

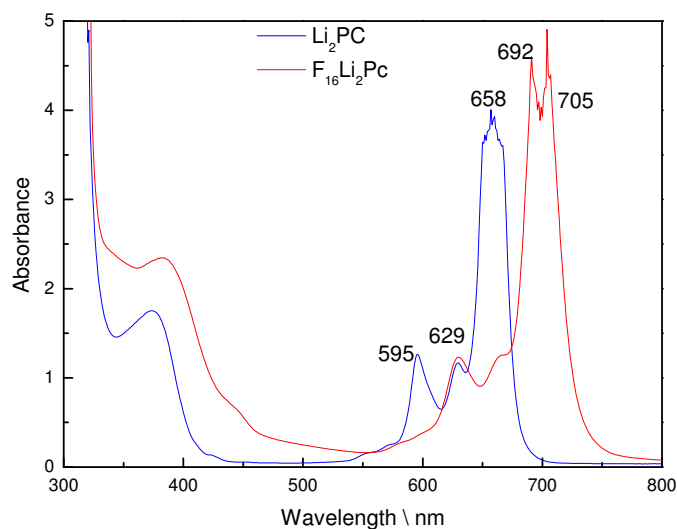


Figure 51. Absorbance spectra of Li_2Pc and $\text{F}_{16}\text{Li}_2\text{Pc}$ taken in acetone.

A comparative UV-Vis spectrum of Li_2Pc and $\text{Li}_2\text{F}_{16}\text{Pc}$ is shown in the figure 50. There is a red shift in the absorbance peak at higher wavelength and also a split in the absorbance peak. But the absorbance spectrum is similar to that of Li_2Pc . This infers the formation of phthalocyanine ring by cyclization of tetrafluorophthalonitrile molecules. The Q absorbance peaks are shifted towards longer wavelength. This could be due to the substitution of octanoxy group on the periphery of the phthalocyanine ring for fluorine. An attempt was made to electrochemically synthesis $\text{F}_{16}\text{Li}_2\text{Pc}$, but the yield was very low for further characterisation. Electrochemical synthesis was done with lithiummethanolate tetrafluorophthalonitrile by electroreduction at 2 V. This form soluble product at cathode compartment and yield is low. These reactions were carried out in a divided H-cell.

3.3 Electrochemical synthesis and crystal structure of organic crystals containing tetracyanoquinodimethane.

Introduction

Organic conductors have attracted considerable attention in the recent past [111,112]. From a structural perspective all existing organic conductors can be divided into two categories: polymers and charge-transfer salts. It has become clear that these materials are also promising for application in electronic devices, electrical and magnetic materials [113,114]. In particular, the unique possibilities offered by the tunability and synthesis of organic molecules together with the possibility of low-cost and large-area fabrication at moderate substrate temperatures appear attractive. The electronic properties of organic conductors are extraordinarily sensitive to even marginal changes in molecular structure [115]. Charge-transfer complexes of 7,7',8,8'-tetracyanoquinodimethane (TCNQ) are highly one-dimensional electronic conductors. They are of special interest because they form unusually stable molecular complexes containing the radical anions TCNQ^- and $(\text{TCNQ})_2^-$. The first organic metal was (TTF-TCNQ) found in 1973, which possessed room temperature conductivity [116]. Since 1980, over 400 organic conductors have been synthesized, of which over 100 are superconducting. Under some physical conditions charge transfer salts may even become superconductors. During this time the superconducting transition temperature in these materials increased from 1.2 K to 12.6 K [117]. The field of practical investigations of organic conductors started in 1960 and 1970 with the discoveries of the molecules TCNQ (tetracyanoquinodimethane) and TTF (tetrathiafulvalene), respectively [118, 119]. The charge transfer salts contain organic molecules with π -conjugated bonds. These molecules play the role of donors and acceptors, with TCNQ acting as acceptor here. The planar molecules of TTF-TCNQ form segregated stacks in a plane-to-plane manner and the molecular π -orbitals can interact preferably along the stacking direction. Some of the compounds act as one-dimensional metals. For this reason, organic conductors exhibit an especially rich variety of behaviors, and their properties can easily be tuned over a wide range. The crystal structure of these compounds play an important role in the electrical properties of these materials. The

materials formed with double anions and mixed valence character show a high electrical conductivity. The donors with higher basicity have resulted in highly-conducting compounds. In the following, the electrochemical synthesis of the title compound and its structural aspects is detailed. The bulky organic cation was chosen to form this salt-like derivative. The interaction between the stacks of cations and anions determines the electron motion in these salts. Planarity (or near planarity) is, in general, a prerequisite for high chemical stability of a radical ion (intramolecular delocalization) and for efficient intermolecular delocalization of charge carriers. Here, the TCNQ anions packed in a different manner in three different crystals are described. Therefore, depending on the stacking, electrons of the plane molecules can be delocalized not only inside a molecule, but also along a pile. TCNQ can form crystalline π -complexes (charge transfer complexes) with aromatic hydrocarbons, amines and polyhydric phenols. Complexes with aromatic π -bases are believed to result from overlap of the respective acid and base π -orbital systems. TCNQ also forms two series of stable, salt-like derivatives, each involving complete transfer of electron to TCNQ with formation of the anion-radical $\text{TCNQ}^{\cdot-}$, which are $\text{M}^{+n}(\text{TCNQ}^{\cdot-})_n$ (simple salt) and $\text{M}^{+n}(\text{TCNQ}^{\cdot-})_n \cdot \text{TCNQ}$ (complex salt). In the following work, different organic salts prepared with macrocyclic as well as alkyl ammonium compounds with varying chain lengths are demonstrated. In particular, the structural aspects and the differences in the mode of packing of the TCNQ anions in these crystals are highly interesting. We also observe disorder amongst the cation and anions under certain conditions, which is discussed in the respective section. This can influence the magnetic and electrical properties of these compounds.

3.3.1. Electrochemical synthesis and crystal structure of Tetrapropyl porphycene Tetracyanoquinodimethane salt.

Introduction

Porphyrins and metalloporphyrins, commanding interest from many points of view, have become targets of interdisciplinary research that encompasses chemistry, the biosciences, physics (especially photophysics), medicine and even materials science. The finding that porphycenes are porphyrin-like pigments promises practical applications in various domains. They also reveal noticeable differences between the two kinds of tetrapyrrolic macrocycles [120-122]. This particularly applies to the electrochemical properties of porphycenes as compared with those of porphyrins [120, 123-127]. The novel porphine structural isomer porphycene is actually more soluble than porphyrin and phthalocyanine macrocycles. Hence, the metalation of porphycenes and recrystallization can be achieved without any difficulty by refluxing the free ligand with metal acetates. [120] Porphycenes and metalloporphycenes have been the subject of numerous physicochemical studies because of their close structural similarity to metalloporphyrins.

[121,122]. Their unique structural properties results in interesting catalytic behaviour and complex formation with metals [128], in contrast to porphine and its metal complexes whose study is impaired by solubility problems. Hence, solubilization and crystallization is promoted by peripheral substitution of the macrocycles, which makes them amenable to almost any physical and chemical investigations. The electrochemical characteristics of porphycenes and porphyrin exhibit quite similar behavior during electrooxidation, but not upon electroreduction. Metalloporphycenes are easier to reduce and less likely to exist in a low-valent metal oxidation state than the corresponding metalloporphyrins containing the same central metal ion. [123,124]. Since the cavity in the porphycene system is smaller than in the porphyrin system the stability of the metalloporphycenes are generally lower than those of the corresponding metalloporphyrins. The porphycene skeleton as a whole is of planar geometry, and in the case of alkylated porphycenes the alkyl groups lie on either side of the planar macrocycle. In the following work the electrochemical oxidation of tetrapropylporphycene along with TCNQ as well as the structural aspects of this interesting compound, are discussed.

Experimental

In general, the synthesis of porphycenes is carried out by reductive coupling of 5,5'-diformyl 2,2'-bipyrrrole with a lower-valent titanium compound. This can be extended to various alkylated porphycenes. Tetra propyl porphycene can be synthesized by a method described by Vogel et al [120]. Here we use tetrapropylporphycene as purchased without any further purification. Tetrapropylporphycene is highly soluble in dimethoxyethane (DME). Hence a DME medium was used in the electrochemical synthesis of tetrapropylporphycene tetracyanoquinodimethane (TPP.TCNQ). Electrochemical oxidation was executed with a solution of Tetrapropyl porphycene, Tetracyanoquinodimethane and Tetrabutylammonium hexafluorophosphate in dimethoxyethane solvent. A three-electrode cell was used for electrochemical synthesis. Pt foil as working and counter electrodes and Ag wire as reference electrode was used in the cell. Initially the solution was subjected to preliminary cyclic voltammetric analysis, after which a galvanostatic electrooxidation was performed for 15 hr. The electrooxidised solution was subjected to slow evaporation of solvent under room conditions. Black, needle-like crystals were separated at the bottom of the Petri dish. Suitable crystals were selected, mounted on glass capillaries and subject to precession measurements so as to identify the best crystal.

Crystal Structure determination

X-ray diffraction data collection was performed at low temperature using a Bruker-AXS APEX Smart-CCD diffractometer equipped with MoK α source with the crystal mounted on the tip of a glass capillary. The cell parameters were determined using reflections within the range $1.8 < \theta < 20.0^\circ$. The crystal structure was solved by the direct method (SHELXS-97) in the monoclinic space group *P1n1* and refined by full matrix least squares (SHELXL-97). All non hydrogen atoms were refined using an anisotropic model for their displacement parameters. Hydrogen atoms were treated by a mixture of independent and constrained refinement. Refinement of F^2 was against all reflections. The weighted *R*-factor $wR2$ and goodness of fit *S* are based on F^2 , conventional *R*-factors *R* are based on *F*, with *F* set to zero for negative F^2 . The threshold expression of $F^2 >$

$2\sigma(F^2)$ is used only for calculating R -factors(gt) *etc.* and is not relevant to the choice of reflections for refinement. R -factors based on F^2 are statistically about twice as large as those based on F , and R -factors based on ALL data will be even larger. General information and details of the structure refinement are given in Table 13.

Like the porphyrins it is found that porphycene is planar and features an π electron system, intermolecular interactions and conjugation pathway. In general, TCNQ forms crystalline π -complexes (charge transfer complexes) with aromatic hydrocarbons. Complexes with aromatic π -bases are believed to result from overlap of the respective acid and base π -orbital systems. Here TPP forms a charge-transfer π -complex with TCNQ. The single crystal structure investigation shows the molecular composition as TPP.TCNQ. This porphycene exhibits geometries of the N4 coordination site which deviate noticeably from the ideal square shape of the porphyrin core. The crystal structure solution shows the composition as TPP.TCNQ (Figure 52 a). The shape of the central N4 cavity is rectangular, enlarged in the direction of the methine bridge C atoms. The N-N distances are in the range of 2.78-2.82 while other two nitrogens are separated by 2.57-2.64 Å. The torsion angle of four nitrogen of pyrrole ring in TPP is 0.669 Å. The molecule is of planar geometry. The planarity of the TPP is unaffected even though four propyl groups are present in the 2,7,12,17-positions. Here the stacking mode is in a column with TPP:TCNQ ratio of one to one. The intermolecular distance between the TPP and TCNQ is in the range of 3.3 -3.4 Å. This shows that it is the non-covalent interaction of TPP donor – TCNQ acceptor within the organic crystal. The adjacent columns are tilted by a certain angle as shown in Figure 53. The conformation of the propyl substituents also determines the stacking mode of TPP to TCNQ in the crystal. The *trans* arrangement of tetrapropyl influences the arrangement of TPP and TCNQ in the adjacent column. Here two of the propyl groups are in *trans* conformation while the other two are in plane with the macrocycle of the porphycene. This packing is influenced by the propyl group of the TPP in the neighboring column.

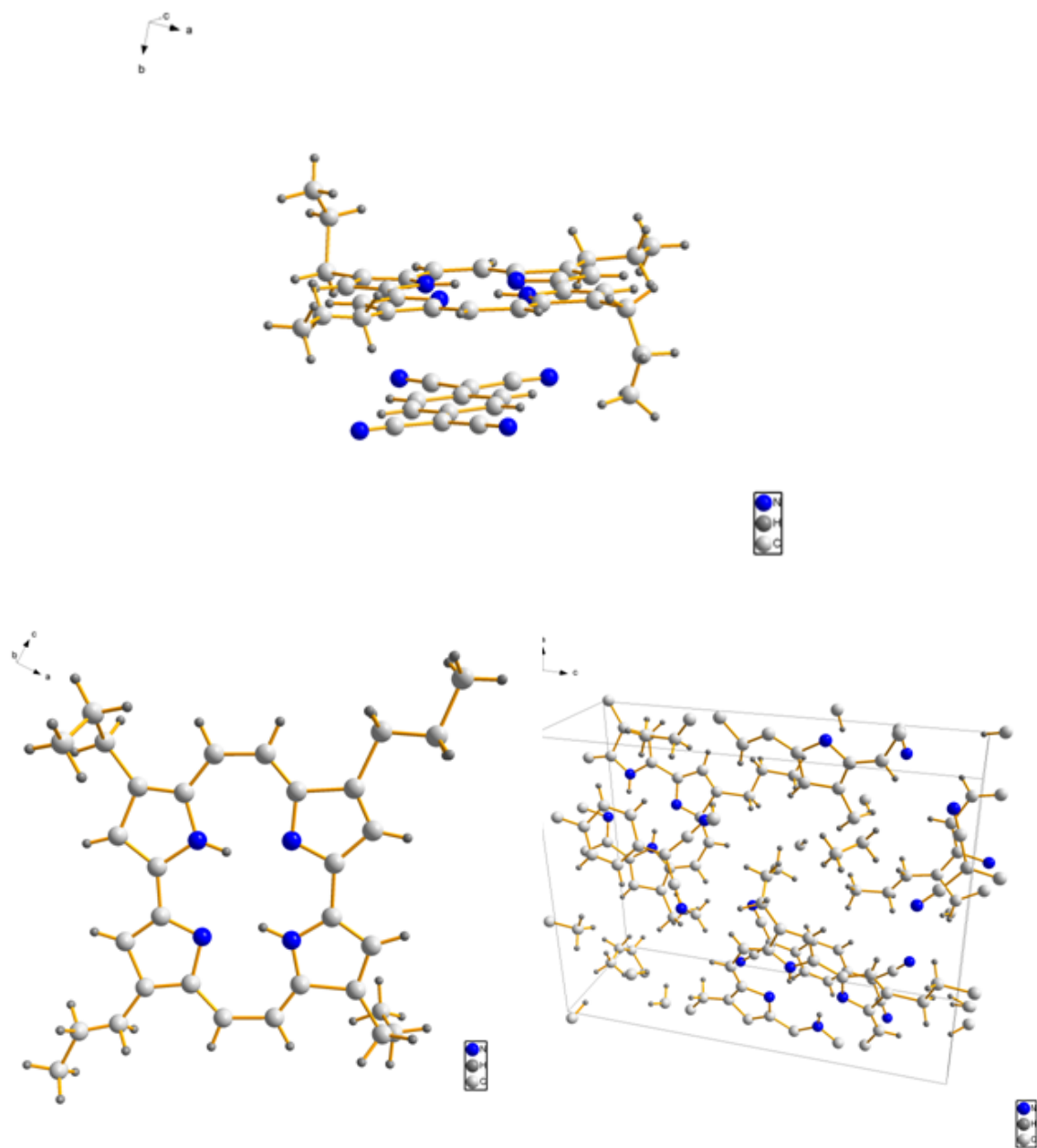


Figure 52: (a) View of TPP.TCNQ, (b) view of TPP in b axis, (c) unit cell of TPP:TCNQ

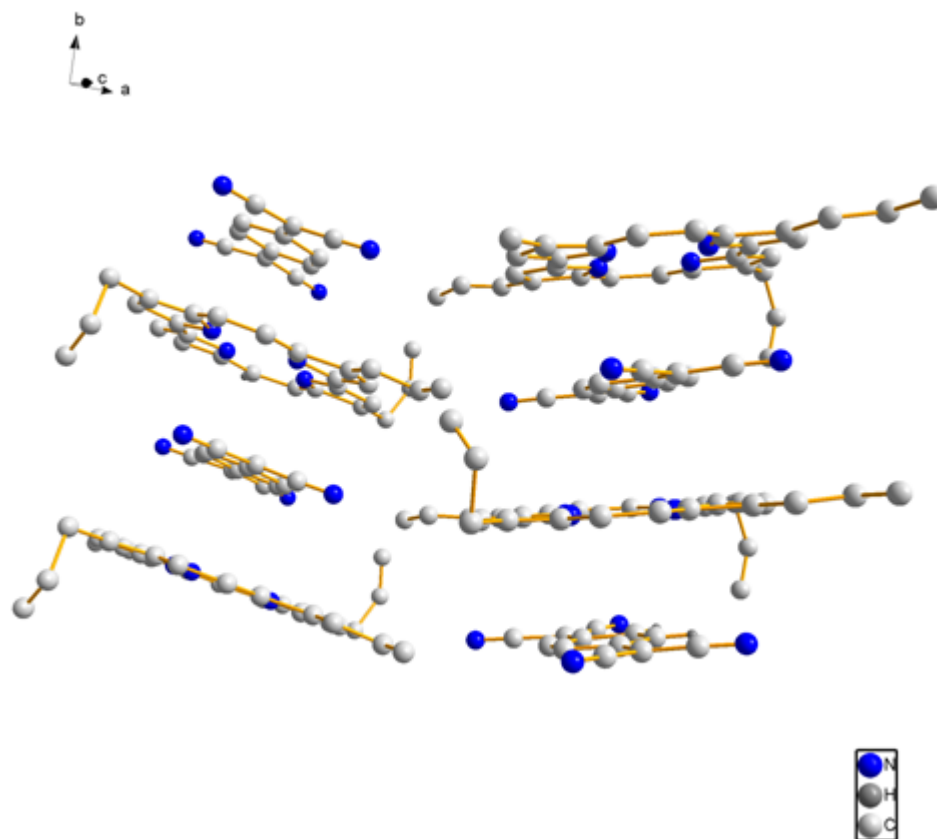


Figure 53: Stacking view of TPP.TCNQ

Table 13. Crystal data for Tetrapropylprophycene. Tetracyanoquinodimethane

Chemical formula	C ₄₄ H ₃₅ N ₈
Formula weight (g/mol)	675.80
Crystal system	<i>Monoclinic</i>
Space group	P 1 n 1 (7)
Z	2
<i>a</i> (Å)	14.2709(10)

3. Special section: Silver Oxides

b (Å)	6.8742(5)
c (Å)	18.9359(13)
β (°)	90.892(2)
V (Å ³)	1857.4(2)
T (K)	100(2)
ρ_{calc} (g/cm ³)	1.208
λ (Å)	0.71073
μ (mm ⁻¹)	0.07
F(000)	710
Index ranges	-13<=h<=13 -6<=k<=6 -18<=l<=18
$R[I > 4(\sigma(I))]$ (%)	5.09
$wR(F^2)$ (%)	13.5
S	1.05
No. of reflections	9130
No. of independent reflections	3476
No. of observed reflections [$I > 2(\sigma(I))$]	2148
$R_{\text{int}}, R_{\text{sigma}}$ (%)	3.61, 1.55
No. of parameters	469
No. of restraints	2
x (Flack parameter)	0 (8)
$\Delta\rho_{\text{min}}, \Delta\rho_{\text{max}}$ (e Å ⁻³)	-0.11, 0.22
$(\Delta/\sigma)_{\text{mean}}, (\Delta/\sigma)_{\text{max}}$	<0.001, 1.262

3.3.2. Electrochemical synthesis and crystal structure of Tetrahexyl ammonium Tetracyanoquinodimethane salt.

Introduction

TCNQ is a strong π -acid and forms charge-transfer or π complexes with a variety of Lewis bases. Complexes with aromatic π -bases are believed to result from overlap of the respective acid and base π -orbital systems. This is shown by the earlier compound Tetrapropylporphycene.TCNQ shown in the previous section. In general, donors of highest basicity give highly conductive compounds. TCNQ undergoes facile one-electron reduction when it is reacted with metal iodides or with reducing metals to form anion radical salts. These metal free organic moieties may be an active magnetic component with spin sites contributing to the magnetism. Several synthetic methodologies were adapted to synthesize organic-based molecular magnets. Electron transfer salts with electron acceptor molecules and their ability to form stable radical species is very versatile. TCNQ is also an efficient organic acceptor molecule that yielded a variety of interesting molecular magnets [129]. In addition, the packing of organic acceptors determines the structural aspects of these compounds that influence electrical and magnetic properties. The stacking mode of TCNQ as columnar stacks or dimers is an interesting aspect of these compounds. The simple and complex salts of these crystals show different modes of stacking. The magnetic sand phase transition can be greatly influenced by the one dimensional characteristics of these compounds.

Experimental

Tetrahexylammonium iodide, tetracyanoquinodimethane and acetonitrile were used. The solution containing 0.05 M Tetrahexylammonium iodide and 0.02 M TCNQ in acetonitrile was used as the electrolytic bath. A galvanostatic electrooxidation experiment was carried out with the solution. There were no crystals grown on the electrode surface. But the solution turns into deep green on prolonged duration of oxidation for about 10 hours. Then the solvent was allowed to evaporate slowly to obtain crystals of the title

compound. The crystals were air-stable, were selected and mounted on glass capillaries, and subjected to single crystal measurements. The data collection was conducted at room temperature and at 100 K. The reflections were collected in the 2 theta range of 1.5 to 25.8°.

Structure description

The single crystal solution obtained from the data collected at 100 K and at 293 K shows that the obtained compound is a simple salt of tetrahexylammonium tetracyanoquinodimethane. Figure 54 shows both room temperature and low temperature molecular structures of the title compound. The interesting point to note in this compound is that only one of the hexyl groups exhibits disorder (at carbon 4, 5 positions) when the measurement was carried out at 293 K. This is clear from the occupancy factors of the respective carbon atoms as shown in the table. The thermal displacement parameters are also only higher for these two carbon positions. Hence the measurement was carried out at 100 K to resolve the disorder. This disorder can be due to repulsive interactions of nearest-lying hexyl groups, which approach each other head-to-head as seen in Figure 2a. The two oppositely lying hexyl groups show a mutually eclipsed conformation. The structural feature of this compound is different from the column structure of NH^+TCNQ^- , alkali-metal-TCNQ TTF-TCNQ compounds. The packing of both cation and anions are different in this compound; they don't form a columnar structure as in lower alkyl ammonium salts. The TCNQ anion radical in this compound packs as dimers, while in salts of tetramethyl ammonium and tetra butyl ammonium they form a continuous column. Although it forms dimers, the formula unit of the compound shows that it is a simple salt with the structure $\text{THA}^+\text{TCNQ}^-$. Also, it is known that the complex salts of tetramethyl ammonium $\text{TCNQ}^-\cdot\text{TCNQ}$ form columnar stacks. Here the dimers are separated by interlaying the long hexyl group. Hence the chain length of the alkyl ammonium ion can also influence the type of structure formed. The interplanar distance between neighbouring TCNQ reflects the magnitude of the charge-transfer interaction. Figure c shows a view of a TCNQ dimer as viewed along the *a*-axis. This dimer of TCNQ anions shows a nearest-lying atom distance of 3.2038 Å and slip distance of 3.2586 Å. Remarkably this is a shorter distance, which shows that it is a tight dimer. This

can show very interesting magnetic characteristics. The packing view of Tetrahexyl and TCNQ is shown in figure 54.

Table 14. Crystal data for Tetrahexyl ammonium tetracyanoquinodimethane

Chemical formula	C36 H56 N5	C36 H56 N5
Formula weight (g/mol)	558.86	558.86
Crystal system	<i>Monoclinic</i>	<i>Monoclinic</i>
Space group	P1 21/n 1 (14)	P 1 21/n 1 (14)
a (Å)	15.839 (2)	15.9025(9)
b (Å)	12.1660 (15)	12.3608(7)
c (Å)	18.732 (2)	19.2218(1)
β (°)	105.054 (2)	105.0680(10)
V (Å ³)	3485.7 (8)	3648.5(4)
Z	4	4
T (K)	100(2)	298(2)
ρ_{calc} (g/cm ³)	1.065	1.017
λ (Å)	0.71073	0.71073
μ (mm ⁻¹)	0.06	0.058
$R[I > 4(\sigma(I))]$ (%)	7.31	5.6
$wR(F^2)$ (%)	18.26	16.5
S	1.06	0.95
No. of reflections	43582	48775
No. of independent reflections	10709	12658
No. of observed reflections [$I > 2(\sigma(I))$]	7817	9520
$R_{\text{int}}, R_{\text{sigma}}$ (%)	8.1,	4.41, 15.5
No. of parameters	374	449
No. of restraints	0	477

3. Special section: Silver Oxides

$\Delta\rho_{\min}, \Delta\rho_{\max}$ ($e \text{ \AA}^{-3}$)	-0.30, 0.73	-0.15, 0.16
$(\Delta/\sigma)_{\text{mean}}, (\Delta/\sigma)_{\text{max}}$	0.002, 0.09	<0.001, 0.04

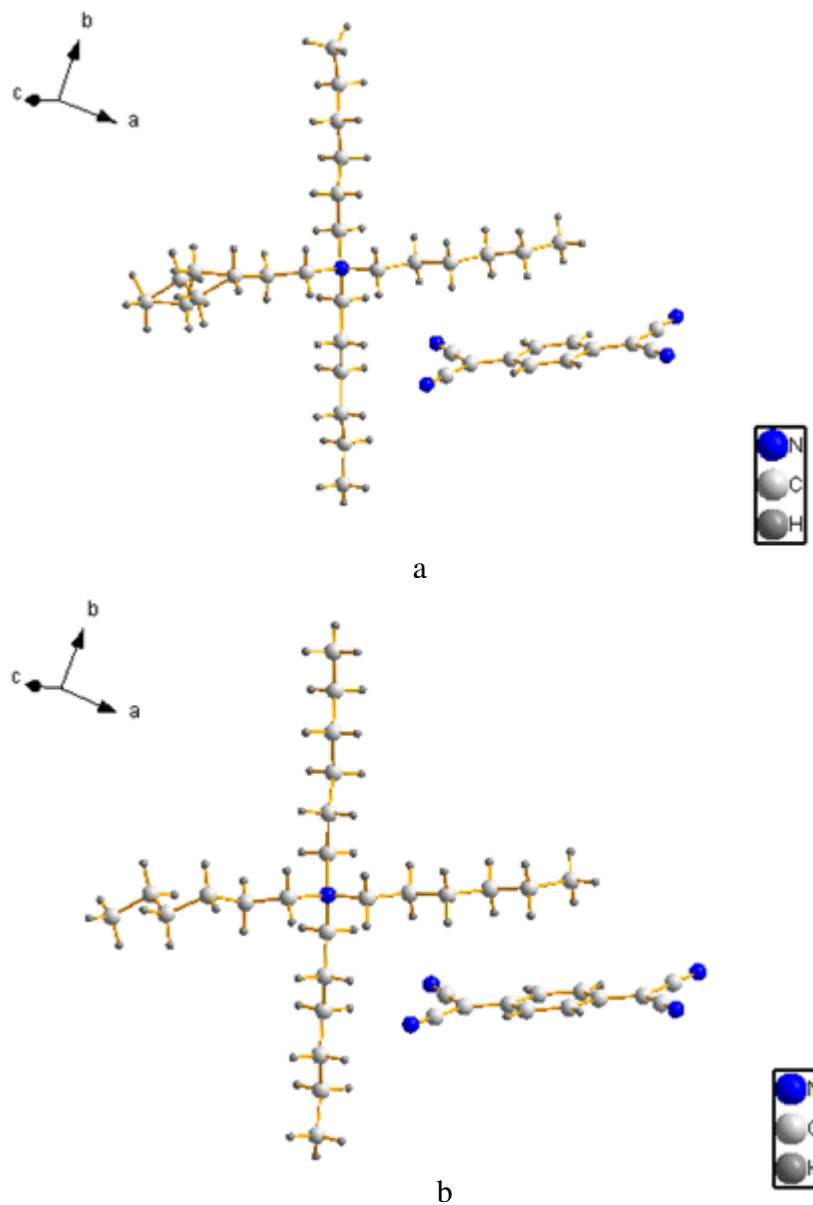


Figure 54. Molecular view of Tetrahexylammonium Tetracyanoquinodimethane. a - 298 K, b - 100 K.

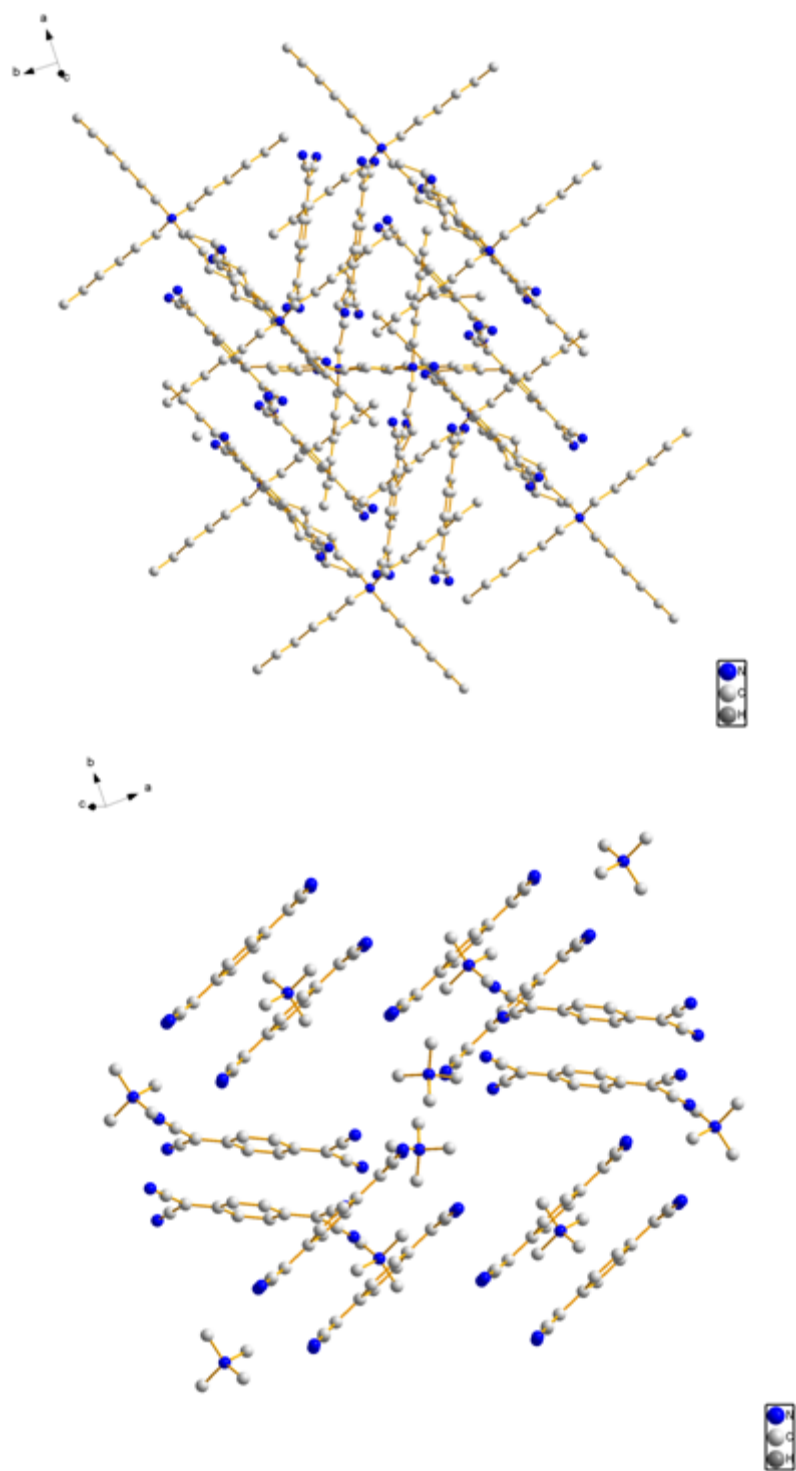


Figure 55. Packing diagram of Tetrahexyl ammonium tetracyanoquinodimethane

3.3.3. Electrochemical synthesis and crystal structure of Tetrabutyl ammonium Tetracyanoquinodimethane.

Introduction

The tetra-alkyl groups with shorter chain lengths can influence the packing mode of TCNQ packing. This determines the charge transfer crystals formed, e.g. a simple or a complex salt. The influence of alkyl group chain length in the crystal structure is shown here. This is evident from the crystal structure of Tetrabutylammonium tetracyanoquinodimethane. The shorter alkyl group can result in a compound with higher electrical conductivity. The intermolecular stacking interactions are higher in the case of lower chain length organic ammonium salts. The nearest-neighbour overlaps of the TCNQ influence the physical properties of the material.

Experimental

Tetrabutylammonium iodide, tetracyanoquinodimethane and acetonitrile were used. The solution containing 0.05 M Tetrabutylammonium iodide and 0.02 M TCNQ in acetonitrile was used as the electrolytic bath. A galvanostatic electrooxidation experiment was carried out with the solution. There were no crystals grown on the electrode surface. But the solution turns to a deep green upon prolonged duration of oxidation for about 10 hours. Then the solvent was allowed to slowly evaporate in order to obtain the crystals of the title compound. The crystals were air-stable. The crystals were selected and mounted on the glass capillary and subjected to single crystal measurements. The data collection was conducted at room temperature and at 100 K. The reflections were collected in the 2 theta range of 1.5 to 25.8°.

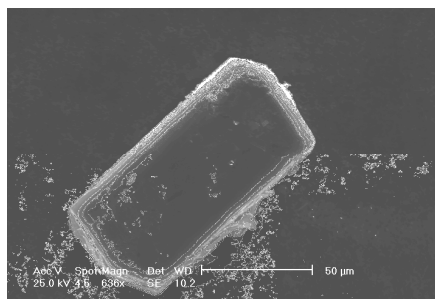


Figure 56. SEM image of Tetrabutylammonium tetracyanoquinodimethane.

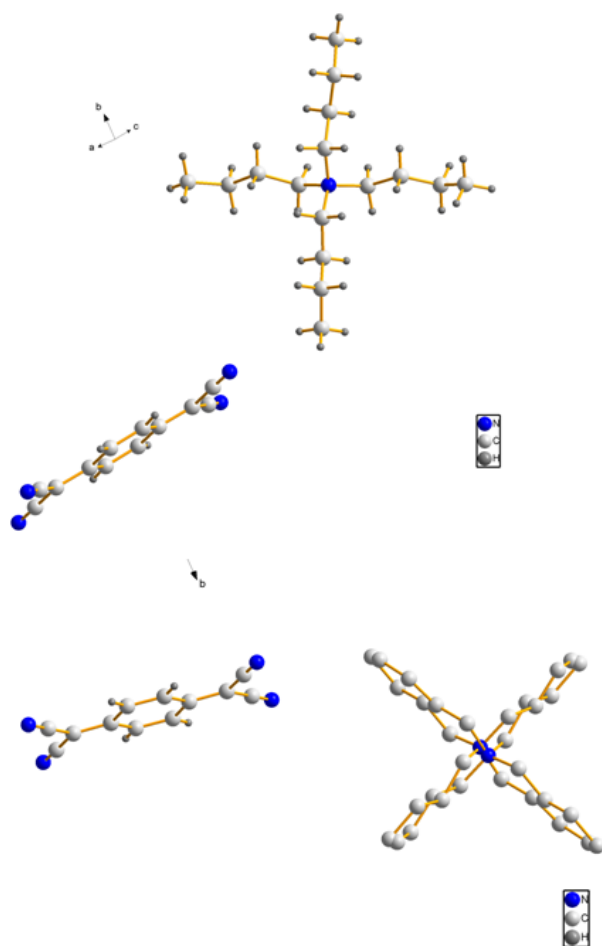


Figure 57. a. Molecular view of Tetrabutylammonium TCNQ, disordered carbon not shown for clarity. b. a view showing with the two position of disordered tetrabutyl group, hydrogen atoms omitted for clarity.

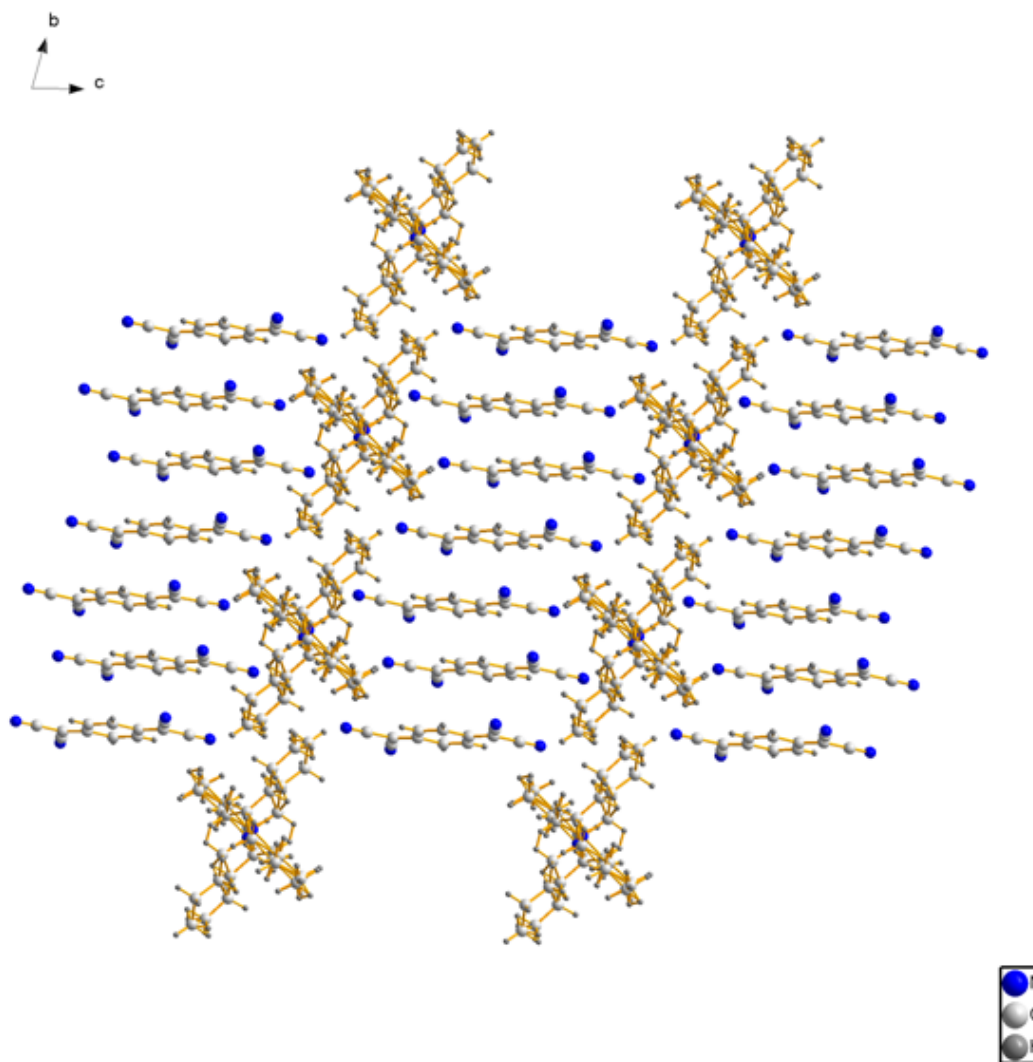


Figure 58. Packing diagram of Tetrabutyl ammonium tetracyanoquinodimethane

The crystal structure analysis shows that the molecular composition is tetrabutylammonium tetracyanoquinodimethane. In the crystal the cation and the anion form continuous stacks. The tetrabutyl ammonium cation and TCNQ anions are arranged as columns. The Tetrabutyl ammonium cation shows disorder in the four alkyl group. This is shown figure 57. The TCNQ forms a continuous stack. The intermolecular contact suggests that in the structure, TCNQ anions are regularly stacked face-to-face to form a

column. The shortest intermolecular distance is about 3.298 Å, which is reflected in the charge transfer interaction. The planar TCNQ is packed in a zigzag manner to form a column structure as shown in Figure 57. It is interesting to note that the stacking mode of the TCNQ anion in Tetrabutylammonium TCNQ is different from Tetrahexylammonium TCNQ. Evidently it is greatly influenced by the chain length of alkyl ammonium cations. Hence, electrochemically-synthesised charge transfer salts of three different modes of stacking of TCNQ are shown in this section.

Table 15. Crystal structure data of Tetrabutyl ammonium tetracyanoquinodimethane

Chemical formula	C ₂₆ H ₄₀ N ₉
Formula weight (g/mol)	437.53
Crystal system	<i>Triclinic</i>
Space group	P-1
<i>a</i> (Å)	7.9638(11)
<i>b</i> (Å)	10.0950(14)
<i>c</i> (Å)	16.106(20)
α (°)	74.117(2)
β (°)	79.573(2)
γ (°)	80.033(2)
<i>V</i> (Å ³)	1214.34(86)
<i>Z</i>	2
<i>T</i> (K)	293.2
ρ_{calc} (g/cm ³)	1.197
λ (Å)	0.71
μ (mm ⁻¹)	0.08
<i>R</i> [<i>F</i> ² > 2(σ (<i>I</i>))] (%)	22
<i>wR</i> (<i>F</i> ²) (%)	33.1
<i>S</i>	1.09

3. Special section: Silver Oxides

No. of reflections	9463
No. of independent reflections	4710
No. of observed reflections [$I > 2(\sigma(I))$]	2719
$R_{\text{int}}, R_{\text{sigma}}$ (%)	22,
No. of parameters	371
No. of restraints	29
$\Delta\rho_{\text{min}}, \Delta\rho_{\text{max}}$ ($\text{e } \text{\AA}^{-3}$)	-0.29, 0.24

3.3.4. Electrochemical synthesis and crystal structure of Tetraphenyl Phosphonium Tetracyanoquinodimethane.

Experimental

Galvanostatic electrochemical oxidation of tetraphenylphosphonium chloride (TPPC) and tetracyanoquinodimethane gave the title compound. This was done in a two electrode electrochemical cell setup. The mixture of TPPC and TCNQ of 1:1 molar ratio (0.01 M) in dry acetonitrile was used for the electrochemical synthesis. The current conditions were determined from the preliminary cyclic voltammetric experiments. The solution was subjected to electrooxidation at 0.05 mA cm^{-2} for a period of 24 hours. The resultant solution was slowly evaporated in a glass Petri dish to obtain rod like crystals, which were washed with n-Hexane and then dried. The crystals were carefully chosen and tested by precession techniques so as to select the best quality crystal for single crystal measurements.

Results and discussion.

Electrochemical oxidation of tetraphenylphosphonium chloride in the presence of TCNQ produces the title compound. The mechanism involved is the electrochemical oxidation of the mixture at the desired galvanostatic conditions, and it evolves chlorine gas at the cathode. Hence in the solution the formation of TCNQ anions is enhanced. Single crystal structure analysis shows the compound is tetraphenylphosphonium tetracyanoquinodimethane ($\text{TPP}^+\text{TCNQ}^-$). The compound crystallizes in triclinic P -1 (2), with $a = 9.0942(8) \text{ \AA}$, $b = 13.1912(12) \text{ \AA}$, $c = 34.4598(30) \text{ \AA}$, $\alpha = 95.019(2)^\circ$, $\beta = 95.946(2)^\circ$, $\gamma = 91.635(2)^\circ$ and $V = 4092.96(63) \text{ \AA}^3$. The single crystal structure analysis shows a special type of anion disorder in the column of anions, which occurs in an alternating manner. This was observed when the data collection was carried out at room temperature. Attempts with low temperature measurements at 100K showed a phase transition.

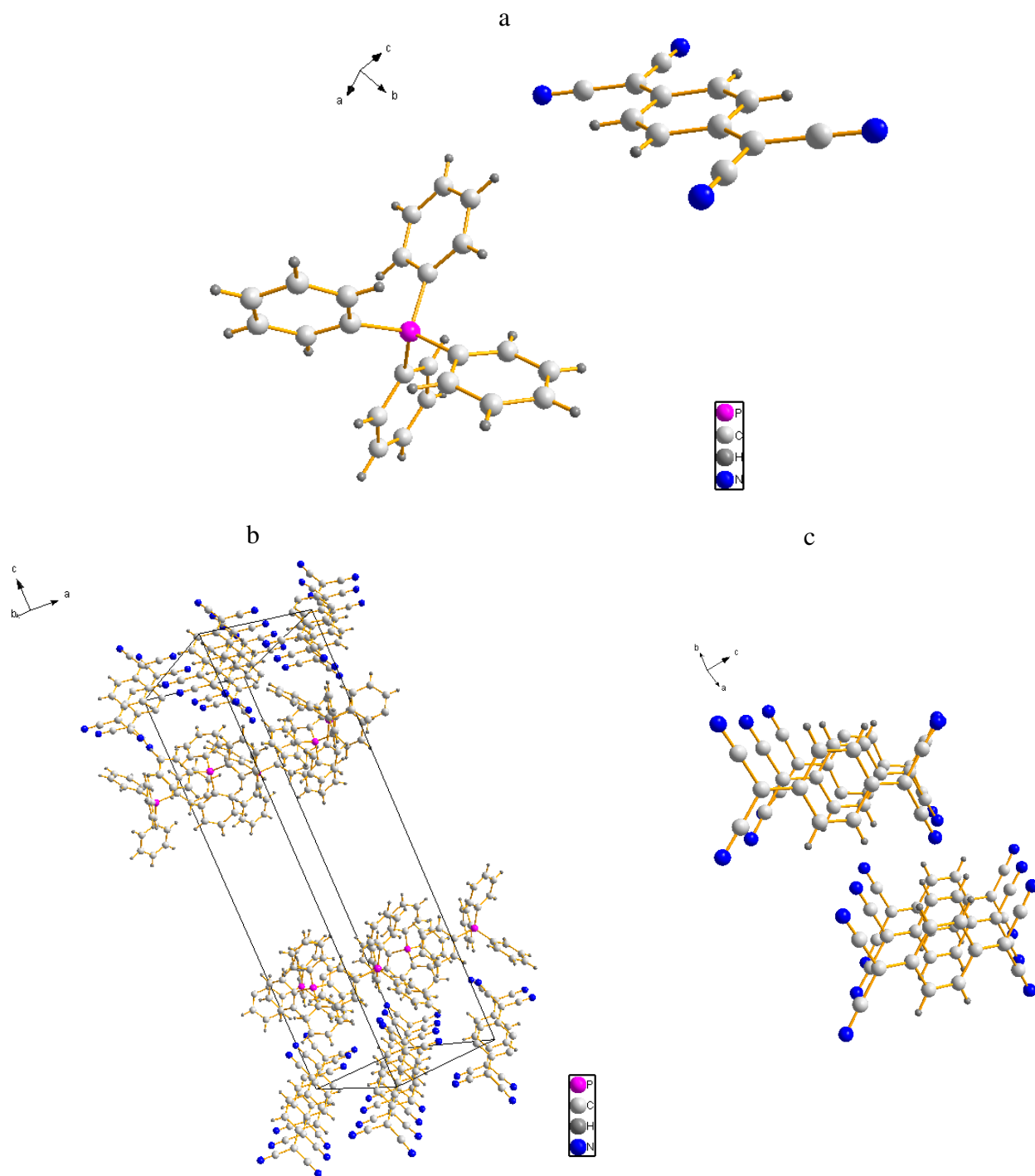


Figure 59. a, View of Tetrabutylphosphonium Tetracyanoquinomethane. b, Unit cell without the disordered TCNQ layer. c, Arrangement of TCNQ in ordered layers.

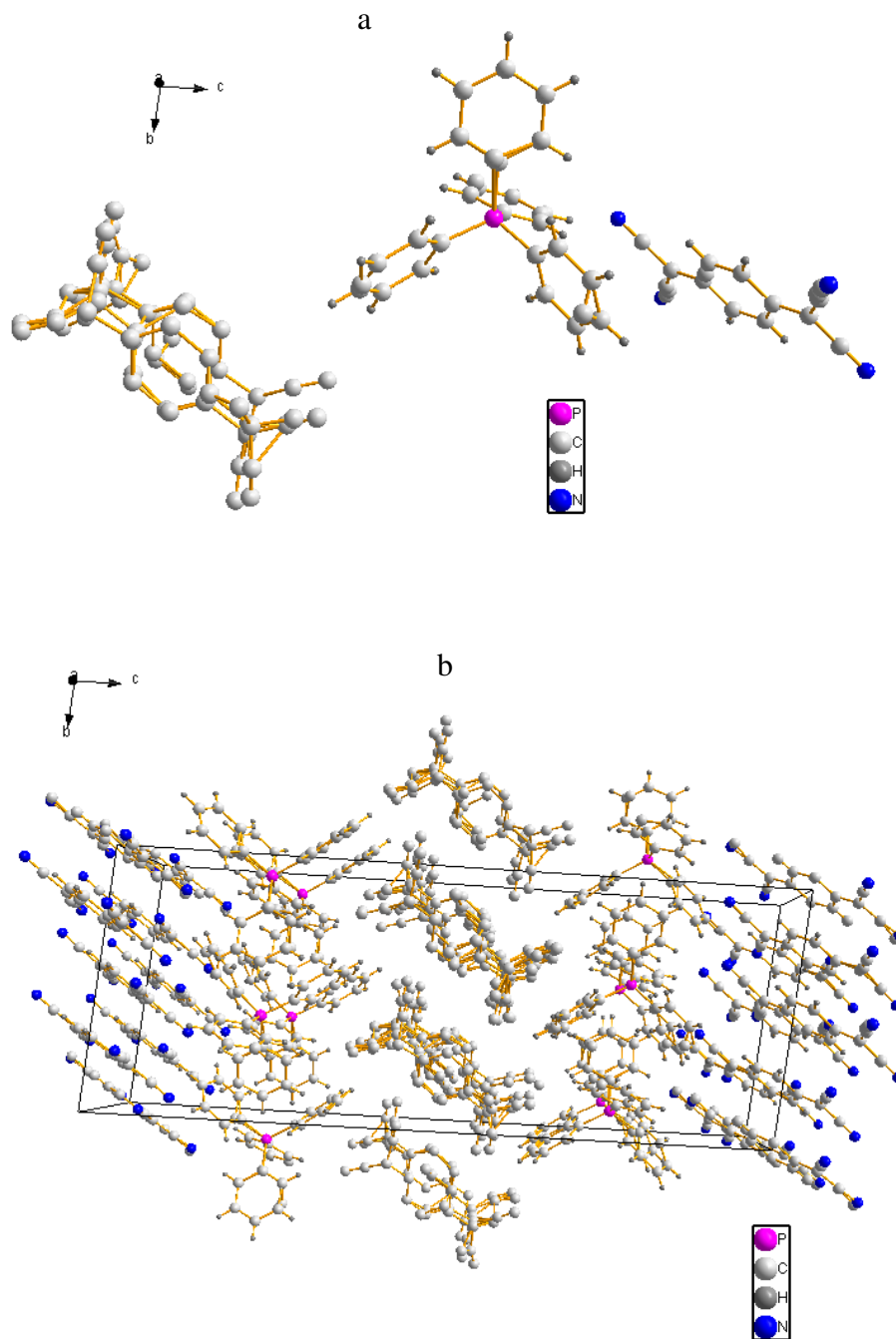


Figure 60. a, View of Tetracyanoquinodimethane b, unit cell with the disordered TCNQ layer.

The structure solution performed with the data collected at room temperature shows a structure with columns of cations and anions in an alternating manner. This is similar to that of TTF.TCNQ, NH₄TCNQ, Tetrabutylammonium TCNQ, and M.TCNQ (where M is an alkali metal cation). Also, the structure is different from that of tetrahexylammonium TCNQ as described in section 3.3.2. The interesting difference noticed here is the disorder in the TCNQ layer in an alternating fashion, shown in Figure 60. The intermolecular TCNQ distance in the ordered layer of TCNQ shows a distance of 3.49 Å. A unit cell structure of the compound is shown in Figure 60. The difficulty in structure solution with the rest of the Q peaks shows that a disordered TCNQ layer also results in high R values. The layers of tetraphenylphosphonium cations show an ordered structure. Thus experiments still have to be carried out so as to produce good quality single crystals and a structure solution. The table of atomic coordinates and displacement parameters are given in table 39, 40.

3.3.4. Electrochemical synthesis and crystal structure of Trimethyl Phenyl Phosphonium Tetracyanoquinodimethane.

Experimental

The same experimental procedure as used in the previous section in tetraphenylphosphonium TCNQ preparation, was employed. The difference lies in the lower solubility of trimethyl phenyl phosphonium chloride (TMPPC). But a saturated solution containing an excess of TMPPC at the bottom of the electrochemical cell allows the same molar concentration to be used, since as the reaction proceeds it undergoes complete dissolution. The electrooxidised solution is slowly evaporated to obtain good quality of single crystals.

Results and discussion

Electrochemical oxidation of trimethylphenylphosphonium chloride in the presence of TCNQ gave crystals of Trimethylphosphonium Tetracyanoquinodimethane. The galvanostatic current conditions had to be controlled to obtain the title product. Following several trials with many different crystals, the single crystal structural refinement was not successful with the data obtained by room temperature measurements. Due to the fact that the data quality obtained from the single crystals measurements was insufficient for structure solution, it exhibits huge disorder. A low-temperature measurement was attempted at 100 K, but it shows a phase change.

3.4. Electrocrystallization of $\text{Ag}_7\text{O}_8\text{HF}_2$ from aqueous medium without use of HF

Introduction

Cu and Ag show a marked difference in their oxidation stability. Silver exists mostly in mixed-valent states in oxides (AgO , Ag_2O_3 , Ag_3O_4). The clathrate phases of silver are in general formulated as $\text{Ag}_7\text{O}_8\text{X}$ ($\text{X} = \text{HSO}_4$, NO_3 , HF_2) and their syntheses and structures were reported [133-136]. These are mixed-valent compounds featuring the +2 and +3 oxidation states of silver. Also, several family members are reported to be superconducting: for example $\text{Ag}_7\text{O}_8\text{NO}_3$ (Tc at 1:04 K), $\text{Ag}_7\text{O}_8\text{BF}_4$ (Tc at 0:15 K), and $\text{Ag}_7\text{O}_8\text{HF}_2$ (Tc at 0:3{1:5 K). [137-139]. Moreover, clathrate-type copper oxide: $\text{Cu}_6\text{O}_8\text{MX}$ (M = copper, X = anion), which has a similar structure to $\text{Ag}_6\text{O}_8\text{MX}$, shows metallic and semiconducting resistivity behavior [140]. Here, the electrocrystallization of $\text{Ag}_7\text{O}_8\text{HF}_2$ from an HF-free aqueous solution containing the salts of silver in presence of CsF, is demonstrated. In comparison with other alkali metal fluorides CsF is known to be a facile fluoride ion donor. This readily facilitates the *in-situ* formation of HF at higher oxidation potential. When NaF was used in the electrocrystallization experiments Ag_3O_4 was formed. The cyclic voltammograms show the behaviour of different reaction baths. Ordinarily, $\text{Ag}_7\text{O}_8\text{HF}_2$ is only preparable from an aqueous HF medium via electrochemical oxidation of a silver salt, however in the following the preparation of the above compound from an HF-free aqueous medium is shown for the first time.

Experimental section

An aqueous solution containing AgPF_6 and CsF in water was electrochemically oxidized by galvanostatic and potentiostatic methods. Initially the cyclic voltammetric experiments were performed so as to probe how the given system behaves under the potentiodynamic conditions.

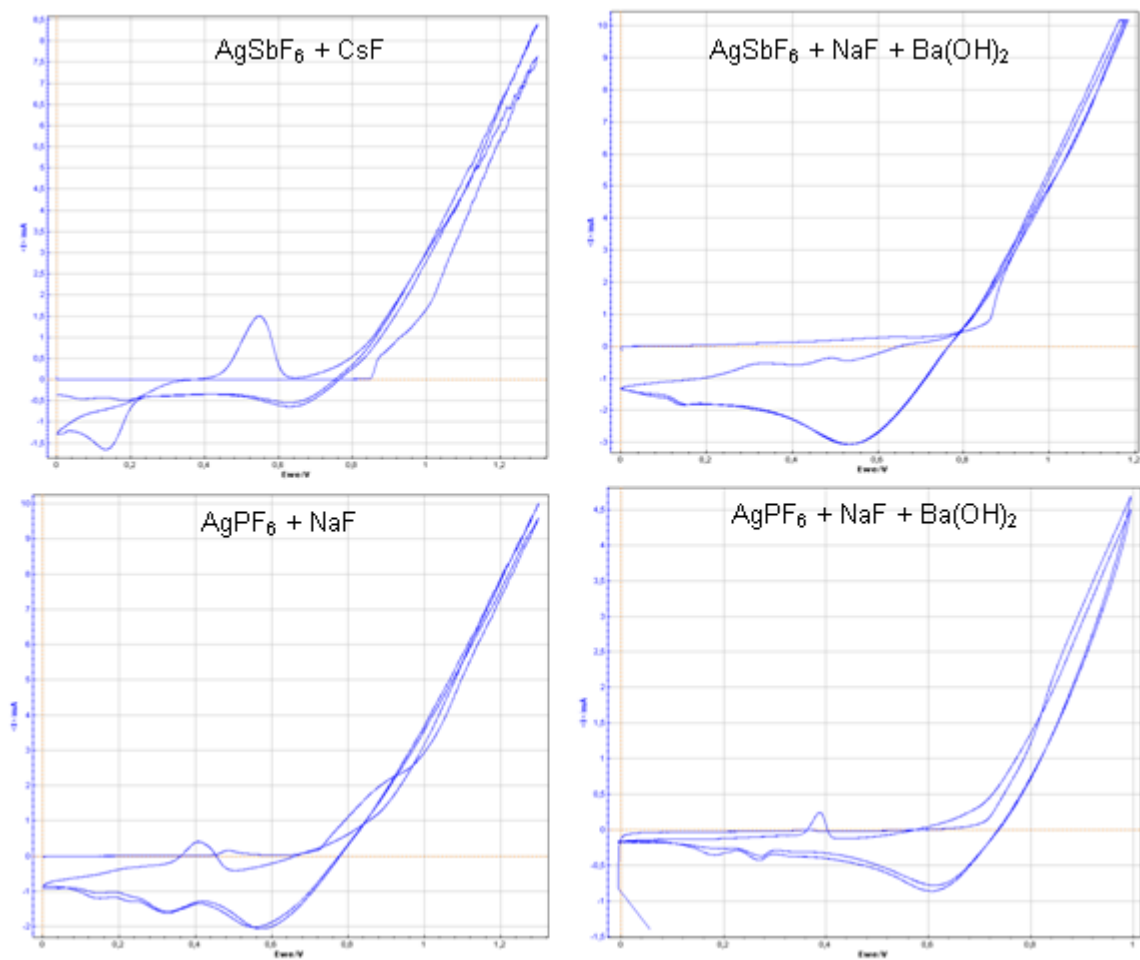


Figure 61. Cyclic voltammograms of aqueous solutions containing different mixtures, as mentioned along with the figure.

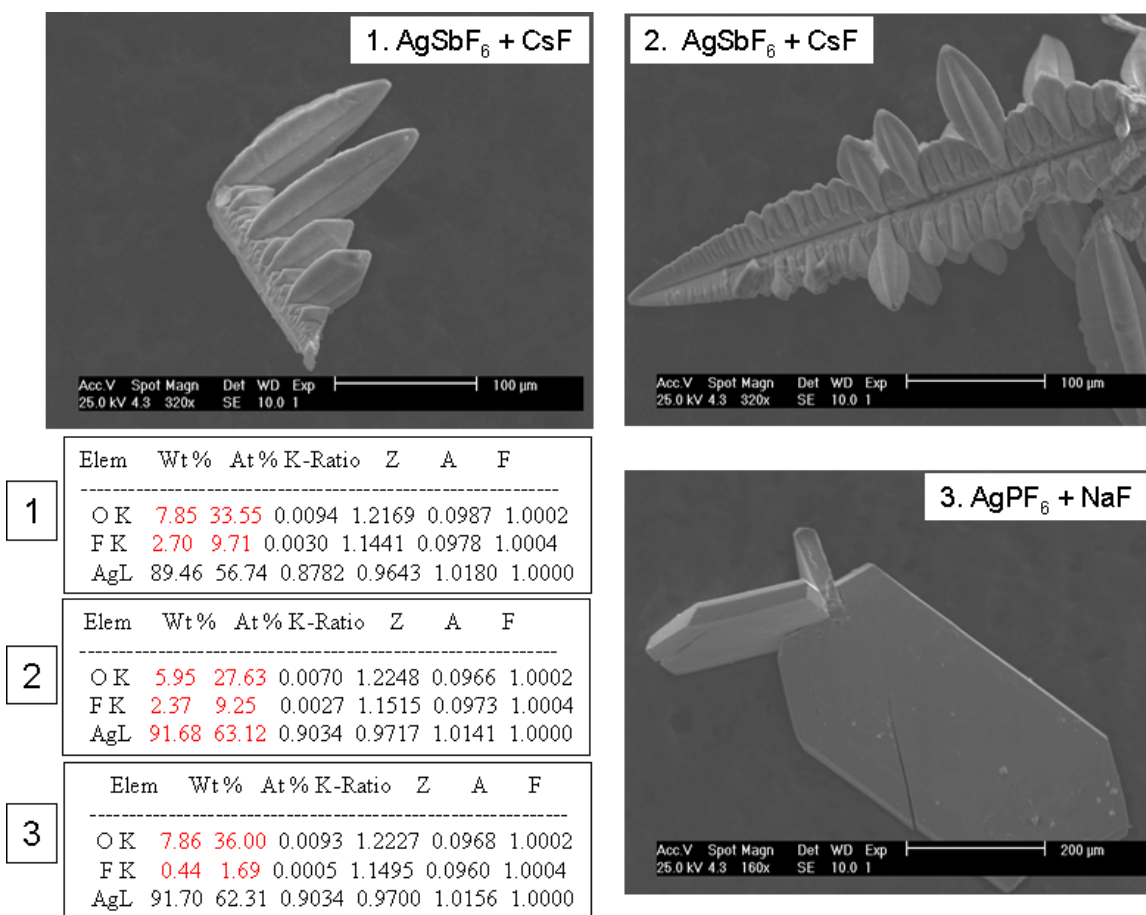


Figure 62. SEM micrographs of crystals obtained from different electrocrystallization experiments, conditions mentioned in the inset of the figure.

X-ray diffraction data collection was performed at room temperature using a Bruker-AXS APEX Smart-CCD diffractometer equipped with MoK α source with the crystal mounted on the tip of a glass capillary. The cell parameters were determined using reflections within the range $3.6 < \theta < 36.1^\circ$. The crystal structure was solved by the direct method (SHELXS-97) in the cubic Fm3m space group and refined by full matrix least squares (SHELXL-97) [11]. General information and details of the structure refinement are given in Table 16.

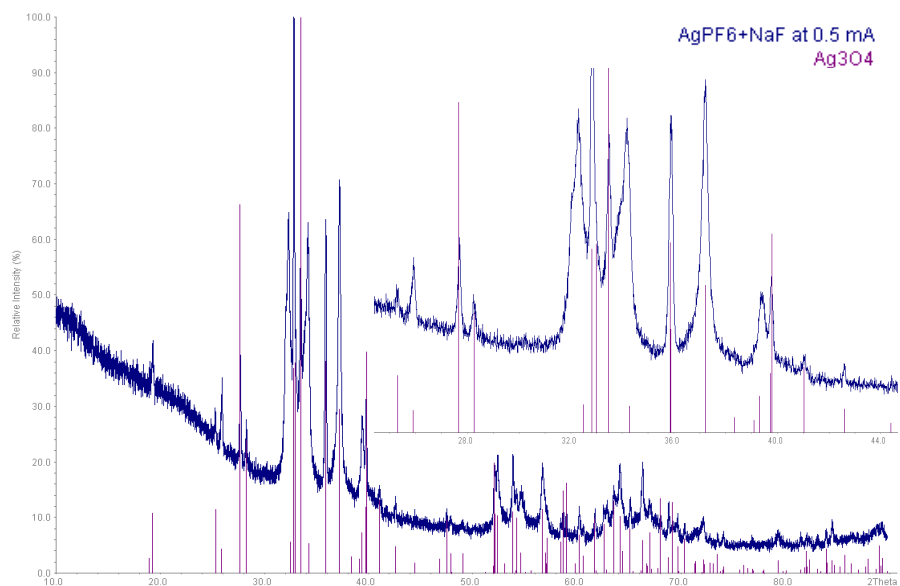


Figure 63. X-ray powder pattern of Ag_3O_4 prepared by electrooxidation of aqueous solution containing $\text{AgPF}_6 + \text{NaF}$.

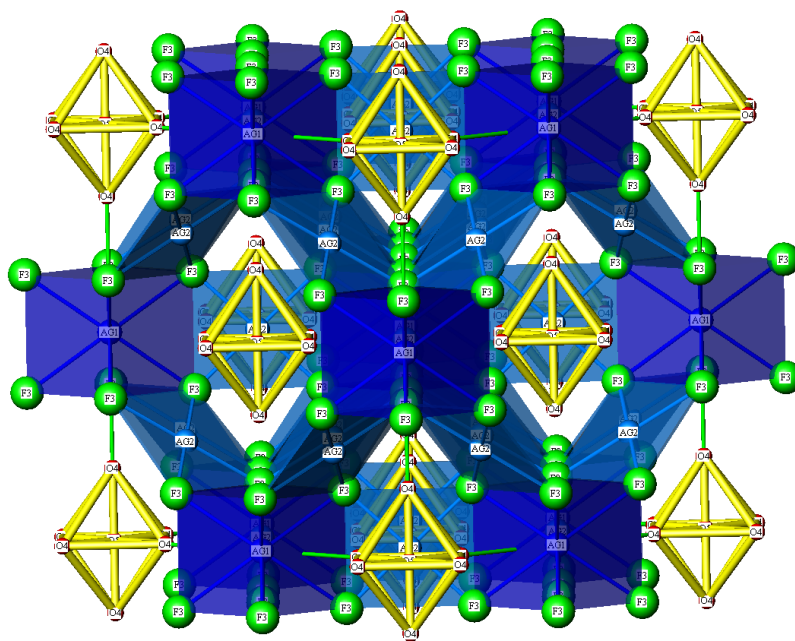


Figure 64. View of $\text{Ag}_7\text{O}_8\text{HF}_2$

Result and discussion

The cyclic voltammograms show vivid differences in line with the different electrolyte compositions as shown in Figure 58. Moreover, the crystal morphologies as observed through scanning electron micrographs, were seen to be very different (Figure 59). The EDAX analysis also confirms the fluorine content (Figure 59). The crystal structure analysis revealed that the crystals correspond to the clathrate phase, $\text{Ag}_7\text{O}_8\cdot\text{HF}_2$. The structure was indexed and solved within the cubic space group $\text{Fm}\bar{3}\text{m}$. This structure has also been discussed in early reports [133,134]. The clathrate phase features mixed-valent silver, in the +2 and +3 oxidation states. The cage-structured family of silver clathrates $\text{Ag}_7\text{O}_8\text{X}$, comprise a three-dimensional network of square planar AgO_4 units forming the surface of the cages. This is similar to the characteristic CuO_4 unit in cuprate superconductors. The silver oxides $\text{Ag}_6\text{O}_8\text{MX}$ (M = silver, X = anion) also have a clathrate-type structure which consists of face sharing Ag_6O_8 . The central cage is occupied by HF_2^- . The electrocrystallization in an HF-free aqueous medium is the most important feature to be noticed in this result. The alkali metal salt (CsF) used in the electrolytic bath acts as source of F^- . CsF is known to be a facile F^- ion donor among the alkali metal fluorides. Thus it is frequently employed in many organic syntheses. Caesium fluoride is also known to be a popular source of fluoride in organofluorine chemistry [141]. For example, it is reported that CsF gives higher yields in Knoevenagel condensation reactions than KF or NaF. This therefore helps to rationalize why the electrolytic bath containing CsF favoured the formation of $\text{Ag}_7\text{O}_8\cdot\text{HF}_2$. Thus a straightforward and moreover safe method for the synthesis of the title compound (which incidentally is also known to be superconducting with a very low T_c) by just varying the composition of electrolytic bath, has been demonstrated. By contrast, electrocrystallization carried out on an aqueous solution containing $\text{AgPF}_6 + \text{NaF}$ results in Ag_3O_4 formation, as shown in Figure 60. This nicely shows how the electrolytic mixture can be slightly tuned to obtain different products.

Table 16. Crystal data for $\text{Ag}_7\text{O}_8\cdot\text{HF}_2$

Chemical formula	$\text{Ag}_7\text{O}_8\text{HF}_2$
Formula weight (g/mol)	906.90
Crystal system	<i>Cubic</i>
Space group	Fm3m
a (Å)	9.8815 (4)
Z	16
V (Å ³)	964.87 (7)
T (K)	298
ρ_{calc} (g/cm ³)	3.990
λ (Å)	0.71073
F_{000}	1056
$R[F^2 > 2\sigma(F^2)]$ (%)	1.94
$wR(F^2)$ (%)	4.1
S	1.29
No. of reflections	4542
No. of independent reflections	155
No. of observed reflections [$I > 2(\sigma(I))$]	155
$R_{\text{int}}, R_{\text{sigma}}$ (%)	4.41, 1.55
No. of parameters	449
No. of restraints	477
$\Delta\rho_{\text{min}}, \Delta\rho_{\text{max}}$ (e Å ⁻³)	-2.87, 7.38
$(\Delta/\sigma)_{\text{mean}}, (\Delta/\sigma)_{\text{max}}$	<0.001, 0.04

Summary

The work carried out consists of four main divisions. (1) Coordination complexes containing silver in +2 oxidation state, (2) Electrochemical synthesis of phthalocyanine compounds, (3) Electrochemical synthesis of organic charge transfer crystals with TCNQ as anion and (4) Electrocrystallization of $\text{Ag}_7\text{O}_8\cdot\text{HF}_2$ from HF free aqueous media.

1. $\text{Ag}(4,4'$ dimethyl 2,2' bipyridine) $_2(\text{NO}_3)_2$

The potential-dependent electrocrystallization of (1) $\text{Ag}(4,4'$ dimethyl 2,2' bipyridine) $_2(\text{NO}_3)_2$ and (2) $\text{Ag}(4,4'$ – dimethyl - 2,2'-bipyridine) $(\text{NO}_3)_2$, from the same electrolytic bath, demonstrates for the first time that the coordination number of silver ions with respect to the ligands can be tuned by the electrocrystallization potential. The single crystal structure analysis [**1**: $C2/c$, $a = 18.6308(15)$ Å, $b = 14.5708(12)$ Å, $c = 11.5867(10)$ Å, $\beta = 126.5910(10)^\circ$, $Z = 4$, $R = 3.9\%$] shows divalent silver to be in an approximately square planar surrounding. The complex is paramagnetic following the Curie law, with magnetic moments of $1.86 \mu_B$.

2. $\text{Ag}(4,4'$ – dimethyl - 2,2' -bipyridine) $(\text{NO}_3)_2$

Single crystal structure analysis shows $P2_1/c$, $a = 8.5865(11)$ Å, $b = 11.0157(14)$ Å, $c = 16.4554(10)$ Å, $\beta = 111.102(10)^\circ$, $Z = 4$, $R = 3.5\%$]. The magnetic measurements show that the compound is paramagnetic and obeys the Curie law with magnetic moment $1.72 \mu_B$.

3. $\text{Ag}(2,2'$ -bipyridine) $(\text{NO}_3)_2$

Electrocrystallization performed at high oxidation potential results in the formation of title compound. The single crystal structure analysis [$P-1$, $a = 7.0000(14)$ Å, $b = 10.1450(2)$ Å, $c = 10.3830(10)$ Å, $\alpha = 113.440(3)^\circ$, $\beta = 100.220(3)^\circ$, $\gamma = 95.620(3)^\circ$, $Z = 2$, $V = 654.1(2)$ R = 11.7 %] shows divalent silver to be in an approximately square planar surrounding of 4+2 with weak axial coordination to the oxygen atoms of the neighbouring nitrate anions.

4. Ag(Tetramethyl tetraaza cyclotetradecane)(PF₆)₂(CH₃CN).

The electrochemical synthesis by a galvanostatic electro-oxidation method and the single crystal structure determination of a complex of silver(II) with a macrocyclic N donor ligand crystallized with hexafluorophosphate anions, is demonstrated. The single crystal analysis shows orthorhombic, *Pmcn* (62), $a = 10.140(5) \text{ \AA}$, $b = 15.071(5) \text{ \AA}$, $c = 17.956(5) \text{ \AA}$, $V = 2744.03(180) \text{ \AA}^3$, $Z = 4$, $R = 9.6 \%$. The crystal structure exhibits a penta-coordinated environment of silver(II) and displacement of the metal center from the rectangular planar configuration of the macrocyclic N donor, which is due to axial coordination by a solvent acetonitrile molecule. Both PF₆⁻ anions were modeled with twofold disorder.

5. *cis*- Coordinated Tetra pyridine Silver dinitrate.

Here, the electrocrystallization and the structural aspects of Ag^{II}(pyridine)₄(NO₃)₂ are presented. The crystal structure analysis of this hexacoordinated silver(II) complex gives *C21*, $a = 14.5872(17) \text{ \AA}$, $b = 11.0169(13) \text{ \AA}$, $c = 7.9723(9) \text{ \AA}$, $\beta = 119.46(0)^\circ$, $Z = 2$ ($R = 4.7 \%$). The divalent silver is coordinated with two nitrate anions in *cis* configuration. The two *cis* pyridine ligands are co-planar, while the other two other pyridines are coordinated in a *trans* manner and in a staggered conformation. The complex is paramagnetic following *Curie's* law with magnetic moments of μ_B .

6. Ag(2,2' Bipyridine)₂(ClO₄)₂

Electrocrystallization was done with the perchlorate salt to produce the title compound. The crystal analysis shows [*P*-1, $a = 7.949 \text{ \AA}$, $b = 10.233 \text{ \AA}$, $c = 14.639 \text{ \AA}$, $\alpha = 78.57(3)^\circ$, $\beta = 81.63(3)^\circ$, $\gamma = 79.60(3)^\circ$, $V = 1140.9(4) \text{ \AA}^3$, $Z = 2$, $R = 5.05\%$]. The divalent silver is weakly coordinated with perchlorate anions.

7. Ag(4,4'-dimethyl-2,2' Bipyridine)₂(ClO₄)₂

Electrocrystallization of the title compound was done from the perchlorate salt of silver. The quality of the crystal was not suitable for single crystal analysis. Powder X-ray

diffraction was used to determine the unit cell. The unit cell determined from the powder pattern indexing is monoclinic - $P2_1/m$, $a = 23.5063 \text{ \AA}$, $b = 5.8629 \text{ \AA}$, $c = 21.3368 \text{ \AA}$, $\beta = 93.092^\circ$, $R_{wp} = 4.9\%$

8. Lithium Phthalocyanine-Tetrabutylammonium Hexafluorophosphate

In this work, the electrochemical synthesis of the title compound, which is dependent on both solvent and the applied potential, is reported. Single-crystal X-ray diffraction structure analysis gives: triclinic, $P-1$, $a = 8.6423(4) \text{ \AA}$, $b = 12.8196(6) \text{ \AA}$, $c = 15.0189(7) \text{ \AA}$, $\alpha = 83.01(0)^\circ$, $\beta = 87.87(0)^\circ$, $\gamma = 74.45(0)^\circ$, $V = 1591.10 (13) \text{ \AA}^3$, $Z = 2$, $R = 5.05 \%$. In this structure, the lithium phthalocyanine shows enhanced distortion of the macrocyclic ring from planarity. The deviation from D_{4h} symmetry may be due to the steric effect induced by tetrabutylammonium hexafluorophosphate. The solid state spectrum of the compound shows a band shift towards shorter wavelengths relative to the Lithium Phthalocyanine radical.

9. Disodium Phthalocyanine (Na_2Pc)

Disodium phthalocyanine acts as precursor for monosodium phthalocyanine prepared by electrooxidation. It can be prepared in a similar procedure as for Li_2Pc , as it shows good solubility in dimethoxyethane. The indexing of powder pattern shows monoclinic $P2_1/m$, $a = 15.3104 \text{ \AA}$, $b = 6.0752 \text{ \AA}$, $c = 9.74626 \text{ \AA}$, $\beta = 122.901^\circ$.

10. Monosodium Phthalocyanine (NaPc)

Electrochemical oxidation of Na_2Pc gave the deposit of microcrystalline NaPc powder on the electrode surface. This is the second monovalent phthalocyanine compound characterised to date. The solvent plays an important role in electrosynthesis of NaPc . The compound shows Tetragonal, $P4/mcc$, $a = 13.8201(12) \text{ \AA}$, $c = 6.5348(5) \text{ \AA}$, $V = 1248.26(14) \text{ \AA}^3$.

11. Silver Phthalocyanine (AgPc)

Preparation of silver phthalocyanine from dilithium phthalocyanine resulted in the presence of metallic impurities. Other methods tailored to prepare the pure phase of silver(II) phthalocyanine were not successful.

12. Mercury Phthalocyanine

Mercury(II)phthalocyanine prepared from dilithium phthalocyanine shows microcrystalline nature. The solubility limitation of HgPc limits its further electrochemical characterization. The powder x-ray diffraction pattern was indexed in triclinic *P*-1, $a = 14.0744 \text{ \AA}$, $b = 11.9801 \text{ \AA}$, $c = 6.4760 \text{ \AA}$, $\alpha = 107.875^\circ$, $\beta = 88.476^\circ$, $\gamma = 102.107^\circ$, $R_{wp} = 5.74\%$

13. Hexadecafluorinated Phthalocyanine

Attempts made to synthesize dilithium hexadecafluorophthalocyanine using lithium metal and tetrafluorophthalonitrile resulted in the formation of LiF in the product. Direct synthesis of silver hexadecafluorophthalocyanine also failed due to poor reducing conditions. The electrochemical method of synthesis resulted in a poor yield and was not successful.

14. Tetrapropyl porphycene Tetracyanoquinodimethane

Herein the electrochemical synthesis of the title compound is demonstrated. The single crystal structure analysis [monoclinic, *P*1*n*1, $a = 14.2709(10) \text{ \AA}$, $b = 6.8742(5) \text{ \AA}$, $c = 18.9359(13) \text{ \AA}$, $\beta = 90.892(2)^\circ$, $V = 1857.4(2) \text{ \AA}^3$] shows the one-to-one stacking of donor TPP and acceptor TCNQ.

15. Tetrahexyl Ammonium Tetracyanoquinodimethane

Here the electrochemical synthesis of the title compound is presented. The crystal structure analysis shows triclinic, *P*-1, $a = 8.6423(4) \text{ \AA}$, $b = 12.8196(6) \text{ \AA}$, $c = 15.0189(7) \text{ \AA}$, $V = 1591.10(13) \text{ \AA}^3$, $Z = 2$, $R = 5.05\%$. Here TCNQ stack in a dimeric fashion unlike in Tetrabutylammonium TCNQ. Also, it is interesting to observe that at room temperature, there is disorder at just two carbon centers of only one alkyl group.

16. Tetrabutyl Ammonium Tetracyanoquinodimethane

Here in this crystal, TCNQ stack to form a column. The cations are disordered in the crystal with all four butyl moieties bearing split positions when the data collection was done at room temperature. The compound crystallizes in triclinic, $P-1$, $a = 7.9638(11) \text{ \AA}$, $b = 10.0950(14) \text{ \AA}$, $c = 16.106(20) \text{ \AA}$, $\alpha = 74.117(2)^\circ$, $\beta = 79.573(2)^\circ$, $\gamma = 80.033^\circ$, $V = 1214.34(86) \text{ \AA}^3$

17. Tetraphenylphosphonium Tetracyanoquinodimethane

Electrochemical oxidation of tetraphenylphosphonium chloride in presence of TCNQ produces the title compound. Single-crystal analysis shows a special type of anion disorder in an alternating manner. This was observed when the data collection was conducted at room temperature. Attempts at low temperature measurements at 100 K showed phase transitions. The compound crystallizes in triclinic, $P-1$ $a = 9.0942(8) \text{ \AA}$, $b = 13.1912(12) \text{ \AA}$, $c = 34.4598(30) \text{ \AA}$, $\alpha = 95.019(2)^\circ$, $\beta = 95.946(2)^\circ$, $\gamma = 91.635(2)^\circ$, $V = 4092.96(63) \text{ \AA}^3$.

18. Trimethylphenylphosphonium Tetracyanoquinodimethane

Electrochemical oxidation of trimethylphenylphosphonium chloride in the presence of TCNQ gave crystals of trimethylphosphonium tetracyanoquinodimethane crystals. The data quality obtained from the single-crystal measurements was not sufficient for structure solution because of the huge disorder. Low temperature measurements at 100 K showed a phase change.

19. $\text{Ag}_7\text{O}_8 \cdot \text{HF}_2$

The electrocrystallization of $\text{Ag}_7\text{O}_8 \cdot \text{HF}_2$ from an HF-free aqueous solution containing salts of silver and in the presence of CsF, is presented. Comparative studies of different electrolytic baths and their effect on product formation were performed. It is shown that among the various alkali metal fluorides, CsF is a facile fluoride ion donor. The cyclic voltammograms show the behaviour of different reaction baths.

Zusammenfassung

Die ausgeführte Arbeit besteht aus vier Hauptteilen: (1) Koordinationskomplexe mit Silber im +2 Oxidationszustand, (2) Die elektrochemische Synthese von Phthalocyaninverbindungen, (3) Die elektrochemische Synthese von organischen 'charge-transfer' Kristallen mit TCNQ als Anion und (4) Die Elektrokristallization von $\text{Ag}_7\text{O}_8 \cdot \text{HF}_2$ mittels HF-freien, wässrigen Medien.

1. $\text{Ag}(\text{4,4' dimethyl 2,2' bipyridine})_2 (\text{NO}_3)_2$

Die potenzialabhängige Elektrokristallizationen von **(1)** $\text{Ag}(\text{4,4' dimethyl 2,2' bipyridine})_2 (\text{NO}_3)_2$ und **(2)** $\text{Ag}(\text{4,4' - dimethyl - 2,2' -bipyridine}) (\text{NO}_3)_2$ aus dem selben elektrolytischen Bad belegen zum ersten Mal, dass die Koordinationszahl um das von von Liganden komplexierte Silberion, durch das Elektrokristallization Potential bestimmt werden kann. Die Einkristallstrukturanalyse [**1**: $C2/c$, $a = 18.6308(15) \text{ \AA}$, $b = 14.5708(12) \text{ \AA}$, $c = 11.5867(10) \text{ \AA}$, $\beta = 126.5910(10)^\circ$, $Z = 4$, $R = 3.9 \%$] deutet auf zweiwertiges Silber, das eine quasi quadratisch planare Koordination aufweist. Der Komplex ist paramagnetisch und folgt dem Curie gesetz, mit magnetischen momenten von $1.86 \mu_B$.

2. $\text{Ag}(\text{4,4' - dimethyl - 2,2' -bipyridine})(\text{NO}_3)_2$

Die Einkristallstrukturanalyse zeigt $P2_1/c$, $a = 8.5865(11) \text{ \AA}$, $b = 11.0157(14) \text{ \AA}$, $c = 16.4554(10) \text{ \AA}$, $\beta = 111.102(10)^\circ$, $Z = 4$, $R = 3.5\%$]. Die magnetische Messung zeigt, dass die Verbindung paramagnetisch ist und demnach das Curie Gesetz folgt, mit dem magnetischen Moment $1.72 \mu_B$.

3. $\text{Ag}(\text{2,2' -bipyridine})(\text{NO}_3)_2$

Elektrokristallization bei hohen Oxidationspotenzialen führten zu der Titelverbindung. Die Einkristallstrukturanalyse [$P-1$, $a = 7.0000(14) \text{ \AA}$, $b = 10.1450(2) \text{ \AA}$, $c = 10.3830(10)$

Å, $\alpha = 113.440(3)^\circ$, $\beta = 100.220(3)^\circ$, $\gamma = 95.620(3)^\circ$, $Z = 2$, $V = 654.1(2)$ Å³, $R = 11.7\%$ belegt die Anwesenheit von zweiwertigem Silber, welches eine quasi quadratisch planare Koordination von 4+2 aufweist, da eine schwache axiale Koordination zu den Sauerstoffatomen der benachbarten Nitratanionen vorliegt.

4. Ag(Tetramethyl tetraaza cyclotetradecane)(PF₆)₂(CH₃CN).

Wir präsentieren die elektrochemische Synthese mittels galvanostatic Electrooxidation und die darauf folgende Kristallstrukturbestimmung eines Komplexes von Silber(II) mit makrozyklischem N Spender ligand und hexafluorophosphat Anionen. Die Einkristallstrukturanalyse zeigt orthorhombisch *Pmcn* (62), $a = 10.140(5)$ Å, $b = 15.071(5)$ Å, $c = 17.956(5)$ Å, $V = 2744.03(180)$ Å³, $Z = 4$, $R = 9.6\%$. Die Kristallstruktur weist pentakoordiniertes Silber(II) auf, sowie auch eine Versetzung des Metallzentrums aus dem Zentrum der rechteckigen planaren Koordinatonsumgebung des makrozyklischen N Spenders, was durch die axiale Koordination eines Lösungsmittelmoleküls, d.h. ein Acetonitril Molekül, zurückzuführen ist. Beide PF₆⁻ Anionen wurden mit einer zweifachen Fehlordnung modelliert.

5. *cis*- Coordinated Tetra pyridine Silver dinitrate.

Wir präsentieren hier die Elektrokristallization und die strukturellen Aspekte von AgII (Pyridin)₄(NO₃)₂. Die Einkristallstrukturanalyse dieses hexacoordinated Silbers(II) Komplexes ergibt *C21*, $a = 14.5872(17)$ Å, $b = 11.0169(13)$ Å, $c = 7.9723(9)$ Å, $\beta = 119.46(0)^\circ$, $Z = 2$ ($R = 4.7\%$). Das zweiwertige Silber ist mit zwei *cis* Nitratanionen koordiniert. Während die zwei *cis* Pyridin Liganden koplanar liegen, sind die zwei *trans* Pyridin Liganden gestaffelt angegliedert. Der Komplex ist paramagnetisch und folgt dem Curie Gesetz mit magnetischen Momenten von μ_B .

6. Ag (2,2' Bipyridine)₂ (ClO₄)₂

Elektrokristallization mit einem Perchloratsalz führte zu der Titelverbindung. Die Einkristallstrukturanalyse zeigt *P-1*, $a = 7.949$ Å, $b = 10.233$ Å, $c = 14.639$ Å, $\alpha = 78.57(3)^\circ$, $\beta = 81.63(3)^\circ$, $\gamma = 79.60(3)^\circ$, $V = 1140.9(4)$ Å³, $Z = 2$ ($R = 5.05\%$). Das zweiwertige Silber wird mit Perchlorat Anionen schwach koordiniert.

7. Ag (4,4'-dimethyl-2,2' Bipyridine)₂ (ClO₄)₂

Elektrokristallization der Titel-Verbindung wurde vom Perchloratsalz des Silbers ausgehend erreicht. Die Qualität der Einkristalle waren jedoch für eine Einkristallstrukturanalyse unzureichend. Daher wurde mittels der Pulverröntgenbeugung die Einheitszelle bestimmt. Die daraus resultierende Zelle ist monoklin $P2_1/m$ mit $a = 23.5063 \text{ \AA}$, $b = 5.8629 \text{ \AA}$, $c = 21.3368 \text{ \AA}$, $\beta = 93.092^\circ$ ($R_{wp} = 4.9 \%$).

8. Lithium Phthalocyanine-Tetrabutylammonium Hexafluorophosphate

Hier wird die elektrochemische Synthese der Titel-Verbindung, was sich als Lösungsmittel- sowie auch Potentialabhängig erweist. Aus Einkristallstrukturanalyse ergibt sich: triklin $P-1$, $a = 8.6423(4) \text{ \AA}$, $b = 12.8196(6) \text{ \AA}$, $c = 15.0189(7) \text{ \AA}$, $\alpha = 83.01(0)^\circ$, $\beta = 87.87(0)^\circ$, $\gamma = 74.45(0)^\circ$, $V = 1591.10 (13) \text{ \AA}^3$, $Z = 2$ ($R = 5.05 \%$). In der Kristallstruktur weist das lithium phthalocyanin eine erhöhte Verzerrung des makrozyklischen Ringes von Planarität auf. Die Abweichung von der D_{4h} Symmetrie kann auf den sterischen Einfluss des tetrabutylammonium hexafluorophosphates zurückgeführt werden. Das Spektrum des festen Zustands dieser Verbindung zeigt eine Bandverschiebung zu kürzeren Wellenlängen im Vergleich zu dem lithium phthalocyanin Radikal.

9. Disodium Phthalocyanine (Na₂Pc)

Disodium phthalocyanin dient als Präkursor für Mononatrium phthalocyanine, und kann mittels Elektrooxidation in das Letztere umgewandelt werden. Da es wie Li₂Pc eine gute Löslichkeit in dimethoxyethane aufweist, kann es auf ähnliche Weise hergestellt werden. Pulverröntgenbeugungsdaten des Produktes führen zu monoklin $P2_1/m$, $a = 15.3104 \text{ \AA}$, $b = 6.0752 \text{ \AA}$, $c = 9.74626 \text{ \AA}$, $\beta = 122.901^\circ$.

10. Mononatrium Phthalocyanine (NaPc)

Die elektrochemische Oxidation von Na₂Pc führte zu der Ablagerung von mikrokristallem NaPc Pulver auf der Elektrode-Oberfläche. Dies ist die zweite

monovalente phthalocyanin Verbindung die bisher aufgeklärt worden ist. Zudem spielt das Lösungsmittel eine wichtige Rolle bei der Herstellung von NaPc. Die Verbindung kristallisiert tetragonal $P4/mcc$, $a = 13.8201(12) \text{ \AA}$, $c = 6.5348(5) \text{ \AA}$, $V = 1248.26(14) \text{ \AA}^3$.

11. Silber Phthalocyanine (AgPc)

Die Vorbereitung von Silber phthalocyanine ausgehend von dilithium phthalocyanine führte zu der Anwesenheit von metallischen Verunreinigungen. Weitere Vorgehensweisen die für die Herstellung von möglichst phasenreinem Silber(II) phthalocyanin angepasst wurden, scheiterten ebenfalls.

12. Quecksilber Phthalocyanine

Quecksilber(II) phthalocyanine von dilithium phthalocyanine ausgehend hergestellt weist eine mikrokristalline Natur auf. Weitere elektrochemische Charakterisierungen waren jedoch durch die begrenzte Löslichkeitsbeschränkung von HgPc nicht möglich. Aus Pulverröntgenbeugungsdaten war eine Indizierung im Triklinen $P-1$, mit $a = 14.0744 \text{ \AA}$, $b = 11.9801 \text{ \AA}$, $c = 6.4760 \text{ \AA}$, $\alpha = 107.875^\circ$, $\beta = 88.476^\circ$, $\gamma = 102.107^\circ$ (Rwp = 5.74 %) möglich.

13. Hexadecafluorinated Phthalocyanine

Versuche dilithium hecadecafluorophthlocyanine durch das Einsetzen von Lithiummetall und tetrafluorophthlonitrilen herzustellen liefen auf die Bildung von LiF im Produkt hinaus. Die direkte Synthese von silber hecadecafluorophthalocyanine versagte auch, in diesem Fall wegen der schlechten, reduzierenden Bedingungen. Die elektrochemische Synthese ergab eine schlechte Ausbeute und blieb unerfolgreich.

14. Tetrapropyl porphycene Tetracyanoquinodimethane

Hier wird die elektrochemische Synthese der Titelverbindung präsentiert. Die Einkristallstruktur Analyse [monoclinic, $P1n1$, $a = 14.2709(10) \text{ \AA}$, $b = 6.8742(5) \text{ \AA}$, $c = 18.9359(13) \text{ \AA}$, $\beta = 90.892(2)^\circ$, $V = 1857.4(2) \text{ \AA}^3$] belegt die eins-zu-eins Stapelung des Spenders TPP und des Annehmers TCNQ.

15. Tetrahexyl-Ammonium Tetracyanoquinodimethane

In diesem Teil wird die elektrochemische Synthese der Titelverbindung beschrieben. Die Einkristallstrukturanalyse ergibt triklin $P-1$, $a = 8.6423(4) \text{ \AA}$, $b = 12.8196(6) \text{ \AA}$, $c = 15.0189(7) \text{ \AA}$, $V = 1591.10 (13) \text{ \AA}^3$, $Z = 2$ ($R = 5.05 \%$). Im Gegensatz zu Tetrabutylammonium TCNQ sind hier die TCNQ in dimerischer Weise gestapelt. Interessant ist auch, dass bei Raumtemperatur eine Fehlordnung bei nur einer Alkylgruppe, und zwar an zwei Kohlenstoff Lagen, zu beobachten ist.

16. Tetrabutyl-Ammonium Tetracyanoquinodimethane

Hier sind die TCNQ gestapelt wodurch sich Säulen bilden. Auf Basis der Datenerfassung bei Raumtemperatur sind die Kationen in diesem Kristall fehlgeordnet und die vier Butyl Gruppen weisen Splitlagen auf. Die Verbindung kristallisiert in Triklin, $P-1$, $a = 7.9638(11) \text{ \AA}$, $b = 10.0950(14) \text{ \AA}$, $c = 16.106(20) \text{ \AA}$, $\alpha = 74.117(2)^\circ$, $\beta = 79.573(2)^\circ$, $\gamma = 80.033(1)^\circ$, $V = 1214.34(86) \text{ \AA}^3$

17. Tetraphenylphosphonium Tetracyanoquinodimethane

Die elektrochemische Oxidation des tetraphenylphosphonium Chlorids in der Anwesenheit von TCNQ erzeugt die Titelverbindung. Die Einkristallstrukturanalyse bei Raumtemperatur zeigt eine spezielle, alternierende Anion Fehlordnung. Versuche bei tieferen Temperaturmaßen um 100 K zeigen Phasenumwandlungen. Die Verbindung kristallisiert triklin $P-1$ $a = 9.0942(8) \text{ \AA}$, $b = 13.1912(12) \text{ \AA}$, $c = 34.4598(30) \text{ \AA}$, $\alpha = 95.019(2)^\circ$, $\beta = 95.946(2)^\circ$, $\gamma = 91.635(2)^\circ$, $V = 4092.96(63) \text{ \AA}^3$.

18. Trimethyl phenylphosphonium Tetracyanoquinodimethane

Die elektrochemische Oxidation des trimethylphenylphosphonium Chlorids in der Anwesenheit von TCNQ ergab Kristalle von Trimethylphosphonium Tetracyanoquinodimethane. Die Datenqualität der Einkristallmessungen war für die Strukturaufklärung bedingt durch die beträchtliche Fehlordnung unzureichend. Bei Tieftemperaturmessungen um 100 K erweist sich eine Phasenumwandlung.

19. $\text{Ag}_7\text{O}_8 \cdot \text{HF}_2$

Hier wird die Elektrokristallisation von $\text{Ag}_7\text{O}_8 \cdot \text{HF}_2$ aus einer HF-freien wässrigen Lösung, die nur Silbersalze und CsF enthält. Vergleichende Untersuchungen mit verschiedenen Reaktion elektrolytischen Bädern und die entsprechende Auswirkung auf die Produktbildung wurden auch unternommen. Dass unter den verschiedenen Alkalimetallfluoriden CsF ein sehr guter Fluorid-Ion-Spender ist, wird beobachtet. Die Zyklovoltammogramme belegen das Verhalten der verschiedenen Reaktionsbädern.

References

1. A. West, *Solid State Chemistry and its applications*, Wiley, New York, 1984.
2. A. F. Holleman, E. Wiberg, *Inorganic Chemistry*, 1st English edition, 2001.
3. *Inorganic materials synthesis and fabrication*, John N. Lalena, David A Cleary, Everett E Carpenter, Nancy F. Dean, John Wiley and sons, 2008.
4. *Electrochemical Methods: Fundamentals and Applications* Allen J Bard, Lerry R Faulkner, Ed. II, Marcel Dekker, 2001.
5. *Modern Electrochemistry 2A: Fundamentals of Electrodicts*, J.O.M. Bockris, Amulya K.N. Reddy, aroia Gamboa-Aldeco, *Electrochemistry*, Carl H. Hamann, Andrew Hamnett, Wolf Vielstich, Wiley –VCH 1998
6. *Inorganic electrochemistry, theory, practice and applications*, Piero Zanello, R.S.C publ. 2003.
7. Fischer H 1943 *Z. Electrochem.* 49, 343, 376, 1951
8. J.O'M. Bockris, G. A. Razumney, *Fundamental Aspects of electrocrystallization*, Plenum Press, New York, 1967.
9. F C Walsh and M E Herron, *J. Phys. D: Appl. Phys.* 24, 217-225, 1991.
10. P. Lustenberger, H. Rohrer, R. Christoph, H. Siegenthaler, *J. Electroanal. Chem.* 243, 225, 1988.
11. M.Paunovic, M. Schlesinger, *Fundamentals of electrochemical deposition*, Wiley-Interscience, New York, 1998.
12. D. P. Barkey, in *Advances in Electrochemical Science and Engineering*, Vol. 7, R. C. Alkire, D. M. Kolb (Eds.), Wiley-VCH, Weinheim, 2001.
13. G. Staikov, K. Ju'ttner, W. J.Lorenz, E. Budevski, *Electrochim.Acta* 1994, 39, 1019. W. Plieth, W. J. Lorenz (Eds.), *Electrochemical Nanotechnology*, Wiley-VCH, Weinheim, 1998.
14. D. M. Kolb, *Electrochim. Acta* 2000,45, 2387.
15. W. Freyland, C. A. Zell, S. Zein ElAbedin, F. Endres, *Electrochimica. Acta* 2003, 48, 3053.

16. Georgi Staikov and Alexander Milchev, *Electrocrystallization in Nanotechnology*. 2007 WILEY-VCH Verlag GmbH & Co. KGaA, Weinheim, 2007
17. G. H. Stout, L. H. Jensen, *X-ray Structure Determination*, 2nd ed., Wiley & Sons, New York, 1989.
18. K. Brandenburger, *Crystal-Impact, Diamond V 2.1, Program for Displaying Crystal Structures*, Bonn, 1998
19. Stoe & Cie, *X-Area: Software for IPDS, Version 1.16*, Darmstadt, 2002.
20. Siemens-Analytical-X-ray-Instruments, *SMART32, Version 5.618: Program for data collection*, Madison, WI, USA, 1997.
21. Stoe & Cie, *X-RED: Data reduction for STADI4 and IPDS, Version 1.22*, Darmstadt, 2001.
22. Siemens-Analytical-X-ray-Instruments, *SAINT32, Version 6.02: Program for data reduction*, Madison, WI, USA, 1999.
23. Stoe & Cie, *X-SHAPE: Crystal Optimisation for Numerical Absorption Correction Version 1.06*, Darmstadt, 1999.
24. G. M. Sheldrick, Bruker-AXS, *SADABS, Version 2.0: Area Detector Absorption Correction*, Madison, WI, USA, 2001.
25. G. M. Sheldrick, *SHELXS97, a program for the solution of crystal structures, computer program*, Universität Göttingen, Germany, 1997.
26. G. M. Sheldrick, Bruker-AXS, *SHELXTL, Version 6.12: Program for the Solution of Structures*, Madison, WI, USA, 2001.
27. V. Petricek, M. Dušek, *JANA2000 - crystallographic computing system*, Institute of Physics, Academy of the Czech Republic, Praha, 2000.
28. ICSD, *Inorganic Crystal Structure Database*, FIZ Karlsruhe.
29. ICDD-JCPDS, *Joint Committee on Powder Diffraction Standards*, Swartmore, USA.
30. A. C. Larson, R. B. von Dreele, *GSAS (Generalized Structure Analysis System)*, Los Alamos National Laboratory Report LAUR 86-748, Los Alamos National Laboratory; Los Alamos, NM, 1994, 86.
31. DASH is a commercial program available from the Cambridge Crystallographic Data Centre (CCDC, <http://www.ccdc.cam.ac.uk/>)
32. DIFFRAC^{plus} TOPAS, Bruker AXS,

33. P.E. Selwood, *Magnetochemistry*, 2nd Ed., Interscience, New York, 1956
34. U. Henseler, M. Jansen, *Sigma-Messung: Ein Programm zur Auswertung von elektrischen Messungen an Festkörpern*, Bonn, 1996.
35. U. Henseler, M. Jansen, *Sigma-Auswertung: Ein Programm zur Auswertung von elektrischen Messungen an Festkörpern*, Bonn, 1996.
36. B. A. Boukamp, *Equivalent Circuit (EQUIVCRT.PAS)*, Version 4.55: The Computer Assisted Electrochemical AC-Immitance Data Analysis System, University of Twente, Niederlande, 1997.
37. M.K. Wu, J.R. Ashburn, C.J. Torng, P.H. Hor, R.L.Meng, L. Gao, Z.J. Huang, Y.Q. Wang, C.W. Chu, *Phys. Rev. Lett.*, 1987, 58, 908.
38. Z. Z. Sheng, A. M. Hermann. *Nature*, 1988, 332, 138.
39. W. Grochala, R. Hoffmann, *Angew. Chem. Int. Ed.*, 2001, 40, 2742.
40. C. Farmer, F. T. Wang, R.A. Hawley-Fedder, P. R. Lewis, L. J. Summers, L. Foiles, *J. Electrochem. Soc.*, 1992, 139, 654.
41. H.N. Po, *Coord. Chem. Reviews*, 1976, 20, 171.
42. J.A. McMillan, *Chem. Reviews*, 1961, 62, 65.
43. B. Standke, M. Jansen, *Angew. Chem.*, 1985, 97, 114; *Angew. Chem. Int. Ed. Engl.*, 1985, 24, 118.
44. A. Jesih, K. Lutar, B. Zemva, B. Bachmann, S. Becker, B.G. Mueller, R. Hoppe, *Z. Anorg. Allg. Chem.*, 1990, 588, 77.
45. R.H. Odenthal, D. Paus, *Z. Anorg. Allg. Chem.*, 1974, 407, 144.
46. R.H.Odenthal, R. Hoppe, *Monatshefte fuer Chemie* 1971, 102, 1340.
47. K.Yvon, A. Bezinge, P. Tissot, P. Fischer, *J. of Solid State Chem.*, 1986, 65, 225.
48. D. Gantar, I. Leban, B. Frlec, J.H. Holloway. *J. of the Chem. Soc. Dalton Transactions, Inorg. Chem.*, 1987, 1987, 2379.
49. C.H.Wong, T.-H. Lu, C.N. Chen, T.-J. Lee. *J. Inorganic and Nuclear Chemistry* **1972**, 34, 3253.
50. R. Fischer, B.G. Mueller, *Z. Anorg. Allg. Chem.*, 2002, 628, 2592.
51. B. Zemva, K. Lutar, A. Jesih, W.J.jr. Casteel, A.P. Wilkinson, D.E. Cox, R.B. von Dreele, H. Borrmann, N. Bartlett, *J. Am. Chem. Soc.*, 1991, 113, 4192.
52. R. Hoppe, R. Hoffmann, *Z. Anorg. Allg. Chem.*, 1970, 379, 193.

53. S.E. McLain, M.R. Dolgos, D. Alan Tennant, J.F.C. Turner, T. Barnes, T. Proffen, B.C. Sales, R.I. Bewley, *Nature Mat.*, 2006, 5, 561.
54. B. Zemva, K. Lutar, A. Jeshi, W.J. Casteel, A.P. Wilkinson, D.E. Cox, R.B. Von Dreele, H. Bormann, N. Bartlett, *J. Am. Chem. Soc.*, 1991, 113, 4192.
55. P. Mailnowski, Z. Mazej, W. Grochala, *Z. Anorg. Allg. Chem.*, 2008, 634, 2608.
56. D. Karweik, N. Winograd, *J. Am. Chem. Soc.*, 1974, 96, 2, 591.
57. F. Kneubuehl, W.S. Caughey, W.S. Koski, *J. Am. Chem. Soc.*, 1961, 83, 7, 1607,
58. T. Kobayashi, D. Huppert, K.D. Straub, P.M. Rentzepis, *J. Chem. Phys.*, 1979, 70, 4, 1720.
59. R.G. Swisher, D.J. Stuehr, J. Knox, B.M. Fox, E.L. Blinn, *J. Coord. Chem.*, 1989, 20, 2, 101.
60. E.K. Barefiel, M.T. Mocella, *Inorg. Chem.*, 1973, 12, 12, 2829.
61. G.A. Bowmaker, S. Effendy, B.W. Marfua, Skelton, A.H. White, *Inorg. Chim. Acta*, 2005, 358, 4371.
62. B. Standke, M. Jansen, *Angew. Chem.*, 1986, 98, 76; *Angew. Chem. Int. Ed. Engl.* 1986, 25, 77.
63. J.L. Atwood, M.L. Simms, D.A. Zatzko, *Cryst. Struct. Comm.* 1973, 2, 279.
64. W. Grochala, *J. Mol. Model*, 2008, 14, 887.
65. K.M. Kadish, X.Q. Lin, J.Q. Ding, Y.T. Wu and C. Araullo, *Inorg. Chem.* 1986, 25, 3236.
66. H. Furuta, T. Ogawa, Y. Uwatoko and K. Araki, *Inorg. Chem.*, 1999, 38, 2676.
67. H. N. Po, E. Brinkman, R. J. Doedens, *Acta. Cryst. Sect. C.*, 1991, C47, 2310.
68. Fowles G. W. A., Matthews R. W., Walton .R. A., *J. Chem. Soc. A*, 1968, 1108
69. Richard V. Biagetti, William G. Bottjer, Helmut M. Haendler, *Inorg. Chem.*, 1966, 5, 3, 379.
70. *The Phthalocyanines: Properties and Applications*, Vol. 3 ed., C.C. Leznoff and A.B.P. Lever, VCH, New York, 1993, 1, 69.
71. R. A. Collins, K. A. Mohammed, *J. Phys. D*, 1988, 21, 142.
72. C. Hamann, M. Hietschold, A. Mrwa, M. Mueller, M. Starke, R. Kilper, *Top. Mol. Organ. Eng.*, 1991, 7, 129.
73. B. W. Flynn, A. E. Owen, J. Mayor, *J. Phys. C*, 1977, 10, 4051.

74. A. H.Ghosh, D. L. Morel, T. Feng, R. F.Shaw, C. A. Rowe, *J. Appl. Phys.*, 1974, *1*, 20.
75. M. Sunil, O. Bertha, P. Su-Moon; I. David, D. Narayan. *J. Electrochem. Soc.*, 1995, 142, 1436.
76. J. H. Zagal, *Coord. Chem. Rev.*, 1992, 119, 89.
77. A. L.Thomas, *Phthalocyanine Research and Applications*; CRC Press: Boca Raton, FL, 1990.
78. R. Madru, G. Guillaud, M. Sadoun, M. Maitrot, J. J.Andre, J. Simon, R. Even, *Chem. Phys. Lett.*, 1988, 145, 343.
79. M. Maitrot, G. Guillaud, B. Boudjema, J. J. Andre, H. Strzelecka, J. Simon, R. Even, *Chem. Phys. Lett.*, 1987, 133, 59.
80. G. de la Torre, T. Torres, F. Agullo-Lopez, *Adv. Mater.*, 1997, 9, 3, 265
81. J. Martinsen, S.M. Palmer, J. Tanaka, R.C. Greene, B.M. Hoffman, *Phys. Rev. B* 1984, 30, 6269.
82. S. Heutz, C. Mitra, W. Wu, A. J. Fisher, A. Kerridge, M. Stoneham, T. H. Harker, J. Gardener, H-H. Tseng, T.S. Jones, C. Renner, G. Aeppli, *Adv. Mater.* 2007, 19, 3618
83. *The Porphyrin Handbook, Volume 20 / Phthalocyanines: Structural Characterization*, by Michael Klaus Engel, E d. Karl M. Kadish, Kevin M. Smith, Roger Guilard, Academic press, 2002
84. J. S. Shirk, R. G. S. Pong, S. R. Flom, H. Heckmann, M. Hanack, *J. Phys.Chem. A*, 2000, 104, 1438.
85. M. Hanack, T. Schneider, M. Barthel, J. S. Shrink, S. R. Flom, R. G. S. Pong, *Coord. Chem. Rev.*, 2001, 235, 219.
86. J. W. Perry, K. Mansour, I. Y. S. Lee, X. L. Wu, P. V. Bedworth, C. T. Chen, D. Ng, S. R. Marder, P. Miles, T. Wada, M. Tian, H. Sasabe, *Science*, 1996, 273, 1533.
87. Y. Chen, L. R. Subramanian, M. Barthel, M. Hanack, *Eur. J. Inorg. Chem.*, 2002, 1032.
88. A. B. P. Lever, P. C. Minor, *Inorg. Chem.*, 1981, 20, 4015.
89. H.Sugimoto, M.Mori, H.Masuda, T.Tagu, *J. Chem. Soc., Chem. Comm.*, 1986, 962.
90. J.A. Cissell and T.P. Vaid, *Inorg. Chem.* 2007, 46, 11, 4360.
91. G. Ilangovan, J.L. Zweier, P. Kuppusamy, *J. Phys. Chem.*, 2000, 104, 4047.

92. M. Brinkmann, C. Chaumont, H. Wachtel, J.J. Andre, *Thin Solid Films*, 1996, 283, 97.
93. M. Brinkmann, J.C. Wittmann, C. Chaumont, J.J. Andre, *Thin Solid Films*, 1997, 292, 192.
94. P. Turek, J-J. Andre, A. Giraudeau, J. Simon, *Chemical Physics Letters*, 1987, 134, 5, 471.
95. M. Sumimoto, S. Sakaki, S. Matsuzaki, H. Fujimoto, *Dalton Trans.*, 2003, 32.
96. P. Turek, J-J. Andre, *Solid State Communications*, 1987, 63, 8, 741.
97. M. Dumm, M. Niklas, A. Loidi, *Synthetic Metals*, 1999, 103, 2070.
98. S. L. Gilat, Thomas W. Ebbsen, *J. Phys. Chem.*, 1993, 97, 3551.
99. M. Dumm, M. Dressel, M. Niklas, P. Lunkenheimer, A. Loidl, M. Weiden, F. Steglich, B. Assmann, H. Homborg, P. Fulde. *Eur. Phys. J. B*, 1998, 6, 317.
100. E. Ortl, J.L. Bredas, C. Clarisse, *J. Chem. Phys.*, 1990, 92, 2, 1228.
101. X. Liu, L-C. Xu, T-J. He, D-M. Chen, F.C. Liu, *Chemical Physics Letters*, 2003, 379, 517.
102. S. Kandaiah, N. Munichandraiah, L.G Scanlon, *J. Electrochem. Soc.*, 2005, 152, 11, C756.
103. H. Homborg, W. Kalz, *Z. Anorg. Allg. Chem.*, 1984, 514, 115.
104. H. Homborg, C.L. Teske, *Z. Anorg. Allg. Chem.*, 1985, 527, 45.
105. *Organic Electrochemistry: An introduction and a Guide*, II Ed. Manuel M. Baizer, Henning Lund, Marcel Dekker, New York, 1983
106. Serena Margadonna, Kosmas Prassides, Yoshihiro Iwasa, Yasujiro Taguchi, Monica F. Craciun, Sven Rogge, and Alberto F. Morpurgo, *Inorg. Chem.*; 2006; 45(26); 10472-10478.
107. Julie A. Cissell and Thomas P. Vaid, *Inorg. Chem.*, 2007, 46 (11), 4360–4361.
108. Leznoff.C.C., McArthur. C.R., *Ain. Y., J. Chem.*, 1993, 71, 1319.
109. Leznoff c.c., Hall. T.W., *Tetrahedron Lett.*, 1982, 23, 3023.
110. Synthesis of substituted phthalocyanines, Victor N. Nemykina, Evgeny A. Lukyanets, *ARKIVOC: Free journal of Organic Chemistry* 2010 (i) 136-208
111. D. Jerome, H.J. Schulz, *Advances in physics*, 1982, 31, 4, 299-490.
112. D. Jerome, *Science*, 1991, 252, 5012, 1509.

113. M. Adam, K. Mullen, *Adv. Mater.* 1994, 6, 439.
114. E. Coronado, P. Day, *Chem. Rev.* 2004, 104, 11, 5419.
115. D. Jerome, *Chem. Rev.* 2004, 104, 11, 5565.
116. P.W. Anderson, P.A. Lee, M. Saitoh, *Solid state comm.*, 1973, 13, 5, 595.
117. T. Ishiguro, K. Yamaji, and G. Saito, *Organic Superconductors*, Second Edition, Springer-Verlag, Berlin, 1998
118. D. S. Acker, R. J. Harder, W. R. Hertler, W. Mabiler, L. R. Melby, R. E. Benson and W. E. Mochel, *J. Am. Chem. Soc.* 1960, 82, 6408.
119. F. Wudl, G. M. Smith and E. J. Hufnagel, *Chem. Comm.* 1970, 13, 1453.
120. E. Vogel, M. Kocher, H. Schmickler, J. Lex, *Angew. Chem., Int. Ed. Engl.* 1986, 25, 257.
121. H. Ofir, A. Regev, H. Levanon, E. Vogel, M. K6cher and M. Balci, *J. Phys. Chem.*, 1987, 91, 2686.
122. J. Schliipmann, M. Huber, M. Toporowicz, M. K6cher, E. Vogel, H. Levanon and K. M6bius, *J. Am. Chem. Soc.*, 1988, 110, 8566.
123. M.W. Renner, A. Forman, W. Wu, C.K. Chang and J. Fajer, *J. Am. Chem. Soc.*, 1989, 111, 8618.
124. J.P. Gisselbrecht, M. Gross, M. Kocher, M. Lausmann and E. Vogel, *J. Am. Chem. Soc.*, 1990, 112, 8618.
125. C. Bernard, J. P. Gisselbrecht, M. Gross, E. Vogel, M. Lausmann, *Inorg. Chem.*, 1994, 33, 2393
126. K.M. Kadish, E. van Caemelbecke, P. Boulas, F. D'Souza, E. Vogel, M. Kisters, C.J. Medford and K.M. Smith, *Inorg. Chem.*, 1993, 32, 4177.
127. K.M. Kadish, P. Boulas, F. D'Souza, M.A. Aukauloo, R. Guilard, M. Lausmann and E. Vogel, *Inorg. Chem.*, 1994, 33, 471.
128. C. Bernard, J.P. Gisselbrecht, M. Gross, E. Vogel and M. Lausmann, *Inorg. Chem.*, 1994, 33, 2393.
129. Hayashi, T., Okazaki, K., Urakawa, N., Shimakoshi, H., Sessler, J. L., Vogel, E. & Hisaeda, Y. *Organometallics*, 2001, 20, 3074.
130. J.S. Miller, A.H. Reis, E. Gebert, J.J. Ritsko, W.R. Salaneck, T.W. Kovnat, R.P. Cape, *J. Am. Chem. Soc.* 1979, 101, 7111.

131. Hayao Kobayashi, *Acta Cryst. B* 1978, 34, 2818.
132. Kistenmacher, T. J., Philips, T. E., Cowan, D. O. *Acta Cryst. B* 1974, 30, 763.
133. J. Selbin, *J. Inorg. Nucl. Chem.* 1961, 20, 91.
134. I. Náray-Szabó and K. Popp: *Z. Anorg. Allg. Chem.* 1963, 322, 286.
135. I. Náray-Szabó, G. Argay, and P. Szabó: *Acta Crystallogr.* 1965, 19, 180.
136. Ph.D thesis , B. Standke, University of Hannover, 1986.
137. M. B. Robin, K. Andres, T. H. Geballe, N. A. Kuebler, and D. B. McWhan, *Phys. Rev. Lett.* , 1966, 17, 917.
138. A. Gossard, D. Hindermann, M. Robin, N. Kuebler, and T. Geballe: *J. Am. Chem. Soc.* 1967, 89, 7121.
139. M. M. Conway, N. E. Phillips, T. H. Gebelle, and N. A. Kuebler: *J. Phys. Chem. Solids* 1970, 31, 2673.
140. K. Budhita, *Physica C*. 1991, 185–189, 2728.
141. Fiorenza, M; Mordini, A; Papaleo, S; Pastorelli, S; Ricci, A, *Tetrahedron Letters* 1985, 26, 787.

Appendix

Table 17. Fractional atomic coordinates and isotropic or equivalent isotropic displacement parameters (\AA^2) for $\text{Ag}(\text{DMBPY})_2(\text{NO}_3)_2$

Atom	X	y	z	$U_{\text{iso}}^*/U_{\text{eq}}$
Ag1	0.5000	0.864345 (15)	0.7500	0.05382 (9)
N1	0.39612 (11)	0.84645 (12)	0.52026 (18)	0.0523 (3)
C2	0.31166 (12)	0.85836 (11)	0.47621 (19)	0.0448 (3)
C3	0.23987 (13)	0.84839 (14)	0.3330 (2)	0.0528 (4)
H3	0.1819	0.8556	0.3050	0.063*
C4	0.25402 (14)	0.82768 (16)	0.2306 (2)	0.0580 (4)
C5	0.34073 (15)	0.81441 (18)	0.2790 (2)	0.0661 (5)
H5	0.3530	0.7995	0.2143	0.079*
C6	0.40969 (14)	0.82314 (18)	0.4230 (2)	0.0631 (5)
H6	0.4679	0.8124	0.4538	0.076*
C7	0.17718 (19)	0.8209 (2)	0.0744 (2)	0.0828 (7)
H7A	0.1793	0.8715	0.0233	0.124*
H7B	0.1220	0.8227	0.0636	0.124*
H7C	0.1811	0.7643	0.0361	0.124*
N8	0.62448 (10)	0.88557 (12)	0.77596 (17)	0.0510 (3)
C9	0.63102 (14)	0.90915 (17)	0.6709 (2)	0.0595 (5)
H9	0.5788	0.9157	0.5781	0.071*
C10	0.71148 (14)	0.92408 (15)	0.6940 (2)	0.0607 (5)
H10	0.7130	0.9376	0.6171	0.073*
C11	0.78988 (13)	0.91893 (15)	0.8312 (2)	0.0582 (4)
C12	0.78217 (12)	0.89849 (15)	0.9410 (2)	0.0558 (4)
H12	0.8333	0.8963	1.0357	0.067*
C13	0.69965 (12)	0.88136 (12)	0.91124 (19)	0.0462 (3)
C14	0.87945 (16)	0.9357 (2)	0.8627 (3)	0.0829 (8)
H14A	0.8752	0.9266	0.7768	0.124*
H14B	0.9224	0.8936	0.9355	0.124*

7. Appendix

H14C	0.8981	0.9975	0.8961	0.124*
N3	0.5000	0.6382 (2)	0.7500	0.0690 (8)
O1	0.5000	0.5547 (2)	0.7500	0.1081 (11)
O2	0.53649 (14)	0.68141 (18)	0.7070 (3)	0.0968 (6)
N4	0.5000	1.0981 (3)	0.7500	0.0722 (7)
O3	0.4510 (2)	1.0531 (3)	0.6428 (2)	0.1403 (12)
O4	0.5000	1.1798 (3)	0.7500	0.1369 (18)

Table 18. Anisotropic displacement parameters ($\text{pm}^2 \times 10^{-1}$) for $\text{Ag}(\text{DMBPY})_2(\text{NO}_3)_2$. The anisotropic displacement factor exponent takes the form: $-2\pi^2 [h^2 a^* U^{11} + \dots + 2 h k a^* b^* U^{12}]$

Atom	U^{11}	U^{22}	U^{33}	U^{12}	U^{13}	U^{23}
Ag1	0.03091 (9)	0.08553 (17)	0.03645 (10)	0.000	0.01545 (7)	0.000
N1	0.0352 (6)	0.0757 (10)	0.0409 (7)	-0.0027 (6)	0.0199 (6)	-0.0072 (6)
C2	0.0337 (7)	0.0580 (9)	0.0366 (7)	-0.0011 (6)	0.0177 (6)	-0.0010 (6)
C3	0.0368 (8)	0.0719 (11)	0.0385 (8)	-0.0039 (7)	0.0164 (7)	-0.0020 (7)
C4	0.0505 (9)	0.0736 (12)	0.0404 (8)	-0.0089 (9)	0.0219 (7)	-0.0056 (8)
C5	0.0584 (11)	0.0924 (16)	0.0496 (10)	-0.0111 (11)	0.0334 (9)	-0.0153 (10)
C6	0.0450 (9)	0.0926 (15)	0.0527 (10)	-0.0056 (10)	0.0296 (8)	-0.0154 (10)
C7	0.0689 (15)	0.117 (2)	0.0405 (10)	-0.0072 (15)	0.0206 (10)	-0.0108 (12)
N8	0.0355 (6)	0.0732 (9)	0.0373 (7)	-0.0031 (6)	0.0180 (6)	0.0021 (6)
C9	0.0471 (9)	0.0834 (14)	0.0411 (8)	-0.0059 (9)	0.0225 (7)	0.0042 (9)
C10	0.0574 (11)	0.0767 (13)	0.0524 (10)	-0.0044 (9)	0.0352 (9)	0.0075 (9)
C11	0.0461 (9)	0.0675 (12)	0.0632 (11)	-0.0008 (8)	0.0337 (9)	0.0087 (9)
C12	0.0347 (7)	0.0752 (11)	0.0492 (9)	0.0003 (8)	0.0205 (7)	0.0073 (8)
C13	0.0348 (7)	0.0600 (9)	0.0392 (7)	0.0007 (6)	0.0196 (6)	0.0020 (6)
C14	0.0545 (12)	0.110 (2)	0.0934 (19)	0.0025 (12)	0.0491 (13)	0.0251 (16)
N3	0.0327 (11)	0.090 (2)	0.0621 (17)	0.000	0.0160 (11)	0.000
O1	0.123 (3)	0.087 (2)	0.099 (2)	0.000	0.058 (2)	0.000
O2	0.0635 (11)	0.1227 (17)	0.1045 (16)	0.0077 (12)	0.0503 (11)	0.0189 (14)
N4	0.0706 (18)	0.094 (2)	0.0599 (16)	0.000	0.0433 (15)	0.000

7. Appendix

O3	0.147 (3)	0.179 (3)	0.0559 (12)	-0.054 (2)	0.0395 (15)	-0.0041 (15)
O4	0.162 (4)	0.087 (2)	0.254 (6)	0.000	0.173 (5)	0.000

Table 19. Fractional atomic coordinates and isotropic or equivalent isotropic displacement parameters (\AA^2) for $\text{Ag}(\text{DMBPY})_2(\text{NO}_3)_2$. $U(\text{eq})$ is defined as one third of the trace of the orthogonalized U_{ij} tensor.

Atom	x	Y	z	$U_{\text{iso}}^*/U_{\text{eq}}$
Ag(1)	2716(1)	9181(1)	1924(1)	49(1)
N(1)	927(4)	7935(3)	1124(2)	43(1)
C(2)	112(6)	7108(4)	1411(3)	51(1)
C(3)	-999(6)	6316(4)	865(3)	53(1)
C(4)	-1313(5)	6344(4)	-24(3)	42(1)
C(5)	-442(5)	7211(4)	-305(3)	42(1)
C(6)	645(4)	8001(3)	261(2)	36(1)
C(7)	1550(5)	8971(3)	2(2)	36(1)
C(8)	1357(5)	9215(3)	-855(2)	40(1)
C(9)	2217(5)	10155(3)	-1064(3)	39(1)
C(10)	3243(5)	10859(4)	-388(3)	42(1)
C(11)	3394(5)	10590(4)	454(3)	42(1)
N(12)	2580(4)	9666(3)	650(2)	38(1)
C(13)	-2537(6)	5505(4)	-645(3)	59(1)
C(14)	2053(6)	10381(4)	-1990(3)	53(1)
N(3)	3932(5)	11431(3)	2778(2)	50(1)
O(1)	4614(4)	10458(3)	2629(2)	55(1)
O(2)	2405(4)	11565(3)	2396(2)	70(1)

7. Appendix

O(3)	4823(5)	12172(3)	3290(2)	74(1)
N(4)	3264(5)	8212(3)	3619(2)	52(1)
O(4)	4073(5)	7707(4)	3235(3)	87(1)
O(5)	2118(5)	8903(4)	3149(2)	81(1)
O(6)	3563(5)	8083(4)	4384(2)	85(1)

Table 20. Anisotropic displacement parameters ($\text{pm}^2 \times 10^{-1}$) for compounds B. The anisotropic displacement factor exponent takes the form: $-2\pi^2 [h^2 a^{*2} U^{11} + \dots + 2 h k a^* b^* U^{12}]$ $\text{Ag}(\text{DMBPY})(\text{NO}_3)_2$

	U^{11}	U^{22}	U^{33}	U^{12}	U^{13}	U^{23}
AG1	0.05846	0.05100	0.03338	-0.00674	0.01090	-0.00196
N1	0.04844	0.03849	0.03865	0.00077	0.01332	0.00163
C2	0.06641	0.04427	0.04192	-0.00169	0.02042	0.00685
C3	0.06038	0.04104	0.06268	-0.00322	0.02816	0.00876
C4	0.03875	0.03596	0.05016	0.00341	0.01381	0.00215
C5	0.04402	0.04439	0.03757	0.00272	0.01310	0.00013
C6	0.03434	0.03735	0.03444	0.00620	0.01183	0.00152
C7	0.03535	0.03319	0.03681	0.00336	0.00880	-0.00025
C8	0.03878	0.04059	0.03722	0.00292	0.01012	-0.00198
C9	0.03691	0.03797	0.04227	0.00727	0.01427	0.00649
C10	0.03891	0.03736	0.05281	0.00108	0.01927	0.00439
C11	0.03826	0.04072	0.04411	0.00005	0.01238	-0.00360
N12	0.03528	0.03899	0.03792	0.00524	0.01027	0.00041
C13	0.05134	0.05403	0.06607	-0.01349	0.01350	-0.00315
C14	0.06194	0.05545	0.04519	-0.00175	0.02254	0.00579
N3	0.05890	0.05277	0.03863	0.00018	0.01733	-0.00358
O1	0.04886	0.05582	0.05232	0.00496	0.00698	-0.01025
O2	0.05300	0.07117	0.07347	0.01052	0.00825	-0.00930
O3	0.08036	0.07233	0.06405	-0.01361	0.01804	-0.02885

7. Appendix

N4	0.06535	0.04005	0.04499	-0.00823	0.01285	-0.00246
O4	0.10071	0.08614	0.07554	0.02223	0.03229	-0.00720
O5	0.08473	0.08283	0.06278	0.02999	0.01031	0.00005
O6	0.11022	0.09822	0.04183	-0.02506	0.02251	0.00936

Table 21. Fractional atomic coordinates and isotropic or equivalent isotropic displacement parameters (\AA^2) for Ag(BPY)(NO₃)₂

Atom	x	y	z	U _{iso} */U _{eq}
Ag1	0.22289 (17)	0.40090 (13)	0.55309 (12)	0.0422 (5)
N1	0.2530 (16)	0.5471 (12)	0.7763 (11)	0.035 (2)
C2	0.269 (3)	0.6904 (19)	0.8277 (16)	0.053 (4)
H2	0.2683	0.7340	0.7641	0.064*
C3	0.288 (3)	0.781 (2)	0.9761 (17)	0.065 (5)
H3	0.3075	0.8819	1.0106	0.078*
C4	0.278 (3)	0.713 (2)	1.0685 (17)	0.062 (5)
H4	0.2826	0.7681	1.1656	0.075*
C5	0.259 (3)	0.559 (2)	1.0120 (18)	0.059 (4)
H5	0.2585	0.5124	1.0733	0.071*
C6	0.242 (2)	0.4764 (17)	0.8652 (14)	0.044 (3)
C7	0.229 (2)	0.3177 (18)	0.7982 (16)	0.047 (3)
C8	0.213 (3)	0.2276 (19)	0.8741 (19)	0.057 (4)
H8	0.2079	0.2695	0.9708	0.068*
C9	0.203 (3)	0.0777 (18)	0.8031 (19)	0.073 (6)
H9	0.1880	0.0184	0.8510	0.087*
C10	0.217 (3)	0.0178 (19)	0.661 (2)	0.067 (5)

7. Appendix

H10	0.2077	-0.0826	0.6116	0.081*
C11	0.244 (3)	0.110 (2)	0.592 (2)	0.060 (4)
H11	0.2626	0.0698	0.4987	0.072*
N12	0.2442 (17)	0.2568 (12)	0.6588 (12)	0.041 (3)
N3	0.266 (2)	0.1882 (15)	0.2712 (14)	0.054 (3)
O1	0.1161 (16)	0.2391 (13)	0.3302 (11)	0.055 (3)
O2	0.421 (2)	0.194 (2)	0.3470 (17)	0.096 (5)
O3	0.218 (3)	0.1307 (17)	0.1348 (15)	0.101 (6)
N4	0.2614 (18)	0.5952 (12)	0.4030 (15)	0.049 (3)
O4	0.1723 (18)	0.5814 (12)	0.4874 (12)	0.059 (3)
O5	0.3643 (17)	0.5080 (13)	0.3403 (13)	0.059 (3)
O6	0.222 (2)	0.6949 (14)	0.3568 (14)	0.068 (3)

Table 22. Atomic displacement parameters (\AA^2) for $\text{Ag}(\text{BPY})(\text{NO}_3)_2$

Atom	U^{11}	U^{22}	U^{33}	U^{12}	U^{13}	U^{23}
Ag1	0.0417 (7)	0.0503 (7)	0.0421 (6)	0.0135 (4)	0.0176 (4)	0.0227 (5)
N1	0.039 (6)	0.038 (6)	0.036 (5)	0.013 (5)	0.018 (5)	0.018 (5)
C2	0.059 (10)	0.062 (10)	0.040 (8)	0.016 (8)	0.005 (7)	0.026 (7)
C3	0.096 (15)	0.063 (11)	0.043 (8)	0.028 (10)	0.026 (9)	0.022 (8)
C4	0.070 (12)	0.078 (12)	0.043 (9)	0.014 (9)	0.024 (8)	0.026 (8)
C5	0.059 (10)	0.085 (13)	0.052 (9)	0.020 (9)	0.026 (8)	0.041 (9)
C6	0.042 (8)	0.065 (9)	0.035 (7)	0.023 (7)	0.017 (6)	0.026 (7)
C7	0.028 (7)	0.064 (10)	0.052 (8)	0.007 (6)	0.019 (6)	0.024 (7)
C8	0.067 (11)	0.061 (10)	0.056 (9)	0.013 (8)	0.019 (8)	0.035 (8)

7. Appendix

C9	0.124 (18)	0.040 (9)	0.054 (10)	0.009 (9)	0.001 (10)	0.030 (8)
C10	0.091 (14)	0.043 (9)	0.082 (13)	0.016 (9)	0.039 (11)	0.033 (9)
C11	0.080 (12)	0.060 (10)	0.070 (10)	0.034 (9)	0.035 (9)	0.045 (9)
N12	0.038 (6)	0.040 (6)	0.046 (6)	-0.003 (5)	0.019 (5)	0.018 (5)
N3	0.057 (9)	0.055 (8)	0.047 (7)	0.009 (6)	0.017 (6)	0.016 (6)
O1	0.043 (6)	0.067 (7)	0.050 (6)	0.008 (5)	0.019 (5)	0.019 (5)
O2	0.083 (11)	0.131 (14)	0.092 (11)	0.054 (10)	0.044 (9)	0.050 (10)
O3	0.172 (18)	0.082 (10)	0.053 (8)	0.032 (10)	0.045 (9)	0.023 (7)
N4	0.043 (7)	0.029 (6)	0.076 (9)	0.007 (5)	0.033 (7)	0.015 (6)
O4	0.065 (8)	0.049 (6)	0.055 (6)	0.015 (5)	0.027 (6)	0.008 (5)
O5	0.050 (6)	0.070 (8)	0.069 (7)	0.021 (5)	0.032 (5)	0.032 (6)
O6	0.085 (9)	0.071 (8)	0.069 (8)	0.024 (7)	0.026 (7)	0.044 (7)

Table 23. Fractional atomic coordinates and isotropic or equivalent isotropic displacement parameters (\AA^2) $\text{Ag}^{\text{II}}(\text{TMTACTD})(\text{PF}_6)_2$

Atom	x	y	Z	$U_{\text{iso}}^*/U_{\text{eq}}$	Occ. (<1)
P2	0.1318 (2)	0.0477 (2)	0.7906 (3)	0.0549 (16)	0.52
F7	0.1148 (6)	0.0403 (7)	0.9446 (4)	0.106 (5)	0.52
F8	0.0706 (5)	-0.0294 (5)	0.7621 (9)	0.145 (6)	0.52
F9	0.0673 (4)	0.1231 (5)	0.7776 (9)	0.073 (3)	0.52
F10	0.1485 (5)	0.0559 (6)	0.6369 (4)	0.061 (3)	0.52
F11	0.1930 (3)	0.1246 (4)	0.8185 (9)	0.0493 (18)	0.52
F12	0.1963 (5)	-0.0272 (5)	0.8039 (11)	0.110 (4)	0.52

7. Appendix

P2A	0.11868 (19)	0.0438 (2)	0.8487 (3)	0.0317 (7)	0.48
F7A	0.1608 (4)	0.0601 (6)	0.9858 (4)	0.044 (2)	0.48
F8A	0.0506 (3)	-0.0039 (4)	0.9258 (7)	0.050 (2)	0.48
F9A	0.0765 (4)	0.1391 (3)	0.8620 (8)	0.045 (2)	0.48
F10A	0.0767 (5)	0.0262 (6)	0.7122 (5)	0.064 (3)	0.48
F11A	0.1872 (3)	0.0918 (5)	0.7741 (7)	0.054 (2)	0.48
F12A	0.1591 (4)	-0.0519 (3)	0.8320 (11)	0.065 (3)	0.48
P1	0.00809 (5)	0.39531 (6)	0.3141 (4)	0.02372 (15)	
N5	0.1495 (2)	0.9753 (2)	0.3104 (13)	0.0415 (8)	
F1	0.0041 (4)	0.2897 (3)	0.3409 (7)	0.087 (3)	0.64
F2	0.0091 (4)	0.3750 (4)	0.1603 (5)	0.0495 (19)	0.64
F3	0.0105 (3)	0.4994 (3)	0.2854 (8)	0.076 (3)	0.64
F4	0.0037 (4)	0.4126 (5)	0.4673 (6)	0.073 (3)	0.64
F3A	0.0059 (8)	0.4839 (5)	0.4040 (9)	0.046 (3)	0.36
F2A	0.0091 (8)	0.4576 (6)	0.1869 (8)	0.053 (3)	0.36
F1A	0.0113 (9)	0.3084 (5)	0.2271 (9)	0.063 (4)	0.36
F4A	0.0169 (7)	0.3362 (6)	0.4444 (8)	0.049 (3)	0.36
C15	0.1124 (11)	1.0325 (10)	0.345 (2)	0.045 (4)	0.56
C16	0.0717 (8)	1.1201 (8)	0.3541 (14)	0.049 (3)	0.56
H16A	0.0487	1.1257	0.4398	0.074*	0.56
H16B	0.0329	1.1227	0.2873	0.074*	0.56
H16C	0.1071	1.1690	0.3410	0.074*	0.56
C15A	0.1140 (10)	1.0388 (10)	0.2913 (18)	0.024 (3)	0.44
C16A	0.0622 (10)	1.1068 (11)	0.2308 (17)	0.045 (4)	0.44

7. Appendix

H16A	0.0487	1.1257	0.4398	0.074*	0.56
H16B	0.0329	1.1227	0.2873	0.074*	0.56
H16C	0.1071	1.1690	0.3410	0.074*	0.56
C15A	0.1140 (10)	1.0388 (10)	0.2913 (18)	0.024 (3)	0.44
C16A	0.0622 (10)	1.1068 (11)	0.2308 (17)	0.045 (4)	0.44
H16D	0.0533	1.1553	0.2923	0.068*	0.44
H16E	0.0146	1.0783	0.2090	0.068*	0.44
H16F	0.0850	1.1307	0.1519	0.068*	0.44
C1	0.3109 (6)	0.7842 (6)	0.5518 (10)	0.058 (3)	
H1A	0.3434	0.8072	0.6216	0.069*	
H1B	0.3365	0.7315	0.5155	0.069*	
C8	0.3201 (6)	0.7836 (7)	0.0783 (10)	0.064 (3)	
H8A	0.3625	0.7996	0.0212	0.076*	
H8B	0.3359	0.7345	0.1362	0.076*	
C3	0.1795 (5)	0.6960 (7)	0.5451 (12)	0.061 (2)	
H3A	0.2043	0.6478	0.4959	0.073*	
H3B	0.1447	0.6680	0.6074	0.073*	
C6	0.1952 (6)	0.7029 (7)	0.0703 (9)	0.069 (3)	
H6A	0.2215	0.6543	0.1165	0.082*	
H6B	0.1624	0.6746	0.0051	0.082*	
C10	0.3766 (3)	0.8502 (5)	0.3491 (7)	0.058 (2)	
H10A	0.4216	0.8757	0.3906	0.069*	
H10B	0.3871	0.7868	0.3300	0.069*	
C2	0.2386 (7)	0.7483 (10)	0.6203 (12)	0.084 (4)	

7. Appendix

H2A	0.2553	0.7099	0.6927	0.101*
H2B	0.2132	0.8002	0.6595	0.101*
C11	0.3057 (4)	0.9485 (4)	0.4974 (8)	0.0489 (15)
H11A	0.2617	0.9527	0.5536	0.073*
H11B	0.3008	0.9908	0.4258	0.073*
H11C	0.3506	0.9624	0.5476	0.073*
C14	0.2718 (6)	0.9401 (5)	0.0685 (9)	0.071 (2)
H14A	0.2585	0.9918	0.1214	0.107*
H14B	0.2288	0.9223	0.0160	0.107*
H14C	0.3136	0.9555	0.0115	0.107*
C9	0.3626 (3)	0.8986 (5)	0.2229 (8)	0.064 (2)
H9A	0.3561	0.9629	0.2404	0.077*
H9B	0.4064	0.8913	0.1654	0.077*
C12	0.0863 (6)	0.8104 (7)	0.5207 (15)	0.070 (4)
H12A	0.0585	0.8462	0.4576	0.105*
H12B	0.1147	0.8499	0.5779	0.105*
H12C	0.0512	0.7752	0.5724	0.105*
C7	0.2527 (7)	0.7567 (9)	-0.0009 (8)	0.081 (3)
H7A	0.2286	0.8113	-0.0343	0.098*
H7B	0.2701	0.7219	-0.0766	0.098*
C4	0.0793 (3)	0.7073 (5)	0.3678 (8)	0.0596 (19)
H4A	0.0395	0.7504	0.3455	0.072*
H4B	0.0560	0.6572	0.4154	0.072*
C5	0.1153 (4)	0.6719 (4)	0.2423 (8)	0.0581 (18)

7. Appendix

H5A	0.1559	0.6297	0.2636	0.070*	
H5B	0.0776	0.6401	0.1896	0.070*	
Ag	0.215090 (12)	0.821688 (15)	0.3140 (3)	0.02081 (6)	
N1	0.3116 (3)	0.8554 (5)	0.4441 (7)	0.0478 (16)	
N4	0.2944 (4)	0.8635 (4)	0.1562 (7)	0.0536 (19)	
N2	0.1364 (4)	0.7522 (5)	0.4540 (8)	0.052 (2)	
N3	0.1465 (5)	0.7502 (4)	0.1665 (7)	0.053 (2)	
C13	0.0965 (9)	0.8174 (8)	0.0898 (15)	0.092 (5)	
H13A	0.0632	0.8484	0.1502	0.139*	
H13B	0.0666	0.7850	0.0258	0.139*	
H13C	0.1282	0.8609	0.0455	0.139*	
F6	0.09887 (14)	0.3951 (3)	0.3180 (7)	0.0614 (9)	
F5	-0.08276 (13)	0.3960 (2)	0.3104 (7)	0.0477 (6)	

Table 24. Atomic displacement parameters (\AA^2) for Ag(TMTACTD) (PF₆)₂

Atom	U ¹¹	U ²²	U ³³	U ¹²	U ¹³	U ²³
P2	0.065 (2)	0.0292 (15)	0.071 (4)	-0.0084 (14)	0.045 (3)	-0.0138 (19)
F7	0.139 (9)	0.081 (7)	0.098 (8)	0.017 (7)	0.057 (7)	0.012 (6)
F8	0.159 (9)	0.104 (7)	0.173 (11)	-0.088 (7)	0.037 (7)	-0.035 (7)
F9	0.037 (4)	0.091 (6)	0.091 (8)	0.006 (4)	-0.005 (4)	-0.038 (5)
F10	0.068 (6)	0.065 (6)	0.051 (5)	0.008 (5)	-0.006 (4)	-0.022 (5)
F11	0.033 (3)	0.064 (4)	0.051 (4)	-0.004 (3)	0.010 (5)	-0.014 (6)
F12	0.159 (8)	0.082 (6)	0.090 (7)	0.071 (6)	0.043 (8)	0.000 (7)
P2A	0.0323 (13)	0.0233 (14)	0.0395 (16)	-0.0003 (10)	0.0053 (12)	0.0044 (13)

7. Appendix

F7A	0.034 (3)	0.057 (5)	0.041 (5)	0.002 (3)	-0.006 (3)	-0.001 (4)
F8A	0.047 (4)	0.042 (4)	0.061 (5)	-0.014 (3)	-0.002 (4)	0.005 (4)
F9A	0.026 (3)	0.029 (3)	0.081 (6)	0.011 (3)	0.002 (3)	0.010 (3)
F10A	0.078 (6)	0.058 (5)	0.056 (5)	-0.004 (5)	-0.011 (5)	0.018 (4)
F11A	0.043 (4)	0.053 (5)	0.066 (6)	-0.003 (4)	0.018 (4)	0.008 (4)
F12A	0.089 (5)	0.029 (3)	0.078 (7)	0.018 (3)	0.022 (6)	0.006 (4)
P1	0.0233 (3)	0.0273 (4)	0.0205 (3)	0.0074 (3)	-0.0009 (11)	-0.0012 (9)
N5	0.0398 (17)	0.0359 (16)	0.049 (2)	0.0103 (14)	0.002 (5)	-0.001 (5)
F1	0.128 (6)	0.038 (3)	0.096 (7)	0.034 (3)	0.064 (5)	0.023 (4)
F2	0.048 (4)	0.084 (5)	0.017 (2)	-0.025 (4)	0.002 (2)	-0.007 (3)
F3	0.071 (4)	0.029 (2)	0.127 (8)	-0.015 (2)	0.022 (5)	-0.007 (4)
F4	0.050 (4)	0.136 (7)	0.034 (4)	-0.012 (5)	0.013 (3)	-0.043 (5)
F3A	0.045 (5)	0.033 (5)	0.060 (7)	0.011 (4)	-0.005 (5)	-0.021 (5)
F2A	0.047 (6)	0.077 (8)	0.034 (5)	0.014 (6)	0.001 (5)	0.030 (5)
F1A	0.060 (7)	0.050 (6)	0.080 (8)	0.019 (5)	-0.033 (6)	-0.041 (6)
F4A	0.025 (4)	0.061 (7)	0.063 (7)	-0.003 (5)	-0.013 (5)	0.042 (6)
C15	0.041 (7)	0.042 (7)	0.051 (7)	0.005 (5)	-0.016 (6)	0.006 (6)
C16	0.040 (5)	0.038 (5)	0.070 (8)	0.014 (4)	-0.007 (5)	0.001 (4)
C15A	0.023 (5)	0.018 (4)	0.031 (8)	0.001 (4)	0.000 (4)	0.005 (4)
C16A	0.044 (7)	0.039 (6)	0.052 (7)	0.007 (5)	0.017 (6)	0.005 (6)
C1	0.088 (5)	0.039 (4)	0.046 (4)	0.007 (4)	-0.028 (4)	-0.006 (3)
C8	0.083 (5)	0.055 (5)	0.053 (5)	0.009 (4)	0.049 (4)	0.008 (4)
C3	0.055 (4)	0.045 (4)	0.083 (6)	0.006 (3)	0.028 (4)	0.025 (4)
C6	0.101 (6)	0.046 (4)	0.059 (4)	0.021 (4)	-0.053 (4)	-0.030 (4)

7. Appendix

C10	0.0191 (18)	0.067 (3)	0.087 (5)	-0.005 (2)	-0.009 (2)	-0.040 (3)
C2	0.091 (6)	0.103 (7)	0.058 (6)	0.027 (5)	0.004 (5)	0.020 (5)
C11	0.048 (3)	0.042 (3)	0.057 (4)	0.004 (2)	-0.015 (3)	-0.025 (3)
C14	0.098 (5)	0.050 (3)	0.066 (4)	-0.003 (3)	0.028 (4)	0.007 (3)
C9	0.048 (3)	0.045 (3)	0.100 (5)	-0.019 (3)	0.042 (3)	-0.021 (3)
C12	0.043 (4)	0.055 (5)	0.113 (9)	0.013 (4)	0.038 (5)	0.036 (5)
C7	0.128 (7)	0.100 (6)	0.016 (2)	0.037 (5)	0.005 (4)	-0.020 (3)
C4	0.026 (2)	0.044 (3)	0.109 (5)	-0.013 (2)	0.009 (3)	0.005 (3)
C5	0.041 (3)	0.037 (3)	0.097 (5)	-0.011 (2)	-0.025 (3)	-0.006 (3)
Ag	0.01694 (8)	0.02705 (10)	0.01843 (8)	-0.00557 (8)	-0.0010 (2)	0.0007 (3)
N1	0.033 (3)	0.044 (3)	0.066 (4)	0.004 (2)	-0.025 (3)	-0.018 (3)
N4	0.069 (4)	0.034 (3)	0.058 (4)	-0.015 (3)	0.046 (3)	-0.010 (3)
N2	0.041 (3)	0.057 (5)	0.056 (4)	-0.007 (3)	0.016 (3)	0.023 (4)
N3	0.071 (5)	0.034 (3)	0.053 (4)	-0.017 (3)	-0.045 (4)	0.005 (3)
C13	0.111 (10)	0.076 (8)	0.089 (8)	-0.007 (6)	-0.081 (8)	-0.004 (6)
F6	0.0266 (11)	0.124 (3)	0.0340 (14)	0.0234 (15)	0.000 (3)	-0.003 (4)
F5	0.0236 (10)	0.0605 (16)	0.0592 (17)	-0.0030 (11)	0.006 (3)	-0.001 (4)

Table 25. Fractional atomic coordinates and isotropic or equivalent isotropic displacement parameters (\AA^2) $\text{Ag}(\text{Py})_2(\text{NO}_3)_2$

Atom	x	y	z	$U_{\text{iso}}^*/U_{\text{eq}}$
Ag1	0.5000	-0.5000	1.0000	0.04158 (16)
N1	0.4393 (9)	-0.6238 (9)	0.7521 (19)	0.069 (2)
C2	0.4470 (8)	-0.7390 (7)	0.7964 (12)	0.0576 (19)
H2	0.4751	-0.7644	0.9235	0.069*

7. Appendix

C3	0.4088 (7)	-0.828 (2)	0.6345 (13)	0.084 (4)
H3	0.4177	-0.9113	0.6599	0.101*
C4	0.3639 (6)	-0.7896 (9)	0.4609 (14)	0.069 (2)
H4	0.3355	-0.8450	0.3599	0.083*
C5	0.3565 (8)	-0.6673 (9)	0.4206 (11)	0.075 (2)
H5	0.3264	-0.6400	0.2940	0.090*
C6	0.3954 (6)	-0.5849 (6)	0.5740 (9)	0.0594 (15)
H6	0.3899	-0.5020	0.5493	0.071*
N2	0.3468 (3)	-0.5007 (12)	0.9873 (5)	0.0473 (9)
C7	0.3312 (5)	-0.5818 (6)	1.1048 (10)	0.0549 (13)
H7	0.3852	-0.6338	1.1855	0.066*
C8	0.2355 (6)	-0.5854 (7)	1.1023 (12)	0.0652 (16)
H8	0.2262	-0.6359	1.1861	0.078*
C9	0.1570 (5)	-0.5151 (13)	0.9774 (10)	0.062 (3)
H9	0.0922	-0.5179	0.9730	0.075*
C10	0.1707 (5)	-0.4373 (7)	0.8529 (12)	0.0652 (16)
H10	0.1166	-0.3874	0.7667	0.078*
C11	0.2684 (5)	-0.4376 (6)	0.8635 (10)	0.0550 (13)
H11	0.2778	-0.3898	0.7769	0.066*
N3	0.4076 (7)	-0.2320 (7)	0.6481 (15)	0.068 (2)
O1	0.4363 (8)	-0.3213 (16)	0.7608 (12)	0.117 (5)
O2	0.3818 (16)	-0.2668 (17)	0.4853 (15)	0.179 (7)
O3	0.4057 (11)	-0.1308 (11)	0.685 (2)	0.140 (5)

Table 26 . Atomic displacement parameters (\AA^2) $\text{Ag(Py)}_2(\text{NO}_3)_2$

Atom	U^{11}	U^{22}	U^{33}	U^{12}	U^{13}	U^{23}
Ag1	0.0474 (2)	0.0372 (2)	0.0411 (2)	0.000	0.02246 (16)	0.000
N1	0.072 (4)	0.060 (4)	0.076 (5)	0.008 (3)	0.037 (4)	0.014 (3)
C2	0.070 (5)	0.057 (4)	0.032 (3)	-0.009 (3)	0.015 (3)	0.000 (3)
C3	0.047 (4)	0.157 (15)	0.043 (4)	-0.009 (6)	0.018 (3)	-0.009 (7)
C4	0.058 (3)	0.074 (5)	0.073 (5)	-0.020 (3)	0.031 (3)	-0.046 (4)
C5	0.094 (5)	0.083 (5)	0.032 (3)	-0.010 (4)	0.019 (3)	-0.009 (3)
C6	0.089 (4)	0.041 (3)	0.047 (3)	-0.008 (3)	0.032 (3)	-0.004 (2)
N2	0.0522 (18)	0.0471 (19)	0.0465 (17)	0.017 (5)	0.0273 (15)	0.003 (5)
C7	0.063 (3)	0.048 (3)	0.062 (3)	-0.001 (2)	0.037 (3)	0.003 (2)
C8	0.076 (4)	0.055 (3)	0.079 (5)	-0.008 (3)	0.050 (4)	0.002 (3)
C9	0.054 (2)	0.060 (7)	0.082 (3)	-0.023 (4)	0.041 (3)	-0.024 (5)
C10	0.052 (3)	0.060 (4)	0.074 (4)	0.005 (3)	0.023 (3)	-0.005 (3)
C11	0.054 (3)	0.048 (3)	0.060 (3)	-0.005 (2)	0.026 (3)	0.002 (2)
N3	0.078 (5)	0.052 (3)	0.079 (6)	-0.007 (3)	0.042 (4)	0.001 (3)
O1	0.074 (5)	0.230 (17)	0.035 (4)	-0.010 (10)	0.018 (3)	0.020 (8)
O2	0.282 (17)	0.186 (15)	0.058 (6)	-0.042 (13)	0.075 (8)	-0.030 (7)
O3	0.196 (12)	0.087 (6)	0.212 (15)	0.004 (7)	0.157 (12)	0.006 (7)

Table 27. Fractional atomic coordinates and isotropic or equivalent isotropic displacement parameters (\AA^2) $\text{Ag(BPy)}_2(\text{ClO}_4)_2$

Atom	x	y	z	$U_{\text{iso}}^*/U_{\text{eq}}$
Ag1	0.68947 (7)	0.68383 (6)	0.72971 (3)	0.0444 (2)

7. Appendix

N1	0.5239 (7)	0.7867 (5)	0.6215 (3)	0.0429 (12)
C2	0.3557 (9)	0.8342 (7)	0.6375 (4)	0.0500 (16)
H2	0.3041	0.8284	0.6991	0.060*
C3	0.2568 (9)	0.8913 (7)	0.5653 (5)	0.0533 (17)
H3	0.1414	0.9268	0.5782	0.064*
C4	0.3317 (10)	0.8950 (7)	0.4737 (5)	0.0560 (18)
H4	0.2670	0.9332	0.4242	0.067*
C5	0.5031 (10)	0.8416 (7)	0.4559 (4)	0.0524 (17)
H5	0.5535	0.8405	0.3946	0.063*
C6	0.6012 (8)	0.7887 (6)	0.5318 (4)	0.0408 (14)
C7	0.7866 (9)	0.7337 (6)	0.5199 (4)	0.0440 (15)
C8	0.8868 (10)	0.7433 (7)	0.4324 (4)	0.0546 (17)
H8	0.8373	0.7858	0.3783	0.066*
C9	1.0587 (10)	0.6896 (8)	0.4272 (5)	0.0602 (19)
H9	1.1256	0.6956	0.3693	0.072*
C10	1.1330 (10)	0.6262 (7)	0.5086 (5)	0.0580 (18)
H10	1.2486	0.5880	0.5059	0.070*
C11	1.0285 (9)	0.6218 (7)	0.5940 (5)	0.0537 (17)
H11	1.0775	0.5836	0.6491	0.064*
N12	0.8582 (7)	0.6711 (5)	0.5995 (3)	0.0446 (13)
N13	0.8127 (7)	0.5324 (5)	0.8381 (3)	0.0449 (12)
C14	0.9219 (9)	0.4226 (7)	0.8225 (5)	0.0557 (17)
H14	0.9621	0.4135	0.7608	0.067*
C15	0.9793 (10)	0.3200 (7)	0.8945 (6)	0.065 (2)

7. Appendix

H15	1.0577	0.2449	0.8817	0.078*
C16	0.9155 (11)	0.3343 (8)	0.9850 (6)	0.068 (2)
H16	0.9510	0.2680	1.0347	0.082*
C17	0.7999 (10)	0.4457 (8)	1.0025 (5)	0.0580 (18)
H17	0.7579	0.4551	1.0639	0.070*
C18	0.7451 (8)	0.5455 (7)	0.9277 (4)	0.0432 (15)
C19	0.6193 (9)	0.6669 (7)	0.9396 (4)	0.0455 (15)
C20	0.5576 (10)	0.7054 (8)	1.0262 (4)	0.0588 (19)
H20	0.5973	0.6530	1.0807	0.071*
C21	0.4383 (11)	0.8202 (9)	1.0319 (5)	0.069 (2)
H21	0.3992	0.8457	1.0898	0.083*
C22	0.3768 (10)	0.8975 (9)	0.9512 (5)	0.066 (2)
H22	0.2936	0.9736	0.9538	0.079*
C23	0.4438 (10)	0.8573 (8)	0.8658 (5)	0.0608 (19)
H23	0.4071	0.9103	0.8108	0.073*
N24	0.5595 (7)	0.7447 (5)	0.8599 (3)	0.0464 (13)
C11	0.5546 (2)	0.58099 (18)	0.28938 (10)	0.0510 (4)
O11	0.6346 (10)	0.4764 (7)	0.2382 (5)	0.109 (2)
O12	0.3961 (14)	0.6286 (11)	0.2589 (7)	0.158 (4)
O13	0.5296 (11)	0.5372 (8)	0.3866 (5)	0.116 (2)
O14	0.6512 (12)	0.6827 (9)	0.2654 (6)	0.135 (3)
C12	-0.0770 (3)	-0.0527 (2)	0.79015 (12)	0.0610 (5)
O21	-0.1482 (9)	-0.0595 (7)	0.8853 (4)	0.0910 (18)
O22	0.0563 (10)	0.0264 (8)	0.7642 (5)	0.107 (2)

7. Appendix

O23	-0.2001 (18)	-0.0265 (14)	0.7318 (9)	0.203 (5)
O24	-0.0031 (11)	-0.1903 (9)	0.7824 (6)	0.127 (3)

Table 28. Atomic displacement parameters (\AA^2) for $\text{Ag}(\text{BPy})_2(\text{ClO}_4)_2$

Atom	U^{11}	U^{22}	U^{33}	U^{12}	U^{13}	U^{23}
Ag1	0.0479 (3)	0.0503 (3)	0.0308 (2)	0.0019 (2)	-0.00432 (17)	-0.00557 (17)
N1	0.046 (3)	0.045 (3)	0.036 (2)	-0.005 (2)	-0.007 (2)	-0.003 (2)
C2	0.051 (4)	0.055 (4)	0.042 (3)	-0.004 (3)	-0.004 (3)	-0.008 (3)
C3	0.044 (4)	0.050 (4)	0.068 (4)	-0.006 (3)	-0.017 (3)	-0.010 (3)
C4	0.068 (5)	0.048 (4)	0.057 (4)	-0.014 (4)	-0.026 (3)	-0.002 (3)
C5	0.075 (5)	0.045 (4)	0.039 (3)	-0.012 (3)	-0.011 (3)	-0.004 (3)
C6	0.053 (4)	0.036 (3)	0.036 (3)	-0.012 (3)	-0.007 (3)	-0.007 (2)
C7	0.054 (4)	0.044 (4)	0.037 (3)	-0.017 (3)	0.001 (3)	-0.011 (3)
C8	0.068 (5)	0.057 (4)	0.040 (3)	-0.017 (4)	0.005 (3)	-0.012 (3)
C9	0.066 (5)	0.064 (5)	0.053 (4)	-0.024 (4)	0.017 (3)	-0.022 (3)
C10	0.050 (4)	0.057 (4)	0.072 (5)	-0.018 (3)	0.008 (3)	-0.024 (4)
C11	0.055 (4)	0.052 (4)	0.056 (4)	-0.009 (3)	-0.007 (3)	-0.010 (3)
N12	0.047 (3)	0.047 (3)	0.040 (3)	-0.008 (3)	0.000 (2)	-0.010 (2)
N13	0.044 (3)	0.048 (3)	0.042 (3)	-0.008 (3)	-0.008 (2)	-0.006 (2)
C14	0.056 (4)	0.052 (4)	0.055 (4)	-0.001 (3)	-0.010 (3)	-0.005 (3)
C15	0.055 (5)	0.046 (4)	0.090 (6)	-0.001 (3)	-0.020 (4)	0.002 (4)
C16	0.071 (5)	0.061 (5)	0.070 (5)	-0.019 (4)	-0.030 (4)	0.020 (4)
C17	0.064 (5)	0.070 (5)	0.042 (3)	-0.023 (4)	-0.013 (3)	0.004 (3)
C18	0.042 (4)	0.054 (4)	0.037 (3)	-0.018 (3)	-0.010 (3)	-0.004 (3)

7. Appendix

C19	0.048 (4)	0.054 (4)	0.038 (3)	-0.020 (3)	-0.004 (3)	-0.007 (3)
C20	0.066 (5)	0.073 (5)	0.039 (3)	-0.015 (4)	-0.001 (3)	-0.014 (3)
C21	0.070 (5)	0.091 (6)	0.053 (4)	-0.021 (5)	0.010 (4)	-0.036 (4)
C22	0.056 (5)	0.074 (5)	0.070 (5)	-0.003 (4)	0.001 (4)	-0.031 (4)
C23	0.064 (5)	0.060 (5)	0.056 (4)	0.002 (4)	-0.007 (3)	-0.017 (3)
N24	0.048 (3)	0.055 (3)	0.036 (2)	-0.003 (3)	-0.001 (2)	-0.014 (2)
Cl1	0.0512 (10)	0.0631 (11)	0.0386 (7)	-0.0070 (8)	-0.0038 (7)	-0.0112 (7)
O11	0.125 (3)	0.099 (3)	0.096 (3)	-0.006 (3)	0.005 (3)	-0.026 (2)
O12	0.146 (4)	0.175 (4)	0.151 (4)	-0.016 (3)	-0.022 (3)	-0.027 (3)
O13	0.128 (3)	0.118 (3)	0.093 (3)	-0.004 (3)	-0.003 (3)	-0.018 (3)
O14	0.143 (4)	0.136 (4)	0.136 (4)	-0.042 (3)	-0.001 (3)	-0.041 (3)
Cl2	0.0592 (12)	0.0783 (13)	0.0416 (8)	-0.0106 (10)	-0.0046 (8)	-0.0023 (8)
O21	0.094 (3)	0.095 (3)	0.078 (3)	-0.006 (2)	-0.001 (2)	-0.016 (2)
O22	0.108 (3)	0.102 (3)	0.111 (3)	-0.028 (3)	-0.003 (3)	-0.021 (3)
O23	0.201 (6)	0.212 (6)	0.194 (6)	-0.035 (3)	-0.035 (3)	-0.020 (3)
O24	0.131 (4)	0.118 (4)	0.128 (4)	-0.023 (3)	0.005 (3)	-0.029 (3)

Table 29.. Fractional atomic coordinates and isotropic or equivalent isotropic displacement parameters (\AA^2) for LiPc.TBAPF₆

Atom	x	y	z	$U_{\text{iso}}^*/U_{\text{eq}}$
P	0.0000	1.0000	0.0000	0.0611 (2)
F1	0.0601 (2)	0.8791 (1)	0.0459 (1)	0.1144 (5)
F2	0.1360 (2)	1.0311 (2)	0.0480 (1)	0.1287 (7)
F3	-0.1140 (2)	1.0273 (1)	0.0835 (1)	0.1013 (5)

7. Appendix

Li	0.5000	0.5000	0.5000	0.0515 (8)
N4	0.4097 (1)	0.6126 (1)	0.2872 (1)	0.0456 (3)
N3	0.6413 (2)	0.3628 (1)	0.5563 (1)	0.0470 (3)
N2	0.5574 (2)	0.4524 (1)	0.3812 (1)	0.0473 (3)
C10	0.5081 (2)	0.5123 (1)	0.3013 (1)	0.0448 (3)
C12	0.2598 (2)	0.7864 (1)	0.3383 (1)	0.0457 (3)
C3	0.6626 (2)	0.3571 (1)	0.3642 (1)	0.0475 (3)
N5	0.7327 (2)	0.2729 (1)	0.4236 (1)	0.0511 (3)
C1	0.7145 (2)	0.2761 (1)	0.5123 (1)	0.0476 (3)
C11	0.3461 (2)	0.6707 (1)	0.3538 (1)	0.0445 (3)
C9	0.5874 (2)	0.4528 (1)	0.2276 (1)	0.0478 (3)
C17	0.2239 (2)	0.8202 (1)	0.4234 (1)	0.0481 (3)
C4	0.6868 (2)	0.3547 (1)	0.2670 (1)	0.0498 (3)
C13	0.2188 (2)	0.8603 (1)	0.2614 (1)	0.0515 (4)
H13	0.2412	0.8381	0.2046	0.06200*
C8	0.5805 (2)	0.4779 (2)	0.1348 (1)	0.0572 (4)
H8	0.5143	0.5430	0.1080	0.06900*
C7	0.6760 (2)	0.4021 (2)	0.0839 (1)	0.0676 (5)
H7	0.6738	0.4169	0.0217	0.08100*
C15	0.1103 (2)	1.0016 (2)	0.3572 (1)	0.0641 (4)
H15	0.0603	1.0745	0.3626	0.07700*
C16	0.1507 (2)	0.9282 (1)	0.4337 (1)	0.0588 (4)
H16	0.1292	0.9508	0.4905	0.07100*
C14	0.1439 (2)	0.9676 (1)	0.2722 (1)	0.0600 (4)

7. Appendix

H14	0.1153	1.0182	0.2217	0.07200*
C5	0.7827 (2)	0.2797 (2)	0.2154 (1)	0.0616 (4)
H5	0.8500	0.2149	0.2419	0.07400*
C6	0.7751 (3)	0.3047 (2)	0.1231 (1)	0.0704 (5)
H6	0.8373	0.2554	0.0868	0.08400*
N1	0.7778 (2)	0.7568 (1)	0.2506 (1)	0.0570 (3)
C21	0.9425 (2)	0.7013 (2)	0.2155 (1)	0.0631 (4)
H21A	0.9649	0.7455	0.1619	0.07600*
H21B	1.0218	0.6997	0.2600	0.07600*
C31	0.6483 (2)	0.7574 (2)	0.1841 (1)	0.0608 (4)
H31A	0.6454	0.6826	0.1816	0.07300*
H31B	0.5452	0.7960	0.2071	0.07300*
C51	0.7417 (2)	0.6956 (2)	0.3383 (1)	0.0615 (4)
H51A	0.7483	0.6213	0.3280	0.07400*
H51B	0.6317	0.7287	0.3553	0.07400*
C41	0.7762 (2)	0.8728 (2)	0.2635 (1)	0.0665 (5)
H41A	0.7984	0.9097	0.2061	0.08000*
H41B	0.8626	0.8700	0.3038	0.08000*
C32	0.6680 (2)	0.8081 (2)	0.0899 (1)	0.0683 (5)
H32A	0.7702	0.7697	0.0657	0.08200*
H32B	0.6689	0.8834	0.0911	0.08200*
C52	0.8489 (3)	0.6915 (2)	0.4169 (1)	0.0733 (5)
H52A	0.8498	0.7650	0.4261	0.08800*
H52B	0.9580	0.6513	0.4041	0.08800*

7. Appendix

C22	0.9640 (2)	0.5868 (2)	0.1931 (2)	0.0753 (5)
H22A	0.9545	0.5398	0.2475	0.09000*
H22B	0.8797	0.5861	0.1525	0.09000*
C33	0.5342 (3)	0.8037 (2)	0.0300 (1)	0.0886 (7)
H33A	0.5324	0.7282	0.0308	0.10600*
H33B	0.4327	0.8427	0.0546	0.10600*
C53	0.7880 (3)	0.6364 (2)	0.5014 (1)	0.0851 (6)
H53A	0.6767	0.6744	0.5114	0.10200*
H53B	0.7919	0.5621	0.4924	0.10200*
C42	0.6208 (3)	0.9402 (2)	0.3005 (2)	0.0871 (6)
H42A	0.5347	0.9477	0.2586	0.10500*
H42B	0.5947	0.9023	0.3565	0.10500*
C43	0.6315 (3)	1.0501 (2)	0.3161 (2)	0.1025 (8)
H43A	0.6582	1.0875	0.2600	0.12300*
H43B	0.7179	1.0421	0.3579	0.12300*
C34	0.5472 (3)	0.8505 (2)	-0.0647 (2)	0.0963 (7)
H34A	0.4581	0.8448	-0.0983	0.14400*
H34B	0.6458	0.8112	-0.0904	0.14400*
H34C	0.5460	0.9258	-0.0665	0.14400*
C24	1.1547 (4)	0.4306 (3)	0.1268 (3)	0.1271 (11)
H24A	1.2592	0.4097	0.0998	0.19100*
H24B	1.0749	0.4274	0.0852	0.19100*
H24C	1.1504	0.3817	0.1800	0.19100*
C44	0.4794 (4)	1.1186 (3)	0.3526 (3)	0.1545 (17)

7. Appendix

H44A	0.4937	1.1884	0.3613	0.23200*
H44B	0.4535	1.0829	0.4089	0.23200*
H44C	0.3937	1.1283	0.3109	0.23200*
C23	1.1230 (3)	0.5441 (3)	0.1507 (2)	0.1048 (9)
H23A	1.2062	0.5465	0.1914	0.12600*
H23B	1.1314	0.5921	0.0966	0.12600*
C54	0.8838 (4)	0.6347 (3)	0.5836 (2)	0.1176 (10)
H54A	0.8402	0.5994	0.6347	0.17600*
H54B	0.8787	0.7081	0.5937	0.17600*
H54C	0.9937	0.5956	0.5748	0.17600*

Table 30. Atomic displacement parameters (\AA^2) for LiPc.TBAPF₆

Atom	U ¹¹	U ²²	U ³³	U ¹²	U ¹³	U ²³
P	0.0714 (4)	0.0724 (4)	0.0412 (3)	-0.0276 (3)	0.0033 (3)	0.0044 (3)
F1	0.1478 (14)	0.0861 (9)	0.091 (1)	-0.0168 (9)	0.0160 (9)	0.0235 (7)
F2	0.1386 (13)	0.2045 (19)	0.0774 (9)	-0.1105 (14)	-0.0138 (9)	0.0006 (10)
F3	0.1147 (10)	0.1166 (11)	0.0678 (8)	-0.0292 (8)	0.0338 (7)	-0.0055 (7)
Li	0.063 (2)	0.0522 (19)	0.0353 (16)	-0.0105 (16)	0.0001 (14)	0.0015 (14)
N4	0.0505 (6)	0.0521 (7)	0.0350 (6)	-0.0167 (5)	-0.0029 (5)	0.0003 (5)
N3	0.0533 (7)	0.0521 (7)	0.0342 (6)	-0.0141 (5)	-0.0003 (5)	0.0009 (5)
N2	0.0568 (7)	0.0504 (7)	0.0339 (6)	-0.0151 (5)	-0.0005 (5)	0.0001 (5)
C10	0.0523 (7)	0.0524 (8)	0.0326 (6)	-0.0202 (6)	-0.0010 (5)	-0.0013 (5)
C12	0.0420 (7)	0.0535 (8)	0.0407 (7)	-0.0142 (6)	-0.0028 (5)	0.0021 (6)
C3	0.0562 (8)	0.0502 (8)	0.0362 (7)	-0.0155 (6)	0.0016 (6)	-0.0028 (6)

7. Appendix

N5	0.0596 (7)	0.0517 (7)	0.0381 (6)	-0.0102 (6)	0.0022 (5)	-0.0014 (5)
C1	0.0499 (7)	0.0519 (8)	0.0385 (7)	-0.0121 (6)	0.0004 (6)	0.0006 (6)
C11	0.0446 (7)	0.0525 (8)	0.0369 (7)	-0.0161 (6)	-0.0027 (5)	0.0012 (5)
C9	0.0578 (8)	0.0540 (8)	0.0356 (7)	-0.0221 (7)	0.0010 (6)	-0.0044 (6)
C17	0.0458 (7)	0.0549 (8)	0.0405 (7)	-0.0107 (6)	-0.0012 (6)	0.0011 (6)
C4	0.0614 (8)	0.0538 (8)	0.0367 (7)	-0.0206 (7)	0.0025 (6)	-0.0044 (6)
C13	0.0483 (8)	0.0628 (9)	0.0411 (7)	-0.0148 (7)	-0.0039 (6)	0.0047 (6)
C8	0.0713 (10)	0.0657 (10)	0.0361 (7)	-0.0224 (8)	-0.0022 (7)	-0.0022 (6)
C7	0.0901 (13)	0.0792 (12)	0.0347 (7)	-0.0241 (10)	0.0041 (8)	-0.0085 (7)
C15	0.0665 (10)	0.0548 (9)	0.0606 (10)	-0.0017 (8)	-0.0073 (8)	0.0027 (7)
C16	0.0597 (9)	0.0603 (9)	0.0481 (8)	-0.0029 (7)	-0.0016 (7)	-0.0023 (7)
C14	0.0589 (9)	0.0607 (9)	0.0524 (9)	-0.0091 (7)	-0.0084 (7)	0.0119 (7)
C5	0.0764 (11)	0.0587 (9)	0.0470 (8)	-0.0134 (8)	0.0063 (7)	-0.0079 (7)
C6	0.0889 (13)	0.0750 (12)	0.0469 (9)	-0.0183 (10)	0.0117 (8)	-0.0169 (8)
N1	0.0543 (7)	0.0697 (9)	0.0525 (7)	-0.0303 (7)	-0.0003 (6)	0.0026 (6)
C21	0.0535 (9)	0.0833 (12)	0.0562 (9)	-0.0290 (8)	0.0022 (7)	0.0013 (8)
C31	0.0553 (9)	0.0726 (11)	0.0590 (9)	-0.0286 (8)	-0.0055 (7)	0.0026 (8)
C51	0.0622 (9)	0.0749 (11)	0.0533 (9)	-0.0335 (8)	0.0012 (7)	0.0039 (8)
C41	0.0711 (11)	0.0703 (11)	0.0658 (10)	-0.0362 (9)	-0.0002 (8)	0.0013 (8)
C32	0.0679 (11)	0.0794 (12)	0.0591 (10)	-0.0281 (9)	-0.0068 (8)	0.0077 (9)
C52	0.0782 (12)	0.0920 (14)	0.0561 (10)	-0.0393 (11)	-0.0075 (9)	0.0059 (9)
C22	0.0655 (11)	0.0834 (13)	0.0782 (13)	-0.0244 (10)	0.0024 (9)	-0.0038 (10)
C33	0.0907 (15)	0.1132 (18)	0.0689 (12)	-0.0472 (13)	-0.0209 (11)	0.0133 (12)
C53	0.0911 (14)	0.1086 (17)	0.0564 (11)	-0.0358 (13)	-0.0002 (10)	0.0086 (11)

7. Appendix

C42	0.0768 (13)	0.0787 (14)	0.1129 (18)	-0.0315 (11)	0.0054 (12)	-0.0157 (13)
C43	0.0983 (17)	0.0940 (17)	0.129 (2)	-0.0403 (14)	-0.0003 (16)	-0.0322 (16)
C34	0.1136 (18)	0.1041 (18)	0.0694 (13)	-0.0301 (15)	-0.0270 (13)	0.0083 (12)
C24	0.108 (2)	0.121 (2)	0.153 (3)	-0.0188 (18)	0.020 (2)	-0.051 (2)
C44	0.110 (2)	0.115 (2)	0.259 (5)	-0.0377 (19)	0.029 (3)	-0.093 (3)
C23	0.0773 (14)	0.128 (2)	0.121 (2)	-0.0359 (15)	0.0230 (14)	-0.0492 (18)
C54	0.126 (2)	0.158 (3)	0.0631 (14)	-0.036 (2)	-0.0168 (14)	0.0086 (15)

Table 31. Atomic coordinates for monosodium phthalocyanine

Atom	x	y	z	U
N1	-0.06120	-0.12296	0.98607	0.0380
C2	-0.01693	-0.20951	0.98611	0.0380
N3	0.07674	-0.22475	0.98609	0.0380
C4	-0.08297	-0.28388	0.98619	0.0380
C5	-0.07776	-0.38447	0.98624	0.0380
H5	-0.01975	-0.41645	0.98625	0.0760
C6	-0.16252	-0.43211	0.98629	0.0380
H6	-0.16114	-0.49835	0.98633	0.0760
C7	-0.24698	-0.38918	0.98630	0.0380
H7	-0.30188	-0.42609	0.98634	0.0760
C8	-0.25530	-0.29386	0.98624	0.0380
H8	-0.31459	-0.26441	0.98624	0.0760
C9	-0.17496	-0.24356	0.98618	0.0380
C10	-0.15475	-0.13935	0.98612	0.0380
Na1	0.00009	0.00017	0.83657	0.0380
N1	0.12324	-0.06111	0.98598	0.0380
C2	0.20980	-0.01684	0.98593	0.0380
N3	0.22503	0.07683	0.98586	0.0380
C4	0.28417	-0.08287	0.98594	0.0380
C5	0.38476	-0.07768	0.98592	0.0380
H5	0.41673	-0.01965	0.98586	0.0760
C6	0.43240	-0.16242	0.98595	0.0380
H6	0.49863	-0.16104	0.98593	0.0760
C7	0.38946	-0.24689	0.98602	0.0380
H7	0.42638	-0.30179	0.98604	0.0760
C8	0.29414	-0.25521	0.98604	0.0380

H8	0.26470	-0.31449	0.98610	0.0760
C9	0.24384	-0.17486	0.98602	0.0380
C10	0.13962	-0.15466	0.98604	0.0380
N1	0.06139	0.12334	0.98588	0.0380
C2	0.01712	0.20989	0.98585	0.0380
N3	-0.07655	0.22513	0.98587	0.0380
C4	0.08316	0.28426	0.98577	0.0380
C5	0.07795	0.38485	0.98572	0.0380
H5	0.01994	0.41683	0.98571	0.0760
C6	0.16271	0.43249	0.98567	0.0380
H6	0.16133	0.49873	0.98563	0.0760
C7	0.24718	0.38955	0.98568	0.0380
H7	0.30208	0.42647	0.98563	0.0760
C8	0.25549	0.29424	0.98572	0.0380
H8	0.31478	0.26479	0.98572	0.0760
C9	0.17515	0.24393	0.98578	0.0380
C10	0.15494	0.13972	0.98586	0.0380
N1	-0.12306	0.06149	0.98598	0.0380
C2	-0.20961	0.01722	0.98603	0.0380
N3	-0.22484	-0.07646	0.98609	0.0380
C4	-0.28398	0.08325	0.98602	0.0380
C5	-0.38457	0.07805	0.98606	0.0380
H5	-0.41654	0.02003	0.98610	0.0760
C6	-0.43220	0.16280	0.98602	0.0380
H6	-0.49844	0.16142	0.98604	0.0760
C7	-0.38927	0.24727	0.98595	0.0380
H7	-0.42619	0.30217	0.98592	0.0760
C8	-0.29395	0.25558	0.98591	0.0380
H8	-0.26451	0.31487	0.98586	0.0760
C9	-0.24365	0.17524	0.98594	0.0380
C10	-0.13943	0.15504	0.98592	0.0380

Table 32. Fractional atomic coordinates and isotropic or equivalent isotropic displacement parameters (\AA^2) for Tetrapropylporphycene.Tetracyanoquinodimethane.

Atom	x	y	z	$U_{\text{iso}}^*/U_{\text{eq}}$
N5	0.6848 (6)	0.2252 (12)	0.2289 (4)	0.069 (2)
N6	0.5241 (5)	0.3004 (11)	0.1625 (6)	0.083 (3)
H6	0.5837	0.2707	0.1684	0.100*
N7	0.6181 (7)	0.2764 (13)	0.0350 (5)	0.077 (2)

7. Appendix

C8	0.1092 (8)	0.2489 (16)	0.7740 (8)	0.084 (4)
C9	0.1266 (7)	0.2510 (15)	0.7045 (6)	0.065 (3)
N8	0.7748 (6)	0.1989 (11)	0.0974 (4)	0.065 (2)
H8	0.7142	0.2217	0.0939	0.079*
C10	0.7413 (9)	0.1856 (17)	0.3380 (6)	0.084 (3)
C3	0.1939 (8)	0.2429 (15)	0.4891 (5)	0.074 (3)
C4	0.2226 (8)	0.2974 (15)	0.6816 (7)	0.083 (3)
H4	0.2699	0.3279	0.7157	0.100*
C5	0.0580 (6)	0.2091 (14)	0.6500 (6)	0.067 (3)
H5	-0.0050	0.1828	0.6625	0.081*
C11	0.6495 (8)	0.2303 (15)	0.2955 (7)	0.091 (4)
C15	0.5649 (9)	0.2642 (18)	0.3217 (7)	0.093 (4)
H15	0.5617	0.2575	0.3717	0.112*
C6	0.1720 (9)	0.2478 (16)	0.5598 (7)	0.076 (3)
C7	0.0823 (8)	0.2070 (14)	0.5819 (5)	0.068 (3)
H7	0.0358	0.1761	0.5473	0.082*
C13	0.3744 (9)	0.3615 (18)	0.1908 (7)	0.096 (4)
C14	0.4790 (9)	0.3087 (17)	0.2867 (7)	0.088 (4)
H14	0.4269	0.3269	0.3167	0.106*
C18	0.7755 (9)	0.1791 (16)	0.2298 (8)	0.095 (4)
C19	0.8212 (10)	0.1747 (16)	0.1574 (8)	0.099 (5)
C16	0.4601 (7)	0.3294 (13)	0.2155 (7)	0.085 (4)
C17	0.4766 (9)	0.3268 (16)	0.0973 (9)	0.106 (5)
C1	0.1196 (11)	0.2044 (16)	0.4355 (7)	0.097 (5)
N4	-0.0652 (9)	0.1890 (17)	0.8184 (6)	0.119 (4)
N3	0.2281 (9)	0.3277 (17)	0.8701 (6)	0.113 (4)
N2	0.0681 (8)	0.1724 (17)	0.3909 (6)	0.108 (4)
N1	0.3558 (10)	0.3191 (16)	0.4464 (8)	0.122 (4)
C2	0.2841 (13)	0.2858 (18)	0.4661 (7)	0.107 (5)
C20	0.3805 (8)	0.3662 (16)	0.1105 (7)	0.092 (4)
H20	0.3316	0.3899	0.0771	0.111*

7. Appendix

C21	0.8091 (8)	0.1606 (14)	0.2975 (6)	0.081 (3)
H21	0.8721	0.1338	0.3114	0.097*
C22	0.6414 (8)	0.2756 (17)	-0.0396 (8)	0.086 (4)
C23	0.5633 (10)	0.3176 (15)	-0.0816 (6)	0.084 (4)
C24	0.4857 (13)	0.3409 (16)	-0.0311 (11)	0.175 (9)
H24	0.4217	0.3687	-0.0413	0.210*
C25	0.7295 (10)	0.233 (2)	-0.0620 (8)	0.113 (5)
H25	0.7354	0.2284	-0.1118	0.135*
C26	0.8184 (10)	0.1926 (16)	-0.0219 (8)	0.103 (5)
H26	0.8721	0.1703	-0.0498	0.124*
C27	0.5268 (11)	0.3135 (16)	0.0322 (7)	0.091 (4)
C28	0.9128 (9)	0.1319 (16)	0.1483 (8)	0.105 (4)
H28	0.9575	0.1055	0.1847	0.127*
C29	0.9295 (9)	0.1332 (19)	0.0778 (9)	0.102 (4)
C30	0.2436 (9)	0.2966 (16)	0.6109 (6)	0.083 (3)
H30	0.3051	0.3281	0.5960	0.100*
C31	0.2796 (8)	0.3953 (19)	0.2260 (6)	0.117 (5)
H31A	0.2324	0.4390	0.1906	0.140*
H31B	0.2857	0.4963	0.2630	0.140*
C32	0.4808 (8)	0.366 (2)	-0.2755 (6)	0.130 (5)
H32A	0.4160	0.3840	-0.2922	0.196*
H32B	0.5076	0.2511	-0.2980	0.196*
H32C	0.5178	0.4812	-0.2877	0.196*
C33	0.5484 (11)	0.327 (2)	-0.1555 (5)	0.136 (6)
H33A	0.5885	0.4370	-0.1696	0.164*
H33B	0.5812	0.2090	-0.1725	0.164*
C34	0.4823 (11)	0.339 (3)	-0.1960 (9)	0.205 (9)
H34A	0.4444	0.4482	-0.1777	0.245*
H34B	0.4450	0.2202	-0.1879	0.245*
C35	0.2262 (12)	0.060 (3)	0.2113 (9)	0.224 (11)
H35A	0.2056	-0.0629	0.2323	0.337*

7. Appendix

H35B	0.2817	0.0367	0.1827	0.337*
H35C	0.1757	0.1129	0.1813	0.337*
C36	0.1711 (9)	0.2947 (18)	0.8287 (7)	0.083 (4)
C37	0.8316 (14)	0.1843 (16)	0.0432 (6)	0.150 (8)
C38	0.8249 (9)	0.1192 (19)	0.4542 (8)	0.127 (5)
H38A	0.8731	0.2155	0.4409	0.152*
H38B	0.8437	-0.0098	0.4360	0.152*
C39	0.0136 (10)	0.2169 (16)	0.7986 (6)	0.083 (4)
C40	0.2469 (10)	0.184 (3)	0.2616 (8)	0.192 (9)
H40A	0.2983	0.1322	0.2917	0.230*
H40B	0.1916	0.2051	0.2916	0.230*
C41	0.7354 (8)	0.174 (2)	0.4251 (9)	0.146 (6)
H41A	0.7167	0.3021	0.4441	0.175*
H41B	0.6876	0.0772	0.4387	0.175*
C43	1.0177 (7)	0.109 (2)	0.0362 (7)	0.110 (5)
H43A	1.0569	0.0078	0.0592	0.131*
H43B	1.0005	0.0615	-0.0116	0.131*
C44	0.8151 (9)	0.112 (2)	0.5372 (7)	0.125 (5)
H44A	0.8760	0.0813	0.5590	0.187*
H44B	0.7695	0.0116	0.5498	0.187*
H44C	0.7935	0.2387	0.5543	0.187*
C42	1.0723 (11)	0.281 (2)	0.0293 (16)	0.241 (12)
H42A	1.1261	0.2563	0.0617	0.290*
H42B	1.0979	0.2682	-0.0187	0.290*
C45	1.0601 (11)	0.4645 (19)	0.0352 (11)	0.178 (7)
H45A	1.1211	0.5299	0.0370	0.267*
H45B	1.0261	0.4921	0.0787	0.267*
H45C	1.0237	0.5123	-0.0055	0.267*

Table 33. Atomic displacement parameters for Tetrapropylporphycene. Tetracyanoquinodimethane.

Atom	U ¹¹	U ²²	U ³³	U ¹²	U ¹³	U ²³
N5	0.074 (6)	0.055 (6)	0.078 (6)	-0.011 (5)	0.029 (5)	-0.008 (5)
N6	0.036 (4)	0.065 (6)	0.150 (9)	0.006 (4)	0.058 (6)	-0.009 (5)
N7	0.090 (7)	0.062 (6)	0.079 (6)	-0.004 (5)	0.018 (5)	-0.004 (5)
C8	0.073 (8)	0.056 (6)	0.122 (12)	-0.006 (6)	0.026 (8)	-0.006 (7)
C9	0.081 (8)	0.055 (6)	0.059 (7)	0.024 (6)	0.018 (6)	0.003 (6)
N8	0.089 (6)	0.067 (6)	0.040 (5)	-0.010 (4)	-0.007 (5)	-0.003 (4)
C10	0.094 (9)	0.087 (8)	0.074 (7)	0.005 (7)	0.018 (7)	-0.002 (6)
C3	0.108 (9)	0.064 (7)	0.050 (7)	0.011 (7)	0.028 (7)	0.011 (6)
C4	0.085 (8)	0.063 (8)	0.102 (9)	-0.002 (6)	0.008 (7)	-0.005 (6)
C5	0.052 (6)	0.053 (7)	0.098 (9)	0.011 (5)	0.014 (7)	-0.008 (6)
C11	0.095 (8)	0.044 (6)	0.139 (11)	-0.001 (5)	0.084 (9)	-0.017 (6)
C15	0.120 (12)	0.082 (9)	0.078 (8)	-0.018 (8)	0.029 (9)	0.003 (6)
C6	0.095 (9)	0.047 (6)	0.087 (9)	-0.009 (6)	0.035 (8)	0.006 (6)
C7	0.080 (8)	0.069 (8)	0.056 (6)	0.010 (6)	0.012 (6)	0.002 (5)
C13	0.081 (10)	0.085 (8)	0.125 (11)	0.001 (7)	0.050 (8)	-0.020 (8)
C14	0.093 (9)	0.085 (9)	0.087 (9)	0.001 (7)	0.013 (8)	0.017 (7)
C18	0.082 (9)	0.065 (8)	0.138 (14)	-0.021 (6)	0.034 (8)	0.016 (7)
C19	0.121 (11)	0.062 (7)	0.116 (11)	-0.011 (6)	0.088 (10)	-0.021 (7)
C16	0.038 (5)	0.053 (6)	0.164 (13)	0.004 (4)	-0.002 (7)	0.006 (6)
C17	0.077 (10)	0.062 (8)	0.178 (14)	-0.010 (6)	-0.051 (10)	0.015 (9)
C1	0.174 (14)	0.051 (8)	0.066 (10)	0.007 (8)	0.040 (9)	0.000 (7)
N4	0.129 (9)	0.125 (10)	0.104 (9)	0.001 (7)	0.057 (7)	0.019 (7)
N3	0.141 (10)	0.100 (9)	0.097 (8)	0.042 (7)	-0.001 (8)	0.004 (7)
N2	0.147 (10)	0.099 (9)	0.079 (8)	-0.012 (7)	0.012 (7)	-0.012 (6)
N1	0.152 (11)	0.088 (8)	0.128 (10)	-0.011 (8)	0.045 (9)	-0.015 (7)
C2	0.172 (14)	0.061 (9)	0.091 (9)	-0.001 (9)	0.055 (11)	0.012 (6)
C20	0.079 (8)	0.070 (7)	0.127 (11)	0.017 (6)	-0.010 (7)	-0.006 (8)
C21	0.094 (7)	0.095 (7)	0.055 (6)	-0.002 (6)	0.059 (6)	-0.005 (5)

7. Appendix

C22	0.063 (7)	0.061 (7)	0.135 (12)	-0.005 (6)	-0.005 (8)	-0.001 (7)
C23	0.112 (10)	0.059 (7)	0.084 (9)	-0.007 (7)	0.055 (8)	0.002 (6)
C24	0.248 (19)	0.049 (7)	0.222 (17)	-0.046 (9)	-0.169 (17)	0.041 (9)
C25	0.136 (13)	0.085 (10)	0.119 (10)	-0.015 (10)	0.055 (10)	-0.027 (8)
C26	0.112 (12)	0.066 (8)	0.133 (13)	0.005 (7)	0.071 (10)	-0.020 (7)
C27	0.111 (11)	0.060 (8)	0.102 (10)	-0.001 (7)	0.040 (10)	-0.027 (6)
C28	0.093 (9)	0.081 (8)	0.145 (12)	-0.021 (6)	0.079 (8)	-0.015 (9)
C29	0.093 (10)	0.074 (9)	0.139 (12)	-0.012 (7)	-0.024 (10)	0.001 (8)
C30	0.100 (9)	0.074 (8)	0.075 (9)	-0.012 (6)	0.017 (7)	0.001 (6)
C31	0.112 (8)	0.130 (11)	0.110 (9)	0.051 (8)	0.059 (8)	-0.003 (9)
C32	0.107 (9)	0.204 (13)	0.081 (9)	0.044 (9)	0.011 (7)	0.024 (9)
C33	0.230 (16)	0.133 (11)	0.044 (6)	-0.025 (10)	-0.050 (8)	0.016 (6)
C34	0.152 (14)	0.37 (3)	0.095 (12)	-0.065 (15)	-0.023 (11)	-0.019 (14)
C35	0.166 (13)	0.39 (3)	0.115 (10)	-0.164 (17)	0.059 (9)	-0.083 (15)
C36	0.085 (8)	0.077 (10)	0.087 (9)	0.027 (7)	0.001 (7)	-0.001 (7)
C37	0.33 (2)	0.086 (8)	0.037 (6)	-0.086 (11)	0.108 (9)	-0.030 (6)
C38	0.102 (9)	0.127 (8)	0.151 (12)	0.024 (7)	0.014 (8)	0.035 (9)
C39	0.111 (10)	0.075 (8)	0.064 (7)	0.007 (7)	-0.004 (8)	-0.011 (6)
C40	0.106 (9)	0.36 (3)	0.110 (9)	-0.052 (13)	0.064 (8)	0.012 (13)
C41	0.075 (8)	0.110 (10)	0.254 (18)	0.002 (7)	0.073 (10)	-0.029 (9)
C43	0.048 (6)	0.154 (13)	0.128 (10)	-0.010 (7)	0.038 (7)	-0.023 (9)
C44	0.136 (11)	0.140 (10)	0.098 (9)	-0.041 (8)	-0.030 (7)	0.010 (8)
C42	0.121 (12)	0.125 (11)	0.48 (4)	-0.010 (10)	0.169 (17)	-0.010 (15)
C45	0.161 (12)	0.112 (10)	0.262 (19)	-0.035 (9)	0.067 (12)	0.027 (11)

Table 34. Fractional atomic coordinates and isotropic or equivalent isotropic displacement parameters (\AA^2) for Tetrahexylammonium TCNQ at 298 K

Atom	x	y	z	$U_{\text{iso}}^*/U_{\text{eq}}$	Occ. (<1)
N1	0.04862 (9)	0.16086 (12)	0.16020 (8)	0.0601 (4)	
C11	-0.01062 (12)	0.24639 (16)	0.11646 (10)	0.0649 (5)	
H11A	-0.0691	0.2171	0.1013	0.078*	
H11B	0.0084	0.2609	0.0734	0.078*	
C12	-0.01415 (15)	0.35275 (17)	0.15499 (12)	0.0785 (6)	
H12A	-0.0415	0.3411	0.1940	0.094*	
H12B	0.0447	0.3782	0.1759	0.094*	
C13	-0.06379 (15)	0.43762 (18)	0.10530 (13)	0.0859 (6)	
H13A	-0.1213	0.4100	0.0819	0.103*	
H13B	-0.0341	0.4525	0.0682	0.103*	
C14	-0.07319 (19)	0.5427 (2)	0.14404 (16)	0.1039 (8)	
H14A	-0.0995	0.5266	0.1831	0.125*	
H14B	-0.0156	0.5719	0.1652	0.125*	
C15	-0.1266 (2)	0.6270 (3)	0.0970 (2)	0.1448 (13)	
H15A	-0.1838	0.5972	0.0748	0.174*	
H15B	-0.0994	0.6448	0.0587	0.174*	
C16	-0.1375 (4)	0.7294 (3)	0.1365 (3)	0.217 (3)	
H16A	-0.1882	0.7233	0.1545	0.325*	
H16B	-0.1441	0.7898	0.1041	0.325*	
H16C	-0.0870	0.7402	0.1760	0.325*	
C21	0.14236 (11)	0.20160 (17)	0.18442 (11)	0.0672 (5)	

7. Appendix

H21A	0.1449	0.2595	0.2190	0.081*
H21B	0.1789	0.1432	0.2092	0.081*
C22	0.18005 (13)	0.24251 (18)	0.12502 (12)	0.0757 (6)
H22A	0.1798	0.1842	0.0912	0.091*
H22B	0.1432	0.2999	0.0993	0.091*
C23	0.27163 (13)	0.28467 (19)	0.15222 (13)	0.0830 (6)
H23A	0.3088	0.2271	0.1773	0.100*
H23B	0.2722	0.3425	0.1865	0.100*
C24	0.30795 (15)	0.3266 (2)	0.09223 (15)	0.0931 (7)
H24A	0.3100	0.2670	0.0598	0.112*
H24B	0.2677	0.3799	0.0652	0.112*
C25	0.39672 (19)	0.3768 (3)	0.1146 (2)	0.1265 (11)
H25A	0.4379	0.3232	0.1401	0.152*
H25B	0.3957	0.4356	0.1479	0.152*
C26	0.4279 (3)	0.4200 (3)	0.0523 (2)	0.1572 (16)
H26A	0.4249	0.3637	0.0173	0.236*
H26B	0.4870	0.4443	0.0694	0.236*
H26C	0.3917	0.4794	0.0305	0.236*
C31	0.04210 (12)	0.06154 (15)	0.11252 (10)	0.0634 (5)
H31A	-0.0189	0.0424	0.0946	0.076*
H31B	0.0635	0.0804	0.0712	0.076*
C32	0.09127 (14)	-0.03695 (17)	0.14837 (12)	0.0759 (6)
H32A	0.1527	-0.0195	0.1656	0.091*
H32B	0.0702	-0.0571	0.1896	0.091*

7. Appendix

C33	0.08016 (15)	-0.13085 (17)	0.09704 (12)	0.0788 (6)	
H33A	0.1001	-0.1100	0.0554	0.095*	
H33B	0.0188	-0.1489	0.0805	0.095*	
C34	0.13137 (18)	-0.23142 (19)	0.13246 (14)	0.0916 (7)	
H34A	0.1917	-0.2111	0.1528	0.110*	
H34B	0.1080	-0.2552	0.1717	0.110*	
C35	0.1284 (2)	-0.3226 (2)	0.08246 (16)	0.1069 (8)	
H35A	0.1534	-0.2997	0.0439	0.128*	
H35B	0.0681	-0.3420	0.0611	0.128*	
C36	0.1770 (2)	-0.4214 (2)	0.11858 (19)	0.1241 (10)	
H36A	0.2378	-0.4048	0.1356	0.186*	
H36B	0.1691	-0.4798	0.0846	0.186*	
H36C	0.1547	-0.4422	0.1585	0.186*	
C41	0.02005 (13)	0.13440 (18)	0.22771 (10)	0.0706 (5)	
H41A	0.0629	0.0864	0.2575	0.085*	
H41B	0.0200	0.2007	0.2547	0.085*	
C42	-0.06892 (14)	0.0821 (2)	0.21513 (12)	0.0903 (7)	
H42A	-0.1118	0.1267	0.1825	0.108*	
H42B	-0.0681	0.0120	0.1927	0.108*	
C43	-0.0947 (2)	0.0683 (3)	0.28454 (16)	0.1002 (8)	
H43A	-0.052 (2)	0.043 (3)	0.3216 (17)	0.129 (11)*	
H43B	-0.106 (3)	0.143 (4)	0.299 (2)	0.190 (18)*	
C44A	-0.1900 (6)	0.0361 (8)	0.2737 (5)	0.113 (2)	0.50
H44A	-0.2028	0.0303	0.3202	0.136*	0.50

7. Appendix

H44B	-0.2271	0.0920	0.2463	0.136*	0.50
C45A	-0.2100 (8)	-0.0703 (8)	0.2344 (7)	0.133 (3)	0.50
H45A	-0.1709	-0.1252	0.2609	0.159*	0.50
H45B	-0.1989	-0.0633	0.1873	0.159*	0.50
C44B	-0.1591 (4)	-0.0276 (9)	0.2843 (4)	0.0962 (19)	0.50
H44C	-0.1318	-0.0948	0.2759	0.115*	0.50
H44D	-0.1710	-0.0323	0.3312	0.115*	0.50
C45B	-0.2446 (4)	-0.0140 (8)	0.2269 (4)	0.097 (2)	0.50
H45C	-0.2732	0.0515	0.2366	0.116*	0.50
H45D	-0.2326	-0.0061	0.1802	0.116*	0.50
C46	-0.3045 (3)	-0.1083 (4)	0.2247 (2)	0.1309 (12)	
H46A	-0.311 (2)	-0.122 (3)	0.275 (2)	0.154 (13)*	
H46B	-0.292 (3)	-0.184 (5)	0.210 (3)	0.24 (2)*	
H46C	-0.374 (4)	-0.062 (4)	0.188 (3)	0.24 (2)*	
C1	0.40606 (11)	0.06160 (15)	0.05448 (10)	0.0616 (5)	
C2	0.40461 (12)	0.09745 (17)	-0.01543 (10)	0.0662 (5)	
H2	0.3542	0.0881	-0.0524	0.079*	
C3	0.47501 (12)	0.14541 (17)	-0.03036 (10)	0.0670 (5)	
H3	0.4716	0.1673	-0.0773	0.080*	
C4	0.55317 (11)	0.16275 (16)	0.02379 (10)	0.0629 (5)	
C5	0.55419 (12)	0.12803 (17)	0.09422 (10)	0.0682 (5)	
H5	0.6042	0.1386	0.1314	0.082*	
C6	0.48418 (12)	0.07978 (17)	0.10897 (10)	0.0683 (5)	
H6	0.4874	0.0581	0.1559	0.082*	

7. Appendix

C7	0.33237 (12)	0.01245 (17)	0.06959 (11)	0.0674 (5)	
C8	0.62572 (12)	0.21269 (16)	0.00801 (11)	0.0676 (5)	
C71	0.33354 (13)	-0.0223 (2)	0.13987 (14)	0.0810 (6)	
N71	0.33491 (14)	-0.0497 (2)	0.19727 (12)	0.1103 (7)	
C72	0.25139 (13)	0.00635 (19)	0.01720 (12)	0.0751 (6)	
N72	0.18515 (12)	0.00440 (19)	-0.02470 (11)	0.0983 (7)	
C81	0.70426 (14)	0.23047 (19)	0.06136 (12)	0.0775 (6)	
N81	0.76811 (13)	0.2449 (2)	0.10434 (12)	0.1097 (8)	
C82	0.62253 (13)	0.2556 (2)	-0.06055 (13)	0.0829 (6)	
N82	0.62019 (16)	0.2919 (2)	-0.11570 (13)	0.1238 (9)	

Table 35. Atomic displacement parameters (\AA^2) Tetrahexylammonium TCNQ 298 K

Atom	U^{11}	U^{22}	U^{33}	U^{12}	U^{13}	U^{23}
N1	0.0520 (8)	0.0646 (9)	0.0612 (9)	-0.0015 (7)	0.0101 (7)	-0.0036 (7)
C11	0.0534 (10)	0.0686 (12)	0.0697 (11)	0.0019 (9)	0.0107 (8)	-0.0002 (9)
C12	0.0782 (14)	0.0716 (13)	0.0858 (14)	0.0077 (11)	0.0214 (11)	-0.0055 (11)
C13	0.0780 (14)	0.0725 (14)	0.1049 (17)	0.0064 (11)	0.0194 (12)	0.0002 (12)
C14	0.115 (2)	0.0759 (15)	0.133 (2)	0.0153 (14)	0.0530 (17)	0.0069 (15)
C15	0.154 (3)	0.097 (2)	0.192 (4)	0.039 (2)	0.062 (3)	0.027 (2)
C16	0.279 (6)	0.095 (3)	0.329 (7)	0.065 (3)	0.177 (5)	0.027 (3)
C21	0.0517 (10)	0.0689 (12)	0.0755 (12)	-0.0039 (9)	0.0067 (9)	-0.0087 (9)
C22	0.0622 (12)	0.0767 (13)	0.0885 (14)	-0.0094 (10)	0.0203 (10)	-0.0107 (11)
C23	0.0619 (12)	0.0768 (14)	0.1093 (17)	-0.0089 (11)	0.0205 (12)	-0.0125 (12)
C24	0.0812 (15)	0.0785 (15)	0.130 (2)	-0.0115 (12)	0.0465 (15)	-0.0198 (14)

7. Appendix

C25	0.0980 (19)	0.116 (2)	0.180 (3)	-0.0374 (17)	0.063 (2)	-0.034 (2)
C26	0.167 (3)	0.139 (3)	0.208 (4)	-0.067 (2)	0.125 (3)	-0.053 (3)
C31	0.0582 (10)	0.0657 (11)	0.0648 (11)	-0.0054 (9)	0.0134 (9)	-0.0076 (9)
C32	0.0697 (12)	0.0693 (13)	0.0862 (14)	0.0025 (10)	0.0155 (10)	-0.0034 (11)
C33	0.0917 (15)	0.0663 (13)	0.0829 (14)	-0.0040 (11)	0.0308 (12)	-0.0032 (11)
C34	0.1067 (18)	0.0732 (14)	0.0957 (16)	-0.0003 (13)	0.0276 (14)	-0.0042 (12)
C35	0.126 (2)	0.0859 (17)	0.115 (2)	0.0069 (16)	0.0410 (17)	-0.0059 (15)
C36	0.136 (3)	0.0789 (17)	0.167 (3)	0.0213 (17)	0.056 (2)	0.0097 (18)
C41	0.0665 (12)	0.0796 (13)	0.0638 (11)	0.0016 (10)	0.0136 (9)	-0.0012 (10)
C42	0.0684 (13)	0.125 (2)	0.0794 (14)	-0.0121 (13)	0.0223 (11)	0.0061 (14)
C43	0.0856 (18)	0.134 (3)	0.0879 (18)	-0.0079 (17)	0.0339 (15)	0.0042 (18)
C44A	0.095 (6)	0.141 (7)	0.117 (6)	0.006 (5)	0.052 (5)	0.002 (5)
C45A	0.109 (7)	0.132 (8)	0.166 (9)	-0.006 (5)	0.055 (7)	-0.010 (7)
C44B	0.080 (4)	0.129 (6)	0.085 (4)	0.005 (4)	0.031 (3)	0.024 (4)
C45B	0.078 (4)	0.125 (6)	0.088 (4)	-0.005 (4)	0.022 (3)	0.020 (4)
C46	0.119 (3)	0.155 (4)	0.129 (3)	-0.028 (3)	0.050 (2)	0.012 (3)
C1	0.0521 (10)	0.0669 (11)	0.0669 (11)	0.0047 (8)	0.0175 (8)	-0.0026 (9)
C2	0.0504 (10)	0.0802 (13)	0.0653 (11)	0.0006 (9)	0.0101 (8)	-0.0009 (10)
C3	0.0567 (11)	0.0795 (13)	0.0624 (11)	-0.0004 (10)	0.0108 (9)	0.0052 (9)
C4	0.0534 (10)	0.0663 (11)	0.0671 (11)	0.0017 (9)	0.0121 (8)	0.0003 (9)
C5	0.0531 (10)	0.0799 (13)	0.0672 (12)	-0.0003 (9)	0.0076 (9)	-0.0004 (10)
C6	0.0598 (11)	0.0850 (14)	0.0599 (11)	0.0022 (10)	0.0152 (9)	0.0031 (10)
C7	0.0531 (11)	0.0793 (13)	0.0721 (12)	0.0011 (9)	0.0203 (9)	-0.0009 (10)
C8	0.0544 (10)	0.0722 (12)	0.0730 (12)	-0.0034 (9)	0.0109 (9)	0.0074 (10)

7. Appendix

C71	0.0618 (12)	0.1027 (17)	0.0823 (15)	-0.0066 (11)	0.0257 (11)	0.0018 (13)
N71	0.0927 (15)	0.152 (2)	0.0904 (15)	-0.0153 (14)	0.0313 (12)	0.0148 (14)
C72	0.0569 (12)	0.0897 (15)	0.0835 (14)	-0.0025 (11)	0.0268 (11)	0.0009 (12)
N72	0.0587 (11)	0.1310 (18)	0.1011 (14)	-0.0092 (11)	0.0135 (10)	0.0075 (13)
C81	0.0592 (12)	0.0864 (15)	0.0864 (14)	-0.0088 (11)	0.0178 (11)	0.0052 (12)
N81	0.0654 (12)	0.145 (2)	0.1085 (16)	-0.0200 (13)	0.0045 (11)	-0.0030 (14)
C82	0.0633 (13)	0.0913 (16)	0.0893 (16)	-0.0074 (11)	0.0112 (11)	0.0176 (13)
N82	0.1113 (18)	0.152 (2)	0.1023 (16)	-0.0126 (16)	0.0178 (13)	0.0500 (16)

Table 36. Fractional atomic coordinates and isotropic or equivalent isotropic displacement parameters (\AA^2) Tetrahexylammonium TCNQ 100 K

Atom	x	y	z	$U_{\text{iso}}^*/U_{\text{eq}}$
N1	0.04932 (7)	0.16136 (9)	0.16173 (7)	0.0185 (2)
C11	-0.01108 (9)	0.24958 (11)	0.11799 (8)	0.0202 (3)
H11A	0.0062	0.2643	0.0718	0.024*
H11B	-0.0715	0.2205	0.1040	0.024*
C12	-0.01070 (10)	0.35751 (12)	0.15887 (8)	0.0236 (3)
H12A	0.0503	0.3833	0.1776	0.028*
H12B	-0.0348	0.3452	0.2020	0.028*
C13	-0.06425 (10)	0.44628 (12)	0.10960 (9)	0.0238 (3)
H13A	-0.1249	0.4198	0.0894	0.029*
H13B	-0.0388	0.4610	0.0675	0.029*
C14	-0.06568 (10)	0.55261 (12)	0.15268 (9)	0.0255 (3)
H14A	-0.0874	0.5360	0.1965	0.031*

7. Appendix

H14B	-0.0051	0.5803	0.1706	0.031*
C15	-0.12209 (12)	0.64280 (14)	0.10819 (10)	0.0342 (4)
H15A	-0.1827	0.6154	0.0895	0.041*
H15B	-0.0998	0.6612	0.0649	0.041*
C16	-0.12287 (15)	0.74668 (14)	0.15391 (13)	0.0448 (5)
H16A	-0.1467	0.7294	0.1959	0.067*
H16B	-0.1593	0.8027	0.1230	0.067*
H16C	-0.0631	0.7745	0.1722	0.067*
C21	0.14352 (9)	0.20216 (11)	0.18541 (8)	0.0213 (3)
H21A	0.1469	0.2632	0.2210	0.026*
H21B	0.1810	0.1419	0.2116	0.026*
C22	0.18000 (10)	0.24171 (12)	0.12268 (9)	0.0241 (3)
H22A	0.1420	0.3007	0.0952	0.029*
H22B	0.1796	0.1802	0.0880	0.029*
C23	0.27304 (10)	0.28532 (12)	0.15058 (9)	0.0254 (3)
H23A	0.2737	0.3461	0.1859	0.030*
H23B	0.3113	0.2260	0.1772	0.030*
C24	0.30864 (10)	0.32663 (13)	0.08740 (10)	0.0280 (3)
H24A	0.3100	0.2645	0.0536	0.034*
H24B	0.2679	0.3825	0.0592	0.034*
C25	0.39945 (12)	0.37663 (17)	0.11134 (12)	0.0404 (4)
H25A	0.4411	0.3202	0.1376	0.048*
H25B	0.3991	0.4374	0.1464	0.048*
C26	0.43052 (15)	0.42052 (18)	0.04623 (13)	0.0507 (6)

7. Appendix

H26A	0.4281	0.3616	0.0101	0.076*
H26B	0.4908	0.4469	0.0639	0.076*
H26C	0.3927	0.4812	0.0229	0.076*
C31	0.04137 (9)	0.06045 (11)	0.11241 (8)	0.0196 (3)
H31A	-0.0210	0.0393	0.0958	0.024*
H31B	0.0607	0.0804	0.0679	0.024*
C32	0.09367 (10)	-0.03847 (12)	0.14867 (8)	0.0228 (3)
H32A	0.0752	-0.0592	0.1934	0.027*
H32B	0.1565	-0.0192	0.1641	0.027*
C33	0.08021 (10)	-0.13583 (11)	0.09551 (8)	0.0219 (3)
H33A	0.0171	-0.1537	0.0793	0.026*
H33B	0.0996	-0.1152	0.0512	0.026*
C34	0.13059 (10)	-0.23694 (12)	0.13090 (8)	0.0229 (3)
H34A	0.1092	-0.2594	0.1739	0.027*
H34B	0.1932	-0.2177	0.1493	0.027*
C35	0.12155 (11)	-0.33338 (12)	0.07773 (9)	0.0263 (3)
H35A	0.1442	-0.3113	0.0353	0.032*
H35B	0.0588	-0.3512	0.0583	0.032*
C36	0.16992 (12)	-0.43587 (13)	0.11302 (11)	0.0334 (4)
H36A	0.2328	-0.4209	0.1283	0.050*
H36B	0.1585	-0.4962	0.0771	0.050*
H36C	0.1496	-0.4565	0.1563	0.050*
C41	0.02241 (9)	0.13331 (12)	0.23204 (8)	0.0209 (3)
H41A	0.0686	0.0870	0.2638	0.025*

7. Appendix

H41B	0.0194	0.2023	0.2592	0.025*
C42	-0.06448 (10)	0.07369 (13)	0.22018 (9)	0.0250 (3)
H42A	-0.0587	-0.0024	0.2033	0.030*
H42B	-0.1095	0.1117	0.1815	0.030*
C43	-0.09258 (10)	0.07114 (14)	0.29235 (9)	0.0273 (3)
H43A	-0.1170	0.1437	0.3002	0.033*
H43B	-0.0407	0.0576	0.3341	0.033*
C44	-0.16099 (11)	-0.01783 (14)	0.29191 (9)	0.0303 (3)
H44A	-0.1358	-0.0902	0.2848	0.036*
H44B	-0.1741	-0.0188	0.3408	0.036*
C45	-0.24599 (11)	-0.00247 (14)	0.23241 (10)	0.0314 (4)
H45A	-0.2326	0.0065	0.1840	0.038*
H45B	-0.2748	0.0657	0.2427	0.038*
C46	-0.30875 (11)	-0.09845 (15)	0.22787 (10)	0.0327 (4)
H46A	-0.2843	-0.1639	0.2102	0.049*
H46B	-0.3651	-0.0803	0.1935	0.049*
H46C	-0.3173	-0.1130	0.2770	0.049*
C1	0.40617 (9)	0.06247 (11)	0.05459 (8)	0.0209 (3)
C2	0.40720 (9)	0.09730 (12)	-0.01753 (8)	0.0222 (3)
H2	0.3565	0.0871	-0.0572	0.027*
C3	0.47967 (9)	0.14538 (12)	-0.03129 (8)	0.0225 (3)
H3	0.4782	0.1674	-0.0803	0.027*
C4	0.55684 (9)	0.16292 (11)	0.02628 (8)	0.0212 (3)
C5	0.55560 (9)	0.12975 (12)	0.09889 (8)	0.0229 (3)

7. Appendix

H5	0.6060	0.1413	0.1387	0.027*
C6	0.48327 (10)	0.08147 (13)	0.11259 (8)	0.0229 (3)
H6	0.4845	0.0602	0.1616	0.027*
C7	0.33107 (9)	0.01325 (12)	0.06859 (8)	0.0222 (3)
C8	0.63178 (9)	0.21176 (12)	0.01200 (8)	0.0226 (3)
C71	0.33065 (10)	-0.02220 (13)	0.14089 (9)	0.0256 (3)
N71	0.33074 (10)	-0.04975 (14)	0.19990 (8)	0.0350 (3)
C72	0.25049 (10)	0.00717 (12)	0.01375 (9)	0.0236 (3)
N72	0.18406 (9)	0.00501 (12)	-0.03016 (8)	0.0307 (3)
C81	0.70998 (10)	0.22773 (12)	0.06836 (9)	0.0236 (3)
N81	0.77408 (9)	0.24086 (12)	0.11336 (8)	0.0316 (3)
C82	0.63230 (10)	0.25505 (13)	-0.05842 (9)	0.0276 (3)
N82	0.63405 (10)	0.29192 (14)	-0.11473 (9)	0.0397 (4)

Table 37. Atomic displacement parameters (\AA^2) Tetrahexylammonium TCNQ 100 K

Atom	U^{11}	U^{22}	U^{33}	U^{12}	U^{13}	U^{23}
N1	0.0178 (5)	0.0094 (5)	0.0278 (6)	-0.0009 (4)	0.0053 (4)	-0.0010 (4)
C11	0.0187 (6)	0.0107 (6)	0.0304 (7)	0.0021 (5)	0.0049 (5)	0.0005 (5)
C12	0.0261 (7)	0.0126 (6)	0.0316 (7)	0.0031 (5)	0.0066 (6)	-0.0016 (5)
C13	0.0240 (7)	0.0126 (6)	0.0342 (8)	0.0011 (5)	0.0062 (6)	-0.0009 (5)
C14	0.0287 (7)	0.0109 (6)	0.0386 (8)	0.0015 (5)	0.0119 (6)	-0.0011 (5)
C15	0.0385 (9)	0.0169 (7)	0.0482 (10)	0.0085 (7)	0.0130 (8)	0.0048 (7)
C16	0.0575 (12)	0.0135 (8)	0.0716 (14)	0.0108 (8)	0.0313 (11)	0.0036 (8)
C21	0.0176 (6)	0.0113 (6)	0.0336 (7)	-0.0015 (5)	0.0045 (5)	-0.0025 (5)

7. Appendix

C22	0.0212 (7)	0.0163 (7)	0.0348 (8)	-0.0024 (5)	0.0074 (6)	-0.0028 (5)
C23	0.0209 (7)	0.0149 (7)	0.0406 (8)	-0.0034 (5)	0.0086 (6)	-0.0020 (6)
C24	0.0283 (8)	0.0146 (7)	0.0450 (9)	-0.0022 (6)	0.0164 (7)	-0.0043 (6)
C25	0.0366 (9)	0.0323 (10)	0.0588 (11)	-0.0154 (8)	0.0242 (9)	-0.0125 (8)
C26	0.0553 (13)	0.0392 (11)	0.0715 (14)	-0.0242 (10)	0.0412 (11)	-0.0215 (10)
C31	0.0206 (6)	0.0097 (6)	0.0282 (7)	-0.0005 (5)	0.0056 (5)	-0.0029 (5)
C32	0.0238 (7)	0.0118 (6)	0.0312 (7)	0.0013 (5)	0.0045 (6)	-0.0026 (5)
C33	0.0244 (7)	0.0112 (6)	0.0305 (7)	-0.0011 (5)	0.0077 (6)	-0.0019 (5)
C34	0.0262 (7)	0.0116 (6)	0.0309 (7)	0.0010 (5)	0.0072 (6)	-0.0004 (5)
C35	0.0325 (8)	0.0116 (6)	0.0361 (8)	0.0009 (6)	0.0114 (6)	-0.0031 (5)
C36	0.0377 (9)	0.0128 (7)	0.0530 (10)	0.0037 (6)	0.0176 (8)	0.0008 (6)
C41	0.0233 (7)	0.0133 (6)	0.0265 (7)	-0.0001 (5)	0.0068 (5)	-0.0005 (5)
C42	0.0237 (7)	0.0218 (7)	0.0306 (7)	-0.0023 (6)	0.0091 (6)	0.0006 (6)
C43	0.0267 (7)	0.0254 (8)	0.0315 (8)	0.0014 (6)	0.0107 (6)	0.0014 (6)
C44	0.0284 (8)	0.0288 (8)	0.0361 (8)	0.0018 (6)	0.0129 (7)	0.0069 (6)
C45	0.0291 (8)	0.0278 (8)	0.0389 (9)	-0.0007 (6)	0.0117 (7)	0.0074 (7)
C46	0.0286 (8)	0.0279 (9)	0.0435 (9)	-0.0026 (7)	0.0127 (7)	0.0035 (7)
C1	0.0195 (6)	0.0141 (6)	0.0291 (7)	0.0012 (5)	0.0066 (5)	-0.0014 (5)
C2	0.0189 (6)	0.0165 (7)	0.0300 (7)	0.0013 (5)	0.0042 (5)	0.0002 (5)
C3	0.0223 (7)	0.0177 (7)	0.0271 (7)	0.0004 (5)	0.0055 (6)	0.0019 (5)
C4	0.0201 (6)	0.0123 (6)	0.0311 (7)	0.0007 (5)	0.0067 (6)	-0.0007 (5)
C5	0.0191 (7)	0.0199 (7)	0.0283 (7)	-0.0001 (5)	0.0038 (5)	-0.0013 (5)
C6	0.0224 (7)	0.0199 (7)	0.0266 (7)	0.0003 (5)	0.0068 (6)	0.0006 (5)
C7	0.0211 (7)	0.0164 (7)	0.0302 (7)	0.0000 (5)	0.0085 (6)	0.0000 (5)

7. Appendix

C8	0.0203 (7)	0.0152 (6)	0.0319 (7)	-0.0007 (5)	0.0059 (6)	0.0009 (5)
C71	0.0191 (7)	0.0228 (7)	0.0354 (8)	-0.0011 (6)	0.0078 (6)	-0.0001 (6)
N71	0.0303 (7)	0.0395 (9)	0.0362 (8)	-0.0038 (6)	0.0104 (6)	0.0036 (6)
C72	0.0230 (7)	0.0164 (7)	0.0337 (7)	-0.0001 (5)	0.0115 (6)	0.0012 (5)
N72	0.0240 (7)	0.0276 (7)	0.0400 (8)	-0.0016 (5)	0.0074 (6)	0.0031 (6)
C81	0.0228 (7)	0.0160 (7)	0.0331 (7)	-0.0012 (5)	0.0089 (6)	0.0003 (5)
N81	0.0250 (7)	0.0270 (7)	0.0413 (8)	-0.0022 (5)	0.0058 (6)	-0.0027 (6)
C82	0.0207 (7)	0.0225 (8)	0.0372 (8)	-0.0037 (6)	0.0032 (6)	0.0034 (6)
N82	0.0320 (8)	0.0410 (9)	0.0427 (8)	-0.0069 (7)	0.0036 (7)	0.0139 (7)

Table 38. Fractional atomic coordinates and isotropic or equivalent isotropic displacement parameters (\AA^2) for Tetrabutylammonium Tetracyanoquinodimethane

Atom	X	y	z	$U_{\text{iso}}^*/U_{\text{eq}}$	Occ. (<1)
N21	0.0663 (6)	0.3642 (5)	0.7721 (3)	0.0849 (13)	
N22	0.4635 (5)	0.2727 (5)	0.9369 (3)	0.0860 (13)	
N1	0.0047 (12)	0.4807 (10)	0.4959 (5)	0.070 (3)	0.526 (4)
C1	0.0136 (11)	0.3930 (9)	0.4345 (6)	0.078 (3)	0.526 (4)
H1A	0.0425	0.4491	0.3758	0.093*	0.526 (4)
H1B	-0.1003	0.3680	0.4386	0.093*	0.526 (4)
C3	0.1240 (17)	0.1708 (13)	0.3898 (9)	0.118 (4)	0.526 (4)
H3A	0.0083	0.1455	0.4026	0.142*	0.526 (4)
H3B	0.1412	0.2231	0.3294	0.142*	0.526 (4)
C5	0.1740 (11)	0.5269 (11)	0.4905 (6)	0.084 (3)	0.526 (4)
H5A	0.2597	0.4452	0.4970	0.100*	0.526 (4)
H5B	0.1696	0.5646	0.5403	0.100*	0.526 (4)
C7	0.4254 (14)	0.6423 (13)	0.3998 (8)	0.107 (4)	0.526 (4)
H7A	0.4872	0.5489	0.4114	0.128*	0.526 (4)
H7B	0.4452	0.6862	0.4431	0.128*	0.526 (4)
C2	0.139 (3)	0.2616 (16)	0.4469 (13)	0.093 (4)	0.526 (4)

7. Appendix

H2A	0.2554	0.2859	0.4347	0.111*	0.526 (4)
H2B	0.1205	0.2096	0.5073	0.111*	0.526 (4)
C4	0.250 (3)	0.0415 (18)	0.4013 (16)	0.155 (8)	0.526 (4)
H4A	0.2339	-0.0124	0.3633	0.186*	0.526 (4)
H4B	0.2322	-0.0119	0.4607	0.186*	0.526 (4)
H4C	0.3650	0.0657	0.3873	0.186*	0.526 (4)
C6	0.2376 (18)	0.634 (3)	0.4091 (12)	0.173 (15)	0.526 (4)
H6A	0.2140	0.6100	0.3583	0.207*	0.526 (4)
H6B	0.1739	0.7241	0.4109	0.207*	0.526 (4)
C8	0.497 (2)	0.7227 (18)	0.3106 (9)	0.105 (7)	0.526 (4)
H8A	0.6164	0.7280	0.3091	0.126*	0.526 (4)
H8B	0.4349	0.8147	0.2982	0.126*	0.526 (4)
H8C	0.4840	0.6765	0.2677	0.126*	0.526 (4)
C1A	-0.1189 (13)	0.6075 (10)	0.4711 (7)	0.090 (3)	0.526 (4)
H1A1	-0.2303	0.5788	0.4738	0.108*	0.526 (4)
H1A2	-0.0825	0.6533	0.4108	0.108*	0.526 (4)
C3A	-0.2932 (19)	0.8253 (14)	0.5120 (9)	0.137 (5)	0.526 (4)
H3A1	-0.2869	0.8727	0.4506	0.164*	0.526 (4)
H3A2	-0.3982	0.7823	0.5287	0.164*	0.526 (4)
C5A	-0.0564 (12)	0.4097 (13)	0.5871 (5)	0.097 (3)	0.526 (4)
H5A1	-0.0346	0.4626	0.6251	0.116*	0.526 (4)
H5A2	0.0116	0.3191	0.6015	0.116*	0.526 (4)
C7A	-0.304 (2)	0.2917 (16)	0.6907 (8)	0.140 (5)	0.526 (4)
H7A1	-0.3163	0.3343	0.7390	0.168*	0.526 (4)
H7A2	-0.2222	0.2078	0.7014	0.168*	0.526 (4)
C2A	-0.143 (3)	0.713 (2)	0.5237 (16)	0.116 (6)	0.526 (4)
H2A1	-0.1535	0.6643	0.5849	0.139*	0.526 (4)
H2A2	-0.0396	0.7578	0.5103	0.139*	0.526 (4)
C4A	-0.305 (3)	0.931 (2)	0.5627 (15)	0.159 (8)	0.526 (4)
H4A1	-0.4036	0.9989	0.5508	0.238*	0.526 (4)
H4A2	-0.2027	0.9756	0.5461	0.238*	0.526 (4)

7. Appendix

H4A3	-0.3161	0.8859	0.6239	0.238*	0.526 (4)
C6A	-0.2459 (13)	0.3897 (19)	0.6069 (11)	0.083 (5)	0.526 (4)
H6A1	-0.3131	0.4798	0.6060	0.099*	0.526 (4)
H6A2	-0.2736	0.3581	0.5599	0.099*	0.526 (4)
C8A	-0.475 (3)	0.259 (4)	0.680 (2)	0.26 (2)	0.526 (4)
H8A1	-0.5219	0.1980	0.7326	0.396*	0.526 (4)
H8A2	-0.4602	0.2158	0.6326	0.396*	0.526 (4)
H8A3	-0.5532	0.3441	0.6675	0.396*	0.526 (4)
C21	0.0165 (5)	0.3358 (4)	0.9976 (2)	0.0482 (9)	
C26	0.0629 (5)	0.3122 (4)	1.0830 (3)	0.0527 (9)	
H26	0.1783	0.2920	1.0908	0.063*	
C22	-0.1643 (5)	0.3663 (4)	0.9894 (2)	0.0485 (9)	
H22	-0.1987	0.3820	0.9349	0.058*	
C27	0.1402 (5)	0.3281 (4)	0.9262 (3)	0.0526 (9)	
C29	0.3188 (5)	0.2964 (4)	0.9330 (3)	0.0595 (10)	
C28	0.0977 (5)	0.3499 (4)	0.8412 (3)	0.0607 (11)	
C24	-0.2382 (5)	0.3485 (4)	1.1439 (2)	0.0520 (9)	
C25	-0.0603 (5)	0.3191 (4)	1.1526 (2)	0.0546 (10)	
H25	-0.0274	0.3042	1.2073	0.066*	
C211	-0.5456 (6)	0.3827 (5)	1.2079 (3)	0.0708 (12)	
C210	-0.3668 (6)	0.3541 (5)	1.2156 (3)	0.0620 (11)	
C23	-0.2835 (5)	0.3725 (4)	1.0591 (3)	0.0535 (10)	
H23	-0.3991	0.3932	1.0518	0.064*	
C212	-0.3261 (6)	0.3260 (6)	1.3029 (3)	0.0784 (14)	
N24	-0.3020 (8)	0.3045 (6)	1.3729 (3)	0.122 (2)	
N23	-0.6885 (6)	0.4071 (6)	1.2026 (3)	0.1004 (15)	
C10	0.8811 (5)	0.0058 (4)	0.0764 (3)	0.0584 (10)	
C12	1.0635 (6)	-0.0272 (4)	0.0791 (3)	0.0637 (11)	
H12	1.1045	-0.0441	0.1321	0.076*	
C13	0.7665 (6)	0.0107 (4)	0.1504 (3)	0.0635 (11)	
C11	0.8242 (5)	0.0343 (4)	-0.0068 (3)	0.0614 (11)	

7. Appendix

H11	0.7073	0.0581	-0.0110	0.074*	
C15	0.8205 (7)	-0.0162 (5)	0.2336 (4)	0.0796 (14)	
C14	0.5845 (7)	0.0434 (5)	0.1487 (3)	0.0781 (13)	
N12	0.8668 (7)	-0.0351 (6)	0.2997 (3)	0.1112 (17)	
N11	0.4391 (6)	0.0684 (6)	0.1471 (3)	0.1055 (16)	

Table 39. Atomic displacement parameters (\AA^2) for Tetrabutylammonium Tetracyanoquinodimethane

Atom	U^{11}	U^{22}	U^{33}	U^{12}	U^{13}	U^{23}
N21	0.093 (3)	0.102 (3)	0.055 (2)	0.005 (2)	-0.011 (2)	-0.022 (2)
N22	0.058 (2)	0.101 (3)	0.094 (3)	0.004 (2)	-0.013 (2)	-0.023 (2)
N1	0.069 (4)	0.087 (7)	0.056 (4)	-0.022 (5)	-0.020 (3)	-0.004 (4)
C1	0.083 (6)	0.099 (7)	0.057 (5)	-0.034 (5)	-0.027 (4)	-0.005 (5)
C3	0.123 (10)	0.117 (10)	0.128 (11)	-0.021 (8)	-0.019 (8)	-0.048 (9)
C5	0.076 (6)	0.117 (8)	0.068 (6)	-0.038 (6)	-0.014 (5)	-0.021 (6)
C7	0.099 (8)	0.107 (9)	0.113 (9)	-0.027 (7)	0.012 (7)	-0.036 (7)
C2	0.093 (9)	0.105 (11)	0.086 (12)	-0.025 (8)	-0.023 (8)	-0.019 (7)
C4	0.164 (17)	0.143 (16)	0.19 (2)	0.000 (13)	-0.054 (13)	-0.081 (14)
C6	0.17 (2)	0.31 (4)	0.088 (13)	-0.16 (2)	0.013 (11)	-0.068 (15)
C8	0.081 (10)	0.096 (10)	0.128 (14)	-0.031 (8)	0.055 (10)	-0.045 (11)
C1A	0.078 (7)	0.114 (9)	0.083 (7)	-0.036 (6)	-0.008 (5)	-0.021 (6)
C3A	0.147 (13)	0.145 (13)	0.105 (10)	-0.010 (10)	0.010 (9)	-0.031 (9)
C5A	0.113 (8)	0.135 (10)	0.048 (5)	-0.045 (7)	-0.016 (5)	-0.011 (5)
C7A	0.123 (12)	0.181 (15)	0.126 (12)	-0.037 (10)	0.016 (9)	-0.067 (11)
C2A	0.113 (12)	0.122 (13)	0.114 (18)	-0.005 (10)	-0.023 (10)	-0.035 (10)
C4A	0.168 (19)	0.139 (15)	0.18 (2)	-0.006 (13)	-0.005 (14)	-0.070 (14)
C6A	0.083 (9)	0.102 (9)	0.058 (7)	-0.029 (7)	0.004 (6)	-0.011 (7)
C8A	0.12 (2)	0.28 (4)	0.30 (5)	-0.04 (2)	-0.01 (3)	0.08 (3)

7. Appendix

C21	0.053 (2)	0.042 (2)	0.052 (2)	-0.0053 (15)	-0.0124 (16)	-0.0114 (16)
C26	0.051 (2)	0.053 (2)	0.057 (2)	-0.0018 (16)	-0.0191 (18)	-0.0132 (18)
C22	0.055 (2)	0.048 (2)	0.045 (2)	-0.0022 (16)	-0.0147 (16)	-0.0127 (16)
C27	0.053 (2)	0.051 (2)	0.056 (2)	-0.0019 (16)	-0.0097 (17)	-0.0183 (18)
C29	0.056 (2)	0.061 (3)	0.061 (3)	-0.0021 (19)	-0.0061 (19)	-0.018 (2)
C28	0.064 (3)	0.059 (3)	0.053 (3)	0.0024 (19)	0.0019 (19)	-0.0162 (19)
C24	0.058 (2)	0.050 (2)	0.051 (2)	-0.0092 (17)	-0.0112 (17)	-0.0162 (17)
C25	0.062 (2)	0.061 (2)	0.046 (2)	-0.0071 (18)	-0.0173 (18)	-0.0144 (18)
C211	0.068 (3)	0.089 (3)	0.060 (3)	-0.015 (2)	-0.001 (2)	-0.027 (2)
C210	0.069 (3)	0.071 (3)	0.051 (2)	-0.014 (2)	-0.0053 (19)	-0.022 (2)
C23	0.051 (2)	0.054 (2)	0.060 (2)	-0.0062 (17)	-0.0143 (18)	-0.0175 (18)
C212	0.084 (3)	0.097 (4)	0.062 (3)	-0.026 (3)	-0.003 (2)	-0.027 (3)
N24	0.162 (5)	0.159 (5)	0.059 (3)	-0.042 (4)	-0.022 (3)	-0.035 (3)
N23	0.068 (3)	0.137 (4)	0.103 (4)	-0.011 (3)	-0.005 (2)	-0.048 (3)
C10	0.066 (3)	0.045 (2)	0.065 (3)	0.0004 (18)	-0.019 (2)	-0.0126 (18)
C12	0.073 (3)	0.058 (2)	0.063 (3)	0.001 (2)	-0.026 (2)	-0.016 (2)
C13	0.074 (3)	0.050 (2)	0.065 (3)	-0.004 (2)	-0.009 (2)	-0.014 (2)
C11	0.057 (2)	0.057 (2)	0.071 (3)	0.0031 (18)	-0.020 (2)	-0.016 (2)
C15	0.092 (4)	0.071 (3)	0.072 (3)	-0.008 (3)	-0.008 (3)	-0.018 (3)
C14	0.080 (3)	0.071 (3)	0.074 (3)	-0.003 (3)	-0.003 (3)	-0.013 (2)
N12	0.139 (5)	0.130 (4)	0.066 (3)	-0.022 (3)	-0.020 (3)	-0.022 (3)
N11	0.076 (3)	0.121 (4)	0.108 (4)	-0.006 (3)	-0.001 (3)	-0.021 (3)

Table 40 Fractional atomic coordinates for Tetraphenylphosphonium
Tetracyanoquinodimethane

Atom	<i>x</i>	<i>y</i>	<i>z</i>
P1	0.8982	0.3995	0.7592
C1	1.0306	0.2334	0.7891
H1	1.0135	0.2643	0.8134
C2	0.9800	0.4834	0.7996
C3	0.7125	0.3656	0.7666
C4	0.9036	0.4646	0.7163
C5	0.9957	0.2832	0.7556
C6	1.1812	0.5472	0.8459
H6	1.2778	0.5414	0.8570
C7	0.6202	0.3182	0.7346
H7	0.6533	0.3102	0.7099
C8	0.8999	0.5640	0.8131
H8	0.8038	0.5707	0.8017
C9	0.6597	0.3773	0.8022
H9	0.7187	0.4094	0.8237
C10	0.7839	0.5174	0.7020
H10	0.6952	0.5132	0.7131
C11	1.0339	0.4714	0.6981
H11	1.1156	0.4356	0.7069
C12	1.0227	0.2367	0.7200
H12	0.9990	0.2688	0.6973
C13	0.7959	0.5773	0.6708
H13	0.7158	0.6144	0.6619

7. Appendix

C14	0.5173	0.3413	0.8064
H14	0.4817	0.3486	0.8308
C15	0.4805	0.2839	0.7400
H15	0.4206	0.2519	0.7187
C16	0.4283	0.2944	0.7742
H16	0.3329	0.2708	0.7768
C17	1.0965	0.6260	0.8600
H17	1.1350	0.6719	0.8808
C18	0.9577	0.6344	0.8428
H18	0.9010	0.6880	0.8512
C19	1.0895	0.1398	0.7864
H19	1.1100	0.1061	0.8089
C20	1.1189	0.0946	0.7505
H20	1.1619	0.0315	0.7489
C21	1.0848	0.1426	0.7177
H21	1.1036	0.1117	0.6935
C22	0.9212	0.5818	0.6537
H22	0.9264	0.6198	0.6323
C23	1.0418	0.5306	0.6675
H23	1.1296	0.5360	0.6560
C24	1.1221	0.4770	0.8151
H24	1.1802	0.4259	0.8054
P2	0.3438	0.1021	0.2404
C31	0.4445	0.2218	0.2451
C32	0.4429	0.2777	0.2124
H32	0.3965	0.2501	0.1883
C33	0.3906	0.0244	0.1991
C34	0.3892	0.0346	0.2832

7. Appendix

C35	0.1522	0.1327	0.2356
C36	0.5066	0.2645	0.2811
H36	0.5043	0.2294	0.3033
C37	0.5758	0.4141	0.2519
H37	0.6223	0.4783	0.2540
C38	0.5097	0.3730	0.2158
H38	0.5105	0.4098	0.1940
C39	0.5531	-0.0246	0.1508
H39	0.6389	-0.0117	0.1393
C40	0.3035	-0.0635	0.1861
H40	0.2209	-0.0796	0.1985
C41	0.2815	-0.0164	0.3001
H41	0.1823	-0.0118	0.2908
C42	0.5368	0.0256	0.2971
H42	0.6110	0.0588	0.2858
C43	0.4620	-0.0825	0.3436
H43	0.4859	-0.1230	0.3639
C44	0.5720	-0.0333	0.3277
H44	0.6703	-0.0393	0.3375
C45	0.3203	-0.0733	0.3302
H45	0.2468	-0.1065	0.3417
C46	0.0641	0.1150	0.2002
H46	0.1002	0.0803	0.1788
C47	0.0964	0.1817	0.2680
H47	0.1548	0.1918	0.2919
C48	-0.0788	0.1499	0.1973
H48	-0.1384	0.1407	0.1736
C49	-0.0451	0.2149	0.2645

7. Appendix

C50	-0.1317	0.1981	0.2298
H50	-0.2285	0.2197	0.2279
C51	0.3417	-0.1273	0.1541
H51	0.2811	-0.1840	0.1446
C52	0.4651	-0.1075	0.1370
H52	0.4896	-0.1503	0.1160
C53	0.5741	0.3634	0.2836
H53	0.6178	0.3932	0.3076
C54	0.5171	0.0414	0.1820
H54	0.5795	0.0973	0.1912
N7	0.2285	0.1635	0.1215
C67	0.3888	0.0242	0.0513
N8	0.5079	0.0019	0.0491
C61	0.1215	0.0281	0.0283
C62	-0.0239	0.0617	0.0341
C63	0.1413	-0.0361	-0.0070
C64	0.2416	0.0547	0.0560
C65	0.2290	0.1152	0.0913
N1	0.4267	0.4271	0.1196
N2	0.0536	0.0694	-0.1204
N3	-0.2575	0.2415	-0.0572
N4	0.7351	0.2529	0.0556
C71	0.2703	0.1862	-0.0327
H71	0.2914	0.1442	-0.0543
C72	0.1221	0.2180	-0.0303
C73	0.3549	0.2783	0.0299
C74	0.2063	0.3090	0.0326
H74	0.1850	0.3493	0.0547

C75	0.0971	0.2811	0.0042
H75	0.0023	0.3034	0.0070
C76	0.3801	0.2158	-0.0042
H76	0.4753	0.1945	-0.0071
C77	0.4686	0.3089	0.0590
C78	0.0082	0.1875	-0.0594
C79	0.0343	0.1238	-0.0936
C80	0.6159	0.2781	0.0571
C81	-0.1398	0.2179	-0.0580
C82	0.4438	0.3721	0.0931
C83	0.3818	0.4682	0.9710
C84	0.5302	0.4354	0.9678
H84	0.5485	0.3924	0.9461
C85	0.6417	0.4649	0.9949
H85	0.7360	0.4421	0.9918
C86	0.2663	0.4374	0.9426
C87	0.2856	0.3706	0.9090
C88	0.1174	0.4679	0.9450
N5	0.2975	0.3166	0.8815
N6	-0.0015	0.4920	0.9461

Table 41. Atomic displacement parameter for Tetraphenylphosphonium
Tetracyanoquinodimethane

Atom	U^{11}	U^{22}	U^{33}	U^{12}	U^{13}	U^{23}
P1	0.03044	0.04471	0.03593	0.00076	0.00594	0.00137
C1	0.04012	0.05625	0.05051	0.00364	0.01396	0.01792
C2	0.03195	0.05677	0.03546	-0.00189	-0.00137	0.00393

7. Appendix

C3	0.03286	0.03812	0.05550	0.00031	0.01178	0.00037
C4	0.05283	0.04375	0.04317	-0.00316	0.00246	-0.00331
C5	0.03233	0.04213	0.04940	-0.00400	0.00899	0.00466
C6	0.06723	0.08029	0.07192	-0.02165	-0.03365	0.01561
C7	0.04341	0.08561	0.07716	-0.00915	0.00851	-0.03419
C8	0.06062	0.05294	0.08191	0.01196	-0.00643	-0.01958
C9	0.04617	0.07623	0.05706	0.00003	0.01607	0.01701
C10	0.07517	0.05977	0.05798	0.02020	0.01222	0.01095
C11	0.06089	0.07528	0.04715	-0.01644	0.01253	0.00951
C12	0.05039	0.05338	0.05005	0.00555	0.00543	0.00119
C13	0.11150	0.08158	0.08348	0.02724	-0.00389	0.02457
C14	0.06336	0.08504	0.09701	0.00695	0.04379	0.02784
C15	0.04635	0.08071	0.12428	-0.01215	0.01281	-0.03694
C16	0.04785	0.06510	0.15358	-0.00856	0.04327	-0.00149
C17	0.12040	0.05128	0.05448	-0.01877	-0.02108	-0.00684
C18	0.09405	0.07304	0.09432	0.00068	0.00128	-0.01840
C19	0.05117	0.06188	0.08614	0.00259	0.01714	0.03154
C20	0.05219	0.05541	0.10384	0.00675	0.01703	0.00154
C21	0.05693	0.06889	0.08262	0.01163	0.01552	-0.02390
C22	0.13057	0.07608	0.04330	-0.01177	0.01937	0.00925
C23	0.10787	0.08508	0.05331	-0.03806	0.02443	0.00758
C24	0.03411	0.05237	0.08273	-0.00306	-0.00045	0.01112
P2	0.03306	0.04892	0.04006	0.00175	0.00524	-0.00352
C31	0.03124	0.05646	0.04025	0.00222	0.00247	0.00061
C32	0.03409	0.06248	0.05157	0.00568	0.00076	0.01167
C33	0.03421	0.05032	0.03685	0.00612	0.00200	0.00648
C34	0.05275	0.05154	0.04783	0.00796	0.00413	0.00000
C35	0.03231	0.04628	0.04257	-0.00218	0.00432	0.00419

7. Appendix

C36	0.05925	0.05367	0.05032	-0.00322	0.00020	-0.00250
C37	0.05347	0.06525	0.11077	-0.00802	0.02086	0.00845
C38	0.04607	0.06814	0.09128	0.00673	0.00445	0.03189
C39	0.05126	0.11327	0.06785	0.01457	0.02152	-0.01759
C40	0.06092	0.05113	0.05904	0.00044	0.01630	-0.01305
C41	0.07223	0.07021	0.05219	-0.00643	0.00759	0.00792
C42	0.06490	0.09787	0.06898	0.01989	-0.00887	0.01944
C43	0.14033	0.07510	0.03921	0.02944	-0.00163	-0.00243
C44	0.09492	0.10752	0.09023	0.05654	-0.00682	0.01789
C45	0.11503	0.07965	0.06975	-0.00685	0.01236	0.02213
C46	0.04497	0.05279	0.04492	0.00199	0.00862	0.00278
C47	0.04512	0.08068	0.05958	0.00635	0.00304	-0.02691
C48	0.04185	0.09052	0.05712	0.00958	-0.00536	0.00676
C49	0.05583	0.06881	0.07341	0.00910	0.00889	-0.02670
C50	0.03737	0.06146	0.10193	0.00282	0.01028	-0.00068
C51	0.08551	0.04156	0.06685	0.00993	-0.00499	-0.01360
C52	0.07510	0.07894	0.04131	0.02765	0.00609	-0.01403
C53	0.07045	0.08451	0.06663	-0.02221	0.00454	-0.03015
C54	0.04145	0.08378	0.06137	0.00190	0.00775	-0.02309
N7	0.07023	0.06696	0.04645	0.00537	0.01803	-0.00887
C67	0.03470	0.05197	0.03171	0.00681	0.00395	-0.00270
N8	0.04283	0.08083	0.04788	0.01899	0.00530	-0.00332
C61	0.03344	0.02588	0.02921	0.00745	0.01111	0.00338
C62	0.03070	0.03737	0.02899	0.00358	0.00970	0.00030
C63	0.03511	0.03715	0.02893	0.00467	0.01000	-0.00348
C64	0.03321	0.03337	0.03697	0.00850	0.00816	0.00211
C65	0.03560	0.04714	0.03928	0.00780	0.00711	0.00439
N1	0.06221	0.10109	0.05760	0.00005	-0.00099	-0.02327

7. Appendix

N2	0.06603	0.07982	0.04933	0.00026	0.00711	-0.01264
N3	0.04884	0.07588	0.08021	0.01759	-0.00939	-0.01992
N4	0.04739	0.10111	0.09556	0.02093	-0.01222	-0.03476
C71	0.03853	0.03953	0.03401	0.01365	0.01091	0.00268
C72	0.03391	0.03349	0.02886	0.00519	0.00513	-0.00239
C73	0.03716	0.03380	0.03251	0.00422	0.00395	-0.00179
C74	0.03858	0.03970	0.03431	0.01109	0.00601	-0.00457
C75	0.03620	0.03189	0.03370	0.01008	0.00777	-0.00161
C76	0.03020	0.03034	0.03425	0.00576	0.00340	-0.00152
C77	0.03689	0.04242	0.03620	0.00334	0.00039	-0.00475
C78	0.03732	0.03475	0.03508	0.00820	0.00455	-0.00212
C79	0.03998	0.05825	0.02952	0.00369	-0.00180	-0.00357
C80	0.04387	0.05462	0.05669	0.00550	-0.00531	-0.01608
C81	0.03957	0.04956	0.04629	0.00959	-0.00389	-0.01282
C82	0.04124	0.06128	0.03483	0.00002	-0.00336	-0.00826
C83	0.04233	0.03184	0.03970	0.01254	0.01589	0.00885
C84	0.04896	0.04442	0.03790	0.01396	0.01934	0.00197
C85	0.04056	0.04684	0.04583	0.01512	0.01973	-0.00028
C86	0.04440	0.03825	0.05097	0.01539	0.01979	0.00966
C87	0.04490	0.05396	0.04844	0.01100	0.01470	0.01140
C88	0.04720	0.05243	0.05437	0.01580	0.00554	0.00240
N5	0.07079	0.07743	0.05486	0.00514	0.02337	-0.00429
N6	0.05801	0.08379	0.07816	0.02754	0.00725	-0.00596

7. Appendix

Table 42. Fractional atomic coordinates and isotropic or equivalent isotropic displacement parameters (\AA^2) for $\text{Ag}_7\text{O}_8\text{HF}_2$

Atom	X	y	z	$U_{\text{iso}}^*/U_{\text{eq}}$	Occ. (<1)
Ag1	0.2500	0.2500	0.0000	0.0131 (2)	
Ag2	0.5000	0.5000	0.5000	0.0104 (3)	
O	0.3588 (3)	0.3588 (3)	0.3588 (3)	0.0169 (8)	
F1	0.148 (3)	0.0000	0.0000	0.063 (8)	0.40 (2)
F2	0.0000	0.0000	0.0000	0.005 (8)	0.28 (6)

Table 43. Atomic displacement parameters (\AA^2) for $\text{Ag}_7\text{O}_8\text{HF}_2$

Atom	U^{11}	U^{22}	U^{33}	U^{12}	U^{13}	U^{23}
Ag1	0.0138 (2)	0.0138 (2)	0.0115 (3)	0.00330 (14)	0.000	0.000
Ag2	0.0104 (3)	0.0104 (3)	0.0104 (3)	0.000	0.000	0.000
O	0.0169 (8)	0.0169 (8)	0.0169 (8)	0.0017 (9)	0.0017 (9)	0.0017 (9)
F1	0.10 (2)	0.042 (7)	0.042 (7)	0.000	0.000	0.000
F2	0.005 (8)	0.005 (8)	0.005 (8)	0.000	0.000	0.000

Acknowledgements

I wish to express my deep gratitude to my advisor Prof. M. Jansen for giving me an opportunity to work under his guidance and realize this thesis in his department. He encouraged me with much kindness throughout the work. In particular, I appreciate his support and many thanks are due to him for the interesting topic in field of solid state electrochemistry.

I express my thankfulness here Dr. Jürgen Nuss, Dr. Hanne Nuss for their support in single crystal measurements and structure solutions. Also I thank Dr. Ivan Halasz and Eva Maria Peters for their great help in solving single crystal structures. So many thanks to Mr. Werner Giering for help in selecting the single crystals by precession measurements and Eva Bruecher for Magnetic measurements. I am so thankful to Dr. Christian Oberndorfer for his initial help and advice in the electrochemistry lab my lab colleagues.

Thanks to Ms. Jeanette Knapp and Ms. Sabine Paulsen for helping me in the administrative work. Thanks to all the Jansen group members for their constant support, encouragement and helpful discussions.

This doctoral work was done from May 2006 to 2010 at Max-Planck-Institut für Festkörperforschung, Stuttgart, supported by a scholarship of the Max-Planck-Gesellschaft which is gratefully acknowledged.

I would also like to thank my dissertation committee members, Prof. Dr. Robert E Dinnebier and Prof. Dr. Thomas Schleid.

My heartfelt thanks to Prof. Dr. N. Munichandraiah (IPC, IISc, Bangalore) for introducing me into field of electrochemistry, deep kindness and support to pursue my PhD. My deep gratitude of thanks to Prof. M. Sharon (IIT Mumbai) for giving me inspiration in research. Finally, I would like to thank my parents, grand parents, brothers and sisters for their encouragement and support. I express my deepest gratitude to my deep thanks to my wife Irene for her somuch care, love and encouragement and also to so many brothers and sisters.

List of Figures

Figure 1. Pictorial representation of three electrode electrochemical cell

Figure 2. Three and two electrodes divided cell setup used for electrochemical synthesis

Figure 3. Schematic representation of Schlenk line

Figure 4. Cyclic Voltammograms of $\text{AgNO}_3 + \text{DMBPY} + \text{TBAPF}_6$ in dry acetonitrile at 20 mV sec^{-1} .

Figure 5. Scanning electron micrograph of $\text{Ag}(4,4' \text{ dimethyl } 2,2' \text{ Bipyridine})_2 (\text{NO}_3)_2$ (A) and $\text{Ag}(4,4' - \text{dimethyl} - 2,2' \text{ -Bipyridine})(\text{NO}_3)_2$ (B)

Figure 6. a) View of molecular structure of $\text{Ag}(4,4' - \text{dimethyl} - 2,2' - \text{bipyridine})_2(\text{NO}_3)_2$; b) the view of hexa-coordinated silver(II), with bond lengths given; c) the unit cell view of the compound.

Figure 7. a) View of molecular structure of $\text{Ag}(4,4' - \text{dimethyl} - 2,2' \text{ -bipyridine})(\text{NO}_3)_2$; b) view of tetra coordinated silver(II), with bond lengths given.

Figure 8. Magnetic susceptibility and reciprocal magnetic susceptibility of compounds $\text{Ag}(4,4' - \text{dimethyl} - 2,2' \text{ -bipyridine})_2(\text{NO}_3)_2$ **1** and $\text{Ag}(4,4' - \text{dimethyl} - 2,2' \text{ -bipyridine})(\text{NO}_3)_2$ **2**

Figure 9. a) A view of $\text{Ag}(\text{II})(\text{BPY})(\text{NO}_3)_2$ axially coordinated with the oxygen of neighboring nitrate anion b) the view of hexa-coordinated silver(II), with bond lengths given.

Figure 10. A chain structural view of $\text{Ag}(\text{II})(\text{BPY})(\text{NO}_3)_2$ axially coordinated with neighboring molecule.

Figure 11. Molecular view of Tetraazacyclotetradecane and Tetramethyl Tetraazacyclotetradecane

Figure 12. Cyclic voltammogram of $\text{AgPF}_6 + \text{TMTACTD} + \text{TBAPF}_6$ in acetonitrile at 20 mV/sec .

Figure 13. Scanning electron micrograph of $\text{Ag}(\text{II})(\text{TMTACTD})(\text{PF}_6)_2(\text{CH}_3\text{CN})$

Figure 14. ORTEP representation of the cation in $\text{Ag}(\text{II})(\text{TMTACTD})(\text{PF}_6)_2(\text{CH}_3\text{CN})$. Ellipsoids are drawn at 50 % probability level and hydrogen atoms are omitted for clarity.

Figure 15. (a) A molecular view of $\text{Ag(II)(TMTACTD)(PF}_6)_2(\text{CH}_3\text{CN)}$ in a pentacoordinated environment, with twofold disorder of PF_6^- anion with two orientations rotated by approximately 45° relatively to each other

Figure 16. (a) A view of Ag^{2+} in a pentacoordinated environment. (b) Twofold disorder of PF_6^- anion with two orientations rotated by approximately 45° relatively to each other and (c) two position disorder of the whole anion. Two orientations of disordered anions are in each case designated with different bond colours.

Figure 17. (a) A molecular view of $\text{Ag(II)(Pyridine)}_4(\text{NO}_3)_2$, b. unit cell view and c. *cis* coordinated Ag(II)

Figure 18. Cyclic voltammograms of $\text{AgClO}_4 + \text{Bipyridine} + \text{TBAClO}_4$ in acetonitrile at 20 mV/sec.

Figure 19. Molecular view of $\text{Ag(II)(Bipyridine)}_2(\text{ClO}_4)_2$

Figure 20. Ag(II) ion in 4+2 coordination. The weak coordination denoted by broken line.

Figure 21. A view of unit cell of $\text{Ag(II)(Bipyridine)}_2(\text{ClO}_4)_2$

Figure 22. Cyclic voltammograms of acetonitrile containing $\text{AgClO}_4 + 4,4'$ dimethyl 2,2' Bipyridine + TBAPF_6

Figure 23. Le Bail fit for $\text{Ag}^{\text{II}}(4,4'$ dimethyl 2,2' Bipyridine) $_2(\text{ClO}_4)_2$

Figure 24. Histogram of research articles on phthalocyanine compounds for every 5 years

Figure 25. View of phthalocyanine and hexadecafluorinated phthalocyanine ligand.

Figure 26. (a) Molecular view of Lithium phthalocyanine radical

Figure 27. Cyclic Voltammograms of $\text{Li}_2\text{Pc} + \text{TBAPF}_6$ in dry acetonitrile (A) and in dimethoxyethane (B) at 20 mV sec^{-1} .

Figure 28. Scanning electron micrographs of (A) Lithium phthalocyanine radical, (B)

Lithium phthalocyanine Tetrabutyl ammonium hexafluorophosphate

Figure 29. ORTEP representation of the cation in LiPc.TBAPF_6 . Ellipsoids are drawn at 50 % probability level and hydrogen atoms are omitted for clarity.

Figure 30. A view of molecular structure of lithium phthalocyanine. Tetrabutylammonium hexafluorophosphate co-crystal.

Figure 31. a) A comparative view of LiPc unit in this compound (A) and in the tetragonal phase of LiPc radical (B).

Figure 32. Unit cell structure of (A) Lithium phthalocyanine Tetrabutyl ammonium hexafluorophosphate, (B) Lithium phthalocyanine radical,

Figure 33. Solid state spectra of LiPc radical (2) and the compound (2) in the KBr pellets

Figure 34. UV-Vis-NIR Spectra of LiPc (1), Li₂Pc (2), LiPc.TBAPF₆ (3)

Figure 35. 2 X-Ray powder pattern disodium phthalocyanine

Figure 36. UV-Vis-NIR spectra of disodium phthalocyanine and dilithium phthalocyanine.

Figure 37. Cyclic voltammograms of Na₂Pc and Li₂Pc in dimethoxyethane containing 0.01 M tetrabutyl ammonium hexafluorophosphate. The continuous cycling and the cycle number in indicated.

Figure 38. Cyclic voltammograms Na₂Pc and Li₂Pc in dimethoxyethane containing TBAPF₆

Figure 39. a, X-ray powder pattern of NaPc showing rietveld refinement profile. b, A comparative X-Ray powder diffraction pattern of LiPc and NaPc.

Figure 40. a - Molecular view of monosodium phthalocyanine and b- packing of neighbouring phthalocyanine molecule with intermolecular weak bonding of N-Na-N.

Figure 41. Solid state absorption spectra of Li₂Pc, Na₂Pc, LiPc and NaPc taken in a KBr medium.

Figure 42. Powder Diffraction pattern of silver phthalocyanine prepared from Li₂Pc + AgNO₃ mixture.

Figure 43. X-Ray powder patterns of LiPc and AgNO₃ treated LiPc.

Figure 44. Solid state silver exchange reaction of lithium phthalocyanine radical with AgNO₃ in CH₃CN - EDAX [Ag:N -0.23:8]

Figure 45. X-Ray powder diffraction of products obtained by treating LiPc with monovalent silver salt in dimethoxyethane.

Figure 46. Powder XRD pattern of LiPc, AgNO₃ treated LiPc and ICDD peak file of elemental Ag

Figure 47. A comparative pattern of LiPc and solid LiPc powder treated with AgNO₃ solution

Figure 48. Powder pattern of mercury phthalocyanine synthesized from Li₂Pc+ HgCl₂

Figure 49. view of hexadecafluorinated metal phthalocyanine

Figure 50. X-Ray powder diffraction of the resultant product of the above reaction.

Figure 51. Absorbance spectra of Li_2Pc and $\text{F}_{16}\text{Li}_2\text{Pc}$ taken in acetone.

Figure 52: (a) View of TPP.TCNQ, (b) view of TPP in b axis, (3) unit cell of TPP:TCNQ

Figure 53: Stacking view of TPP.TCNQ

Figure 54. Molecular view of Tetrahexylammonium Tetracyanoquinodimethane.

Figure 55. Packing diagram of Tetrahexyl ammonium tetracyanoquinodimethane

Figure 56. SEM image of Tetrabutylammonium tetracyanoquinodimethane.

Figure 57. a. Molecular view of Tetrabutylammonium TCNQ, disorder carbon not shown for clarity. b. a view showing with the two position of disordered tetrabutyl group, hydrogen atoms omitted for clarity.

Figure 58. Packing diagram of Tetrabutyl ammonium tetracyanoquinodimethane

Figure 59. a, View of Tetraphenylphosphonium Tetracyanoquinomethane. b, Unit cell without the disordered TCNQ layer. c. Arrangement of TCNQ in the ordered layer.

Figure 60. a, View if Tetraphenylphosphonium Tetracyanoquinodimethane b, unit cell with the disordered TCNQ layer.

Figure 61. Cyclic voltammograms of aqueous solution containing different mixture mentioned along with the figure.

Figure 62. SEM micrographs of crystals obtained from different electrocrystallization experiments, conditions mentioned in the inset of the figure.

Figure 63. X-ray powder pattern of Ag_3O_4 prepared by electrooxidation of aqueous solution containing $\text{AgPF}_6 + \text{NaF}$.

Figure 64. View of $\text{Ag}_7\text{O}_8\text{HF}_2$.

List of Table

Table 1. Crystal data and structure refinement for compounds $\text{Ag(II)(DMBPY)}_2(\text{NO}_3)_2$ and $\text{Ag(II)(DMBPY)(NO}_3)_2$

Table 2. Selected interatomic distances (\AA) and bond angles ($^\circ$) of $\text{Ag(II)(DMBPY)}_2(\text{NO}_3)_2$ and $\text{Ag(II)(DMBPY)(NO}_3)_2$

Table 3. Crystal data for $\text{Ag(II)(Bipyridine)(NO}_3)_2$

Table 4. Selective interatomic distance and bond lengths $\text{Ag(II)(BPY)(NO}_3)_2$

Table 5. General and crystallographic parameters for $\text{Ag(II)(TMTACTD)(PF}_6)_2(\text{CH}_3\text{CN})$.

Table 6. Selected geometrical parameters for $\text{Ag(II)(TMTACTD)(PF}_6)_2(\text{CH}_3\text{CN})$.

Table 7. Hydrogen bonds of the C-H \cdots F type between the macrocyclic ligand and one of the PF_6^- anions.

Table 8. Crystal data and structure refinement of $\text{Ag}^{\text{II}}(\text{pyridine})_4(\text{NO}_3)_2$

Table 9. Selected interatomic distances (\AA) and bond angles ($^\circ$) for the $\text{Ag(II)(Pyridine)}_4(\text{NO}_3)_2$

Table 10. Crystal data and structure refinement of $\text{Ag}^{\text{II}}(\text{pyridine})_4(\text{ClO}_4)_2$

Table 11. Crystal data for LiPc.TBAPF_6

Table 12. Selected bond angles and bond distances for LiPc.TBAPF_6

Table 13. Crystal data for Tetrapropylporphycene tetracyanoquinodimethane

Table 14. Crystal structure data of Tetrahexyl ammonium tetracyanoquinodimethane

Table 15. Crystal structure data of Tetrabutyl ammonium tetracyanoquinodimethane

Table 16. Crystal data for $\text{Ag}_7\text{O}_8.\text{HF}_2$

List of table in Appendix

Table 17. Atomic coordinates and equivalent isotropic displacement parameters ($\text{pm}^2 \times 10^{-1}$) for compounds $\text{Ag}(\text{DMBPY})_2(\text{NO}_3)_2$ (A) $U(\text{eq})$ is defined as one third of the trace of the orthogonalized U^{ij} tensor.

Table 18. Anisotropic displacement parameters ($\text{pm}^2 \times 10^{-1}$) and the anisotropic displacement factor for $\text{Ag}(\text{DMBPY})_2(\text{NO}_3)_2$

Table 19. Atomic coordinates and equivalent isotropic displacement parameters ($\text{pm}^2 \times 10^{-1}$) for compound $\text{Ag}(\text{DMBPY})(\text{NO}_3)_2$ (B). $U(\text{eq})$ is defined as one third of the trace of the orthogonalized U^{ij} tensor.

Table 20. Anisotropic displacement parameters for $\text{Ag}(\text{II})(\text{DMBPY})(\text{NO}_3)_2$

Table 21. Fractional atomic coordinates and isotropic or equivalent isotropic displacement parameters (\AA^2) for $\text{Ag}(\text{II})(\text{BPY})(\text{NO}_3)_2$

Table 22. Atomic displacement parameters (\AA^2) for $\text{Ag}(\text{BPY})(\text{NO}_3)_2$

Table 23. Fractional atomic coordinates and isotropic or equivalent isotropic displacement parameters (\AA^2)

Table 24. Atomic displacement parameters (\AA^2) for $\text{Ag}(\text{TMTACTD})(\text{PF}_6)_2$

Table 25. Fractional atomic coordinates and isotropic or equivalent isotropic displacement parameters (\AA^2) $\text{Ag}(\text{Py})_2(\text{NO}_3)_2$

Table 26. Atomic displacement parameters (\AA^2) $\text{Ag}(\text{Py})_2(\text{NO}_3)_2$

Table 27. Fractional atomic coordinates and isotropic or equivalent isotropic displacement parameters (\AA^2) $\text{Ag}(\text{BPy})_2(\text{ClO}_4)_2$

Table 28. Atomic displacement parameters (\AA^2) for $\text{Ag}(\text{BPy})_2(\text{ClO}_4)_2$

Table 29. Fractional atomic coordinates and isotropic or equivalent isotropic displacement parameters (\AA^2) for LiPc.TBAPF_6

Table 30. Atomic displacement parameters (\AA^2) for LiPc.TBAPF_6

Table 31. Atomic coordinates for monosodium phthalocyanine

Table 32. Fractional atomic coordinates and isotropic or equivalent isotropic displacement parameters (\AA^2) for Tetrapropylporphycene.Tetracyanoquinodimethane.

Table 33. Atomic displacement parameters for Tetrapropylporphycene. Tetracyanoquinodimethane.

Table 34. Fractional atomic coordinates and isotropic or equivalent isotropic displacement parameters (\AA^2) Tetrahexylammonium TCNQ 298 K

Table 35. Atomic displacement parameters (\AA^2) Tetrahexylammonium TCNQ 298 K

Table 36. Fractional atomic coordinates and isotropic or equivalent isotropic displacement parameters (\AA^2) Tetrahexylammonium TCNQ 100 K

Table 37. Atomic displacement parameters (\AA^2) Tetrahexylammonium TCNQ 100 K

Table 38. Fractional atomic coordinates and isotropic or equivalent isotropic displacement parameters (\AA^2) for Tetrabutylammonium Tetracyanoquinodimethane

Table 39. Atomic displacement parameters (\AA^2) for Tetrabutylammonium Tetracyanoquinodimethane

Table 4044 Fractional atomic coordinates for Tetraphenylphosphonium Tetracyanoquinodimethane

Table 41. Atomic displacement parameter for Tetraphenylphosphonium Tetracyanoquinodimethane

Table 42. Fractional atomic coordinates and isotropic or equivalent isotropic displacement parameters (\AA^2) for $\text{Ag}_7\text{O}_8\text{HF}_2$

Table 43. Atomic displacement parameters (\AA^2) for $\text{Ag}_7\text{O}_8\text{HF}_2$

List of Abbreviations

a. u.: arbitrary units

HT: High Temperature

RT: Room Temperature

EDX: Energy Dispersive X-ray spectrometry

PSD: Position Sensitive Detector

SQUID: Spin Quantum Interference Device

T_c : Curie temperature

Å: Angstrom

K: Kelvin

q: Theta temperature in Kelvin

T: Tesla

AC – Alternating current

List of publications

1. Electrochemical synthesis and crystal structure of a penta-coordinated silver(II) macrocyclic complex, Sakthivel Kandaiah, Ivan Halasz, Robert E Dinnebier, Martin Jansen, *Inorganica Chimica Acta*, 2009, 362, 11, 4009-4012.
2. Electrocrystallization of Tetra- and Hexa-coordinated Silver(II) Compounds Based on 4,4'-Dimethyl-2,2'-Bipyridine Ligand - Single Crystal Structures and Magnetic Studies, Sakthivel Kandaiah, Eva Maria Peters, Martin Jansen, *Zeitschrift für Anorganische und Allgemeine Chemie*, 2008, 634, , 2483-2486.
3. Electrodeposition of adherent films of lithium phthalocyanine on platinum and stainless steel substrates by oxidation of dilithium phthalocyanine, Sakthivel. Kandaiah, N. Munichandraiah, Lawrence G Scanlon, *J. Electrochemical Soc.*, 2005, 152, 11, C756-C763
4. Analysis of electrochemical impedance of dilithium phthalocyanine, Munichandraiah Nookala, Sakthivel Kandaiah, Lawrence G Scanlon, *Electrochemical and solid state letters*, 2005, 8, 5, E45-E48.
5. Electrochemical Synthesis, Crystal Structure and Optical Properties of Lithium Phthalocyanine-Tetrabutylammonium Hexafluorophosphate. Sakthivel Kandaiah, Ivan Halasz, Robert E Dinnebier, Martin Jansen, (*under preparation*),
6. Electrocrystallization and Single Crystal structure Investigation of a *cis* - Coordinated Tetrapyrindine Silver(II) Dinitrate. Sakthivel Kandaiah, Eva Maria Peters, Martin Jansen, (*under preparation*)
7. Electrochemical synthesis and crystal structure of Tetrahexyl ammonium tetracyanoquinodimethane. Sakthivel Kandaiah, Jürgen Nuss, Martin Jansen (*under preparation*)
8. Single crystal structures and magnetic studies of electrocrystallized silver(II) compounds containing weakly coordinated perchlorate anions. Sakthivel Kandaiah, Eva Maria Peters, Martin Jansen (*under preparation*)
9. Electrochemical synthesis and crystal structure of Tetrapropyl porphycene tetracyanoquinodimethane. Sakthivel Kandaiah, Hanne Nuss, Martin Jansen (*under preparation*)

-
10. Electrocrystallization of monosodium phthalocyanine, Sakthivel Kandaiah, Martin Jansen (*under preparation*)
 11. Electrochemical synthesis of Teraphenylphosphonium tetracyanoquinodimethane. Sakthivel Kandaiah, Hanne Nuss, Martin Jansen (*under preparation*)

Curriculum vitae

Sakthivel Kandaiah

Education

Ph. D. in Inorganic Chemistry 2006- 2010

Max-Planck Institute for Solid State Research, Stuttgart, Germany

Dissertation: 'Electrochemical synthesis of new coordination compounds with higher valent silver, metallo- phthalocyanines, and some organic charge transfer crystals.'

Advisor: Prof. Dr. Dr. h. c. Martin Jansen

M. Sc. in Applied Chemistry 2000-2002

Government College of Technology, Bharathiar University, Coimbatore, India

Thesis: 'Preparation and characterization of carbon anode for alkaline fuel cell '

Advisor: Dr. M. Sharon (Indian Institute of Technology – Mumbai)

B. Sc. in Chemistry 1997-2000

Hindu College, Manonmaniam Sundaranar University, Tirunelveli, Tamilnadu, India

Work Experience

Project student, 2002

Indian Institute of Technology, Mumbai, India

Project: 'Preparation and characterization of carbon nanomaterials' under Guidance of Prof. Maheswar Sharon

Research Assistant, 2003-2004

Indian Institute of Science, Bangalore, India

Project: 'Synthesis and electrochemical characterisation of nanomaterials, chemically modified electrodes self assembled monolayer'

Research Assistant 2004-2006

Indian Institute of Science Bangalore, India

Project 'New Electrode and Electrolyte materials for Lithium Batteries', Collaboration with U.S Naval Research Lab, with Lawrence G Scanlon and Advisor: Prof.N.Munichandraiah (IISc-Bangalore)

Personal Information

Date of Birth: 1st Nov 1978

Place of birth: Ambasamudram, Tamilnadu, India

Gender: Male

Hiermit versichere ich an Eides statt, dass ich diese Dissertation unter Verwendung der angegebenen Hilfsmittel selbstständig angefertigt und bisher noch keinen Promotionsversuch unternommen habe.

Stuttgart, den ,

Sakthivel Kandaiah